



UNIVERSITÀ
DEGLI STUDI
DI PADOVA

**UNIVERSITÀ DI PADOVA
FACOLTÀ DI INGEGNERIA**

-

Dipartimento di Tecnica e Gestione dei Sistemi Industriali

-

**SCUOLA DI DOTTORATO IN INGEGNERIA INDUSTRIALE
Indirizzo: Meccatronica e Sistemi Industriali
XXIII Ciclo**

**Critical analysis and economic optimization in the foundry
after introduction of
primary aluminum alloys for premium castings**

Ch.mo Prof. Paolo Francesco BARIANI, **Direttore della Scuola**

Ch.mo Prof. Alberto TREVISANI, **Coordinatore di Indirizzo**

Ch.mo Prof. Franco BONOLLO, **Supervisore**

Dottorando: Federico Casarotto

8 Marzo 2011

*“Sono due perle,
il bene piú prezioso...
Non permettere a nessuno
di fare mai loro del male.”*

Preface

This doctoral thesis is the result of three years of work and study, carried-out at the Department of Management and Engineering (DTG) in Vicenza - University of Padova, in collaboration with the german company Rheinfelden Alloys GmbH & Co. KG, located in Rheinfelden Baden and the italian company Microtech Solution s.r.l. in Flero (BS).

Professor Franco Bonollo was the main supervisor of this work, coordinated in Microtech by Emanuele Ferrari and Claudio Gatti.

Some of the activities carried-out within the framework of this work have been reported and published in the following papers, books and proceedings:

- D. Shimosaka, M. Kim, Y. Harada, S. Kumai, S. Watanabe, F. Casarotto, *Microstructure refinement and toughness improvement of rapidly-solidified aluminium alloys including inherent brittle dispersed particles*, Proceedings from PFAM XVIII – Processing and Fabrication of Advanced Materials, pp 223-230, Tohoku University, Sendai, December 2009.
- F. Casarotto, *Premium HPDC-alloys for automotive applications*, Proceedings from the 2010 Korea International Eco-DieCasting Symposium, Ulsan, South Korea, October 2010.
- F. Casarotto, A. J. Franke, R. Franke, *Advanced materials in automotive bodies, chassis and interiors*, from the book “Enabling Materials and Manufacturing Technologies”, published by Woodhead Publishing Limited, Cambridge, UK (accepted on 31.10.2010 – print in progress).
- G. Luvará, P. Piccardo, F. Casarotto, L. M. Volpone, *Studio di saldabilità (LBW, FSW, EBW) di leghe da pressocolata a base di alluminio*, 33° Conv. Naz. Associazione Italiana di Metallurgia, Novembre 2010.

In addition, the following M.S. theses have been supervised:

- E. Caruso, *Chemical optimization of Castasil-37 for the economic production of ductile high-pressure diecastings*, DTG, Università di Padova, Facoltà di Ingegneria, Supervisors: F. Bonollo, A. J. Franke, D. Apelian, F. Casarotto, A.A. 2007-2008.
- F. Rando, *L'alluminio nelle applicazioni motociclistiche*, DTG, Università di Padova, Facoltà di Ingegneria, Supervisors: F. Bonollo, F. Casarotto, A.A. 2007-2008.
- G. Raffaelli, *Strengthening while maintaining ductility in HPDC-Alloys for automotive application*, DTG, Università di Padova, Facoltà di Ingegneria, Supervisors: F. Bonollo, A. Zambon, F. Casarotto A.A. 2008-2009.

**Critical analysis and economic optimization in the foundry
after introduction of
primary aluminum alloys for premium castings**

Questa tesi di dottorato é il frutto di tre anni di lavoro presso il Dipartimento di Tecnica e Gestione dei Sistemi Industriali (DTG) di Vicenza - Università di Padova – e della collaborazione tra l’azienda tedesca Rheinfelden Alloys GmbH & Co. KG di Rheinfelden, Baden e la società italiana Microtech Solution s.r.l. di Flero (BS).

Rheinfelden Alloys è un produttore di leghe di alluminio da fonderia, la cui filosofia trova forti radici nelle attività di ricerca e sviluppo. Negli anni '90, l’azienda ha sviluppato ed introdotto sul mercato alcuni materiali innovativi per il settore automotive, accoppiando alla leggerezza dell’alluminio una maggiore resistenza meccanica e duttilità. Questo ha reso più agevole il processo di continua riduzione del peso delle moderne autovetture, favorendone al contempo l’abbassamento delle emissioni.

Microtech Solution è un’azienda di consulenza, che progetta e sviluppa getti pressocolati su richiesta del cliente. I getti nascono dalle prime fasi di engineering, passando per la prototipazione rapida, fino alla produzione di serie in fonderia. Microtech è attiva principalmente nel settore auto, che serve in outsourcing per quel che concerne getti strutturali e componenti chassis in generale.

Uno dei recenti sviluppi di Rheinfelden Alloys in termini di leghe d’alluminio da pressocolata è Magsimal[®]-59, chimicamente designata come AlMg5Si2Mn. La lega è stata scelta come materiale da utilizzare per la realizzazione di un sistema di apertura/chiusura di capote rigida in 5 pezzi di una famosa auto sportiva. Microtech è stata incaricata di gestire il progetto in veste di capo commessa.

L’obiettivo di questo lavoro é di fornire un’immagine completa della catena logistico-produttiva di un moderno “sistema fonderia”, integrandone diverse funzioni e discipline. Il lavoro è stato strutturato su due livelli: quello del fornitore di materia prima e quello della fonderia ovvero del fornitore di getti in lega leggera. Tradizionalmente, i due livelli sono stati considerati indipendenti e separati, con la gestione delle attività produttive da monte a valle, nell’ottica di soddisfare le richieste del cliente finale; il produttore di leghe di alluminio è visto soltanto come colui che fornisce il materiale necessario alla produzione del pezzo finito.

Al contrario, un approccio moderno alla fonderia combina trasversalmente il know-how di tutti i membri della catena di fornitura, sfruttando al meglio le sinergie che ne derivano. In questo modo, ad esempio, un componente si progetta tenendo conto delle accortezze che il materiale prescelto richiede. Un’accurata ed integrata metodologia di lavoro permette di controllare al meglio l’entità dell’investimento iniziale, il costo del prodotto, il time-to-market e, punto fondamentale, problemi nella fase di avviamento produttivo.

Al fine di collegare i diversi protagonisti della filiera produttiva coinvolti nel progetto, i processi di produzione della materia prima e dei getti pressocolati sono stati analizzati in parallelo, con lo stesso approccio.

Il capitolo 1 raccoglie in maniera organica dati tecnici sulla lega Magsimal[®]-59, facendo riferimento ad informazioni disponibili in letteratura e ad esperienze dirette di fonderia. Il valore aggiunto della lega sono le sue proprietà meccaniche e la sua resistenza a fatica allo stato grezzo di colata, di gran lunga superiori rispetto a quelle

di materiali tradizionali. Si fornisce un ritratto completo della lega, descrivendone composizione chimica e microstruttura. Parametri di trattamento termico, resistenza a corrosione, trattamenti superficiali e tecniche di giunzione applicabili a Magsimal[®]-59 completano il quadro.

Il capitolo 2 presenta il processo manifatturiero della Rheinfelden Alloys, basato su logistica snella, sottolineandone le fasi cruciali dell'implementazione in fonderia. La produzione del metallo si scompone nei suoi nuclei elementari tramite il diagramma di flusso, ponendo l'attenzione sulle variabili fondamentali per l'ottenimento di proprietà meccaniche superiori. La descrizione del modello di business e delle dispendiose misure adottate nel Sistema Qualità gettano le basi per la costificazione dei componenti RHT, effettuata nel capitolo 3.

Il cuore del lavoro è presentato nel terzo capitolo, in cui si descrive nei dettagli l'applicazione, in ciascuna delle tre parti costituenti la capote rigida: capote carrier, main roof racket e side frame. Il profilo dei requisiti dei componenti è stato discusso alla luce dei maggiori ostacoli incontrati a livello produttivo. Il processo di pressocolata è stato scomposto nelle sue fasi elementari tramite flow chart, al fine di evidenziarne le criticità; opportuni cambiamenti sono stati quindi introdotti in fonderia. I risultati ottenuti su prototipi, campionature, pre-serie e getti di serie sono stati infine correlati alle misure adottate sul nuovo layout di fonderia.

Valutazioni generali sulla qualità dei getti e la gestione complessiva di processo sono state effettuate utilizzando come termine di paragone una lega secondaria AlSi9Cu3(Fe), di comune utilizzo in fonderia. La lunga messa a punto del processo di pressocolata con Magsimal[®]-59 ha portato alla conclusione che, se da una parte il cliente finale è affascinato dalle proprietà meccaniche superiori della lega allo stato grezzo, dall'altro la fase di ingegnerizzazione ne richiede profonda conoscenza, poiché il componente deve essere progettato in funzione delle caratteristiche fisiche della lega.

In chiusura, è stato valutato l'impatto economico di operazioni aggiuntive e misure necessarie alla gestione di una cella di pressocolata in Magsimal[®]-59, tramite costificazione a consuntivo dell'intero processo produttivo. Il valore percentuale ottenuto è di notevole rilievo: + 150 %, che legittima l'uso di leghe alto-prestazionali solamente laddove lo giustifica un profilo di requisiti altrettanto elevato. D'altra parte si consideri che il fattore "costo" comporta l'adozione di soluzioni nella maggior parte dei casi non propriamente compatibili con le richieste tecniche presentate. L'approccio suggerito è quindi quello di potenziare l'impiego delle risorse disponibili in fase di ingegnerizzazione, sia di processo che di prodotto, utilizzando, ad esempio, moderni tools CAD/CAE.

Lo specifico potenziale applicativo della lega Magsimal[®]-59 è stato valutato anche in relazione a processi di fonderia innovativi. Il capitolo 4 presenta uno studio centrato sulla tecnologia High-Speed Twin-Roll Casting (HSTRC), caratterizzata da elevate velocità di solidificazione, in grado di determinare sensibili affinamenti della microstruttura. L'attività sperimentale presentata è stata condotta al fine di valutare la possibilità di un ulteriore miglioramento delle proprietà meccaniche statiche e dinamiche del metallo. Si è cercato di correlare i dati sperimentali con microstruttura

ottenuta e duttilità, confrontando piastre realizzate in twin-roll ed in pressocolata tradizionale.

I miglioramenti attesi a livello di trazione non sono stati confermati dai campioni testati, a causa della presenza di difetti di colata e di una microstruttura non omogenea osservabile sulle piastre realizzate in twin-roll. Una revisione dei parametri di colata in HSTRC è quindi indispensabile al fine di migliorare la qualità fusoria del prodotto. Risultati positivi si sono invece ottenuti con il test Erichsen: l'energia assorbita a cricatura E_i e l'energia unitaria di iniziazione della cricca UE_i è circa 1,7 volte superiore al valore rilevato per piastre pressocolate di spessore paragonabile. Inoltre, il test Erichsen si è rivelato poco sensibile alla presenza di difetti interni di colata, profilandosi come alternativa valida alla prova di strappo per la valutazione della tenacità di un metallo.

Le leghe primarie da fonderia sono ampiamente utilizzate in automotive, settore in cui le richieste in termini di duttilità e saldabilità del getto pressocolato si fanno sempre più severe. Per quel che concerne la saldabilità, i processi di giunzione più comunemente utilizzati sono quelli ad arco tradizionali, come TIG e MIG, che hanno lo svantaggio di generare ampie zone termicamente alterate con precipitazioni di fasi fragili. Di qui l'esigenza di uno studio di saldabilità con processi alternativi come Laser Beam Welding (LBW), Electron Beam Welding (EBW) e Friction Stir Welding (FSW).

Il capitolo 5 presenta la sperimentazione effettuata con queste tecnologie su piastre in leghe AlSi, saldate con la tecnica "beads-on-plate", cioè direttamente sul metallo base. Lo scopo dello studio è verificare la compatibilità di moderne tecniche di giunzione con leghe primarie ad alte prestazioni e di definire in tal caso i migliori parametri di saldatura, al fine di ottenere giunti privi di difettosità.

La procedura sperimentale adottata ha permesso la realizzazione di giunti LBW, EBW e FSW, analizzati qualitativamente al microscopio ottico e tramite profili di microdurezza.

Tecniche di saldatura che portano a fusione il metallo danno origine a giunti dalla maggiore micro e macro porosità. La tecnologia LBW non si è rivelata in grado di produrre giunti saldati di qualità accettabili, mentre la tecnica EBW porta a risultati positivi, previa adozione della doppia passata e di un'eventuale passata cosmetica. In tal caso, velocità di saldatura fino a 90 mm/s non hanno inficiato la qualità dei cordoni ottenuti. Entrambe le tecniche ad energia concentrata determinano un incremento di durezza di circa 25-30 punti Vickers in corrispondenza del giunto saldato. Il metodo FSW si è rivelato applicabile entro un ampio intervallo di parametri di saldatura, generando giunti di qualità molto soddisfacente. Un calo di durezza di circa 25 HV è stato osservato in prossimità del nugget.

Nei paragrafi successivi si fornisce una sintesi più dettagliata dei capitoli in lingua italiana, al fine di condensare i tratti essenziali del lavoro.

Capitolo 1: Magsimal[®]-59

Magsimal[®]-59 é una lega da pressocolata primaria del tipo AlMg5Si2Mn, la cui composizione chimica completa è riportata in tab. 1.1. Gli alliganti principali sono magnesio, silicio e manganese. Il rapporto tra magnesio e silicio determina le caratteristiche meccaniche del metallo. La presenza del manganese supplisce all'assenza del ferro e favorisce l'estrazione del getto dalla cavità dello stampo.

[%]	Si	Fe	Cu	Mn	Mg	Zn	Ti	Be	others total
min.	1,8			0,5	5,0				
max.	2,6	0,2	0,05	0,8	6,0	0,07	0,20	0,004	0,2

Tab. 1.1: composizione chimica di Magsimal[®]-59.

La lega è trattata con ca. 30-40 parti per milione di berillio, al fine di ridurre la naturale tendenza del magnesio all'ossidazione.

A livello microstrutturale, la lega presenta una fase primaria α ricca in alluminio e una fase eutettica ternaria, costituita da alluminio e Mg_2Si . Il manganese si aggrega sotto forma di intermetallici poligonali del tipo Al_6Mn . La particolarità della lega risiede nel fatto che il meccanismo naturale di nucleazione e crescita dei cristalli di Mg_2Si viene modificato artificialmente in fase di produzione. Ne consegue una morfologia globulare indotta della fase Mg_2Si , profondamente diversa dalla sua struttura lamellare tipica. Si vedano a titolo di confronto le due micrografie di fig. 1.1 e 1.2, che affiancano Magsimal[®]-59 ad una normale AlMg5Si2Mn.



Fig. 1.1: la microstruttura di Magsimal[®]-59. 1000X.



Fig. 1.2: la microstruttura di una comune AlMg5Si2Mn. 1000X.

Le conseguenze a livello di proprietà meccaniche sono apprezzabili in maggiori allungamenti a rottura, con carichi di allungamento superiori ai 220 MPa, tab. 1.2. La resistenza a fatica raggiunge i 100 MPa, riferita a curve di Wöhler al 5% di probabilità di rottura in condizioni $r = -1$ per spessori di parete di 4 mm. Un trattamento termico completo influenza negativamente queste caratteristiche, motivo per cui la lega viene utilizzata quasi esclusivamente allo stato grezzo di colata (F) o post trattamento termico monostadio (T5 oppure O).

Wall thickness [mm]	$R_{p0,2}$ [MPa]	R_m [MPa]	A [%]
< 2	> 220	> 300	10 – 15
2 – 4	160 – 220	310 – 340	12 – 18
4 – 6	140 – 170	250 – 320	9 – 14
6 – 12	120 – 145	220 – 260	8 – 12

Tab. 1.2: caratteristiche meccaniche di Magsimal[®]-59 allo stato grezzo.

La lega possiede un'ottima resistenza alla corrosione ed una buona attitudine alla giunzione tramite saldatura e rivettatura.

A fronte di questi vantaggi, la lega mostra alcuni lati critici, quali il maggior ritiro volumetrico, dovuto alla presenza di un tenore limitato di silicio, ed una colabilità inferiore rispetto alle leghe alluminio-silicio. Inoltre, temperatura di fusione e colata più elevata, unita alla maggior reattività del metallo primario con l'acciaio, rendono i fenomeni di usura sugli utensili di fonderia molto più spinti rispetto a leghe da pressocolata tradizionali.

Capitolo 2: il processo produttivo di Magsimal[®]-59

Le attività di produzione della lega sono gestite da Rheinfelden Alloys secondo le linee guida della logistica snella. In particolare, l'alluminio primario viene acquistato sulla borsa di Londra - London Metal Exchange (LME) - sulla base del portafoglio ordini clienti e secondo filosofia "back-to-back". Questo tipo di approccio ha il vantaggio di eliminare i rischi speculativi legati alle fluttuazioni delle quotazioni dell'alluminio e al tempo stesso di limitare al minimo i quantitativi di lega presenti a magazzino. Il cliente riceve quindi metallo di fresca produzione, senza far uso di un polmone o buffer intermedio.

Il ciclo di produzione della lega Magsimal[®]-59 si articola nelle seguenti fasi:

- ricezione e stoccaggio materie prime
- preparazione della carica
- fusione ed alligaggio
- trattamento di trasformazione del bagno
- colata dei lingotti
- pallettizzazione e marcatura
- controllo qualità e approvazione
- spedizione al cliente

La fase di maggior interesse risulta quella del trattamento di trasformazione del bagno, con cui si induce il cambio a livello microstrutturale del metallo.

Il trattamento effettuato ha un "grado di riuscita" variabile, funzione delle condizioni di fusione e di colata contingenti. In base all'efficacia del trattamento, si può stilare una scala di misura percentuale, in cui lo zero corrisponde a risultati nulli e il 100 alla piena riuscita del lotto. Sulla base del know-how interno e dell'esperienza pluriennale in fonderia, l'aspetto ed il colore della superficie di rottura del metallo si

sono correlate alle proprietà meccaniche della lega, in particolare alla sua duttilità/tenacità. La scala di riferimento è riportata in tab. 2.1.

	YTS [MPa]	UTS [MPa]	e [%]	Efficacia trattamento [%]
Magsimal®-59 AlMg5Si2Mn	178	313	20,6	75-100
AlMg5Si2Mn	187	328	13,4	50-75
AlMg5Si2Mn	183	319	8,4	25-50
AlMg5Si2Mn	186	321	7,7	0-25

Tab. 2.1: correlazione tra proprietà meccaniche della lega AlMg5Si2Mn ed efficacia del trattamento di trasformazione.

A migliori risultati del trattamento di trasformazione corrispondono valori di allungamento maggiori. La superficie di rottura del metallo cambia progressivamente da un colore azzurrastro a rottura poco duttile ad un colore bianco, con dinamiche di fratture molto più tenaci. Infine, la microstruttura si modifica gradualmente da quella di fig. 1.2 a quella di fig. 1.1. Solo lingotti in cui il trattamento di trasformazione mostri efficienze superiori al 75% sono considerati lingotti di Magsimal®-59.

Capitolo 3: l'applicazione

Il sistema di apertura e chiusura della capote rigida (RHT) in 5 parti di una famosa vettura sportiva è stata progettata con l'ausilio di getti pressocolati in lega leggera, al fine di ridurre le masse in gioco e quindi l'inerzia del meccanismo cinematico. La lega designata per la realizzazione dei componenti è Magsimal®-59. In tab. 3.1 si riportano le caratteristiche meccaniche richieste sul nodo portante a telaio (capote carrier), sul nodo per la rotazione del tettuccio (main roof bracket) e sull'apribauetto (side frame) con un'immagine descrittiva. Ciascun componente è presente in una versione destra (RH) ed una sinistra (LH), per la simmetria costruttiva della capote.

Il processo produttivo dei getti è stato strutturato secondo le seguenti fasi:

- ricezione e stoccaggio della materia prima
- fusione e trattamento del bagno
- pressocolata
- tranciatura
- sabbiatura
- lavorazione meccanica
- verniciatura cataforetica (solo per il capote carrier ed il side frame)

- packaging e spedizione al cliente finale



Capote carrier

YTS	> 150 MPa
UTS	> 250 MPa
e%	> 7 %
HB	> 70 HB



Main roof racket

YTS	> 150 MPa
UTS	> 250 MPa
e%	≥ 8 %



Side Frame

YTS	> 150 MPa
UTS	> 250 MPa
e%	≥ 8 %

Tab. 3.1: profilo di requisiti per il capote carrier, main roof bracket e side frame.

La qualità fusoria dei getti è stata monitorata dalla fase di prototipazione fino alla produzione di serie. Il main roof bracket ed il side frame non hanno presentato particolari difficoltà nel raggiungimento dei valori da disegno, mentre il capote carrier ha richiesto una fase di ottimizzazione piuttosto complessa. A livello di fonderia, il sistema forno fusorio/siviera/forno di mantenimento è stato sostituito dal forno fusorio e di trattamento a bordo macchina. La procedura di degasaggio è stata prolungata ed effettuata con Ar anziché N₂; la scorifica potenziata con un sale apposito sviluppato per Magsimal[®]-59. Si è inoltre deciso di utilizzare una pressa dal tonnellaggio maggiore, passando da 1 100 t a 1 600 t, la cui lubrifica è stata garantita da agenti distaccanti calibrati in concentrazione e composizione sulla lega. Numerose modifiche della geometria del carrier capote sono state apportate a fini migliorativi della qualità fusoria del getto. Simulazioni di riempimento, solidificazione e distribuzione della temperatura sono state implementate per velocizzare il processo di messa a punto del componente.

Al termine di questa procedura, le proprietà meccaniche determinate sui pressocolati e riportate in tab. 3.2 hanno soddisfatto le specifiche richieste. Il capote carrier ha superato il test di roll-over previsto dal costruttore e la produzione di serie dei getti è stata avviata.

Capote carrier

(RH)

YTS	150 MPa
UTS	248MPa
e%	8,8 %

(LH)

YTS	179 MPa
UTS	246MPa
e%	8,9 %

Main roof racket

YTS	158 MPa
UTS	240 MPa
e%	10 %

Side Frame

YTS	178 MPa
UTS	283 MPa
e%	8 %

Tab. 3.2: caratteristiche meccaniche sui getti di serie.

Infine, i parametri di processo principali sono stati raccolti in maniera sistematica. Alla luce della loro valutazione e tenendo conto di fattori come fermi macchina e tempo ciclo, tasso di scarto, fenomeni di usura su stampo e su pareti dei forni, lubrificazione dello stampo e del sistema di iniezione, nonché dei costi unitari di servizio della pressa da 1 600 t, si è redatta la tabella 3.3, in cui si paragonano le condizioni di lavoro con una comune lega AlSi9Cu3(Fe) e Magsimal[®]-59.

Il valore percentuale ottenuto è di notevole rilievo: + 150 %, che legittima l'uso di leghe alto-prestazionali solamente laddove lo giustifica un profilo di requisiti altrettanto elevato. D'altra parte si consideri che il fattore "costo" comporta l'adozione di soluzioni nella maggior parte dei casi non propriamente compatibili con le richieste tecniche presentate. L'approccio suggerito è quindi quello di

potenziare l'impiego delle risorse disponibili in fase di ingegnerizzazione, sia di processo che di prodotto, utilizzando, ad esempio, moderni tools CAD/CAE.

	Leghe AlSi secondarie	Magsimal[®]-59	Impatto sui costi
Operatori	1 per 2 isole HPDC	1 per 1 isola HPDC	+ 15 %
Fusione	Forno fusorio Siviera Forno di mantenimento	Forno di fusione e mantenimento a bordo pressa	- 20 %
Perdita di fusione	5%	10%	+ 5%
Costo del metallo	1,71 €/kg ¹ 1,89 €/kg ²	2,48 €/kg ³	+ 45 % + 31 %
Riciclo materozze	100 %	50% - 50 %	+ 10 %
Sali di scorifica	No	Si	+ 3 %
Pressa	1 100 t - 150 €/ora - tempo ciclo: 75 sec - t.t.p. ⁵ : 640 getti/gg. - t.r.p. ⁶ : 600 getti/gg.	1 100 t - 150 €/ora - tempo ciclo: 75 sec - t.t.p. ⁵ : 640 getti/gg. - t.r.p. ⁶ : 260 getti/gg.	
		1 600 t - 170 €/ora - tempo ciclo: 85 sec - t.t.p. ⁵ : 560 getti/gg. - t.r.p. ⁶ : 520 getti/gg.	+ 13 %
Lubrifica sistema di iniezione	No	Si	+ 5 %
Diluizione agente distaccante	1,8-2,2 %	3,3 %	+ 10 %
Fermi macchina	1	1,1	+ 10 %
Scarti	1	1,05	+ 5 %
Usura sistema di iniezione	4 000 colpi	2 000 colpi	+ 20 %
- rame	8 000 colpi	N.A.	
- integrale	35 000 colpi	N.A.	
- pistone con anello			
Usura stampo	20 000 colpi	5 000 colpi	+ 20 % ⁴
Usura pareti forno	1x 6 mesi	1x 5 mesi	+ 10 %
Totale			+ 150 %

Tab. 3.3: riepilogo dei costi di gestione della lega Magsimal[®]-59 e di leghe secondarie tradizionali.

¹ media listino WVM del 2009 per la lega 226 – AlSi9Cu3

² media listino WVM del 2009 per la lega 233 – AlSi10Mg(Cu)

³ media listino Rheinfelden del 2009

⁴ trattamenti di nitrurazione sullo stampo

⁵ tasso teorico di produzione

⁶ tasso reale di produzione

Capitolo 4: Twin-roll casting

Al fine di potenziare ulteriormente le proprietà meccaniche statiche e dinamiche di Magsimal[®]-59, si sono valutati alcuni processi di fonderia innovativi. Alligaggio, trattamento termico o tecnologie come l'AMS e lo stirring elettromagnetico sembrano, infatti, aver esaurito il loro specifico contributo di miglioramento del materiale. Risulta pertanto più interessante concentrarsi su tecnologie in grado di modificare la microstruttura finale durante la colata, ovvero la fase di formatura del getto. In particolare, la tecnologia denominata High-Speed Twin-Roll Casting (HSTRC) è in grado di garantire elevate velocità di solidificazione e quindi sensibili affinamenti della microstruttura.

Si è quindi deciso di procedere con un'attività sperimentale, volta alla valutazione quantitativa delle proprietà a trazione e di deformazione a imbutitura (Erichsen test) di piastre twin-roll, confrontandole con quelle di prodotti di spessore simile, realizzati in pressocolata tradizionale. In tab. 4.1 e 4.2 si riportano i risultati ottenuti rispettivamente da test di trazione e test Erichsen.

Tecnologia	Spessore di parete [mm]	Stato di trattamento	YTS [MPa]	UTS [MPa]	e [%]
HPDC	2	F	230	354	10,3
HPDC	3	F	186	320	10,5
HPDC	2	O	257	358	9,7
HPDC	3	O	203	311	7,4
HSTRC	2,5	F - (A1)	122	221	4,1
HSTRC	2,5	F - (A2)	132	241	5,1
HSTRC	2,5	O - (B1)	138	232	4,6
HSTRC	2,5	O - (B2)	142	246	4,9

Tab. 4.1: test di trazione su piastre twin-roll (HSTRC) e pressocolati (HPDC).
Stato O: 250 °C per 60 minuti

A1: test effettuati nella direzione di laminazione

A2: test effettuati nella direzione perpendicolare a quella di laminazione

B1: test effettuati nella direzione di laminazione

B2: test effettuati nella direzione perpendicolare a quella di laminazione

I miglioramenti attesi a livello di trazione non sono stati confermati dai campioni testati, a causa della presenza di difetti di colata e di una microstruttura non omogenea osservabile sulle piastre realizzate in twin-roll. La messa a punto dei parametri di colata in HSTRC è quindi indispensabile al fine di migliorare la qualità fusoria del prodotto.

Risultati positivi si sono invece ottenuti con il test Erichsen: l'energia assorbita a cricatura E_i e l'energia unitaria di iniziazione della cricca UE_i è circa 1,7 volte superiore al valore rilevato per piastre pressocolate di spessore paragonabile. Inoltre, il test Erichsen si è rivelato poco sensibile alla presenza di difetti interni di colata, profilandosi come alternativa valida alla prova di strappo per la valutazione della tenacità di un metallo.

Tecnologia	Spessore di parete [mm]	Stato di trattamento	E_i [J]	UE_i [Nmm ⁻¹]
HPDC	2	F	15,9	50,6
HPDC	3	F	21,0	66,9
HPDC	2	O	15,3	48,6
HPDC	3	O	19,1	60,7
HSTRC	2,5	F	26,6	84,7
HSTRC	2,5	O	20,1	63,9

Tab. 4.2: energia assorbita a criccatura E_i ed energia unitaria di iniziazione della cricca UE_i su piatti twin-roll (HSTRC) e pressocolati (HPDC).
Stato O: 250 °C per 60 minuti

I dati sperimentali ricavati nel capitolo 4 sono in accordo con quanto determinato in [34].

Capitolo 5: Saldabilità di leghe di alluminio

Le leghe primarie da fonderia sono ampiamente utilizzate in automotive, settore in cui le richieste in termini di duttilità e saldabilità del getto pressocolato si fanno sempre più severe. Per quel che concerne la saldabilità, i processi di giunzione più comunemente utilizzati sono quelli ad arco tradizionali, come TIG e MIG, che hanno lo svantaggio di generare ampie Zone Termicamente Alterate (ZTA) con precipitazioni di fasi fragili.

Di qui l'esigenza di uno studio di saldabilità con processi alternativi come Laser Beam Welding (LBW), Electron Beam Welding (EBW) e Friction Stir Welding (FSW). I processi EBW e LBW sono denominati ad energia concentrata¹ ed hanno il vantaggio di generare cordoni di saldatura di dimensione molto limitata. Il metodo FSW permette la giunzione di cianfrini metallici per mezzo del calore generato dall'attrito di una testa saldante; non si genera una zona fusa, ma il materiale plasticizza e viene meccanicamente rimescolato.

La sperimentazione è stata effettuata su piastre pressocolate in Silafont[®]-36, AlSi9MgMn, ed in Castasil[®]-37, AlSi9Mn, dello spessore di 2 e 4 mm, con la tecnica nota come "beads-on-plate", cioè direttamente sul metallo base. Lo scopo dello studio è verificare la compatibilità di moderne tecniche di giunzione con leghe primarie ad alte prestazioni e di definire in tal caso i migliori parametri di saldatura, al fine di ottenere giunti privi di difettosità. Si sono realizzati giunti LBW ed EBW facendo variare i seguenti parametri:

- portata e tipo di gas protettivo (He o N₂)
- potenza del fascio laser (LBW)
- corrente di filamento (EBW)
- velocità di saldatura
- numero di passate

¹ LBW~ 1MW/cm²; EBW~ 10MW/cm²; traditional arc welding techniques ~ 0,01 MW/cm²

In FSW si é variata soltanto la velocità di rotazione della testa saldante e la velocità di saldatura.

I giunti realizzati sono stati valutati al microscopio ottico; per quelli piú interessanti si sono tracciati profili di microdurezza, partendo dal materiale base fino alla zona fusa, passando dalla ZTA. Tecniche di saldatura che portano a fusione il metallo danno origine a giunti affetti da maggiore micro e macro porositá. In particolare, la tecnologia LBW non si è rivelata in grado di produrre risultati di qualità accettabile; si veda a tal proposito la fig. 5.1, in cui il giunto risulta addirittura deformato meccanicamente a seguito di tensioni introdotte in fase di saldatura.



Fig. 5.1: giunto LBW in Castasil®-37.



Fig. 5.2: giunto EBW in Castasil®-37.



Fig. 5.3: giunto FSW in Castasil®-37.

La tecnica EBW porta a risultati positivi, previa adozione della doppia passata e di un'eventuale passata cosmetica. Velocità di saldatura fino a 90 mm/s non hanno in tal caso inficiato la qualità dei cordoni ottenuti, visibili in fig. 5.2. Entrambe le tecniche ad energia concentrata determinano un incremento di durezza di circa 25-30 punti Vickers in corrispondenza del giunto saldato. Il metodo FSW si è rivelato applicabile entro un ampio intervallo di parametri di saldatura, generando giunti di qualità molto soddisfacente, fig. 5.3. Un calo di durezza di circa 25 HV è stato osservato in prossimità del nugget.

Summary

This doctoral thesis is the result of three years of work and study, carried-out at the Department of Management and Engineering (DTG) in Vicenza - University of Padova, in collaboration with the german company Rheinfelden Alloys GmbH & Co. KG, located in Rheinfelden - Baden and the italian company Microtech Solution s.r.l., located in Flero (BS).

Rheinfelden Alloys GmbH & Co. KG is a manufacturer of primary aluminium foundry alloys, strongly oriented to an active R&D approach. In the past years, the company has developed innovative materials for the automotive sector, with the aim of coupling the lightness of aluminium to improved strength and ductility, as key factors for weight and, in turn, emission reduction of vehicles.

Microtech Solution s.r.l is a consulting company, which designs and develops high-pressure die-castings on customer's requirements. The castings are engineered for the final clientele, starting from the prototypes until the green light for series production. Microtech is mainly active in the automotive field through the outsourced manufacturing, among others, of structural parts for chassis and body.

One of the developments of Rheinfelden Alloys is a HPDC primary alloy called Magsimal[®]-59, chemically corresponding to an AlMg5Si2Mn. The alloy has been specified as raw material to be used for the 5 parts Retractable Hard Top (RHT) of a famous sport car. Microtech Solution has been chosen as project leader for the manufacturing of the castings.

The aim of the doctorate is giving an overview of the supply and production chain of a modern foundry system, integrating different key functions and disciplines. The work has been structured at two levels: the first one involves the supplier of metal; the second one the foundry, supplier of castings. Traditionally, the two areas have been considered independent and detached; in most cases every ring of the supply chain plays its role individually and concentrates its activities downstream, to follow customers' requirements. The suppliers upstream have been considered often just as a supplier of goods, necessary as input to the final product.

On the contrary, a modern foundry system combines the transversal know-how of each single ring of the supply chain. The integrated approach to activities allows the positive exploitation of synergies towards the common target. Thus, the design of a HPDC parts can be suited to the selected casting material, taking into account its peculiarities. An accurate and reliable integrated methodology allows the control of original investments, product costs, time to market and, in particular, can avoid start-up problems.

In order to synchronise the activities of the partners taking part to the project, both manufacturing processes have been described with the same approach.

The first chapter of this work collects data on Magsimal[®]-59, from available literature and past foundry experiences. The key features of the alloy are superior mechanical properties and fatigue resistance in the as-cast state. A complete portrait of the material is given, as well as background information on its basic chemistry and microstructure. Heat-treatment parameters, corrosion resistance, surface treatments,

joining techniques and designed criteria to be adopted with Magsimal[®]-59 are briefly discussed.

Chapter 2 presents the details concerning the lean production system of Rheinfelden Alloys and its implementation on the shop floor. The general process flow diagram for the manufacturing of Magsimal[®]-59 is outlined, underlining the key phases for the achievement of improved mechanical properties. The description of the business model and of the measures adopted for quality assessments clears the impact on the final cost by raw materials in the break-down of the RHT.

The core of this work is presented in the third chapter. The profile of requirements and the application of Magsimal[®]-59 are presented into the details for each part of the RHT car set: capote carrier, main roof bracket and side frame. The focus has been put on the main technical hurdles faced during the manufacturing of the castings. The HPDC process has been described phase-by-phase according to its flow chart. The results obtained during prototyping, sampling, pre-series and series production have been correlated to the improvements introduced on the shop floor. Outcomes have been evaluated both on the castings, and on the process management, setting as benchmark a common AlSi9Cu3(Fe).

The long phase of process optimization has led to the conclusion that, if on one side the use of Magsimal[®]-59 fascinates the final end-user, as highest performances are targeted in the as-cast state, on the other side, the design engineer is required being well-experienced on casting alloys, as the requirements in terms of mechanical properties need to be translated in the correct design of the parts

Finally, a cost break-down of the whole process has been made, on the basis of the additional operations and measures adopted for running a common HPDC-foundry with primary metal. The figure obtained is impressive: + 150 % compared to common secondary alloys, which legitimates the use of high-performing premium alloys just when highest technical requirements are posed. The driving factor “cost” calls for solutions which are in most cases contrasting with the technical requirements set on the parts. However, if insufficient resources are invested in the development of the casting, also taking into account the hardware needed for its manufacturing, significant if not even higher-than-budget costs are falling due.

Chapter 4 presents a study based on an innovative casting process - called High-Speed Twin-Roll Casting (HSTRC) - applied to Magsimal[®]-59. This technology provides ultra high-cooling rates and therefore a significant refinement of the final achieved microstructure. Experimental activities have been carried-out with Magsimal[®]-59, in order to determine if a further improvement of static and dynamic properties is possible and at which extent. A correlation between tensile properties, results of Erichsen tests, microstructure and toughness has been attempted, setting as benchmarks the HPDC process.

The expected improvements of HSTRC technology on the tensile properties of Magsimal[®]-59 have not been observed, due to the lack of an adequate casting quality of twin-rolled strips. In particular, the presence of casting defects and the non-homogeneity to a microstructural level have been considered the main factors for the impairing of mechanical performance. The further optimization of casting parameters has therefore to be implemented.

Nevertheless, positive results have been obtained with the Erichsen test: the absorbed energy until cracking E_i and the unit crack initiation energy UE_i is ca. 1,7 times higher in comparison to HPDC plates of similar wall-thickness. Additionally, Erichsen test has shown its reduced sensitivity to the presence of casting defects and provides therefore a good alternative to tear toughness test for the evaluation of ductility.

Primary HPDC alloys are widely used in automotive, where the requirements and demands in terms of structural and weldable parts are constantly increasing. The most common joining techniques are arc welding processes, such as TIG or MIG. However, in many circumstances the given geometry of castings can be incompatible with the adopted welding technique and the use of traditional welding torches difficult. Hence, the need for alternative joining processes such as Laser Beam Welding (LBW), Electron Beam Welding (EBW) and Friction Stir Welding (FSW). Chapter 5 presents a study on these welding technologies applied to AlSi primary alloys according to the approach “beads-on-plate”, i.e. directly on base material. The aim of the study is the understanding of compatibility of modern joining processes with premium casting alloys and the definition of the correct welding parameters for the obtainment of sound weld seams.

The main issues of standard arc welding techniques have been briefly discussed. The experimental procedures adopted for LBW, EBW and FSW have produced welding seams, qualitatively evaluated with the light microscopy and through microhardness profiles.

Results and conclusions have been finally drawn. Welding processes, which cause the melting of the chamfers, result in seams with gaseous porosities. High-energy processes have shown conflicting results. The experimentation with LBW has proven to be unsuccessful, as fault-free welding seams could not be produced. The technology EBW has shown acceptable results with the adoption of a double run. Welding speeds of 90 mm/s could be reached with satisfactory seam quality. The increase on the microhardness of the melt zone is around 25-30 HV.

FSW technology has shown a higher degree of liberty in the tuning of welding parameters and welding seams of satisfactory quality have been produced. A decrease of microhardness of around 25 HV has been observed in the nuggets.

Table of contents

Preface	I
Sintesi in italiano	III
Summary	XVII
1. Magsimal[®]-59	1
1.1 Introduction	2
1.2 Chemical composition	2
1.3 Thermal analysis and resulting microstructure	5
1.4 Static mechanical properties	7
1.5 Dynamic mechanical properties	12
1.6 Corrosion resistance	14
1.7 Joining technology	16
1.7.1 Welding	16
1.7.2 Self-pierce riveting	18
1.8 Surface treatments	19
1.9 Designing with Magsimal [®] -59	19
1.10 Tool life	20
2. Manufacturing of Magsimal[®]-59	21
2.1 Introduction	22
2.2 Rheinfelden Alloys GmbH & Co. KG	22
2.3 The “Back-to-Back” Philosophy and the Lean Production Model	23
2.4 Process Flow Diagram	26
2.4.1 Good receipt and raw materials	26
2.4.2 Melting preparation	27
2.4.3 Melting and alloying	29
2.4.4 Melting treatment	29

Table of contents

2.4.5 Casting of ingots	30
2.4.6 Stacking and marking	30
2.4.7 Final control and product approval	31
2.4.8 Dispatch and shipping to customer	32
2.5 Fracture surface, microstructure and ductility	33
2.6 FMEA Analysis	38
Appendix A	39
3. Manufacturing of Magsimal[®]-59	43
3.1 Introduction	44
3.2 The application	44
3.3 The manufacturing process	51
3.3.1 Advanced Product Quality Planning (APQP)	51
3.3.2 General Activity Planning (GAP)	52
3.3.3 Process Flow Chart	53
3.3.3.1 Melting, high-pressure die-casting and press control	53
3.3.3.2 Shearing	57
3.3.3.3 Sand blasting	58
3.3.3.4 Machining	59
3.3.3.5 Cataphoretic painting	61
3.3.3.6 Packaging	62
3.4 Evaluation of the castings	63
3.4.1 Capote carrier bracket	63
3.4.1.1 Prototyping	63
3.4.1.2 First sampling	64

3.4.1.3 Second sampling	71
3.4.1.4 Third sampling – pre-series parts	76
3.4.1.5 Series manufacturing die	79
3.4.1.6 Protection from cataphoretical painting and machining	82
3.4.2 Roof main bracket	83
3.4.2.1 First sampling	83
3.4.2.2 Second sampling	85
3.4.2.3 Third sampling	86
3.4.2.4 Series manufacturing die	87
3.4.3 Side frame	89
3.4.3.1 Preliminary modifications	89
3.4.3.2 First sampling	91
3.4.3.3 Second sampling	93
3.4.3.4 Series manufacturing die	94
3.4.3.5 Shearing die	95
3.4.3.6 Protection from cataphoretical painting and machining	98
3.4.4 Series production of the car set	99
3.5 Outcomes	100
3.5.1 Shop floor and melting	100
3.5.2 Down-times and cycle-times	100
3.5.3 Scrap rate, shrinkages and porosities	101
3.5.4 Die-lubrication	105
3.5.5 Die-wear	106
3.5.6 Shot-sleeve lubrication and wear	107

Table of contents

3.5.7 Dimensional stability	107
3.6 Cost impact	107
3.7 Conclusions	110
4. Twin-roll casting	115
4.1 Introduction	116
4.2 Twin-roll casting	120
4.2.1 Conventional Twin-Roll Caster for Aluminium alloys (CTRCA)	121
4.2.2 High-speed Twin-roll Caster for Aluminium Alloys (HSTRC)	121
4.3 High-speed twin-roll casting and toughness	124
4.4 Tear toughness of Magsimal [®] -59	126
4.5 Tear toughness and Erichsen test	127
4.6 Experimental procedure	128
4.6.1 HPDC plates	128
4.6.2 Twin-rolled plates	128
4.6.3 Design of experiments	129
4.7 Results and discussion	131
4.7.1 Surface appearance and X-rays	131
4.7.2 Tensile tests	135
4.7.3 Erichsen test	139
4.7.3.1 Real-time Erichsen test	142
4.7.3.2 Absorbed energy and unit initiation crack energy	145
4.7.4 Microstructural evaluation	151
4.7.4.1 Fracture surfaces	151
4.7.4.2 Light microscopy on tensile specimens	152

4.7.4.3 Light microscopy on Erichsen plate	157
4.7.5 Microhardness	160
4.8 Conclusions	161
4.9 Applications and outlooks	162
5. Weldability of primary aluminium HPDC alloys	163
5.1 Introduction	164
5.2 Traditional welding techniques and aluminium alloys	165
5.3 Materials and samples	167
5.4 Design of experiments	167
5.4.1 Laser Beam Welding	168
5.4.1.1 Results of LBW test procedure	170
5.4.2 Electron Beam Welding	172
5.4.2.1 Results of EBW test procedure	174
5.4.3 Friction Stir Welding	177
5.4.3.1 Results of FSW test procedure	180
5.5 Conclusions	183
Acknowledgements	185
References	187

Chapter 1
Magsimal[®]-59

1.1 Introduction

Magsimal[®]-59 is the registered trademark used by Rheinfelden Alloys GmbH & Co. KG to define its primary aluminium casting alloy, chemically corresponding to an AlMg5Si2Mn. This alloy was developed and patented by Aluminium Rheinfelden in 1995 and was logically and historically following the concept of Silafont[®]-36, AlSi9MgMn, the very first low-iron high pressure die-casting alloy for aluminium die-castings. At those times, an AlMgSi-alloy for HPDC was unusual; so far this alloy system had been used almost only for permanent mould casting and mainly for sea-water applications.

The main reasons leading to the design of this new material were the requirements set by the automotive sector, booming in the 80ies and the 90ies, especially in Germany, and the desire of combining the superior mechanical properties of the AlMg-system with its application in HPDC purely in the as-cast state.

Safety parts in automotive body construction, such as suspension parts, steering wheels, cast nodes and crossbeams were demanded in order to reduce the car weight, while maintaining the required mechanical properties. The culminating result was the launch on the market of the A8, the first aluminium-intensive car by Audi. The space-frame of the Audi A8 had 35 HPDC-nodes in Silafont[®]-36, which were cast with a Müller-Weingarten Vacural System [1]. In order to achieve the required static mechanical properties (YTS >130 MPa; UTS > 210 MPa and $\epsilon > 15,0\%$) the castings needed to be heat-treated. Solutionizing was not an option; the risk of distortion during quenching was in turn the main side effect.

The need of an alloy with superior mechanical properties in the as-cast state within common HPDC wall thicknesses of 2-6 mm was therefore clear. Magsimal[®]-59 was developed in this context [2]. This AlMg5Si2Mn alloy is becoming more and more important, as high yield strength in conjunction with high elongation and ductility is coupled with excellent energy absorption capacity. Fatigue strength is also sensibly higher than for conventional HPDC-alloys.

The scope of this chapter is giving a complete portrait of the alloy in its main features. Basic chemistry, microstructure, mechanical properties and further background technical information are reported in the following paragraphs.

1.2 Chemical composition

Magsimal[®]-59 is an AlMg5Si2Mn HPDC alloy. The nominal chemical composition is reported in tab. 1.1. The main alloying elements are magnesium, silicon and manganese. Magnesium goes into solution and results in high yield strength by forming coherent and semi-coherent phases in the α -aluminium phase. The ratio magnesium/silicon is very important to get the desired share of 35-45 % eutectic. This favours in turn sufficient castability and feeding during solidification. No free silicon must be available, in order to grant the outstanding corrosion behaviour [19]. Excess magnesium forms Mg₂Si compounds – to be seen in the typical ternary eutectic microstructure. Manganese prevents sticking to the die and lowers the solubility of iron into the aluminium, thus substituting the function of iron itself [6] [7].

Previous experiences on low-iron high-pressure die-casting alloys have shown that an optimal content of 0,5-0,8 % Mn must be present in order to guarantee a good ejection behaviour of the casting from the die cavity [3][4]. Manganese is responsible for forming Al₆Mn intermetallics, whose morphology is of irregular polygons. Iron content is kept below 0,2 % to minimize the formation of the needle-like β-AlFeSi phases, whose morphology would initiate cracks in the casting under load, deteriorating tensile strength, elongation and fatigue strength.

Titanium is normally used for grain-refining purposes. Metallographic studies have shown, however, that a grain-refinement with titanium/boron has a deteriorating effect on the fine morphology of the ternary eutectic of Magsimal[®]-59. For this reason, no TiB₂ particles should be added. Magsimal[®]-59 has a special long-term grain refinement performed during manufacturing and targeting the AlMg₂Si-eutectic. Ca. 240-250 ppm of vanadium and zirconium are additionally alloyed, in order to further grain-refine the structure and to improve the tensile properties.

AlMg-melts with Mg contents over 2 % have a tendency towards an increased dross formation, especially if the melt is kept for a long time in holding furnaces at elevated temperatures [5]. Beryllium has the capability of increasing the density of the superficial oxide skin, forming a BeO film on its surface [13]. Alloying 30-40 ppm Be¹ during manufacturing allows to improve the resistance to oxidation of Magsimal[®]-59 melts, as less aluminium and magnesium diffuse to the external surface.

[%]	Si	Fe	Cu	Mn	Mg	Zn	Ti	Be	others total
min.	1,8			0,8	5,0				
max.	2,8	0,2	0,05	0,8	6,0	0,07	0,20	0,004	0,2

Tab. 1.1: the chemical composition of Magsimal[®]-59 by Rheinfelden.

The alloy is produced on the basis of 99,8 % pure aluminium. The control of impurities and minor elements is therefore guaranteed. Copper and zinc are kept under the maximum levels respectively of 0,05 % and 0,07 %. This complies with the automotive standards and provides for an outstanding corrosion resistance. Calcium and sodium are limited to max 15 ppm, as they enhance hot-tearing tendency of the castings and lead to poor fluid flow.

Contamination by phosphor must be absolutely avoided, as its influence on the eutectic fineness is deleterious already in the range of 10-15 ppm. According to internal researches, also the presence of few part per million As, Ba, Te, Hg, Be, K have the same negative effect.

The highest fineness of ternary eutectic is the special feature of Magsimal[®]-59 and can be achieved by a special manufacturing process, which transforms the Mg₂Si eutectic from its normal coarse brittle plate-like structure into a more ductile fine fibrous structure. Micrographs shown in figure 1.1 clearly depict the difference between Magsimal[®]-59 and a common HPDC AlMg₅Si₂Mn alloy.

¹ The Be-content between 30 and 40 ppm is not harmful to health. Safety precautions have to be taken just when castings in Magsimal[®]-59 are welded, in order to avoid gas inhalation.

SEM pictures have been additionally reported in fig. 1.2 in order to show three-dimensionally the induced modification. A clearly superior behaviour of Magsimal[®]-59 can be observed in terms of mechanical properties, especially elongation, see par. 1.4.

The research work reported in chapter 4 has the main aim to investigate if the fineness of the eutectic phase of Magsimal[®]-59 can be achieved just by this special manufacturing process or if any other parameters, such as solidification rate, can play a role in modifying the growth mechanism of Mg₂Si particles.

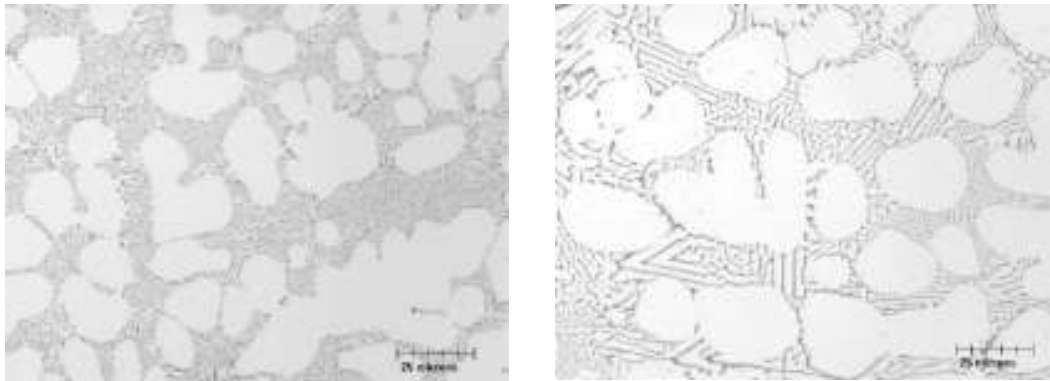


Fig. 1.1: the microstructure of Magsimal[®]-59 (left) compared to a common AlMg5Si2Mn alloy (right). The different morphology of eutectic is the key feature for superior elongation and fatigue strength.

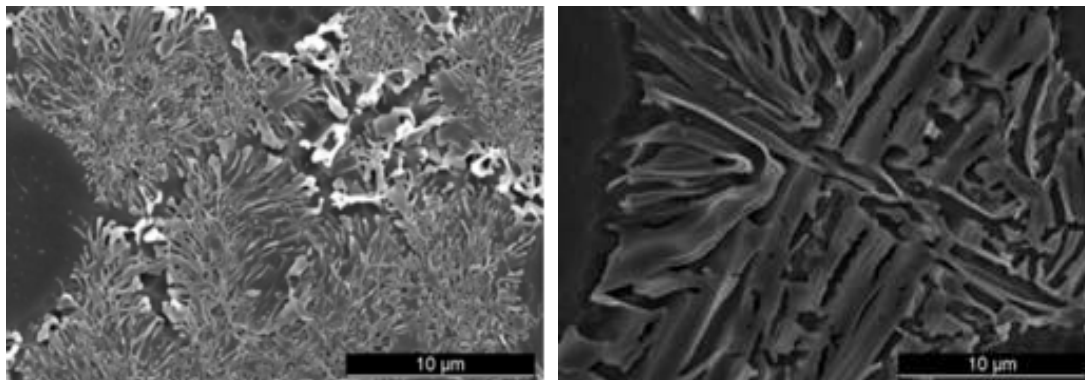


Fig. 1.2: SEM pictures of the Mg₂Si eutectic phase of Magsimal[®]-59 (left) and of a common AlMg5Si2Mn (right). Finer eutectic means higher deformation capabilities, higher resilience and therefore higher energy absorption. See par. 1.4.

It can be easily deduced that the special chemistry of Magsimal[®]-59 needs to be managed in the proper way. This must be in turn translated into a precise foundry practice [24]. Dedicated crucibles should be used, avoiding contaminations by impurities. Quarz-free refractories with high alumina (Al₂O₃) content are preferred. The melting of the ingots should be rapid to avoid gas pick-up, magnesium oxidation and melt oxidation, possibly in a gas fired furnaces. Convection helps in fact the homogeneous mixing into the melt.

Temperature after melting should not exceed 780°C and should not be sunk under 650°C during holding, to avoid segregations by manganese. No degassing tablets, modification or grain-refining additives should be used. The expected loss of magnesium is normally between 0,10 % and 0,15 %, depending on melting conditions. Internal experiments showed that a rectification of the Mg-content should be avoided: adding pure magnesium can be done up to 0,5 %. Beyond this value, the microstructure will be inevitably coarsened.

For the same reason, the maximum scraps and returns should not exceed 50 %. A 30 % recycling ratio is the recommended value for series production. Only ingots should be used, if highest elongation values and fatigue strength are the key-points on the final casting. The aluminium share in the dross can be reduced by using appropriate salts developed for Magsimal[®]-59. Covering the melt delivers drier dross than mixing the salts into the melt. Nitrogen and/or argon rotor degassing is considered a common practice in a modern foundry. This operation should be intensified when scraps and returns are remelted.

1.3 Thermal analysis and resulting microstructure

The thermal analysis of Magsimal[®]-59 shows a liquidus temperature of about 618°C and a solidus temperature of 580°C. A pronounced holding point, resulting as a plateau of the cooling curve, defines the eutectic temperature at 592°C (fig. 1.4), which is 25°C than common AlSi-alloys. Comparative cooling curves of Magsimal[®]-59 and a common AlSi9Cu3(Fe) are reported in fig. 1.5. High cooling rates, typical of HPDC, are the basis for the formation of uniform and fine α -dendrites surrounded by the AlMg₂Si- eutectic and the AlMn₆-intermetallics, see fig. 1.3.

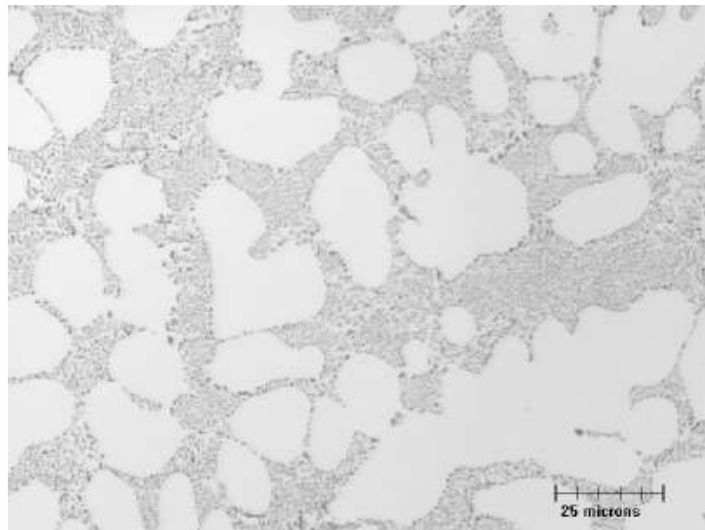


Fig. 1.3: the ternary eutectic microstructure of Magsimal[®]-59.

This very fine ternary eutectic is the special feature of Magsimal[®]-59 and results in high mechanical properties and ductility in the as-cast state.

A visual evaluation of this can be simply done by observing the fracture surface of an ingot of Magsimal[®]-59: it looks white. In fact, the finer the eutectic, the brighter the fracture surface, the higher the elongation values. As soon as the eutectic gets coarser, the fracture surface will get a blue nuance, corresponding to an increase in the tensile strength and to a dramatic drop of elongation values, see 2.5.

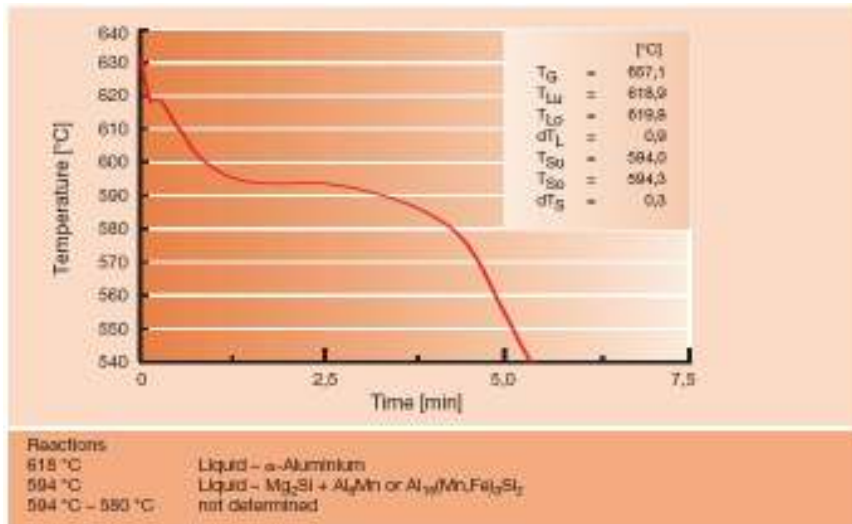


Fig. 1.4: thermal analysis of Magsimal[®]-59, AlMg5Si2Mn. (Quick-Cup-Crucible).

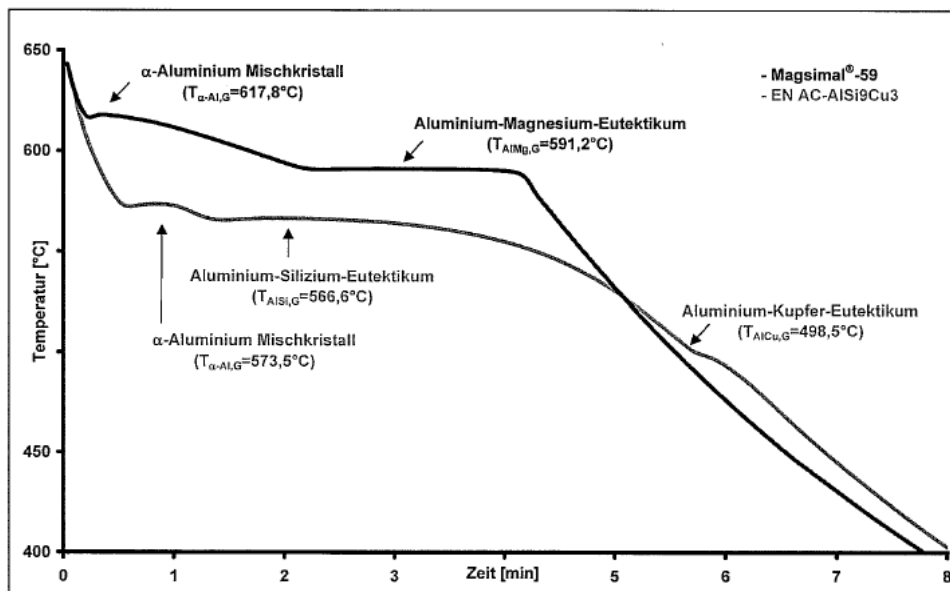


Fig. 1.5: thermal analysis of Magsimal[®]-59, AlMg5Si2Mn, compared to a common AlSi9Cu3(Fe).

1.4 Static mechanical properties

Generally speaking, mechanical properties of HPDC alloys depend on the secondary dendrite arm spacing (SDAS). The lower the solidification rate, the longer the dendrite arm distances, and the poorer the deformation behaviour [16]. However, the mechanical properties of AlMg-HPDC alloys, such as Magsimal[®]-59, show a more pronounced decay by increasing wall thicknesses in comparison to AlSi-HPDC alloys.

Fig. 1.6 shows the relationships between the wall thickness of a Magsimal[®]-59 casting, local solidification time, measured SDAS and outgoing mechanical properties. Elongation falls from 18 % to less than 4 %, YTS from 185 MPa to 106 MPa and UTS from 310 MPa to 220 MPa, when increasing wall thickness from 3 to 18 mm. This is a boundary condition and a guideline, which the experienced engineer has to take into account, e.g. by designing a limit of 6 mm on wall thickness, whereas interesting technological properties of Magsimal[®]-59 in temper F can be exploited.

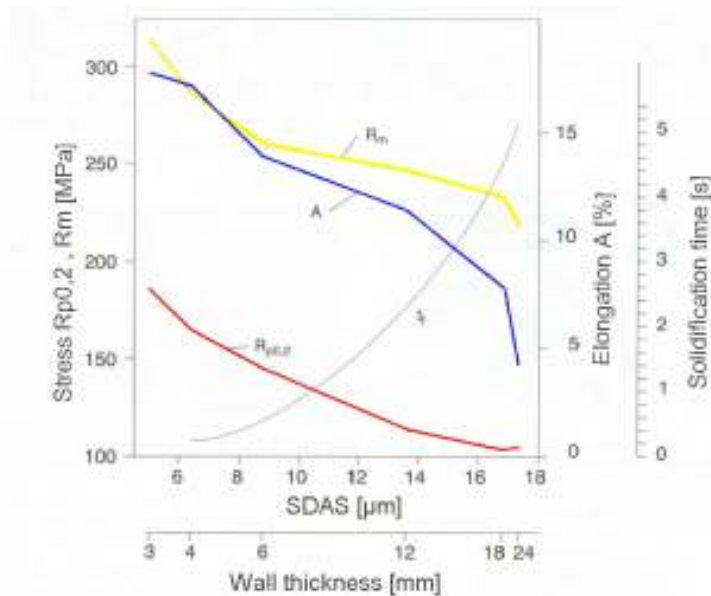


Fig. 1.6: dependence of mechanical properties of Magsimal[®]-59 on local solidification time, SDAS and wall-thickness.

The “value-added” of Magsimal[®]-59 can be considered the delivery of superior mechanical properties in the as-cast state, i.e. after casting without any further heat treatment, see tab. 1.2. The reported mechanical properties have been evaluated on cast-apart test samples, as the values can be dispersed within the casting, being generally better in proximity of the gate and worse in the gate-opposite area, far from ingates and in correspondence of overflows.

Wall thickness [mm]	$R_{p0,2}$ [MPa]	R_m [MPa]	A [%]
< 2	> 220	> 300	10 – 15
2 – 4	160 – 220	310 – 340	12 – 18
4 – 6	140 – 170	250 – 320	9 – 14
6 – 12	120 – 145	220 – 260	8 – 12

Tab. 1.2: mechanical properties of Magsimal[®]-59 in the as-cast state.

Some sources report that an ageing process at room temperature occurs within the first 30 days after casting, which causes an increase of the yield strength (ca. + 25 %) and a slight decrease of the elongation (ca. -11 %) [15].

As already mentioned in par. 1.2, the special mechanical properties of Magsimal[®]-59 can be achieved thanks to a special refining treatment during its manufacturing process by which a change of the Mg₂Si eutectic is induced. If this modification is partially induced or neglected, an impact on the tensile outcomings can be clearly observed. Tab. 1.3 summarizes the tensile values of different AlMg5Si2Mn alloys, chemically identical to Magsimal[®]-59, but manufactured with a limited or even without this special treatment, whose “efficacy” has been quantified between 0 % and 100 %. Benchmark is Magsimal[®]-59 with a reference treatment efficiency of 100 %.

	YTS [MPa]	UTS [MPa]	e [%]	Treatment [%]
Magsimal [®] -59 AlMg5Si2Mn	178	313	20,6	100
AlMg5Si2Mn Variant 1	187	328	13,4	75
AlMg5Si2Mn Variant 2	183	319	8,4	25
AlMg5Si2Mn Variant 3	186	321	7,7	0

Tab. 1.3: tensile tests results with Magsimal[®]-59 and common AlMg5Si2Mn HPDC alloys.

YTS and UTS are not influenced by the refining treatment to a high extent; elongation on the other side is strongly influenced.

These results are strictly connected to the microstructural change induced in the growth of the Mg₂Si phase. Strength impact results reported in par. 1.5 confirm the increased ductility of Magsimal[®]-59. A correlation between efficacy of treatment and microstructural induced changes is presented in par. 2.5.

A curious and typical feature of AlMg-alloys is the so-called “strain-induced ageing” of the material, when undergoing to tensile testing. This phenomenon occurs in the plastic area of the stress-strain curve and can be seen by a lot of small irregularly distributed peaks. From an atomic point of view, this is an interaction between solid solution atoms and migratory dislocations in the microstructure, which causes a momentary low stress reduction in the tensile curve itself, see fig. 1.7. The phenomenon is also called “Portevin - Le Chatelier effect” [9].

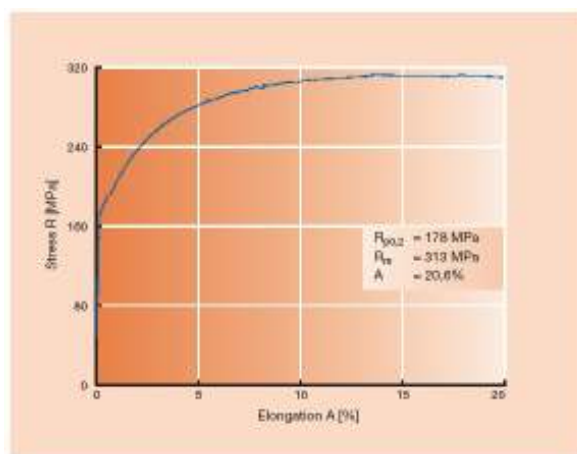


Fig. 1.7: stress-strain curve for Ma-59, in the as-cast state for a 3 mm-wall thick sample.

Full heat-treatments are normally not carried-out with Magsimal[®]-59 for two main reasons:

- 1.) the as-cast properties of the alloy are targeting and approaching the performance of common AlSi-alloys in T6 state
- 2.) full heat-treatments do not show brilliant improvements of the mechanical properties in AlMgSi systems [10][17]

Additionally, all cons connected to full heat-treatments of high-pressure die-castings are avoided. However, heat-treating Magsimal[®]-59 is possible, according to the following modalities:

- T5 to increase the yield strength
- O to increase of the elongation

T5 consists in quenching the castings in water directly after their removal from the die and subsequently artificially-age to a well-defined temperature and time.

The yield strength can be increased by a T5-treatment, when the required value, often in association with defined hardness Brinell, can not be reached in temper F. Figure 1.8 and 1.9 show how YTS and e% are influenced by a T5 heat-treatment, depending on the wall thickness of the castings.

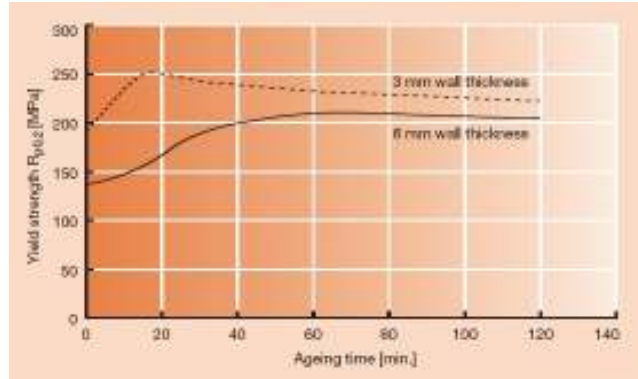


Fig. 1.8: YTS as a function of ageing time. Ageing temperature: 250°C.

It is of a vital importance to quench the castings immediately after removal from the die, in order to “freeze” the soluted magnesium into the matrix and to allow the subsequent hardening. Internal trials have shown that air cooling is not effective and does not result in the desired mechanical properties after ageing. Further heat-treatment optimization trials have shown that the T5 parameters to get the best compromise between UTS and e % are 250°C for 60 minutes: UTS increases to 200-210 MPa and elongation maintained around 8-10 %.

Stable outcomes by age-hardening can be generally observed after ca. 60 minutes treatment. 200-250 MPa can be targeted on 3mm-thick castings. Yield strength over 200 MPa can be obtained also on thicknesses of 6 mm. Elongation suffers of a T5 treatment and the values sink to average 10 % and 4 % respectively for 3 and 6 mm wall thickness, after 60 minutes ageing time.

Summarizing, a T5-heat-treatment can influence the yield strength with an increase up to 30 %, while reducing elongation up to 30 %.

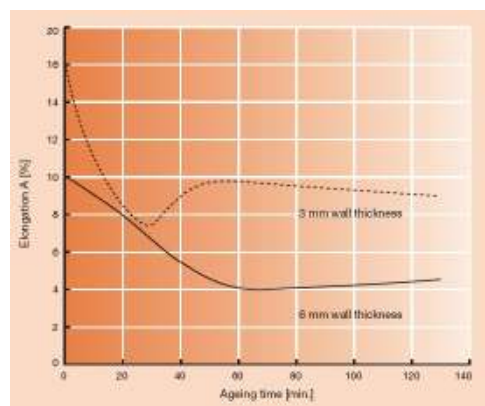


Fig. 1.9: e% as a function of ageing time. Ageing temperature: 250°C.

The so-called “O”- treatment consists in a simple annealing at low temperature, commonly set between 320°C and 380°C. Typical annealing times are 30 to 180 minutes. Actually two main kinds of O tempers can be defined:

- O (I) with annealing at lower temperature, i.e. ca. 320°C
- O (II) with annealing at lower temperature, i.e. ca. 380°C

As annealing at low temperatures does not have a strong impact on the mechanical properties of Magsimal[®]-59 such as a T5-treatment, O temper is normally intended as O(II). Figure 1.10 and 1.11 show how annealing influences the yield strength and the elongation of the alloy. Several annealing temperatures have been investigated. Higher ductility can be however thought just by means of annealing temperatures higher than 350°C for 60 minutes treating time.

Summarizing, an O heat-treatment can influence the yield strength with a decrease up to 30 %, while increasing elongation up to 30 %.

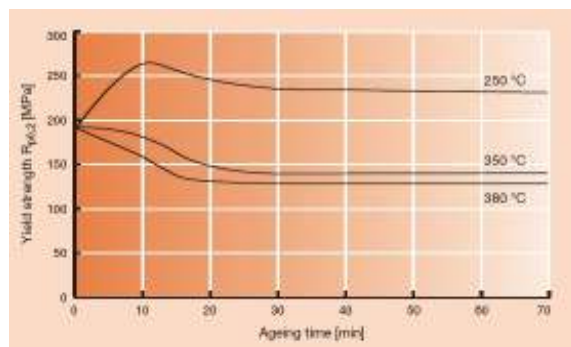


Fig. 1.10: YTS as a function of ageing time. Wall-thickness: 3mm.

The choice of the correct treatment to be performed occurs after evaluation of the profile of requirements set by the designers. The definition of the correct treatment parameters takes place as fine tuning, ad hoc on the casting geometry.

Stabilizing castings, which are working under thermal stress is recommended. This can be done simply by heating up the castings slightly over the working temperature for 2 to 3 hours.

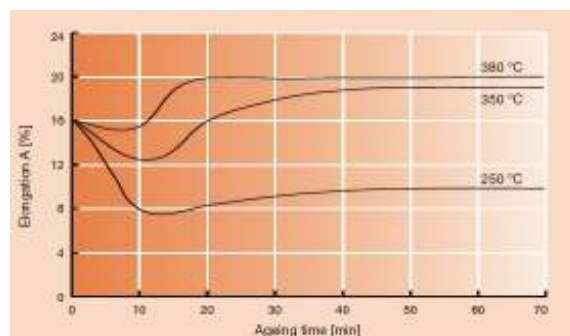


Fig. 1.11: e% as a function of ageing time. Wall-thickness: 3 mm.

1.5 Dynamic mechanical properties

The properties of a material under dynamic load or undergoing to multi-axial stresses are a fundamental criterion for the design engineer. In fact, they reflect the behaviour of castings during their operating life with more precision.

Fatigue performances are a direct function of the chemistry and solidification rates of the metal. Surface conditions, heat-treated state and metallurgical defects of test specimens influence however the fatigue strength to a huge extent. Therefore, the reliability of test results can be transferred to the real operative conditions just to a limited extent and the testing of a real casting is strongly recommended [20].

Measurements carried-out with a high-frequency pulse generator (approx. 110 Hz) and a 200 kN load give as results the Wöhler's curves traced in fig. 1.12 for 5, 50 and 95 % fracture probability. If the 5 % fracture probability curve and the value of 10^6 cycles are considered, as common practice, Magsimal[®]-59 shows fatigue strength of 100 MPa in the as-cast state.

This value is significantly higher than the AlSi-alloys one. Under the same loading conditions an AlSi7Mg0,3 (A356) sample, cast in permanent mould and heat-treated to the T6 state show a fatigue limit of 93 MPa. All standardized² HPDC-alloys show fatigue limits of 60-90 MPa [10]. Silafont[®]-36, AlSi9MgMn, in temper F has fatigue strength of 89 MPa [25]; Castasil[®]-37 in temper F has fatigue strength of 86 MPa [22].

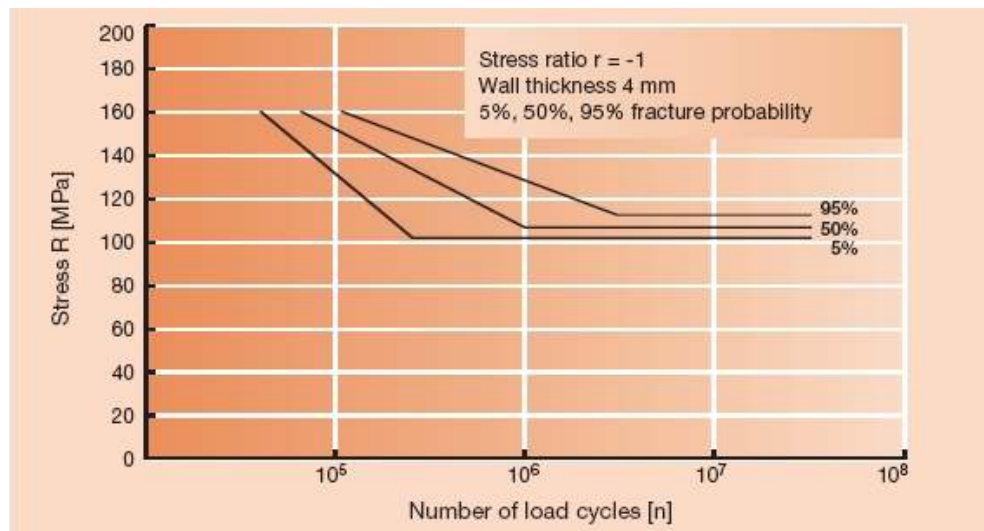


Fig. 1.12: Wöhler's curve for Magsimal[®]-59.

Tensile tests under dynamic conditions³ showed that the yield strength increases of 16,5 % and therefore to a slighter extent compared to AlSi-alloys. UTS and E improve respectively of 5,1 % and 23,0 % compared to static tensile tests. Tab. 1.4 compares average static to dynamic tensile test results for Magsimal[®]-59.

² EN 1706 : 1998

³ i.e. traction speed = 6 m/s which equals to strain rates around 300 s^{-1}

The behaviour of a real casting in terms of energy absorption is therefore supposed being better if stressed in a dynamic way, e.g. in case of crash, than in static conditions.

	YTS [MPa]	UTS [MPa]	e [%]
Magsimal [®] -59 Static	170	316	17,4
Magsimal [®] -59 Dynamic	198	332	21,4
Variation	+ 16,5 %	+ 5,1 %	+ 23,0 %

Tab. 1.4: static versus dynamic tensile tests of Magsimal[®]-59.

A stress-strain curve of a low and high speed tensile test for Magsimal[®]-59 are reported and superimposed in fig. 1.13.

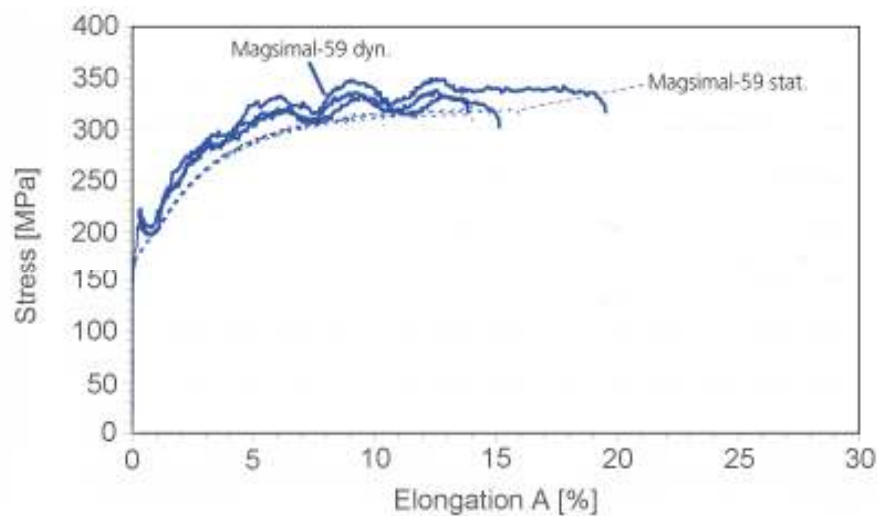


Fig. 1.13: high-speed tensile test for Magsimal[®]-59.

U-notches strength impact samples have been tested for Magsimal[®]-59 and for common AlMg5Si2Mn alloys. The samples have dimensions of 10 x 10 x 60 mm with a 2,5 mm U-notch, according DIN EN 10 045-01.

The results are reported in tab. 1.5 and show the huge gap in energy absorption within alloys with the same nominal chemical composition, but different microstructures.

	Impact strength [KJ/m ²]	Treatment [%]
Magsimal [®] -59 AlMg5Si2Mn	156	100
AlMg5Si2Mn Variant 1	146	75
AlMg5Si2Mn Variant 2	38	25
AlMg5Si2Mn Variant 3	33	0

Tab. 1.5: strength impact tests results with Magsimal[®]-59 versus common AlMg5Si2Mn HPDC alloys.

1.6 Corrosion resistance

Generally speaking, AlMg-alloys are the best choice in terms of corrosion behaviour and this explains why they were adopted first in sea-water applications. Classifying casting alloys according their corrosion resistance and castability results into the diagram of fig. 1.14, where Magsimal[®]-59 appears as the best compromise.

Salt spray corrosion tests with a 5 % NaCl solution for 48 hours at 35°C according MIL-STD-810E have shown that Magsimal[®]-59 is clearly superior to HPDC-AlSi-alloys: no local pit corrosion has been detected.

The adoption of AlMg-systems for safety components does immediately pose the question of tendency towards stress-cracking-corrosion. In fact, pure AlMg-alloys with Mg-contents over 3 % suffer from SCC and intercrystalline corrosion. This is due to Mg₂Al₃-phases, which are precipitating at the grain boundaries, if the temperature increases up to 60-150°C. These phases are not precipitated by Magsimal[®]-59. SCC trials have been conducted according ASTM G 47-90: 4 mm-thick test samples in Magsimal[®]-59 have been tested with as-cast and machined surface (0,3 mm from each side). A 75 %-UTS load has been introduced to the samples using isolated steel pliers. The samples have been dipped into a 35 g NaCl/l salt solution for 10 minutes, than dried in air for 50 minutes. The procedure has been continued for 30 days. After the test cycles were finished, the tensometer has shown no relaxation or drop of load for each sample, confirming no tendency to SCC.

		Castability			
		average	good	very good	excellent
Corrosion resistance	with surface protection	Al-47/-48 Al-52/-60	Si-70		
	from weathering	Ca-30/-50		Si-30 Uf-90 Uf-04 Cl-37	Si-13 Si-20 Si-09 Si-36
	from salt water	Ac-04 Pe-30/-36 Pe-50/-56	Ac-50 Ac-70/78dv Ac-71 Ac-72	Ma-59	

Fig. 1.14 : castability and corrosion resistance of various aluminium casting alloys.

Coupling corrosive atmosphere with dynamic loads means putting a material into severest operating conditions and taking it to its limits. This is however a typical example of automotive applications, such as crossbeams, engine cradles or integral mountings.

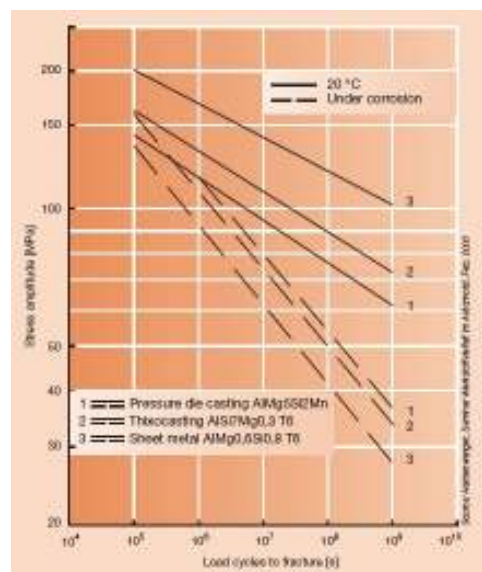


Fig. 1.15: fatigue properties of different alloys in corrosive context.
Curve 1 depicts the behaviour of Magsimal[®]-59.

Fig. 1.15 shows how pressure die-castings in Magsimal[®]-59 can compete with thixo-castings in common AlSi7Mg0,3 T6 and with fully heat-treated sheet metals of 6 000 series.

This can be explained by the chemistry and in turn by the uniform microstructure of Magsimal[®]-59, which does not present any precipitates at the grain boundaries, where corrosion can easily initiate. The corrosion resistance of Magsimal[®]-59 can be further boosted by means of polishing, artificial thickening of the oxide layer, cataphoretic painting and coating.

1.7 Joining technology

Several joining technologies have been successfully applied with Magsimal[®]-59. The most common ones are welding techniques, but self-pierce riveting, glueing, screwing and flanging have delivered promising positive results.

1.7.1 Welding

Aluminium alloys are generally weldable, but when ranking HPDC materials according to their suitability to be welded, AlSi-alloys are taking the leading position compared to AlMg-Alloys [14][21][23]. This is due to the fact that AlMg alloys have higher shrinkage rates and therefore shrinkage forces during solidification. However, the presence of manganese in Magsimal[®]-59 enhances the resistance to hot cracking during solidification of the HAZ.

Weldability can be confirmed when a material can be joined by a given welding technique and in line with a suitable production process, see fig. 1.16, and should always be evaluated taking into account its three main aspects: welding suitability, capability and reliability. Welding suitability is the capability of welding a certain material without considerably impairing its properties; welding capability can be assessed when the welds can be performed under the selected manufacturing conditions. Finally, welding reliability is the capability of the welded joints to bear all operation-inherent loads without any function-impairing damage [8].

When dealing with castings to be welded, the HPDC process calls for special considerations both during the casting design and casting operations, in order to meet simultaneously economic and qualitative requirements.

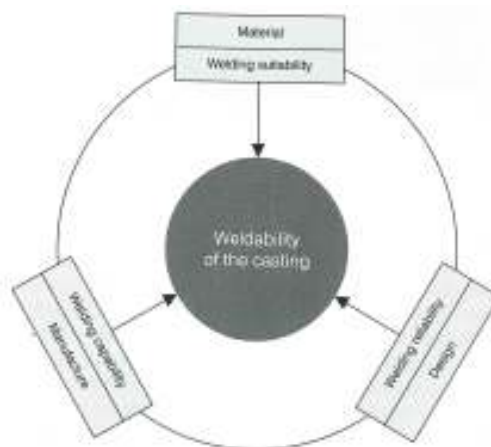


Fig. 1.16 : weldability of components.

The chemistry of a casting alloy is for sure important to determine the final result of a welding, but it is worth underlining how the ability to be welded of a casting depends to a large extent on the melting treatment and on the HPDC process, tuned in its three main leverages:

- air inclusion control
- injection of metal
- lubrication

The evaluation of a welded part should be always related to a preset level of quality, chosen as applicative goal [11]. According to this, the adequateness of the casting process needs to be tuned in its elementary and necessary progresses, as depicted in fig. 1.17.

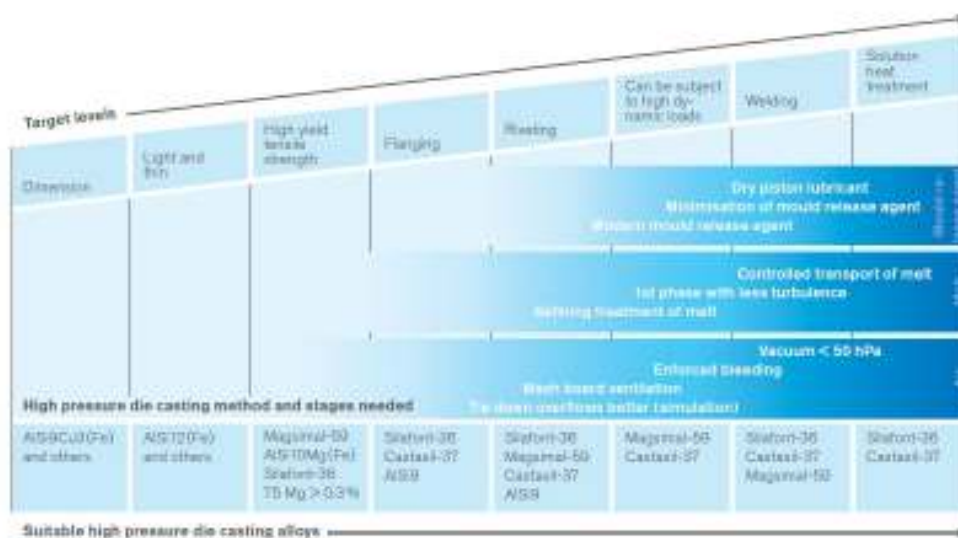


Fig. 1.17: the eight quality steps leading to premium quality weldable diecastings.

Dimensional stability for high-performing light and thin parts is nowadays a standard for AlSi9Cu(Fe) or AlSi12(Fe) alloys. If flanging is required, a change to a primary alloy is necessary. Self-piercing capabilities means the adoption of high ductile HPDC casting alloys, like Magsimal®-59, Silafont®-36 or Castasil®-37.

Dynamically stressed and fatigue loaded parts require additional precautions on the process itself, with the use of vacuum systems, intensive cleaning and careful handling of the metal, as well as CAD Tools to optimize the filling of the part.

A key-factor to obtain sound welding seams is the use of die-lubricants recently developed for AlMg-alloys, which reduce to a minimum their application on the die and therefore their residual presence into the castings. Finally, weldable structural parts and fully heat-treatable castings do require additional care during lubrication.

Nevertheless, TIG structural welding with Magsimal®-59 can be carried out by using as filler metal an AlMg4,5MnZr master alloy. As known, elongation values are affected to a larger extent in the HAZ after welding, if compared to the static strength properties, see tab. 1.6. From a microstructural point of view, a coarsening of the globular Mg₂Si phase can be observed at the edge of the HAZ.

Experiences with Magsimal[®]-59 show that elongation drops even more, if the filler metal is a common AlSi5. For this reason, welded seams are normally positioned in low loaded areas by the experienced casting designer; they should also be located not far from the ingate, taking into account the nature of the high-pressure die-casting process.

Wall thickness 4 mm	$R_{p0,2}$ [MPa]	R_m [MPa]	A [%]
unwelded	165	287	17
welded*	148	246	6

* Manual welding, MIG process, filler metal AlMg4,5Mn

Tab. 1.6: tensile tests performed on welded and non-welded samples.
Manual MIG welding with AlMg4,5Mn filler metal.

Electron beam welding can also be successfully adopted. Industrial application of Magsimal[®]-59 for the production of welded HPDC-rims showed that no through-holes occurred both with electron and laser beam welding for the total length (1,4 m) of the seam [18]. Tolerable porosity levels < 6 % has been observed, depending on the welding speed, as reported in tab. 1.7.

Welding speed [m/min]	Average porosity [%]
2	3,2
4	3,9
6	5,8

Tab. 1.7 : porosity of laser welded seams as function of the welding speed.

Spot welding has been successfully adopted for the assembly of door frame nodes with an average wall thickness of around 2 mm.

1.7.2 Self-piercing riveting

Self-piercing riveting is a very modern joining technique, particularly suitable for thin-walled components. It gives the possibility of joining different materials such as pressure die-castings and metal sheets. The rivet is normally anchored into the casting and just the other material is cut or drilled.

Different riveting conditions have been tested with Magsimal[®]-59. If the casting is pierced as upper layer, it should be min. 2 mm thick, in order to guarantee higher elongation and in turn the required wall deformability. If the casting constitutes the lower layer of the joint, it should not be thicker than 3-4 mm, in order to allow a failure-free anchoring of the rivet.

The best results have been observed by using a rivet die with flat geometry and wide matrix radii. Perfect jointed parts have been obtained with a 1,5 mm AlMg3 sheet as upper layer and a 4 mm plate of Magsimal[®]-59 in the as-cast state as lower layer.

A combination of self-piercing riveting and structural gluing is compatible with the alloy and is considered nowadays a common joining method.

1.8 Surface treatments

Castings in Magsimal[®]-59 can be easily painted or powder coated. Cathodetical painting is the most common method used nowadays. Polishing and protective anodizing can be carried out with relative good results. Polishing produces a typical light blue colour on the surface gloss. The surface should be finally protected against scratches by a transparent varnishing. Gray-shaded zones are visible after anodizing, due to the presence of silicon. Glass blasting is recommended for balancing the heterogeneous look of the surface.

If the oxidation layer has just protective purposes, no further technical issues have to be taken into account. Also if the aesthetic of Magsimal[®]-59 after anodization is much better than the one of AlSi-alloys, chromium coatings are recommended when a decorative meaning is wished.

1.9 Designing with Magsimal[®]-59

Magsimal[®]-59 presents itself like a “difficult” alloy to deal with, as its physical properties are significantly different from the commonly used AlSi-alloys.

Due to its silicon content of average 2 %, the alloy has higher volumetric shrinkage compared to AlSi-alloys. Internal trials in Rheinfelden on a 1 meter mould have resulted in reference values for linear shrinkage of respectively 0,6-1,1 % for Magsimal[®]-59 and 0,4-0,6 % for AlSi-alloys.

Therefore, some guidelines should be kept in mind by an experienced engineer, while designing with Magsimal[®]-59. Ribs should not be designed too thick, as the alloy delivers its best performances in thin sections. 1-2 mm ribs connected to 6 mm walls are not recommended. The whole construction would show a highly undesired rigidity. Additionally, deformation under stress would be located at the walls of the castings, and not on the ribs.

Nodal points with massive material presence should be avoided. A sinking of the surface could be observed, because of the higher volume contraction. Material agglomerations on internal radii can also cause sinking points. A solution is given by the so called “crow’s feet”, shown in fig. 1.18.

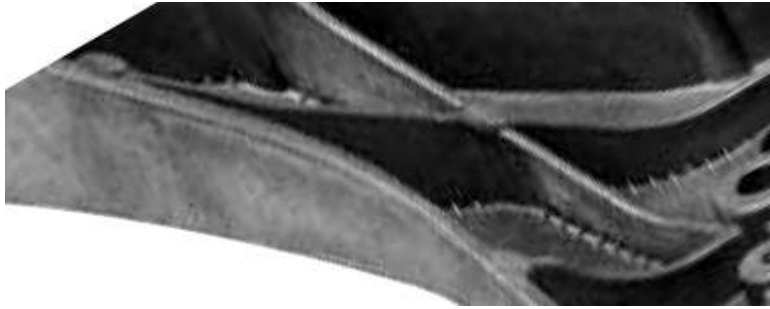


Fig. 1.18: solving inner edge problems through “crow’s feet”.

In unfavourable solidification conditions and for given castings, shrinkages can end into a central line, normally located on the central neutral fibres of the material itself. They do not have any evident effect on the strength of the casting. However, it is extremely important in this instance that the shrinkage does not get any contact with the open surface of the heavy-duty section of the casting.

Wide casting surfaces with high requirements should be designed considering a laminar flow of the metal. Opening and drillings should be machined after casting and not obtained as cast holes. Regular wall-sections should be evaluated together with uniform temperature distribution on the die. If hot spots are present, a premature crack of the casting could occur. Draft angles should be generous, above $1,5^\circ$ even better if over 2° .

1.10 Tool life

Tooling and die equipment is one of the most important positions contributing to the total cost of a casting.

Magsimal[®]-59 is a primary alloy with a max iron content of about 0,2 % and its eutectic temperature is ca. 30°C higher than the one of an AlSi10Mg(Fe) or AlSi9Cu3(Fe). These factors must be considered, while manufacturing the dies.

Die-lubricants should be used at 30-50 % higher concentration, if compared to traditional AlSi-alloys. Last generation die-lubricants developed for Mg-alloys can help in protecting the die longer at higher temperatures, while favouring the flow of metal into the die-cavity.

Generally speaking, dissipating heat from the die just by means of die-lubrication, i.e. from the die surface shortens the die-life. Water-cooled or oil-cooled tools with heat-exchangers show improved die-life.

Experiences in the series production of steering wheels in Magsimal[®]-59 showed that the die life can be quantified in roughly 50 000 shots/die. The die life is however strongly dependent on casting parameters and temperature, see par. 3.5.5 [7]. Linings of furnaces working with AlMg melts show also an increased wear and the necessity of earlier maintenance.

Chapter 2
Manufacturing of Magsimal[®]-59

2.1 Introduction

This chapter presents the details concerning the lean production system of Rheinfelden Alloys GmbH & Co. KG and its application for the series manufacturing of primary casting alloys. The general process flow diagram of Magsimal[®]-59 is presented, underlining its key features. Aim of the chapter is helping in understanding the impact on the final cost for raw materials used for the car set, see chapter 3.

2.2 Rheinfelden Alloys GmbH & Co. KG

Rheinfelden Alloys GmbH & Co. KG (RA) manufactures primary aluminium casting alloys and serves the European market with innovative and traditional materials. The main delivered sector is the automotive, followed by the civil and electrical engineering ones, as well as machine components, ship building and food industry.

Rheinfelden Alloys is built-up by four main units:

- Sales and Marketing (RASM)
- Supply Chain Management (RASC)
- Advanced Casting Materials (RACM)
- ISO TS 16949 Management System (RATS)

RASM's core activity is the selling of metals to customers with the assistance of a dedicated marketing department. Customer assistance and CRM activities are a part of the value added offered as a service accompanying RA's products.

RASC's targets are oriented to the lean production of casting alloys by means of a strict collaboration and coordination within production facilities, production planning and process technology.

R&D activities are carried out by RACM, which is focussed on four main thematics:

- powertrain
- structural components
- self-hardening alloys
- nano-materials

RATS, also called ISO TS 16949 Management System, which is mandatory for an automotive supplier, is transversally permeating all units. RATS takes care of all quality issues arising from RA's units and grants for the implementation of audits, norms, regulations, such as UE directives, IMDS and REACH.

RA produces the complete spectrum of primary casting alloys in form of 8 kg ingots. The finished products can be grouped into two main streams:

- 1.) Standard aluminium casting alloys, whereas RA tailors their specifications on customers' input, according short-term delivery dates and required quantity. The complete RA's product portfolio is described in [12].

- 2.) Patent pending casting alloys and material developed by Rheinfelden’s Tech-Centre. These products are specialties by RA and always connected to particular applications. Their use is justified by clear economical advantages for the end-customers, who consider the product a Value Innovator. Well-known trademarks by Rheinfelden are Silafont[®]-36, AlSi9MgMn, Castasil[®]-37, AlSi9MgMn and Magsimal[®]-59, AlMg5Si2MgMn. A detailed portrait of these materials is depicted in [5].

2.3 The “Back-To-Back” Philosophy and the Lean Production Model

RA sets operates in a business niche, privileging just-in-time orders with small lot sizes, short lead-times and a widened product portfolio.

The business model consists in buying raw materials in bulk, manufacturing of tailored order- and quantity-related casting alloys with final delivering at retailers, with a back-to-back strategy, operated through all the production process, starting from purchase of the raw materials until batch delivery.

As logic consequence, products are delivered from running fresh manufacturing and just seldom from stocks. The product portfolio becomes wider and embraces a great variety of specifications, which are not mass produced in standardized lots, but lean-produced in customized ones.

Fig. 2.1 depicts the consequences of this new approach, showing the average lot size of RA on a basis of ca. 2000 deliveries. Most records are referred to quantities of <1, 1, 2 and 5 metric tons; full truck loads – typically of 24 t – follow, as it is the most economical choice in terms of freights. Downsizing of supplied deliveries fits the downsizing of the final products batches delivered to final customers.

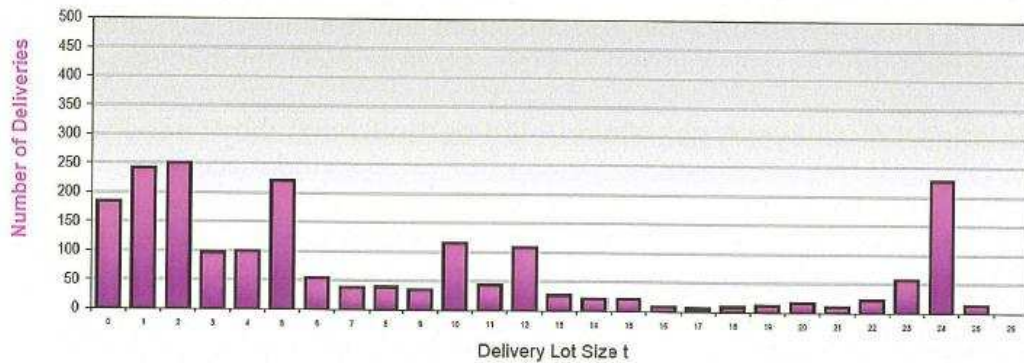


Fig. 2.1: average lot sizes distribution of RA.

The implementation of the Back-to Back philosophy presupposes the translation of the operational principles into a lean production model with a corresponding flexible layout of the plant and its facilities, see 2.4. RA’s lean roadmap is the reference document to translate concept into practice, see fig. 2.2.

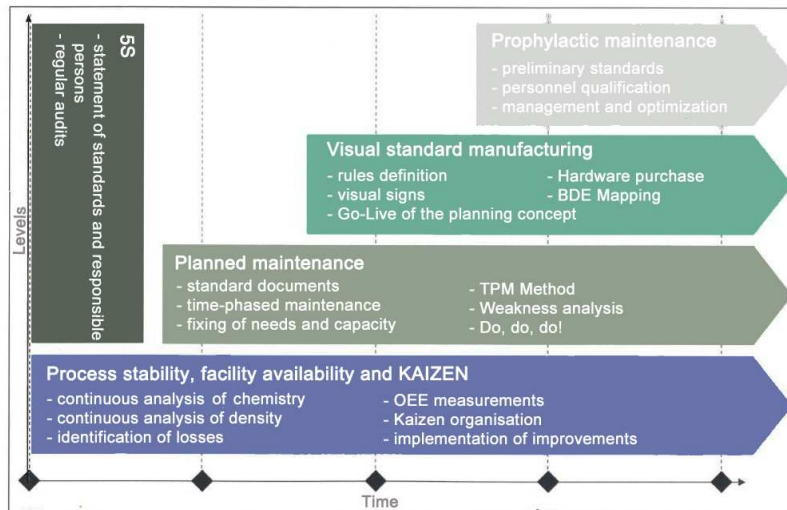


Fig. 2.2: RA's Lean Roadmap.

* OEE stays for Overall Equipment Efficiency; BDE stays for Betriebsdatenerfassung = Operational Data Collection; TPM stays for Total Productive Maintenance.

The purchasing of raw materials is managed by the Risk Management Department (RM), which is directly controlled by the Executive Holding Management. This occurs by a short term Back-to-Back coverage determined soon after the selling of final products to customers. RASM translates the inquiries by the clientele into an input for RM. Consequently, RM interfaces with the London Metal Exchange (LME): immediately after a sale operation, pure aluminium is purchased on the LME by a broker. It is extremely important to coordinate RASM's and RM's activities and to translate them into an immediate action on the LME, in order to minimize or even cancel the speculative risk. In fact, the notation in London changes very rapidly and the volatility of the raw materials can be very pronounced, see fig. 2.3.

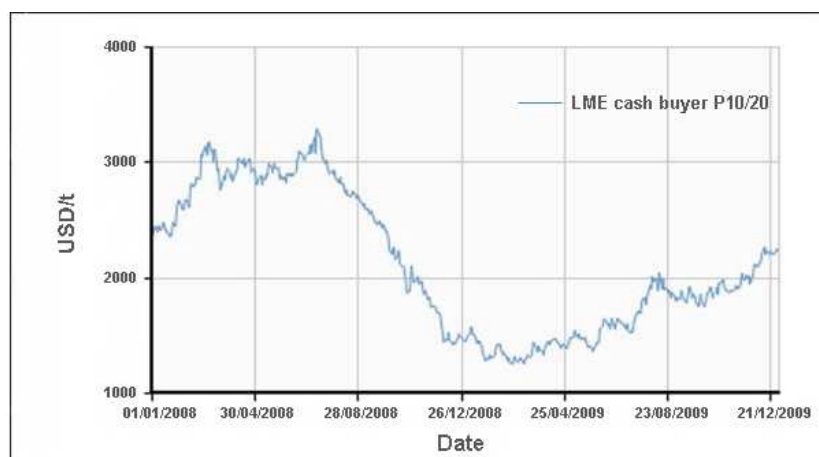


Fig. 2.3: LME quotation for P10/20 (cash buyer values) from 01.01.2008 to 31.12.2009. Statistic from http://www.lme.com/aluminium_graphs.asp.

The current situation of the raw material pipeline is revised by the internal Hedge Committee, with the aim of assessing the short-term buying policy. Finally, RM provides for the securing of master alloys and alloying elements, such as silicon, magnesium, titanium, etc. on the basis of the current market situation. RASM proposes casting alloys to customers and provides for the smooth information flow between inner and outer environment. Material requirements and specifications are evaluated in collaboration of RATS; deliveries are planned JIT with RASC.

The Quality Department (RATS) confirms the feasibility of inquired alloys and may communicate any particular requirements for the purchase of constituents for special alloys. Continuous feedback to RASM is provided on produced batches; RATS and RASM schedule with RASC's production planning the manufacturing of required products. Finally, RATS gives final product approval, before shipment to customers.

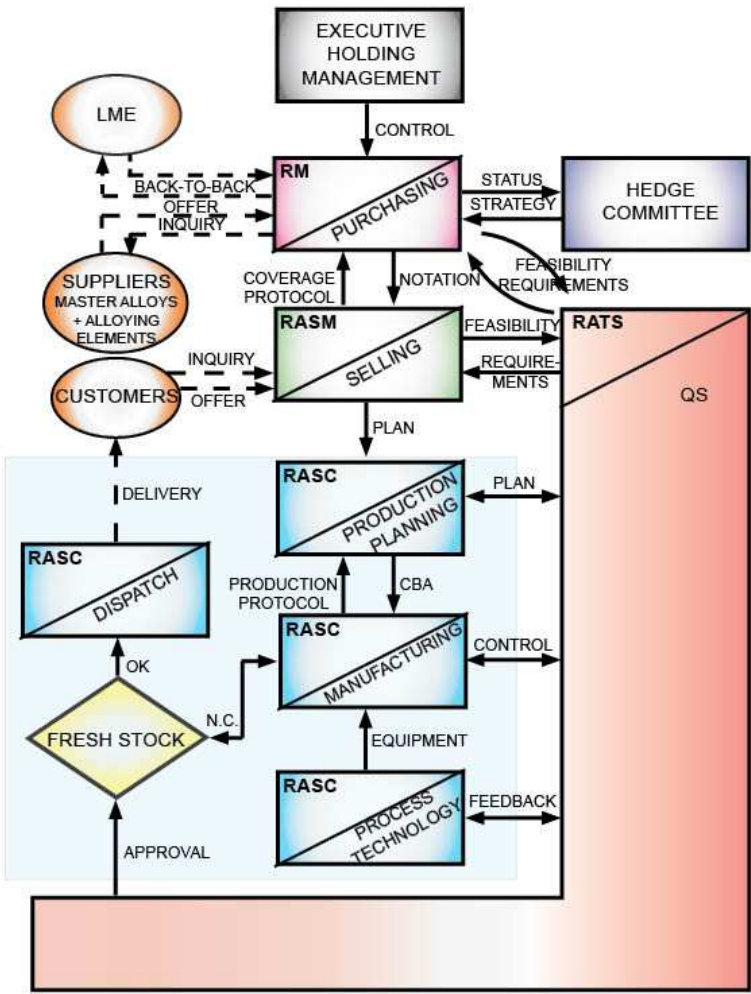


Fig. 2.4: RA's Lean Production Model.

RASC's activities constitute the core competence of RA. They are marked in the blue shaded area of fig. 2.4 and described in their details in par. 2.4.

The batch number 3682 of Magsimal[®]-59 - used for the production of the car sets - has been taken as template for describing the manufacturing process.

2.4 Process Flow Diagram

The manufacturing process of Magsimal[®]-59 is structured according to the process flow diagram reported in fig. 2.5. A description of the main phases is given below. Every stage of the manufacturing process has to be carried out while meeting the Control Plan, approved by the internal Quality System for series production.

Process Flow

1	Goods receipt and raw material <ul style="list-style-type: none"> - Approved suppliers - Raw material control and inspection
2	Melting and Alloying <ul style="list-style-type: none"> - Melting of raw aluminium and main elements - Adding of alloying elements - Check and control of the melt - Temperature setting of the melt - Transferring of the melt
3	Melt treatment <ul style="list-style-type: none"> - Melt cleaning with active and inert gases - Melt treatment with metallurgical means - Accompanying process-oriented Quality Controls
4	Casting of ingots <ul style="list-style-type: none"> - Casting of ingots into the continuous casting line - Accompanying process-oriented Quality Controls
5	Stacking and Marking <ul style="list-style-type: none"> - Stacking of cast ingots - Visual inspection of the surface of ingots - Labelling of the alloy and batch number - Marking of single ingot - Accompanying process-oriented Quality Controls
6	Final control and product approval <ul style="list-style-type: none"> - Double-checking of the record keeping process - Checking of the QS-measures and data - Approval according to the "I.O."-report
7	Dispatch and shipping to customers <ul style="list-style-type: none"> - Weighing and weight note - Dispatch specific identification - Dispatch details according customers' order - Accompanying product documents - Delivery approval

Fig. 2.5: process flow diagram of Magsimal[®]-59.

2.4.1 Good receipt and raw materials

From a logistic point of view, metal and master alloys are delivered via barge or truck to Rheinfelden. Upon receipt, the goods are identified and weighed two times with final recording into the SAP-Management System.

After unloading in the dedicated stocking area, a first visual control and inspection is performed: the presence of oxides and cleanliness of the T-bars or sows are double-checked. 99,8 % pure aluminium is controlled at the spectrometer, comparing the delivered certificate of analysis with the specifications determined by RA. If the chemistry matches, raw aluminium is approved for production; if not, a non conformity is notified and the metal quarantined until clearance.

Granular low-P-silicon is used for series manufacturing. The deleterious effects of this element on the microstructure of Magsimal[®]-59 have been described in par. 1.2. The presence of SiO₂ agglomerates causes a reject of the raw material.

Pure magnesium is alloyed in form of ingots, whose required purity is 99,8 %. Randomly chosen batches are metallographic controlled, in order to see if at 300X and 500X MgO nests are to be detected. Titanium is delivered in form of AlTi 90/10 master alloy. Waffles must be free of dross residues, superficial oxides and H₂. Beryllium is alloyed in granulated form, as its percentage in Magsimal[®]-59 is very low. Al-Manganese briquettes or tablets are preferred with a dosage of 20/80, in order to make the melting down faster and easier. 10% Vanadium master alloys in form of waffles or ingots have been chosen for series manufacturing.

Every delivery of raw materials is recorded into SAP with its charge number, lot size, certificate of origin and quality; although a list for approved suppliers has been issued, incoming goods are double-checked: acceptance rate has been fixed to 100 %.

New suppliers are requested to submit a trial batch, before being approved in the official list.

2.4.2 Melting preparation

After the input of the order by the Sales Department, the Planning Manager issues the so-called “CBA”- Sheet or Batch Production Order. The foundry manager, the QS-Manager and the responsible person for the charge making-up are contemporary notified with a hard copy of the CBA-Sheet.

Quantity, batch number and casting oven are defined and reserved, on the basis of the current real time foundry planning and of the requirements by the alloy.

The preparation of a batch is made by RASC’s foundry men, starting from its basic recipe, called “production protocol”, see fig. 2.6. Depending on the chemistry of Magsimal[®]-59 and on the batch quantity to be produced, alloying elements and pure metal are picked-up from the storage area and located next to the melting furnace 53, dedicated to AlMg-alloys.

RA Metallbestandsführung: Fertig-Charge Herstellprotokoll					
Rheinfelden ALLOYS		Herstell-Protokoll		24.08.2010	
ZIMM_FWLCHAR01/P00		Fertigwaren-Chargen		07:43:24	
Ersteller: HI0B				Seite: 1	
Charge: 8003682-00 Werkstoff: 100060522 MA-59					
Wiegen von: 02.03.2010 11:36:06 bis: 02.03.2010 19:27:22					
	WE-Charge	Mat-Nr.	Material-Bezeichnung	Gewicht	Me
1	0100003742	1-20000170	MAGNESIUM 99,8%, 8 kg Masse1	833,000	KG
2	0100003741	1-20000140	Silizium-Metall "Phosphorarm	270,000	KG
3	0100003559	1-20000330	AL-TITAN 90/10	118,000	KG
4	0100003779	1-20000460	AL-MANGAN 20/80	123,000	KG
5	0100003395	1-20000420	AL-BERYLLIUM 95/5	10,450	KG
6	0100003801	1-10000060	Aluminium 99,8 P06/10	7.934,000	KG
7	0100003832	1-10000060	Aluminium 99,8 P06/10	5.620,000	KG
8	0100003119	1-20000430	AL-VANADIUM 90/10	10,050	KG
9	0100003742	1-20000170	MAGNESIUM 99,8%, 8 kg Masse1	50,050	KG
10	0100003395	1-20000420	AL-BERYLLIUM 95/5	1,250	KG
			Summe	14.969,800	KG

Fig 2.6: production protocol of a 15t-batch Magsimal[®]-59.

Contemporarily, the calculation of raw material costs can be easily carried out, according to tab. 2.1, referred to one metric ton of metal. The nominal weight of single alloying elements is taken out of the basic chemistry of Magsimal[®]-59.

Raw material	Nominal weight [%]	Price [€/t]	Share [€]
Pure aluminium	91,261	96,02	89,87 €
Silicon	2,200	109,12	2,45 €
Magnesium	5,700	119,33	6,87 €
Titanium	0,110	147,63	1,62 €
Beryllium	0,004	1.000,00	0,80 €
Vanadium	0,025	323,12	0,81 €
Manganese	0,700	116,99	1,02 €
TOTAL	100,000		103,45 €/t
			103,00 €/t

Tab. 2.1: metal voucher for Magsimal[®]-59.

The percentage loss of metal is determined according to the common practice and experience in the foundry. Purchasing prices of master alloys and elements are purely indicative. Shares are actually calculated as the product of nominal weight and acquisition prices divided by the loss in weight during melting. The metal voucher constitutes a reliable and up-to-date basis for the quoting activities by RASM, see par. 2.3.

2.4.3 Melting and alloying

The foundry CBA-Sheet contains a step-by-step description of the production process. The final target chemical composition is listed with eventual limitations for polluting elements or additional notes to foundry operations.

RASC'S process technology grants for the preparation of the manufacturing facilities and for the availability of necessary equipment, under constant dialogue with RATS.

The first melting procedure is performed into a gas-fired crucible melting furnace with a total capacity of 13 tons, which is a part of a casting facility called "S&A"¹.

The melting furnace is identified by number 53 in fig. 2.7, showing the layout of the whole casting line. The first bath is created with the pure aluminium and the main alloying elements, such as Mg, Si, Mn, V and Be. Mg-loss during melting is taken into account. Melting temperature is strictly controlled within an interval of 30°C.

Stirring is performed to homogenize the chemistry into the melt. The process is described and tuned phase by phase by a Quality Sheet which is filled-out by the operator in real time. After skimming, a first control of the chemical composition and melt temperature is made on this preliminary melt and the nominal/actual values are double-checked on the batch production order (CBA-Sheet).

If no deviation occurs, the approval for melt transferring is given. The metal is thus cast from melting oven 53 either into the casting oven 26 or 27 by means of a ladle.

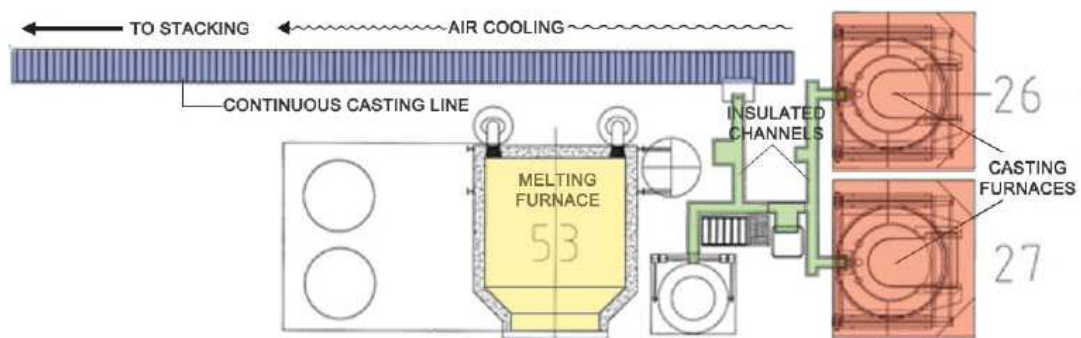


Fig. 2.7: Schmitz & Apelt casting line.

2.4.4 Melt treatment

In the casting furnace, the final chemistry of the metal is achieved by grain refining through TiB_2 nuclei.

Melt cleaning with active and inert gases by means of rotor degassing is performed as well. This is a crucial phase for the manufacturing of Magsimal[®]-59, as the special foundry treatment modifying the growth mechanism of Mg_2Si eutectic platelets is performed. This step is therefore fundamental to get the final mechanical properties of Magsimal[®]-59 and the high amount of quality measurements performed at this stage is herewith justified.

The number of gas treatments in the melt depends on the effectiveness of the treatments themselves and is a direct function of the feedback by the QS-Department.

¹ S&A stays for Schmitz & Apelt casting line

The control of the chemistry and the melt temperature is made soon after a rotor degassing treatment. The H₂-content in cm³/100g is recorded and 1 kg ingot is cast for the evaluation of the surface of fracture, its cleanliness and its degree of ductility. The same operation is made on a permanent mould cast-apart sample (cylinder sample), which is stored for further consultation in case of any need.

Surface fracture controls are performed visually, according to the internal know-how and experience of the workers and taking into account a scale of reference developed for Magsimal[®]-59, see par. 2.5.

After the last rotor degassing, no alloying and further grain refining is allowed. The metal is fluxed and after a determined resting time skimmed. After final approval by the QS on chemistry and fracture surface, the green light for casting is given.

2.4.5 Casting of ingots

The casting procedure is performed from the ovens 26 or 27 into the continuous casting line through a system of insulated transfer channels. As the accomplished microstructure can be influenced by several factors, further quality assessments are performed during the casting operation into the casting line.

Two further permanent mould cast-apart samples, respectively at the beginning and at the end of casting procedures, and three 1kg-test-ingots, respectively at the beginning, in the middle and at the end of the batch casting, are cast. The same controls as in par. 2.5 are performed. Temperature is measured into the feeder of the casting furnace and the H₂-content as well as the DI² are recorded.

One real casting ingot is taken out from the batch, in order to perform once again all tests of par. 2.5 and be stored 10 years long, thus complying with the requirements of the ISO TS 16949 certification for automotive suppliers.

The ingots running into the casting line are cooled down in forced air and conveyed to the stacking station. The single ingot moulds are water-cooled after casting and pre-heated via gas burners before casting. A visual control of the surface of the ingots by the operator closes the casting operation.

2.4.6 Stacking and marking

A laser-controlled device provides a check of the dimensional and weight tolerances of the ingots. Ingots outside these tolerances are automatically rejected; the others are first alternatively turned then stacked in 1 t – bundles and tied-up with plastic stripes, after complete cooling down.

² The Density Index is determined by means of the low pressure test.



Fig. 2.8: a double bundle of Magsimal[®]-59.

Every single bundle is marked with the stamp “Ma-59”, see fig. 2.8. Feet are cast manually in Magsimal[®]-59, in order to provide the same chemical composition with a smart logistic solution. An automatic system for the marking of single ingots by ink printing is being currently implemented in Rheinfelden and will soon available as a standard.

2.4.7 Final control and product approval

During this stage, a re-melted sample is produced, taking out two ingots, respectively from the beginning and the end of the cast batch, and re-melting them in a small induction crucible furnace.

The sample serves to the simulation and monitoring of the final quality expected by the end customer, i.e. the foundry, which will of course melt down the delivered ingots. The record keeping is gathered and evaluated. Chemical composition is definitely approved by the QS on the basis of the specifications listed on the batch production order. The process values collected on the protocols during production are evaluated.

The metallographic laboratory gives its end approval on the microstructure observed at the optical microscope on ingots from the batch production. The approval threshold has been fixed in a 75 % efficiency of the treatment, see par. 2.5. The evaluation is made according to a precise procedure, taking into account 16 different positions on the ingot at 200x magnifications and the resulting average value.

If all tests are successful, the so-called “i.O.” report is issued and the approved metal is ready for delivery to customers.

In addition to this standard procedure, a re-qualification approval for the series production is done once a year throughout the complete manufacturing process. Additionally, the determination of the mechanical properties of series Magsimal[®]-59 ingots is carried-out by the Tech Lab on a six month time-horizon.

The main target is granting invariable premium quality of the delivered material.

2.4.8 Dispatch and shipping to customer

RASC’s dispatch department takes care of the final operations on the stacked metals. The bundles are weighed, labelled and temporary stored on stock. According to the input of RASM, particular wishes by customers on the final packaging, spray marking and transportation are implemented. The specific dispatch identification is carried out, arranging the bundles according to the order quantity. A certificate of analysis is issued. Customer details, delivery address, contract number, kind of alloys and packaging, number of bundles, gross and net weight, incoterms, carrier name and complete spectrometric analysis are given on the delivery note, see fig. 2.9.

RHEINFELDEN ALLOYS GmbH & Co. KG		RHEINFELDEN																																						
Ein Unternehmen der ALUMINIUM RHEINFELDEN Group																																								
Versandanzeige / Analysenattest Advice of Dispatch/Analysis Certificate Avis d'Expédition/Certificat d'Analyse																																								
RHEINFELDEN ALLOYS GmbH & Co. KG, Postfach 1004, D-79607 Rheinfelden MicroTech Srl, Via Galvani 24-28 I-25010 FLERO (BS)	No. of 1200103519	Date 22.10.2009	Warehouse/Plant No. Contract No. 11081928 00																																					
Adresse/Address to party/Clerk 123430 Warehouse/Shipping to party/Desk/office 12343003 Incoterms/For order/Your company tel. Sig. Gatti / 28.09.2009 Warehouse/Contract/Desk/office Production Plant Via Galvani 24-28 I-25010 FLERO (BS)																																								
No. of bundles / No. of 1 bundle / 1 piece	Packaging DOPPELSTAPEL	Weight Net of Gross 1,8																																						
Marking / Branding / Code MA-59	Marking / Marking / Marking	Location / Delivery Location																																						
Material / Alloy MA-59	Formwork / Piece count / Code DEP Inno																																							
Order No. / No. of Quality No. of Goods 1-00060520	Description / Designation / Description MAGSIMAL-59 GBD-ALMG5512M Primary Aluminium Alloy	Location / Form / Form ingots																																						
Order Buyer Grieshaber	Date of order 23.10.2009	Gross weight kg 19.405	Net weight kg 19.405																																					
We accept no liability for the fitness of our products for the use intended by buyer/user.																																								
Analysenattest/Analysis/Analyse																																								
<table border="1"> <thead> <tr> <th>Stück Piece</th> <th>Charge</th> <th>Si</th> <th>% Fe</th> <th>% Cu</th> <th>% Mn</th> <th>% Ni</th> <th>% Cr</th> <th>% Zn</th> <th>% Ti</th> <th>% BB</th> <th>%</th> </tr> </thead> <tbody> <tr> <td>10</td> <td>8002512-00</td> <td>2,220</td> <td>0,107</td> <td>0,007</td> <td>0,685</td> <td>5,389</td> <td>0,001</td> <td>0,001</td> <td>0,084</td> <td>0,003</td> <td></td> </tr> <tr> <td>8</td> <td>8002511-00</td> <td>2,220</td> <td>0,109</td> <td>0,006</td> <td>0,689</td> <td>5,460</td> <td>0,001</td> <td>0,000</td> <td>0,079</td> <td>0,003</td> <td></td> </tr> </tbody> </table>	Stück Piece	Charge	Si	% Fe	% Cu	% Mn	% Ni	% Cr	% Zn	% Ti	% BB	%	10	8002512-00	2,220	0,107	0,007	0,685	5,389	0,001	0,001	0,084	0,003		8	8002511-00	2,220	0,109	0,006	0,689	5,460	0,001	0,000	0,079	0,003					41190
Stück Piece	Charge	Si	% Fe	% Cu	% Mn	% Ni	% Cr	% Zn	% Ti	% BB	%																													
10	8002512-00	2,220	0,107	0,007	0,685	5,389	0,001	0,001	0,084	0,003																														
8	8002511-00	2,220	0,109	0,006	0,689	5,460	0,001	0,000	0,079	0,003																														
<small> Stichtag/Date of analysis: 23.10.2009 Hersteller/Manufacturer: RHEINFELDEN ALLOYS GmbH & Co. KG Unterschrift/Signature: _____ </small>																																								

Fig. 2.9 : certificate of analysis and delivery note by RA.

On customer’s request, an official delivery note, valid as inspection certificate according EN 10204 3.1 with a complete 30 element-chemistry, tensile properties and radioactivity measurements can be additionally issued. Custom clearance formalities are carried-out and connected paperwork issued for extra EU-deliveries. Once the metal is ready and has been approved for dispatch, a record will be registered under the corresponding delivery date into the SAP-Platform dedicated to the forwarder, who is immediately notified. International deliveries via air freight or sea freight are arranged directly by the Sales Department, according to the best current available freights. After loading, the metal is weighed one additional time at the main gate. Leaving date and time from Rheinfelden is recorded.

2.5 Fracture surface, microstructure and ductility

The quality monitoring procedures listed in par. 2.4.1 to 2.4.7 are laborious and time-consuming to a huge extent, if considering that they are performed on every batch.

Chemical composition, temperature of the melt and H_2 values are standing measured during melt treatment and casting; two cast-apart cylinder samples and three test ingots per batch are broken; one additional cylinder sample and test ingot are evaluated after every treatment in order to assess its outcomes. 1x series production ingot is fractured; a re-melted sample from series ingots is cast; micrographs are taken on three series ingots per batch.

The reason for this effort lies in the strict relationship between manufacturing parameters, the aspect of the fracture surface of the metal, its microstructure and its final mechanical properties.

The special foundry treatment performed in Rheinfelden changes the Mg_2Si growth mechanism, resulting in a very fine ternary eutectic, the special feature of Magsimal[®]-59. Direct effects of the treatment can be observed simply looking to the fracture surface of an ingot of Magsimal[®]-59: it looks white. The finer the eutectic, the brighter the fracture surface, the higher the elongation values. As soon as the eutectic gets coarser, the fracture surface will get a blue nuance, corresponding to an increase in the tensile strength and to a dramatic drop of elongation values.

According to internal experiences, a quantification of the treatment efficacy has been defined between 0 % and 100 %. Depending on this percentage, different mechanical properties can be observed on alloys with identical chemical composition.

The aspect of fractured ingots through out all manufacturing steps described previously is presented in fig. 2.10. The corresponding microstructure of the alloy is reported from fig. 2.11 to 2.15. Finally, tab. 2.3 summarizes typical tensile properties of Magsimal[®]-59 depending on the outcomes of the foundry treatment.

Positions A and B in fig. 2.10 show the broken surface of test ingots, respectively after the first and second melt treatment with 0 % and 10 % efficiency. The fracture is fragile. Fig. 2.11 shows the microstructure revealed in A after one treatment, which have not led to positive outcomes. Mg_2Si eutectic phase can be observed in its plate-like morphology. After the third treatment, 75 % efficiency has been achieved (ingot C, fig. 2.11) and therefore casting has been approved. Test ingots D, E and F refer respectively to the beginning, middle and end of the casting procedure. A very effective treatment (80-90 %) has been found in this stage.

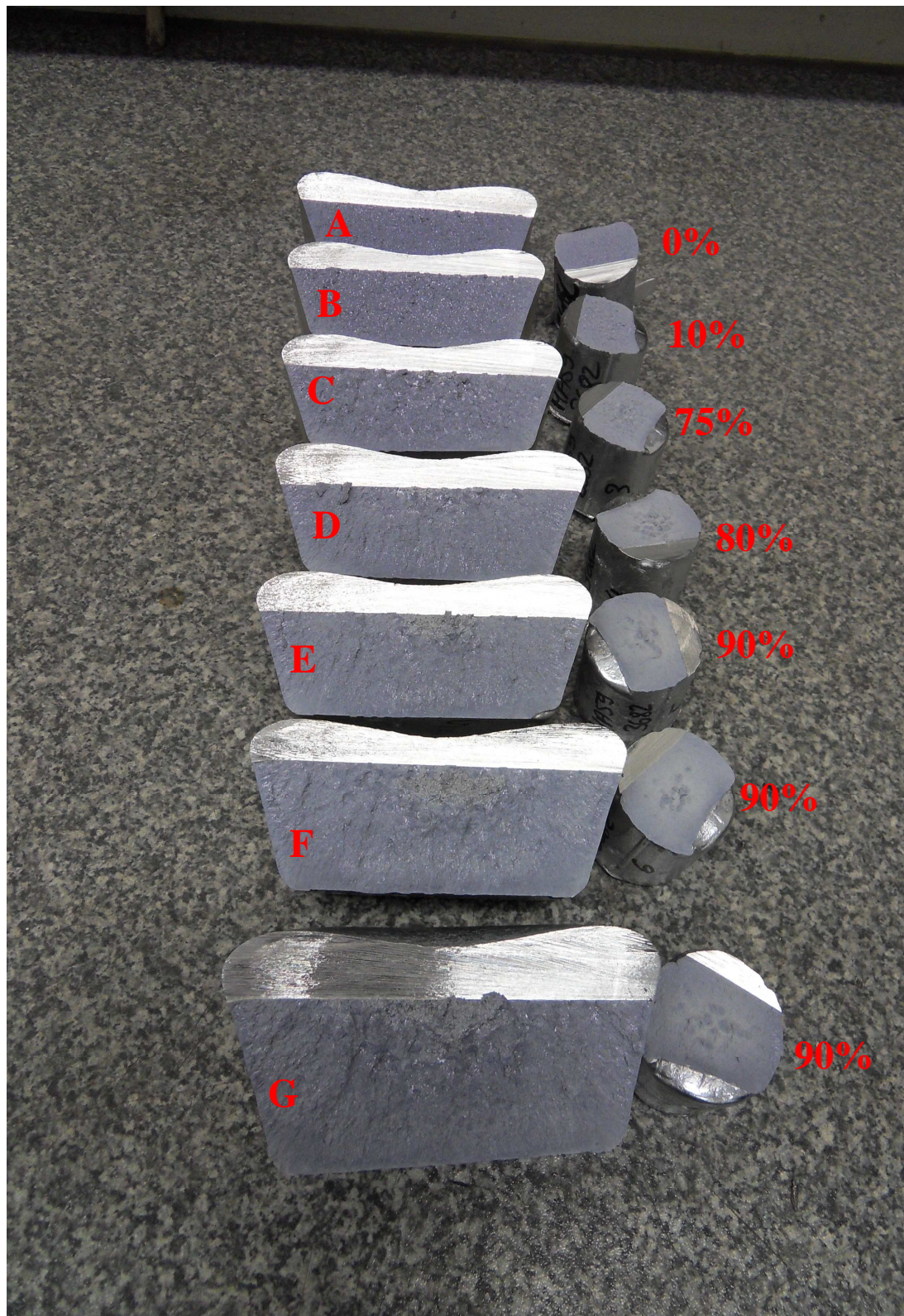


Fig. 2.10: cylinder samples, test ingot and series production ingot of Magsimal[®]-59. Batch 3682.

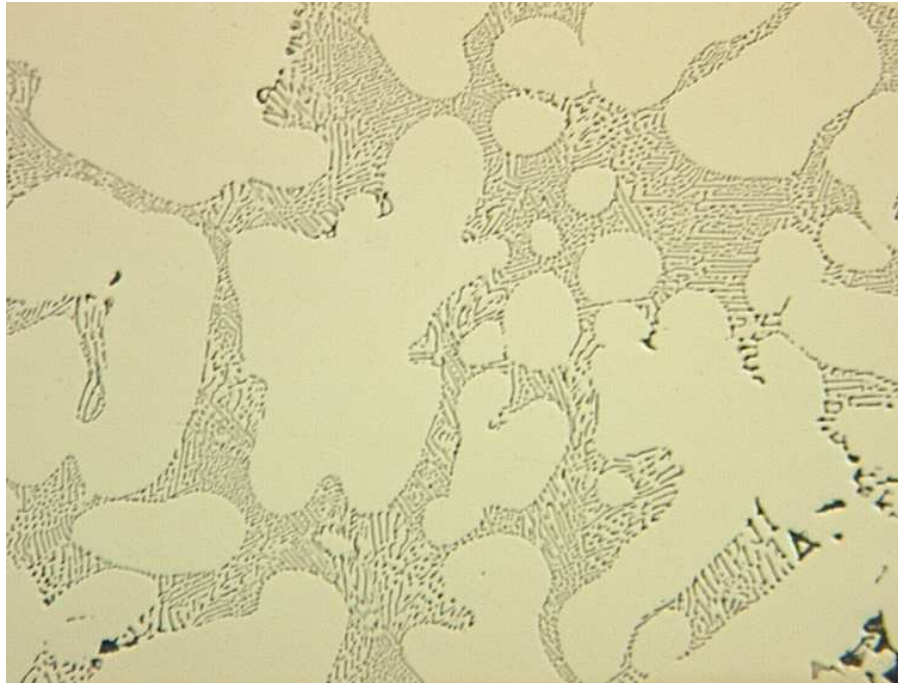


Fig. 2.11: microstructure of a Magsimal[®]-59 test ingot of batch 3682.
Treatment 0 % - ingot “A” of fig. 2.10.

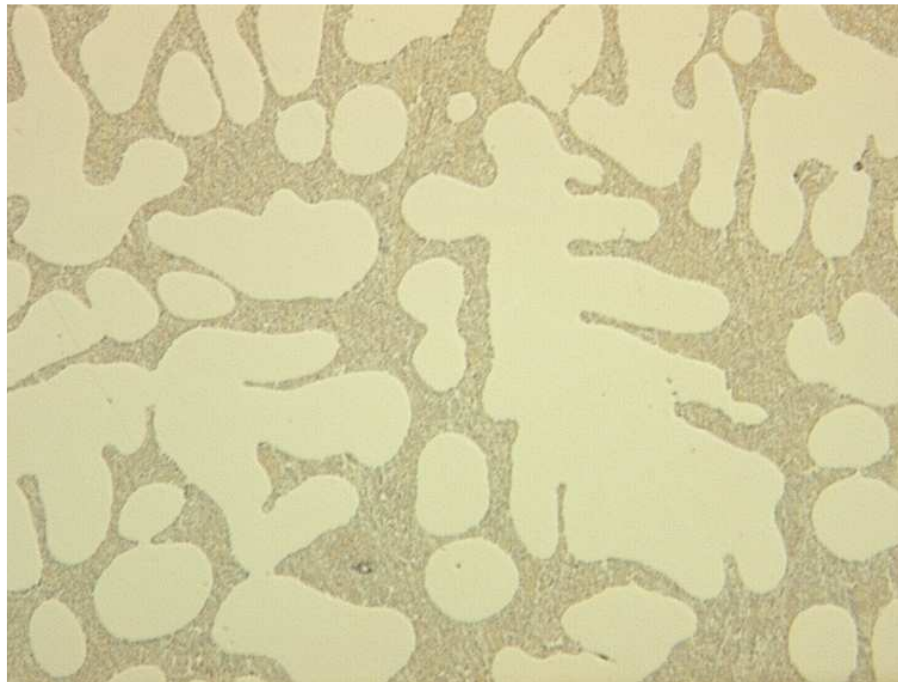


Fig. 2.12: microstructure of a Magsimal[®]-59 test ingot of batch 3682.
Treatment 90 % - ingot “G” of fig. 2.10.

The micrographs in fig. 2.13 and 2.14 show the change in morphology of the Mg₂Si crystals, which appear now in a fine coral-like form.

SEM pictures showing the phenomenon in a 3D perspective are to be seen in chapter 1, fig. 1.2. The fracture surface of the ingots turns brighter with a ductile breaking dynamic. Position G refers to an 8 kg series production ingot of Magsimal[®]-59. The fineness of the eutectic is appreciable in fig. 2.12, taken at 500x magnifications.

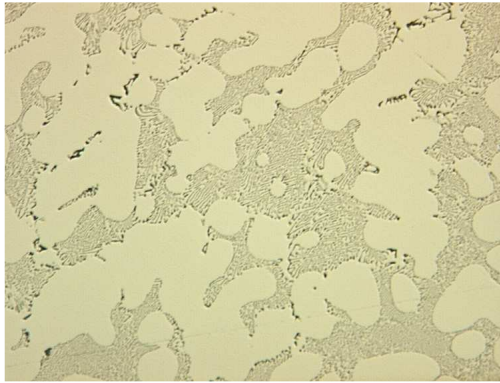


Fig. 2.13: microstructure of a series Magsimal[®]-59 ingot.
Batch 3682 - beginning of casting - ingot
“D” of fig. 2.10

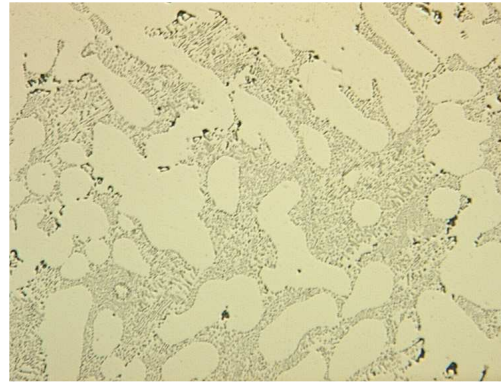


Fig. 2.14: microstructure of a series Magsimal[®]-59 ingot.
Batch 3682 - end of casting - ingot
“F” of fig. 2.10

The two micrographs of fig. 2.15 show the microstructure of the re-melted sample cast by series ingots of Magsimal[®]-59. The result is still satisfactory with a 90 % efficiency of the treatment, which remains fully effective after one melting procedure.

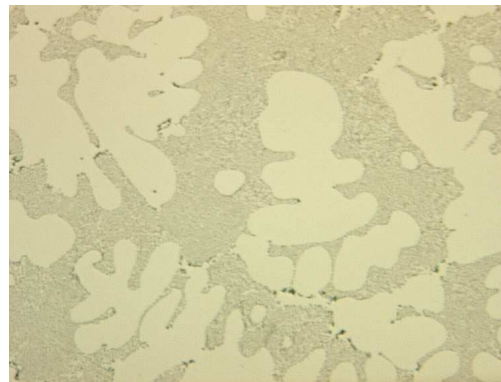
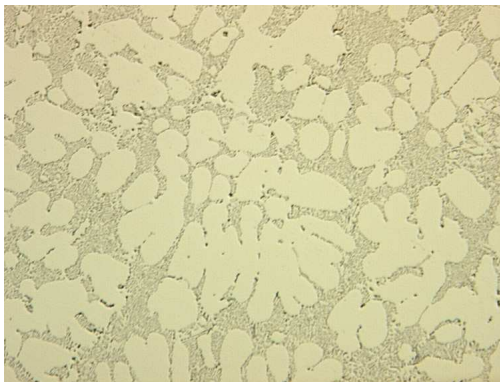


Fig. 2.15: microstructure of re-melted Magsimal[®]-59.
Batch 3682.

It has to be taken into account that just ingots with % treatment > 75 % are considered suitable for delivery to final users. Lower treatment performances do not necessarily mean bad mechanical properties.

Therefore a classification according to this criterion can be made, resulting in two additional alloys, whose trade names are Magsimal[®]-33 and Peraluman[®]-07.

As reported in tab. 2.2, Magsimal[®]-33 has a percentage efficiency treatment between 50 % and 75 %; Peraluman[®]-07 between 0 and 50 %. Further details to these alloys can be consulted in [5] and [26].

Trade mark by Rheinfelden Alloys	Treatment [%]
Magsimal [®] -59 AlMg5Si2Mn	75-100
Magsimal [®] -33 AlMg5Si2Mn	50-75
Peraluman [®] -07 AlMg5Si2Mn	0-50

Tab. 2.2: trademarks by Rheinfelden according to the efficiency of the treatment.

Tab. 2.3 compares results of tensile tests collected for different “quality levels” of Magsimal[®]-59, classifying them into main four families according the treatment efficiency.

	YTS [MPa]	UTS [MPa]	e [%]	Treatment [%]
Magsimal[®]-59 AlMg5Si2Mn	178	313	20,6	75-100
AlMg5Si2Mn (Magsimal [®] -33)	187	328	13,4	50-75
AlMg5Si2Mn (Peraluman [®] -07)	183	319	8,4	25-50
AlMg5Si2Mn (Peraluman [®] -07)	186	321	7,7	0-25

Tab. 2.3: tensile tests results with Magsimal[®]-59 and different treatment efficiency.

YTS and UTS are influenced to a slight extent by the outcomes of the manufacturing process; on the other hand side, elongation shows a huge sensitivity to the foundry treatment. Toughness and fatigue behaviour are influenced at the same extent of ductility.

Fig. 2.17 to 2.25 of Appendix A show once again the significant difference on the microstructural point of view. Fig. 2.17 to 2.19, top and bottom, show a Peraluman[®]-07 with average 10 % treatment efficiency. Fig. 2.20 to 2.22, top and bottom, show a Magsimal[®]-33 with average 55 % treatment efficiency. Finally, fig. 2.22 to 2.25, top and bottom, show a Magsimal[®]-59 with average 70 % treatment efficiency.

The change in the mechanism of growth of Mg₂Si platelets is visible.

2.6 FMEA Analysis

A FMEA³ is implemented through all the production process as effective tool for controlling errors and overcoming their side-effects. Failures are prioritized according to their impact in terms of consequences, how frequently they occur and how easily they can be detected.

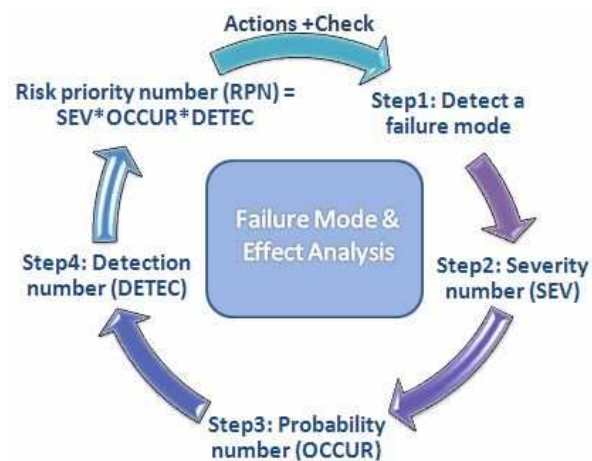


Fig. 2.16: FMEA analysis.

RPN-values are recorded for all main phases listed into the process flow. As a mandatory tool by the formal quality system ISO TS 16949, the FMEA is used for process control before and during ongoing operations, kept up-to-date as soon as the process flow is changed.

³ Failure Modes and Effect Analysis

Chapter 2
Manufacturing of Magsimal[®]-59

APPENDIX A



Fig. 2.17: Peraluman®-07 – 200X.

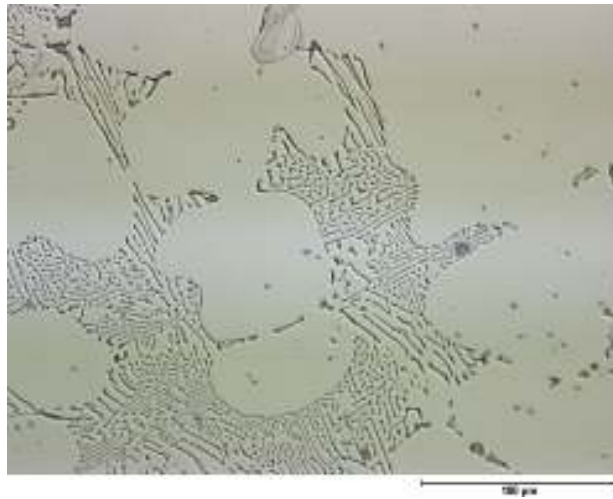
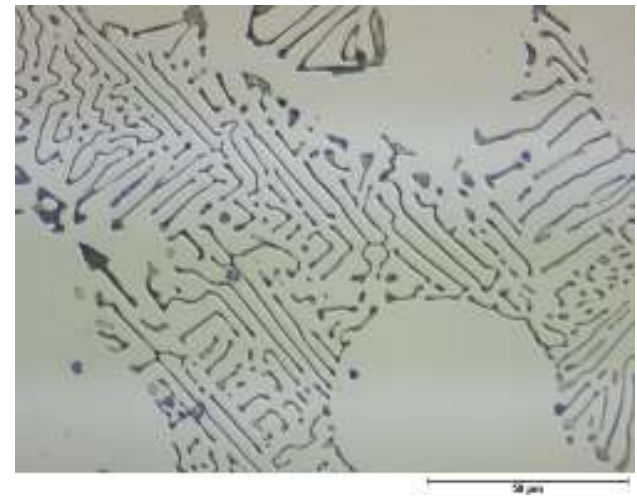


Fig. 2.18: Peraluman®-07 – 500X.



Fig. 2.19: Peraluman®-07 – 1000X.



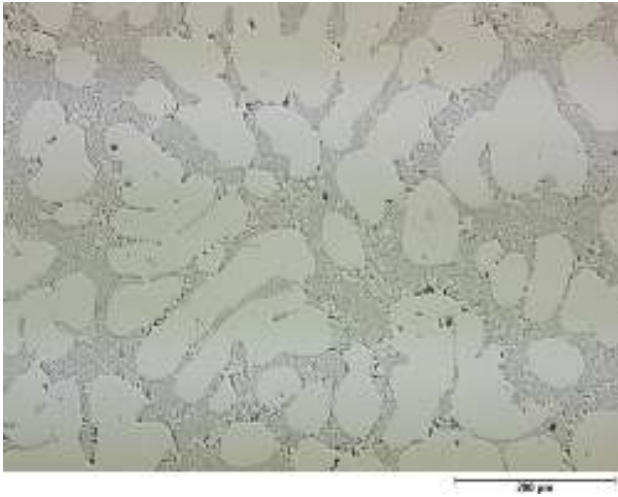


Fig. 2.20: Magsimal[®]-33 - 200X.

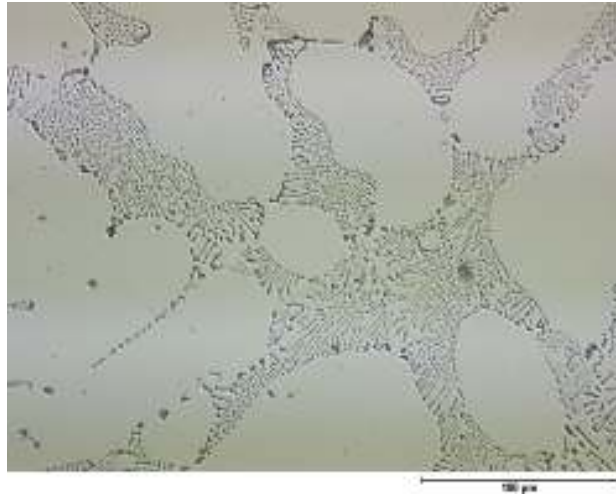


Fig. 2.21: Magsimal[®]-33 - 500X.

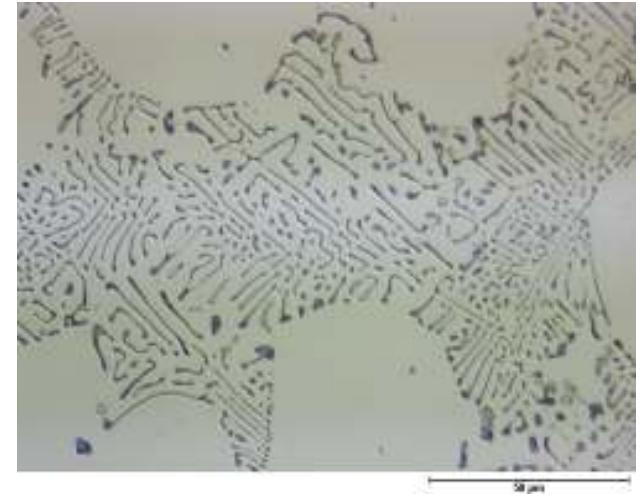


Fig. 2.22: Magsimal[®]-33 - 1000X.

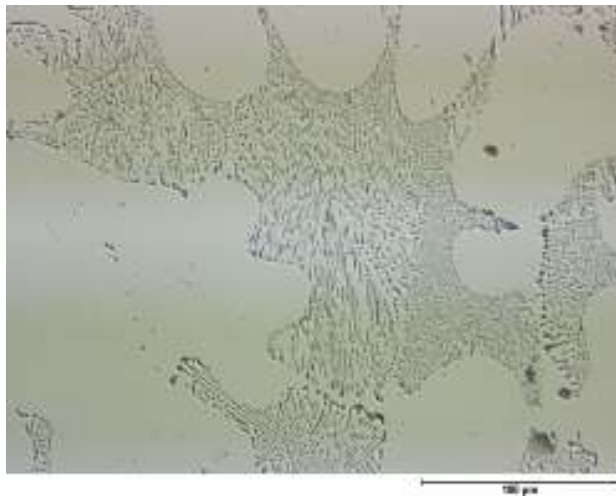
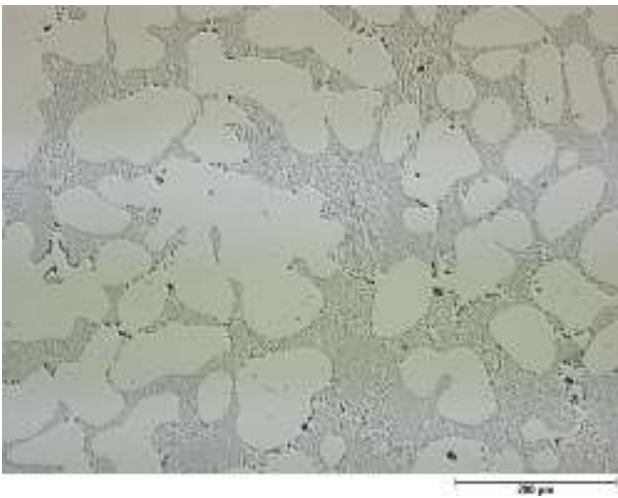




Fig. 2.23: Magsimal®-59 - 200X.

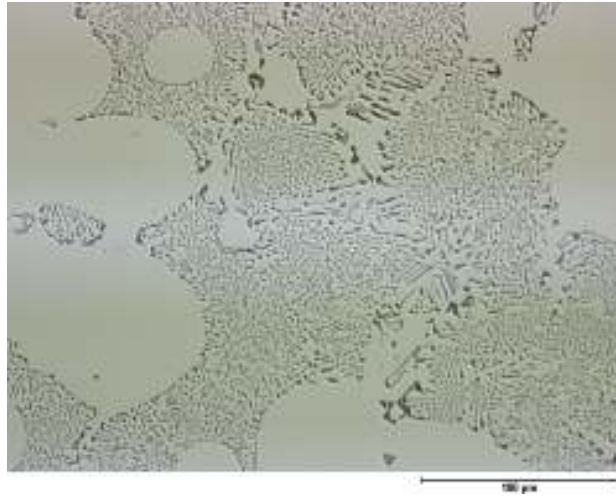


Fig. 2.24: Magsimal®-59 - 500X.

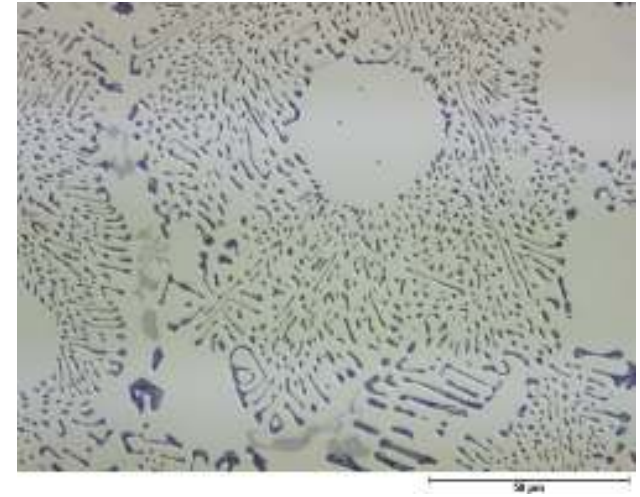
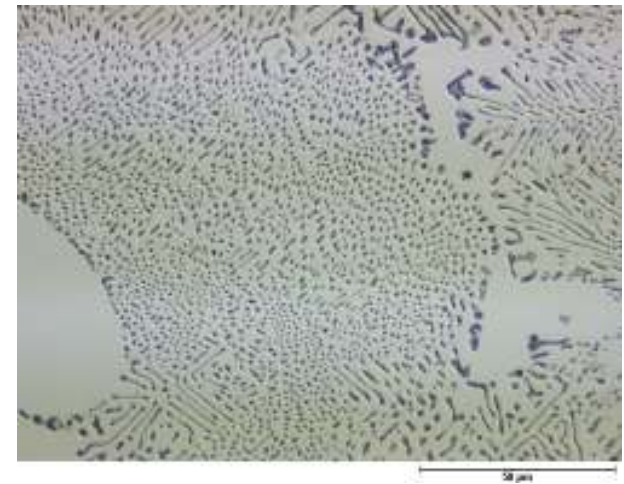
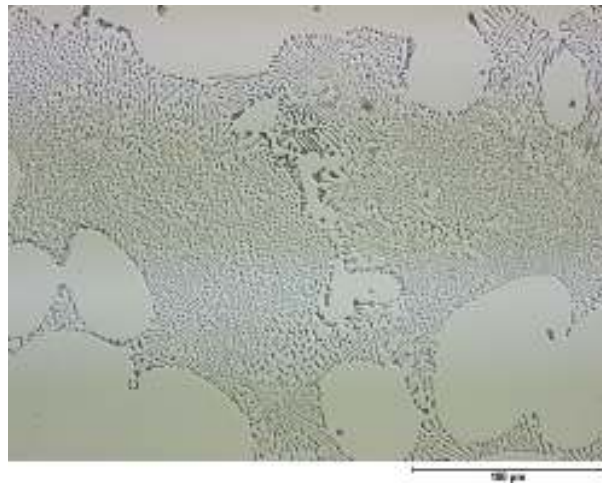
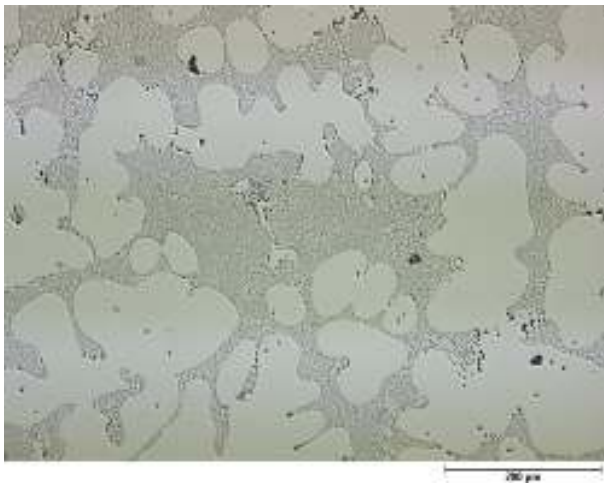


Fig. 2.25: Magsimal®-59 - 1000X.



Chapter 3
The application

3.1 Introduction

This chapter describes the application of Magsimal[®]-59 to the chassis of a modern convertible car, focussing on the main technical hurdles faced during the manufacturing of the castings. After the definition of the requirements, the manufacturing process has been described in its managerial part and phase-by-phase according its process flow chart.

The results obtained during prototyping, sampling, pre-series and series production have been correlated to the improvements introduced on the shop floor.

Outcomes have been evaluated both on the castings, referring to the main requirements for automotive parts, such as shrinkage, porosity and dimensional stability and on the process management, underlining the main difficulties arisen in terms of process stability and tooling life, while casting Magsimal[®]-59 and benchmarking a common AlSi9Cu3(Fe).

Finally, a cost break-down of the whole process has been attempted, on the basis of the additional operations and measures adopted for running a common HPDC-foundry with primary metal. This has been done as the main dilemma of a caster facing new alloys is their impact on operating costs. The figure obtained is impressive: + 150 % compared to common secondary AlSi-alloys. The conclusion is therefore clear: the use of high-performing premium alloys is justified where the highest technical requirements are set on castings.

3.2 The application

The castings investigated in this work are high-pressure die cast nodes, manufactured for the famous Italian carmaker Ferrari. The complete assembled construction made by 6 castings in Magsimal[®]-59 (3+3, respectively right-hand RH and left-hand LH) is a portion of the 5-part retractable hart top (5-part RTH), mounted on the new Ferrari California model, called also F149. The 6-part car set has been developed and delivered by Webasto as finished solution ready for the final assembly. Microtech has taken care of the manufacturing of the castings.

The aim of the work is giving an overview of the manufacturing process in the foundry system from the production of the raw material ingots to the delivery of finished castings, integrating many functional areas involved in the process itself.

The foundry system is intended therefore as foundry of level one, supplier of raw materials, and as foundry of level two, supplier of HPD castings. These two players are normally evaluated each as a single ring of the supply chain. A unified vision allows for a better understanding of the faceted aspects to be taken into account for this challenging application.

The reasons leading to this study are several.

First of all, the design engineers have chosen a low-iron primary AlMg-HPDC alloy as material for this application. The intention is limiting the total weight of the RTH and therefore improving the balancing masses. On one side, the choice is justified by the high mechanical properties of this alloy system; on the other side however, it poses hurdles connected to the particular handling of the metal itself, see chapter 1.

The evaluation of the technical and economical pros and cons of this application has proven very interesting in understanding when and at which expenses primary alloys can be used.

Additionally, the parts can be considered at the state-of-the art in their application field. With this model, the final customer enters the segment of the RTH-cars and brings further its light-weight design, adopting a 100 % aluminium chassis. The innovation degree of the application superimposes the innovative possibilities Magsimal[®]-59 opened in 1995 after its launch on the market.

The Ferrari California made its official debut at the Paris Show; it is an open top car, designed on the famous past California 250 from 1950s. The manufacturing volumes have been planned as 7000 cars/year until end of 2013. The car has a dry weight of ca. 1630 kg. Lightweight construction can be noticed on different car parts. Electrically adjustable magnesium-framed seats are mounted as default, but new seat with all-carbon-fibre frame is available as optional. Diamond-finish 19" 5-spoke aluminium alloy wheels are a standard, but a further set of diamond-finish 20" forged 5-spoke alloy wheel can make the car further 11 kg lighter. The chassis and body shell are both made entirely from aluminium. Thanks to the use of different aluminium technologies - extrusions and shell casts - the onboard comfort has not added to chassis weight or to the dimensions of the structural sections. Traditional steel construction would have caused a significant increase of the total chassis weight. The use of aluminium on the traditional double wishbone suspension to the front and on a new multilink system to the rear allows the car to absorb in practice any unevenness, in terms of noise and vibrations.

The Ferrari California's signature feature is its retractable hard top (RHT). It is made from aluminium panels and has a cast aluminium weight-bearing structure in Magsimal[®]-59, which has reduced its overall weight and the moving masses involved. This proves to be one of the most important technical advantages of the use of Magsimal[®]-59 in the RHT. In fact, the entire opening/closing cycle can be completed in just 14 seconds and thanks to the improved construction of this modern stowage system, the California's boot space remains extremely generous regardless of whether it is up or down.

The most relevant safety aspect is an ejectable roll-bar to ensure that its occupants are protected should the car overturn. The system is installed behind the backrests of the rear seats and is hidden by the trim of the same. Ejection time is under 190ms.

The car set in Magsimal[®]-59 is mounted to the chassis by the main capote carrier, see fig. 3.1, which is screwed to the bodywork as shown in fig. 3.2. The capote bracket carrier has a structural function as main node on the chassis. At the same time it provides the connections chassis-RTH and chassis-roll bar. The complete assembled mechanism is shown in fig. 3.3, together with the bearing steel levers of the RTH.



Fig. 3.1: the 5-part RTH of the Ferrari F149.



Fig. 3.2: the location of the car set in the F149.



Fig. 3.3 capote carrier and roof bracket assembled on a F149. On the top-right a black-coated side frame is visible.

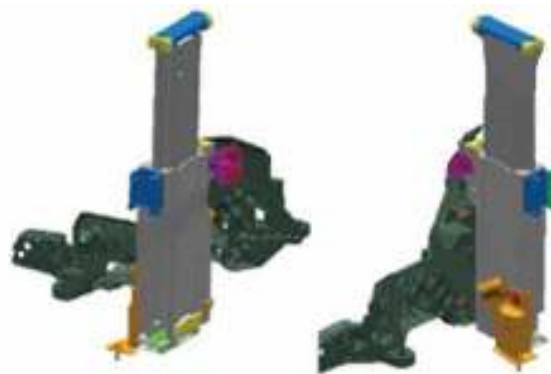


Fig. 3.4: the capote carrier with roll-bar.

Fig. 3.4 shows the capote carrier, which is the biggest part of the car set with its net weight of 3,2 kg and its dimensions of ca. 600 x 350 x 280 mm. The minimum

requirements in terms of mechanical properties for the sand prototypes of this part are the following:

- YTS > 150 MPa
- UTS N.A.
- e% > 1 %

Concerning series production parts, the minimum requirements set by the constructor in terms of mechanical properties have been defined as following:

- YTS > 150 MPa
- UTS > 250 MPa
- e% > 7 %
- HB > 70 HB

Evaluation of tensile properties is carried-out on specimen cut off the region shown in fig. 3.6 according the german DIN 50125 E3x8x35. The general wall-thickness of the carrier is 4 mm, one millimetre higher compared to the side frame and the roof carrier. Rib radii for all ribs are $R=1$ with the exception of the profile of the rib with $R=0,5$ and a progressive thinning with 2° . A cataphoretic black painting with a thickness of 20 to 30 μm has been indicated on the drawing.

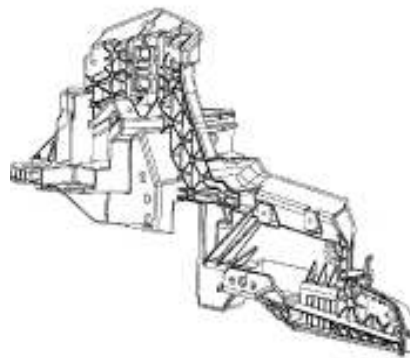


Fig. 3.5: a 3D-sketch of the capote carrier.

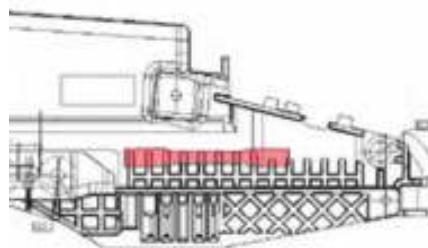


Fig. 3.6: positioning of the tensile specimen of the carrier capote.
Zooming of fig. 3.4.

As the capote carrier is the most requiring part of the car set, the component has been tested under particular conditions with the aim of simulating real operating circumstances. The modalities and parameters have been defined by the car maker in the so-called “Roll-Over” test; a testing bay been designed to this purpose, as depicted in fig. 3.6.



Fig. 3.7: the testing bay designed for the carrier capote on the Roll-Over.

According the indication of the constructor, the carrier capote is mounted on the test bench and connected to the roll bars, as visible in fig. 3.7. The anchorage of the carrier to the roll bar is made by means of three screws M8x65 and washers $\text{Ø } 25 \times 1,5$ mm. The fixing on the bench test is granted by two M10x75 screws with washers $\text{Ø } 35 \times 3,0$ mm. The roll-bars are mounted on the test stand through 1 M8x25 screw with a $\text{Ø } 25 \times 1,5$ mm-washer.

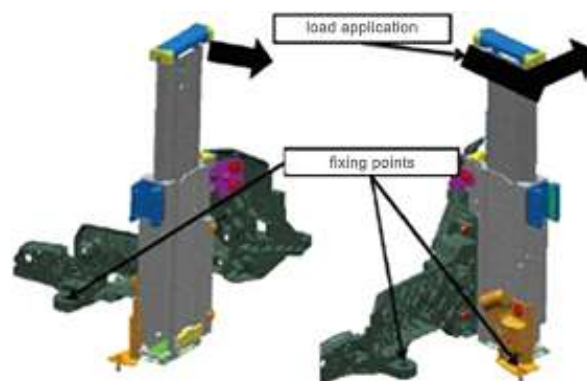


Fig. 3.8: the sketch for load application during the Roll-Over test.

The load is applied by an oil plunger as shown in fig. 3.8; the measurement of the transmitted force is made by a 50 kN-load cell. The test is considered passed and valid if the whole construction withstands an applied force of 15 000 N. This kind of evaluation has the advantage of referring to the performance of a whole casting, by-

passing thus the influences of machining on tensile properties and the transferability of results from specimens to real castings. Fig. 3.9 shows the main bracket roof with a weight of ca. 0,85 kg and dimensions of ca. 230 x 220 x 120 mm and therefore the smallest casting of the car set. The main bracket is screwed on the capote carrier and its main function is granting the rotational movements, and therefore the de-folding and the folding of the two parts of the RTH, while opening and closing.

As for the carrier, the minimum requirements on sand prototypes are the following:

- YTS > 150 MPa
- UTS N.A.
- e% > 1 %

HPDC series parts are required to perform according the following tensile properties:

- YTS > 150 MPa
- UTS > 250 MPa
- e% \geq 8 %

The position for the cutting-off of the tensile specimen is shown in fig. 3.10, according DIN 50125 E3x8x35. General wall-thickness of the part is 3 mm.

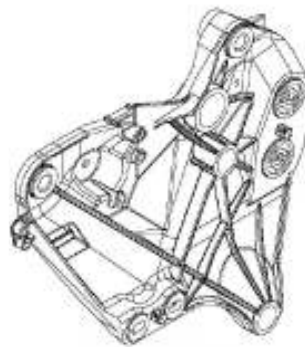


Fig. 3.9: a sketch of the main bracket roof.



Fig. 3.10: positioning of the tensile specimen of the roof main bracket.

Fig. 3.11 shows the side frame which weights around 1,3 kg and has typical dimensions of ca. 740 x 130 x 125 mm. The main function of this casting consists in its tilting, thus granting the opening and closing movement of the back door.

The minimum requirements in the prototyping phase have been specified as following:

- YTS > 140 MPa
- UTS > 240 MPa
- e% > 1 %
- Hardness > 70 HB

On series HPDC production parts, the minimum requirements have been defined as following:

- YTS > 150 MPa
- UTS > 250 MPa
- e% \geq 8 %

The position for the cutting-off of the tensile specimen is shown in fig. 3.12. General wall-thickness is 3 mm; minimum wall-thickness at the end of the ribs must be 2,5 mm. A cataphoretic black painting with a thickness of 20 to 30 μm has been required on this part.



Fig. 3.11: a sketch of the side frame.

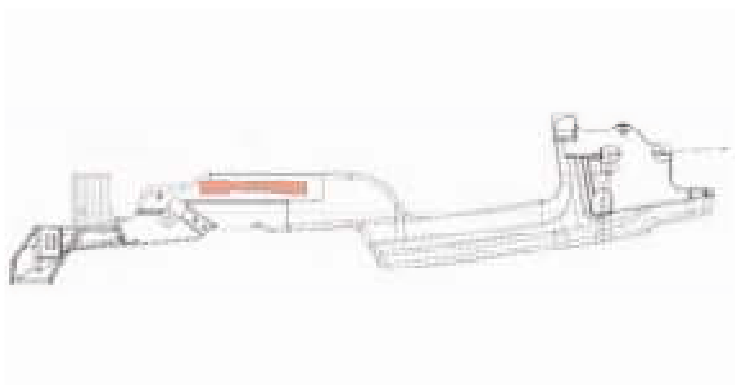


Fig. 3.12: positioning of the tensile specimen of the side frame.

For all parts, the mechanical values are required being satisfied by every batch. The average values of three tensile tests are considered the basis for the evaluation of the components. Two further specimens are allowed, if one of the tensile tests does not reach the characteristic values specified on the drawing. The whole batch has to be scrapped, if the new specimens do not reach the specifications.

As common for automotive applications, parts are serially numbered with LH or RH marking, production date of the batch and material definition.

General tolerances for mechanical processes, i.e. machining, are defined according ISO2768-1; general tolerances for HPDC are defined by GTA 14/5 DIN 1688-4.

Tolerances are given as $\pm 0,5$ mm, radii $R=1$ and draft angles as 2° , if not different specified on the drawing. Roughness has been defined as $R_z=100$ before machining and $R_z=16$ to 25 after machining. The constructor gives full liberty to the die-caster in setting the layout of the parts, their ingates and overflows: no specifications at this extent are given. However, direction of ejection is given for the three parts. Compliance with EU-directives 2000/53/EG and 2005/673/EG is required.

3.3 The manufacturing process

This paragraph deals with the manufacturing of the castings. As the foundry practice adopted for all parts is actually the same, the capote bracket carrier has been taken as reference. Specific notes on the side frame and the roof carrier have been inserted, if necessary.

The managerial side of this core process is presented first. APQP for the implementation of the project, the general activity planning (GAP), process flow chart with references to the control plan and its FMEA are briefly introduced.

The original HPDC layout is described, underlining the necessary modifications to suit Magsimal[®]-59 and their qualitative impact on the outcomes. PPAP parts, pre-series sampling and final HPD-castings have been tested according the constructor's indications: outcomes and results have been summarized. Corrective measures in case on non-compliance with the requirements are described.

3.3.1 Advanced Product Quality Planning (APQP)

A modern approach to activity management provides always a milestone document, called Advanced Product Quality Planning (APQP). The customer establishes in this way a pattern the suppliers have to comply with, allowing in turn a synchronization of all key partners taking part into the supply chain and a uniform levelling of operative sequences at the same time. According to this planning instrument, all involved participants are listed. A team leader is selected to coordinate all suppliers' internal activities and to interface with the customer's project manager. Subsequent build levels - prototypes, pre-series and PSW-parts - and corresponding deadlines for delivery are defined.

The manufacturing process of the bracket carrier capote has been divided into 23 core activities. For each of them, a dedicated file shows the detailed tasks to be done or requirements to be fulfilled; completed activities are filled-out. A status indicator is kept for each core activity and shows its progress in percentage.

The total APQP progress index, expressed in percentage, summarizes all sub-phase indicators, thus reflecting the status of the whole project.

Simultaneously with the APQP, the feasibility of the bracket carrier capote has been evaluated by different functional areas of the supplier. Manufacturing engineering, production control, quality management and purchasing department work together to confirm the feasibility of the profile of requirements. This involves technical specifications, quality inspections and available capacities.

3.3.2 General Activity Planning (GAP)

The general activity planning, GAP, visualizes by means of a Gantt's diagram the core activities leading to the manufacturing of the capote bracket carriers. The detailed GAP is reported for the left-hand casting in fig. 3.13. Phase and sub-phase descriptions, responsible members, lead-times in weeks and deadlines are gathered in a single table, showing activities in parallel processing.

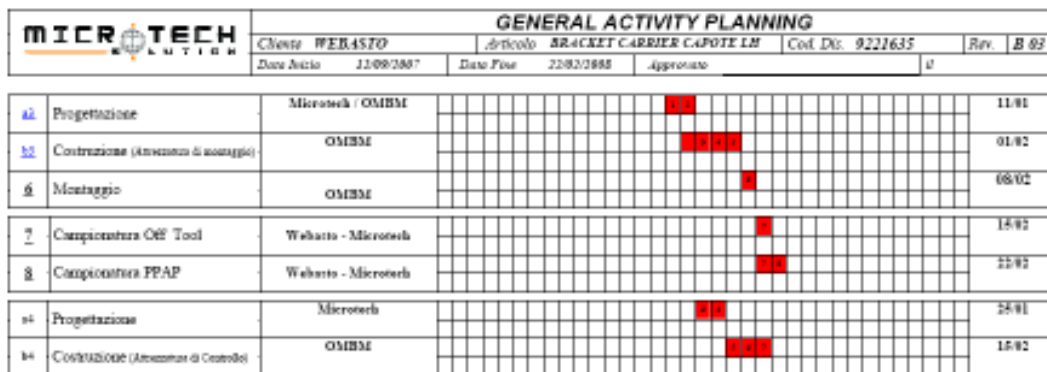


Fig. 3.13 GAP of the capote bracket carrier.

The main activity steps have been scheduled according the following list:

- kick-off
- order to suppliers for HPDC-tooling design and making
- casting process
- order to suppliers for shearing-die and tooling
- shearing
- order to suppliers for machining tooling
- machining
- order to suppliers for assembly tooling
- assembly
- off-tool prototyping
- PPAP prototyping
- order to suppliers for quality control tooling

The planned timeframe for all design activities embraces 24 weeks; calling-up a batch production covers 8 weeks.

3.3.3 Process Flow Chart

The manufacturing of the bracket carrier capote in HPDC includes different phases, from the official order kick-off and raw material inquiry to the final delivery of finished parts by the dispatch department. The logical stream of process is summarized by the so-called process flow chart, which has been zoomed in its main constitutive steps through the use of simplified diagrams. Each of them corresponds to the single operations performed on the castings:

- melting, high-pressure die-casting and press control
- shearing
- sand blasting
- machining
- cataphoretic painting
- packaging

Methods of manufacturing, control procedures and corresponding paperwork are listed in the Control Plan (CP), as well as responsible entities, frequency and recordings. Operations, control levers, methodologies and records are additionally deepened by FMEA, in order to double-check the CP and to provide corrective actions in case of error. A detailed description of the manufacturing process is reported below.

3.3.3.1 Melting, high-pressure die-casting and press control

Operational activities start with the manufacturing of the castings in the foundry. The outline of this first stage is represented in fig. 3.14. The corresponding activities and generated documents are listed in the tab. 3.2. As the casting process has been outsourced, an order for production is formally issued. The die for the bracket carrier capote is called-up from the tooling department and mounted on the press.

Raw ingots of Magsimal[®]-59 are double-checked in their chemical composition and approved for production.

The melting procedure has been originally planned with the typical layout: melting furnace + ladling + maintenance furnace. On the basis of the results of 3.4.1.2 and due to the presence of oxides in the microstructure of the sampled parts, this layout has been changed by the using of a melting furnace feeding directly the press, according fig. 3.15.

Originally, melting have been performed in a 2,5 t-gas-fired melting furnace. The metal has been transferred to a 400 kg ladle and degassed with a N₂-rotor impeller for 5 minutes. After skimming, pouring into a 3 t-maintaining furnace concludes the melting procedure.

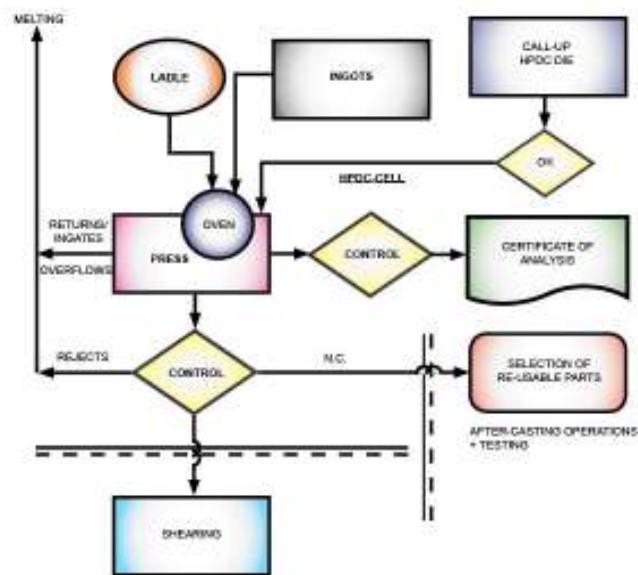


Fig. 3.14: synoptic outline of the melting phase in its original configuration.

The new configuration adopted for series manufacturing has consisted in pre-heating the ingots of Magsimal[®]-59 and melt them into a 3 000 kg hearth gas-fired furnace. The melt has been constantly degassed by blowing pure argon through a lance with porous head; the use of a rotor degassing has not been possible anymore, as the degassing station is a fixed one. The melting/holding furnace has been refilled with the necessary top-up quantity average 1x hour.

Skimming with a special salt for AlMg-alloys has been introduced and afterwards regularly performed; an additional covering has been provided while maintaining the melt overnight.

Casting activities have been carried-out on a double shift of 7 hours, i.e. totally 14 hours/day. Series manufacturing has been carried out with a 50/50 ratio of virgin ingots versus returns. Casting temperature has been set between 720°C and 730°C.

During the start-up phase, a 100 % visual control of the castings has been performed to observe the presence of cracks or deformations; sticking phenomena have been

evaluated on ejectors and steel cores. Press parameters have been recorded; mass of the casting compared to a standard¹ and recorded in a data-sheet as in fig. 3.17. X-Ray controls with a 50 % frequency have been carried out until standard casting conditions have been reached.

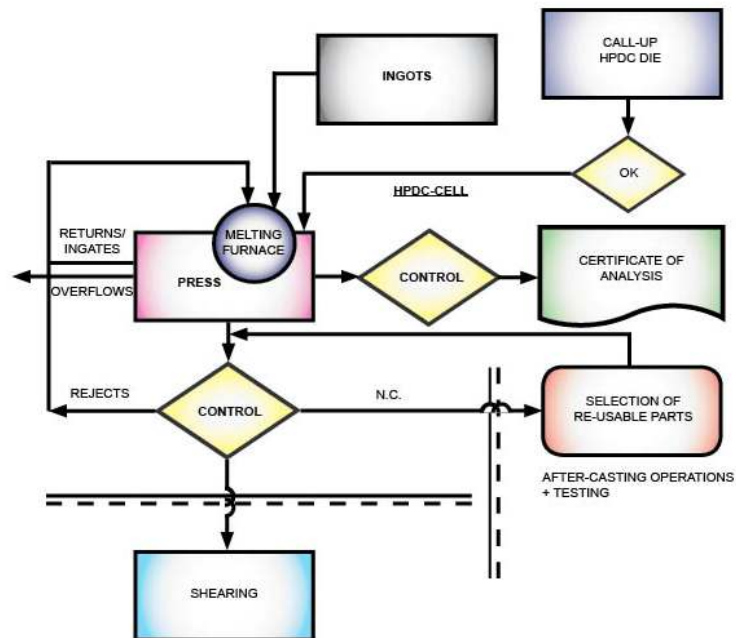


Fig. 3.15: synoptic outline of the melting phase in its final configuration.

As soon as series manufacturing conditions have been accomplished, the chemical composition of the melt has been checked and monitored, in order to guarantee in-spec cast material. Corresponding certificates of analysis have been stored; a 100 % visual control carried out on the parts; X-rays performed with 1/20 frequency; dimensional control has taken place with 1/20 ratio. Sound castings have been approved for the shearing phase; discarded castings correspondently identified and stored until a second melting procedure.

The manufacturing of the castings has been originally planned on a 1100 t-HPDC Idra press, mainly for economical reasons. Theoretically, this would have allowed the production of ca. 640 castings/day with a cycle time of ca. 75 seconds. Due to the reasons presented in 3.4.1.2 real production rates have been recorded around 260 castings/day. Therefore, the decision of shifting to a 1600 t-HPDC-machine has been taken, see fig. 3.16, while achieving real production rates of average 520 castings/day with cycle-times of 85 seconds. In spite of higher hourly operating costs, quality standard levels and stability of the entire process could be guaranteed.

¹ Norma Fiat Auto 9.50305

Die-casting parameters have been set as following:

- $v_1 = 0,2 \text{ m/s}$
- $v_2 = 3,6 \text{ m/s}$
- multiplication at 350 bars for 8 seconds

The die has been maintained closed for 5 further seconds without multiplication, allowing ingate solidification. Die operating temperatures have been recorded between 230-270°C. No vacuum has been used; die-lubrication has been performed using a modern die-lub, originally developed for Mg-HPDC alloys. External and internal lubrication of the shot sleeve by mineral oil has proven to be necessary in order to lower wear while injecting. The castings have been collected by a robot at ejection. A laser control is performed to check dimensional tolerances. No water quenching or water cooling to room temperature has been performed for the reasons presented in par. 3.5 simple air cooling has been adopted.



Fig. 3.16: the 1600 t IDRA machine used for the production of the car sets.

O.F.C.		REGISTRAZIONE AUTOCONTROLLO SU CALIBRO FISSO				CICLO N°	DATA
ESD. ARTICOLO	DESCRIZIONE ARTICOLO	DIMENSIONI		CICLO N°			DATA
	Caricatore	100x100		1000			10/06/16
REF. PRESSI. PRESSI.	FASE ELAVAZIONE			1000			
CARATTERISTICHE DA CONTROLLARE							
N°	CARATTERISTICA DA CONTROLLARE	SOGLIA	TOLLERANZA	TREC	FREEL	TIPO	CONTROLLO
1	mm	0,5	0,1	1000	1000	1000	Visual
 							
REGISTRAZIONE AUTOCONTROLLO							
Pezzi	Data/Turno/Operai	Pezzi	Data/Turno/Operai	Pezzi	Data/Turno/Operai		
1	10/06/16	21	10/06/16	41			
2	10/06/16	22	10/06/16	42			
3	10/06/16	23	10/06/16	43			
4	10/06/16	24	10/06/16	44			
5	10/06/16	25	10/06/16	45			
6	10/06/16	26	10/06/16	46			
7	10/06/16	27	10/06/16	47			
8	10/06/16	28	10/06/16	48			
9	10/06/16	29	10/06/16	49			
10	10/06/16	30	10/06/16	50			
11	10/06/16	31	10/06/16	51			
12	10/06/16	32	10/06/16	52			
13	10/06/16	33	10/06/16	53			
14	10/06/16	34	10/06/16	54			
15	10/06/16	35	10/06/16	55			
16	10/06/16	36	10/06/16	56			
17	10/06/16	37	10/06/16	57			
18	10/06/16	38	10/06/16	58			
19	10/06/16	39	10/06/16	59			
20	10/06/16	40	10/06/16	60			

Fig. 3.17: dimensional control of the carrier on a fixed calibre.

Phase	Operation	Control	Method/Instrument	Records
F 1. 1	Issue of a production protocol	Acceptance of protocol	Production protocol	
F 2. 1	Control and approval raw material	- Certificate of analysis raw material - Correspondence to production protocol	Visual by the operator	- ID card raw material - Certificate of analysis
F 3. (1-2)	Die preparation			
F 4. (1-2)	Die: mounting + settino	Check of Production Order	- Visual by the operator - Production Order List	
F 5. 1	Press parameters	Check inserted press parameters	- Template: press parameters	Press
F 6. (1-3)	Production Start-up	- Check real press parameters - X-ray control	- Visual - X-ray hardware	Control report
F 7. (1-8)	HPDC	Chemical composition	Spectrometer	Certificate of analysis of the melt
		Visual control of castings	Control instructions through comparative pictures	- Batch ID-cards - WARNING Cards
		X-ray control	Spectrometer	Control report
		Dimensional control	- Caliber - Drawing	Control report

Tab. 3.1: tracing documents for melting, HPDC and press control area.

3.3.3.2 Shearing

After cooling to room temperature, the castings have been sheared. A formal order is issued. Shear dies are called-up from stock, mounted and prepared to operation. A 100 % visual control of the castings has been performed on the basis of reference pictures; castings batch numbered, identified by Kanban cards and approved for sand blasting. Distorted or non suitable castings are discarded.

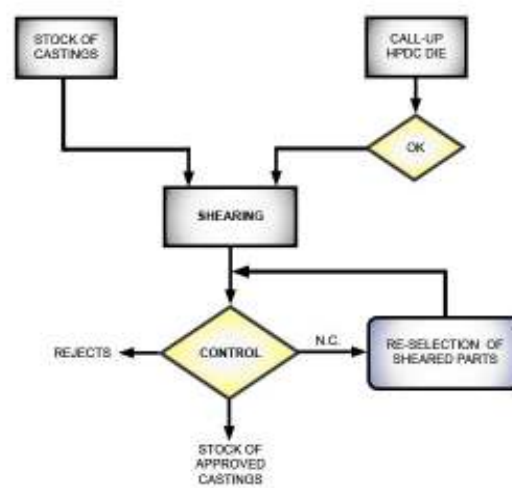


Fig. 3.18: synoptic outline of shearing.

Ingates have been collected separately in marked containers for one additional melting procedure; risers and overflows managed apart and “declassified” for further use, while processing secondary AlSiCuMg-alloys.

Phase	Operation	Control	Method/Instrument	Records
T 1. 1	Issue of a shearing protocol	Acceptance of protocol	Shearing protocol	
T 2. 1	Die preparation		- Software GESPRO 7	
T 3. (1-2)	Die: mounting + setting	Check of Production Order	- Visual by the operator - Production Order List	
T 4. (1-3)	Shearing (Shear press)	Visual control of castings	Control instructions through comparative pictures	- Batch ID-cards - WARNING Cards

Tab. 3.2: tracing documents for shearing.

3.3.3.3 Sand blasting

After shearing, flashes have been manually removed, if necessary. A formal order is issued for sand blasting; blasting parameters have been defined in 10 minutes with green sand fewer than 2 bars pressure. Sand-blasting has been carried out indoor by the foundry.

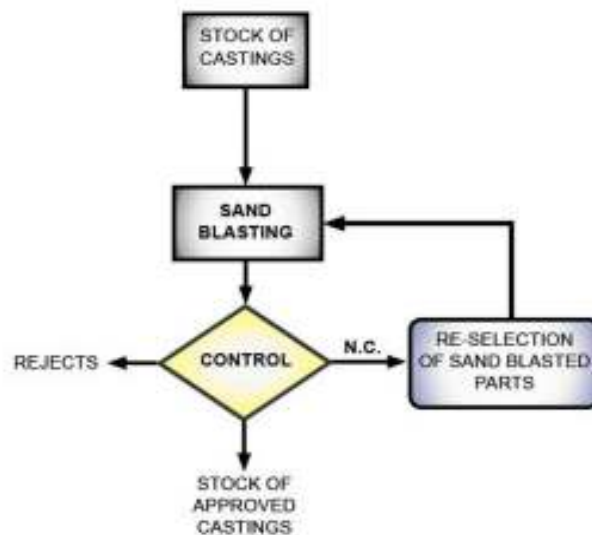


Fig. 3.19: synoptic outline of sand blasting.

Parts have been 100 % visually checked after treatment: approved ones identified for machining; discarded castings can either be treated again or sent to the remelting area.

Phase	Operation	Control	Method/Instrument	Records
S 1. 1	Issue of a sand blasting protocol	Acceptance of protocol	Sand blasting protocol	Delivery template
S 2. 1	Sand blaster parameters	Visual by the operator	Visual (Supplier requirements)	Supplier template
S 3. (1-2)	Sand blasting (Sand blasting machine)	Visual control of castings	Control instructions through comparative pictures	- Batch ID-cards - WARNING Cards

Tab. 3.3: tracing documents for sand blasting.

3.3.3.4 Machining

Machining operations have been outsourced. A formal order is therefore issued; the CNC centre equipped and preset; dimensional tolerances of the tooling have been double-checked by comparators. The brackets have been machined on twelve different positions, first visually controlled through reference pictures and subsequently with calibres and a micrometer, on the basis of the CAD drawings. 3D-dimensional controls are carried out to control functional and critical features, marked respectively as YS (1 to 62) and YC (1 to 63) on the drawing. Quotas and threads tolerances, eventual defects, such as discovering of under skin porosities, are marked. A control report is issued.

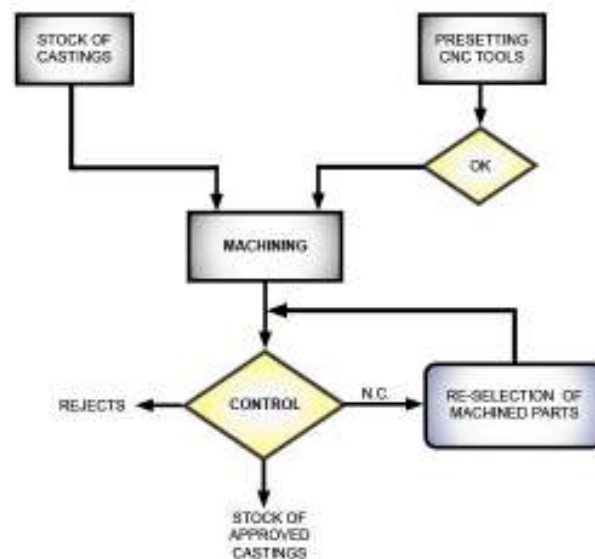


Fig. 3.20: synoptic outline of machining.

Fig. 3.21: records of the machining operations.

Phase	Operation	Control	Method/Instrument	Records
LM1. 1	Issue of a machining protocol	Acceptance of protocol	Machining protocol	
LM2. (1-2)	Tooling: mounting + setting	Check of Machining Order	- Visual by the operator - Machining Order List	
LM3. (1-2)	CNC: mounting + setting	Visual by the operator Dimensional by the operator	Maintenance plan CNC - Comparators - Tool drawing	
LM4. (1-7)	Machining (CNC)	Visual control of castings Dimensional control	Control instructions through comparative pictures Control instructions through comparative pictures - Caliber - 3D Measurements - Drawing	- Batch ID-cards - WARNING Cards

Tab. 3.4: tracing documents for machining.

After machining, castings are identified and approved for painting.

3.3.3.5 Cataphoretic painting

Cataphoretic painting has been designed for the carrier capote and for the side frame; the roof carrier is mounted on the RTH without additional protective coating. The varnishing process has been outsourced; a formal order is therefore raised to the supplier. Cycle parameters are preset: a first washing has been performed in distilled water, a second one in demineralised water; pH values and electrical conductivity recorded after each washing. Painting cycle has been carried out in 180 seconds under control of temperature, pH and electrical conductivity. Two further washings have been performed before baking the coating for 50 minutes at 165-185°C. Baking curve has been stored for each batch and black painted castings evaluated at the light bench with a 100 % frequency by comparison to a sample part, to individuate non-uniformities or bubbling of the coating.

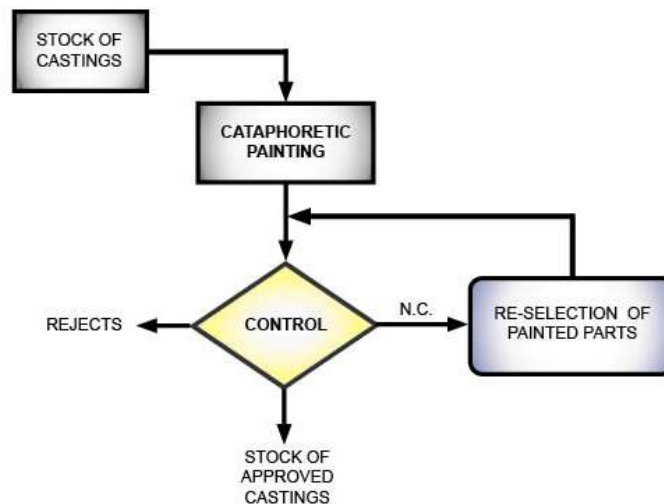


Fig. 3.22: synoptic outline of cataphoretic painting.

The layer thickness is measured on one part per batch, according the Fiat Norm 9.55842 (§ 2.4). The resistance and strength of the layer is determined with the so-called “pencil test” according ASTM D 3363 and the Fiat Norm 9.55842 (§ 2.5). The corrosion resistance is determined in a 120 hours saline suspension test, according ISO 3768 and the Fiat Norm 9.55842 (§ 2.10.1) with a frequency of 1 casting/year. Resistance to moisture is carried out according to ISO 6270 / DIN 50017 with a frequency of 1 casting/year. Painting certificates have been issued for every mentioned test. Approved castings are ready for packaging.

Phase	Operation	Control	Method/Instrument	Records
V 1. 1	Issue of a c. painting protocol	Acceptance of protocol	Cataphoretic painting protocol	
V 2. (1-5)	Cataphoretical painting	Visual control of castings	Control instructions through comparative pictures	- Batch ID-cards - WARNING Cards
		Check of the cataphoretic layer thickness (15-20 µm)	Thickness measurement	Certificate of cataphoretic painting
		Check of the mechanical resistance of the cataphoretic layer	Pencil hardness test (according to ASTM D 3363)	Certificate of cataphoretic painting
		Check of the corrosion resistance of the cataphoretic layer	Salt spray test (according to ISO 3768)	Certificate of cataphoretic painting
		Check of the moisture resistance of the cataphoretic layer	Hygrometer (according to ISO 6270/DIN 50017)	Certificate of cataphoretic painting

Tab. 3.5: tracing documents for cataphoretic painting.

3.3.3.6 Packaging

Parts qualitatively matching the requirements are set ready for shipment. The completed technical paperwork is gathered and castings stored in containers, according to their packaging data sheets. Supplier data, part name, part number, yearly delivered castings, tare and net weight and department of destination are reported. The layout of the castings in the boxes, quantity, dimensions and level numbers are specified. A visual control of the final packaging is made before dispatch to forwarder.

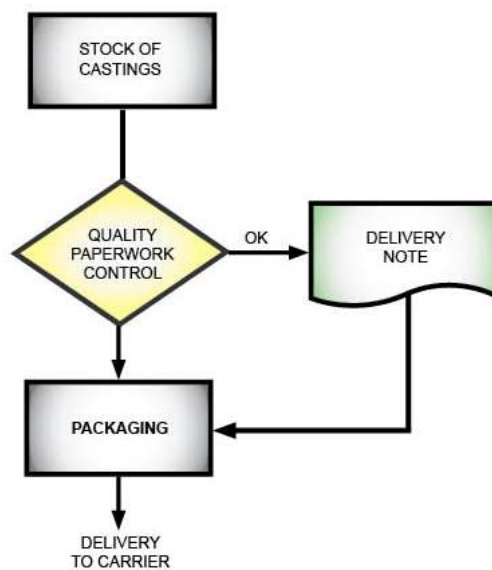


Fig. 3.23: synoptic outline of packaging.

Phase	Operation	Control	Method/Instrument	Records
I 1.1	Issue of a packaging protocol	Acceptance of protocol	Packaging protocol	
I 2. (1-2)	Packaging	Visual control of castings	- Control instructions through comparative pictures - Packaging manual	- Batch ID-cards - WARNING Cards
I 2. (1-2)	Acceptance control	Acceptance control		
I 3. 1	Dispatching	Delivery note		Certificate

Tab. 3.6: tracing documents for packaging.

3.4 Evaluation of the castings

3.4.1 Capote carrier bracket

The following paragraphs present the testing procedures of prototypes, samplings and pre-series parts, until the final approval for series production of capote carrier brackets. The results of testing, characterization and key modifications introduced into the carriers are presented according to their chronology, in order to show the logical steps which have brought from the very first product to its final configuration.

3.4.1.1 Prototyping

Prototypes of the carrier capote have been cast in sand in order to perform a first basic characterization of the metal and a check of the dimensional tolerances of the castings. The chemical composition of the prototype complies with the specification of Magsimal[®]-59. Measured values are reported in tab. 3.7.

[%]	Si	Fe	Cu	Mn	Mg	Zn	Ti	Be	Others
Min.	1,8			0,5	5,0				
Max.	2,6	0,2	0,05	0,8	6,0	0,07	0,20	0,004	0,2
Prototype	2,4	0,1	0,05	0,5	5,6	0,05	0,1	N.A.	Ni 0,01 Ga<0,1

Tab. 3.7: chemistry of the first sand prototypes.

YTS	120 MPa
UTS	120 MPa
e%	1 %
HBW _{2,5-62,5}	66 HB

Tab. 3.8: results of the tensile test according UNI EN 10 002.

Hardness has been tested with a round penetrator of 2,5 mm diameter and a load of 62,5 N. The value reported in tab. 3.8 is the average of three measurements.

The mechanical properties have been tested according to DIN 50125 E4x8x35. Results have been reported in tab. 3.8. As expected, the tensile values are very low, as consequence of the solidification conditions. No deformation after yielding of the cast could be observed. Fracture was immediate.

3.4.1.2 First sampling

Capote carriers have been sampled a first time to verify and evaluate the behaviour of the final component in high-pressure die-casting. The chemical composition has been found complying with the specification of Magsimal[®]-59. Measured values are reported in tab. 3.9.

[%]	Si	Fe	Cu	Mn	Mg	Zn	Ti	Be	Others
Min.	1,8			0,5	5,0				
Max.	2,6	0,2	0,05	0,8	6,0	0,07	0,20	0,004	0,2
Samples	2,5	0,2	0,05	0,8	6,0	0,07	0,2	N.A.	Ni<0,1 Ga<0,1

Tab. 3.9: chemistry of the samples.

The whole part has been tested twice, according the modalities described in 3.2. The values recorded by the 50 kN load cell are reported in tab. 3.10 and show that both parts failed.

Carrier 1	7 500 N
Carrier 2	13 000 N
Minimum required	15 000 N

Tab. 3.10: failed test for the capote carriers in Magsimal[®]-59.

As the Carrier 1 has shown the worst results in terms of load bearing, a closer look on the casting has been taken. The carrier showed three fracture positions: position A corresponds to the area where the casting is fixed to the roll bar in its lower part; position B is located where the area for tensile testing has been placed; position C corresponds to the area where the casting is fixed to the roll bar in its upper part. An overview of the broken carrier and of positions A, B, C is shown in fig. 3.24.



Fig. 3.24: the carrier 1 with its three fractures (up-left). Fracture A on the lower anchoring point to the roll-bar (up-right), fracture B in the area where tensile bars are cut-off (low-left), fracture C on the upper anchoring point to the roll-bar (low-right).

The mechanical properties of the carrier have been tested by cutting-off a tensile sample in the area B, according to DIN 50125 - geometry E4x8x35 - and the drawing, with the following results:

YTS	132 MPa
UTS	132 MPa
e%	0-1 %
HBW _{2,5-62,5}	74 HB

Tab. 3.11: results of the tensile test according UNI EN 10 002.

The sample cracked without showing any ductile behaviour, presenting mechanical properties far under the requirements.

The fracture surfaces have been investigated. Macros taken with a stereo microscope on section A and C show the presence of oxides, see fig. 3.25 and 3.26. Fracture B shows a flat crack, which can be traced-back to a compression load, see fig. 3.27. Micrographs on section B confirm the strong deformation of the microstructure, see fig. 3.28 and 3.29.

Additionally, looking to the eutectic structure of fig. 3.30, an efficiency of just 10 % ca, can be observed, see chapter 2. A presence of P has not been detected through the quantometer, as the P channel is not present, but a pollution by this element has been taken into account.



Fig. 3.25: section A.



Fig. 3.26: section C.



Fig. 3.27: section B.



Fig. 3.28: section B; the metal has been visibly compressed. HF 1 %.



Fig. 3.29: section B; the metal has been visibly compressed. HF 1 %.

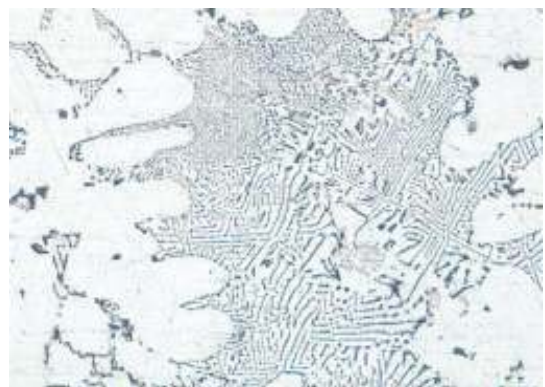


Fig. 3.30: section B, 200x, HF 1 %.

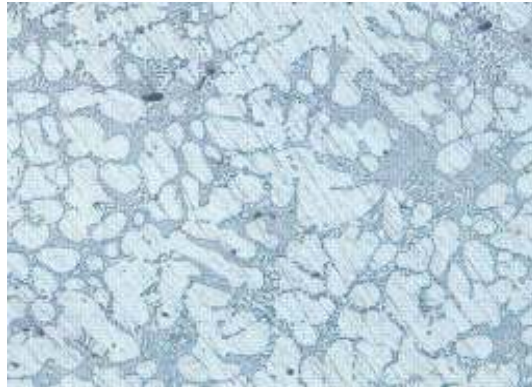


Fig. 3.31: micrograph of section B, 100x, HF 1 %.

In order to improve the quality of the melt and lower the oxide content, some countermeasures have been taken concerning the melting and the handling of the metal, compatibly with the available solutions. In particular:

- melting procedure has been changed. Transferring of the molten aluminium has been eliminated, preferring melting and maintaining the bath next to the HPDC-cell. See 3.3.3.1;
- skimming and drossing by means of special salts for Magsimal[®]-59 has been introduced;
- degassing with argon has been introduced, while substituting N₂. A porous-headed lance must be adopted, as the rotor degassing station could not be moved;

Modifications of the capote carrier have been suggested both in the geometry of the part itself and on the HPDC-die, in order to solve the problems arising while sampling for the first time. The gray shadowed areas of fig. 3.32 show the proposed modification of the part. The fixing point to the car chassis has been lightened, in order to limit the formation of shrinkages (left); the fin facing the slide “rounded” (right.)

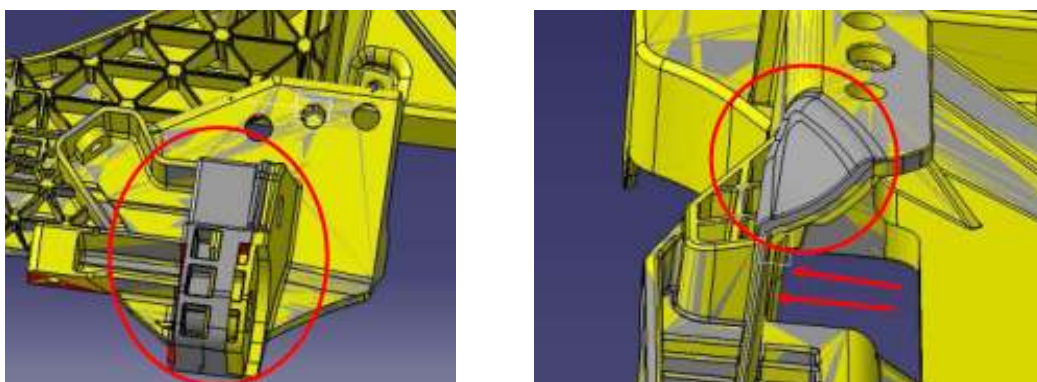


Fig. 3.32: suggested geometry modification of the capote carrier.

The connection fin next to the section “A”, where the prototype broke, has been increased in its thickness, in order to strengthen it, see fig. 3.33. Higher connecting radii ($R=2$) have been proposed for the area of fig. 3.34, 3.35 and 3.36, where sticking to the die has been observed. The introduction of a fin has been proposed on the ring of fig. 3.37, connected to the chassis of the car.

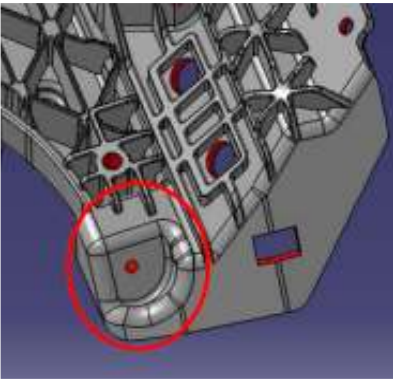


Fig. 3.33: suggested geometry modification next to “A”.

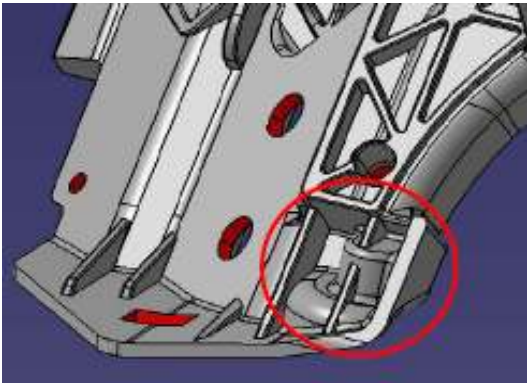


Fig. 3.34: suggested geometry modification where sticking has been observed.

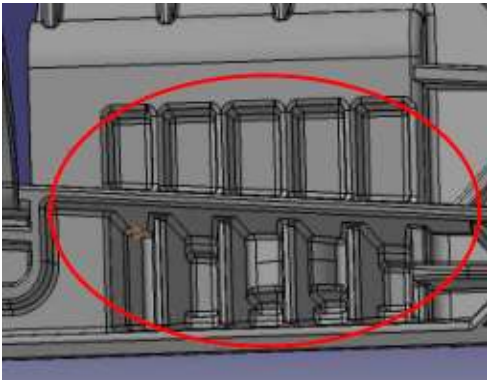


Fig. 3.35: suggested geometry modification in the finning.

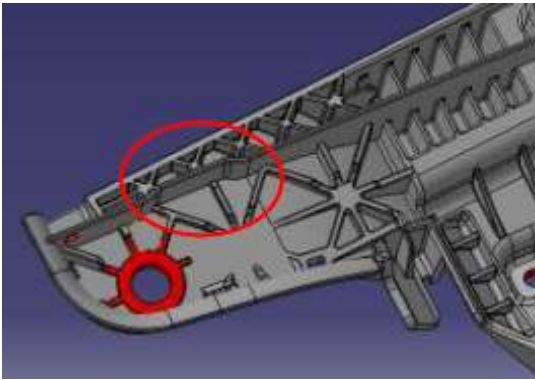


Fig. 3.36: suggested geometry modification in the wing area.

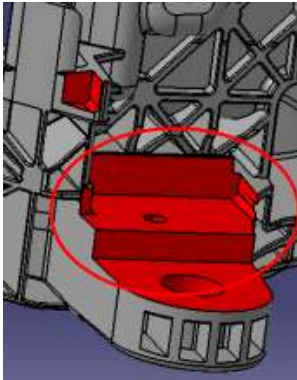


Fig. 3.37: suggested geometry modification on the main ring.

The die has been corresponding modified after confirmation of these changes. The revisions have been carried out on both dies: RH and LH capote carrier. The steel cores of position 1, fig. 3.38, have been levelled to the parting line. The openings marked with “2” and the hole of position “4” have been provided with a 0,5 flash, in order to maintain the front of melt flow compact while casting. Forming flashes have been eliminated on the profile marked by the dotted line in position 3.

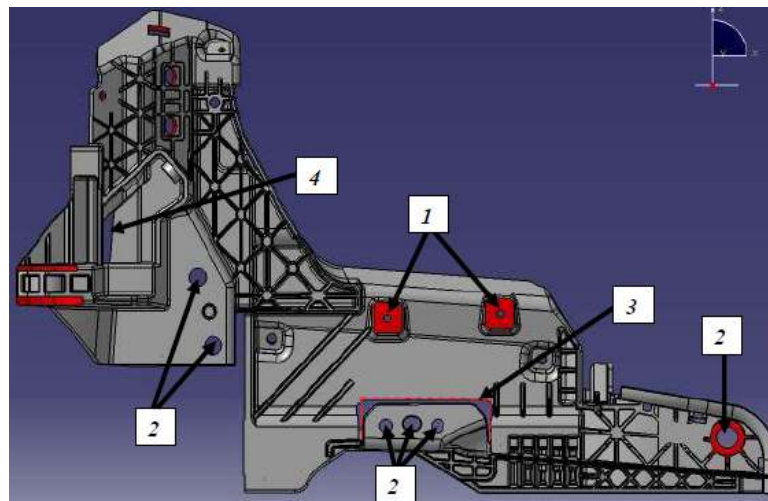


Fig. 3.38: introduced modifications on the capote carrier.

At the centre of the steel cores marked with “2” in fig. 3.39 a conical overflow has been inserted, with an ingate of 1,2 mm. This has been done in order to improve the quality of the casting on the two rings, where shrinkages have been observed and expected. A 0,5 mm thick connecting flash has been introduced in position 3 of fig. 3.39.

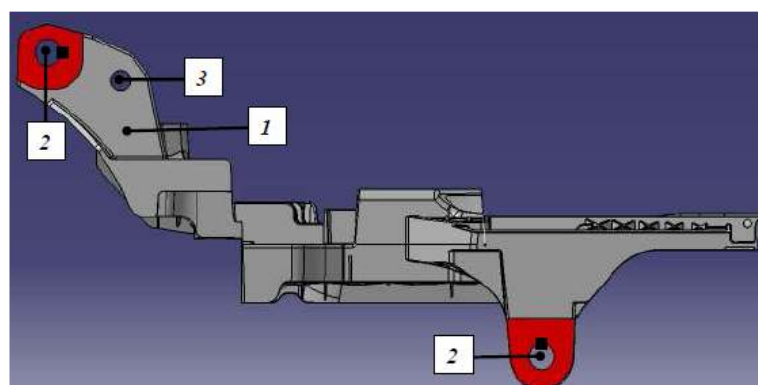


Fig. 3.39: introduction of flashes and steel cores.

The overflow, designed in the area “1” of fig. 3.40 has been enlarged and the ingate increased to 1,8 through all the circular connection profile.

A 5 mm-thick and 4,5 mm-high fin has been introduced in area 2, with a die inclination of 2° , in order to feed better the ring. Ribs of fig. 3.41 have been increased in their die inclination and corresponding surface polished to diminish sticking phenomena.

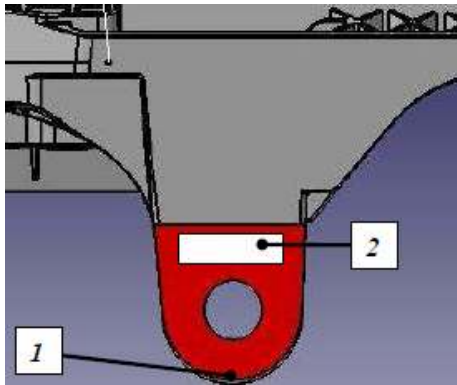


Fig. 3.40: feeding rib on the ring.

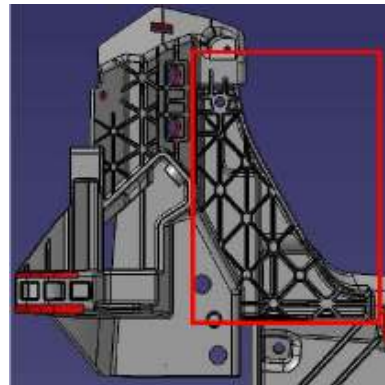


Fig. 3.41: increasing die inclination.

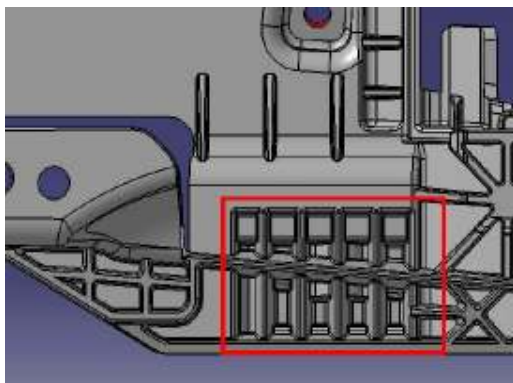


Fig. 3.42: increasing die inclination.

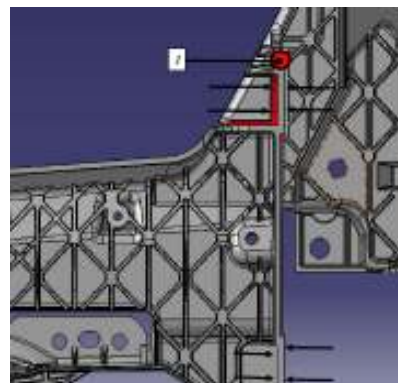


Fig. 3.43: insertion of a ejector.

The same operations have been performed on the fins of fig. 3.42. An ejector has been inserted in position 1 of fig. 3.43, in order to prevent deformations during extraction of the part.

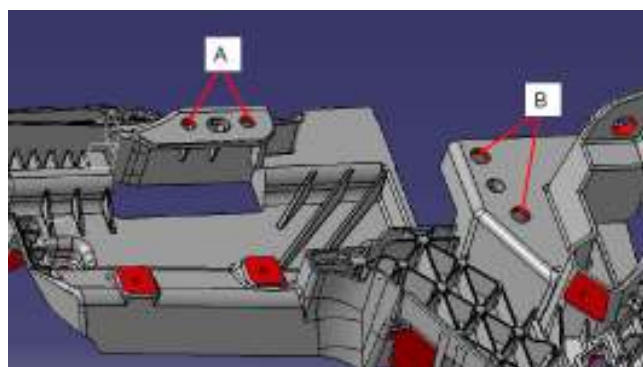


Fig.3.44: introduction of flashes and steel cores.

The steel cores “A” and “B” of fig. 3.44 have been modified in their diameter respectively to $8,85 \pm 0,3$ mm and $10,60 \pm 0,3$ mm. Additionally, all remaining overflows have been increased at their ingate to 1,6 mm and the critical area where sticking has been observed polished.

3.4.1.3 Second sampling

After changing the melting procedure and modalities as specified in the previous paragraph, a second sampling in HPDC have been carried out. Chemistry and mechanical properties of the capote carries have been evaluated.

[%]	Si	Fe	Cu	Mn	Mg	Zn	Ti	Be	Others
Min.	1,8			0,5	5,0				
Max.	2,6	0,2	0,05	0,8	6,0	0,07	0,20	0,004	0,2
Measured (1)	2,3	0,1	0,05	0,6	6,0	0,06	0,1	N.A.	Ni<0,05 Ga<0,1
Measured (2)	2,5	0,14	0,02	0,73	5,50	0,01	0,048	0,004	Ni<0,05

Tab. 3.12: the chemical composition of the second sampled carriers.

The tolerances for Magsimal[®]-59 are respected. Mechanical properties and hardness have been evaluated as average of three tests, with the following results:

YTS	188 MPa
UTS	255 MPa
e%	8 %
HBW _{2,5-62,5}	98 HB

Fig. 3.13: results of the tensile test according UNI EN 10 002.

Requirements are therefore fulfilled. As from the results of the first samples the main stressed areas have been found on the connections of the roll bar, a pull-out test of the screw thread has been performed. The screw thread of section A, see 3.4.1.2, has been tested on a LH carrier and has resisted beyond the required 15 000 N, see tab. 3.14.

Thread	Test temperature [°C]	Force to crack [N]	Fail/pass [N]
M8x1,25	20	20 050	15 000

Tab. 3.14: Results of the pull-out test.

The components have been finally tested on the bench, according to the modalities of 3.2. However, the testing bay construction has been modified by fixing the roll bar on a steel rod and mounting the load cell and the oil plunger on a steel column. The original construction and the fixing points of the capote carrier on the roll-bar of a real F149 are shown in fig. 3.45 and 3.46.



Fig. 3.45: the fixing of the carrier on the roll bar of a F149 RTH.



Fig. 3.46: the fixing of the carrier on the roll bar of a F149 RTH.

The details of the testing facility are to be seen in fig. 3.31 to 3.37. The maximum measured load has been of 14 040 N, after which a strong deformation of the mounting link has been observed. The screw threads on the roll-bar have been broken, as well as the whole bearing bush, see fig. 3.52. The roll-bar suffered of heavy distortions which brought to the breaking of the lower fixing point to the test bench, see fig. 3.51. No damage, deformation or cracks have been noticed on the carrier. The test on the carrier could have reached higher values if the testing bench had resisted to the applied loads.



Fig. 3.47: the testing bay before testing.



Fig. 3.48: final configuration of the testing assembly after the test.



Fig. 3.49: the bearing bush before the test.



Fig. 3.50: the connection carrier-roll bar after the test. Heavy deformation is visible.



Fig. 3.51: screw and threads on the roll-bar after testing.



Fig. 3.52: the bearing bush after testing.



Fig. 3.53: broken fixing point roll bar to test bench.

Therefore, it has been decided to repeat the test with new carriers. Under the same conditions, the maximum recorded load has been 16 850 N, at which no failure could be detected on the carriers. The test has been interrupted due to the fact that the end of the 150 mm piston stroke was reached. As the registered load was superior to the requirements, the test has been considered passed and the components approved.

In order to optimize the quality of the castings, further modifications have been introduced on the die. The steel core “1” of fig. 3.54 has been reduced of 1 mm on its profile, in order to give some more machining allowance. The same operation has been made with the passing hole “3”. Tamping steel cores have been introduced and levelled to the die. Opening marked with “2” have been eliminated and the holes have been obtained by machining. The openings marked with “1” and “2” in fig. 3.55 have been modified at the same extent, eliminating 2 mm of the steel cores in order to give more allowance.

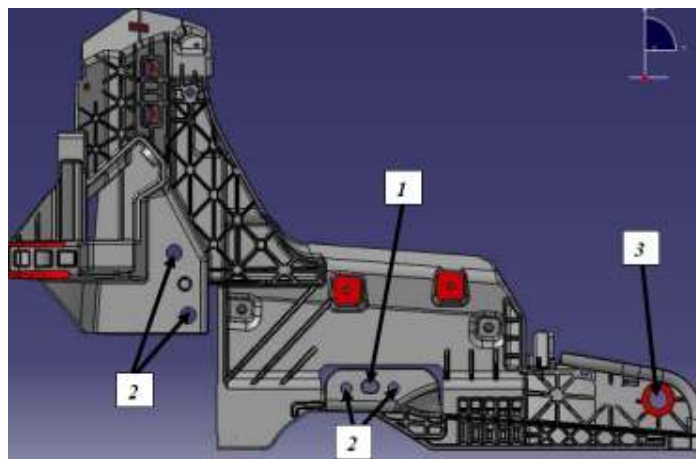


Fig.3.54: modifications after the second sampling. Capote carrier.

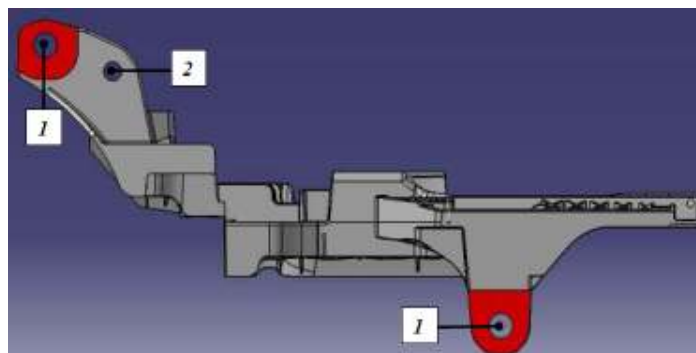


Fig.3.55: modifications after the second sampling. Capote carrier.

The final customer has decided to slightly modify the geometry of the component, as presented in fig. 3.56.

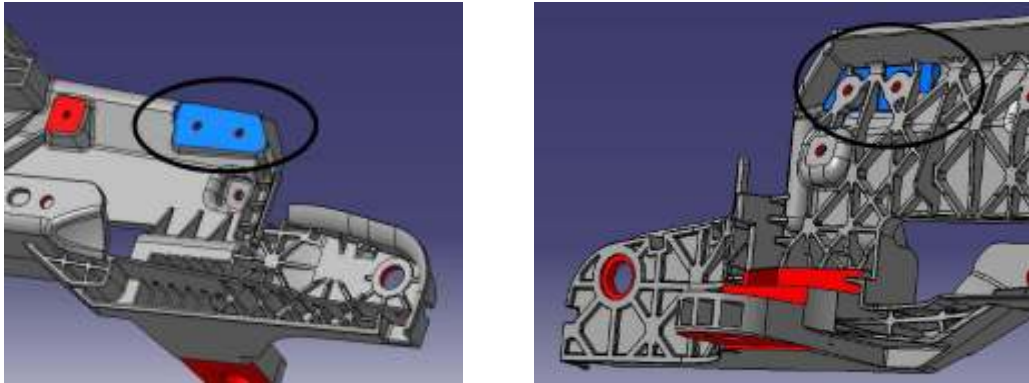


Fig.3.56: modifications on the capote carrier.

Connecting radii have been augmented to $R=3$ in the red-circled areas of fig. 3.57, where sticking phenomena are visible and sensible.

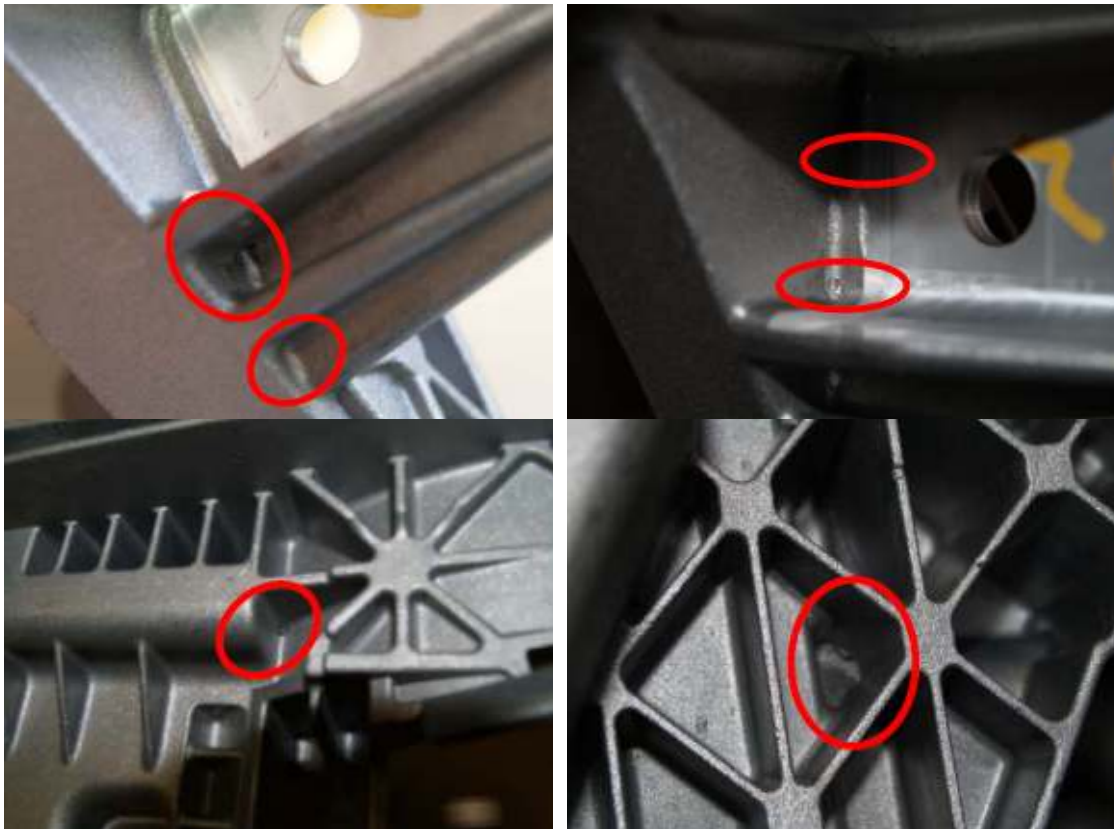


Fig.3.57: increasing die inclination.

Finally, the dimensional control of second sampling has been carried out and missing tolerances indicated. The closing and coupling of the moving and fix die has been double-checked as the formation of flashes on the parting line has been observed.

3.4.1.4 Third sampling (pre-series parts)

After the carrying out of these changes, a third and final sampling, called pre-series sampling, has been cast. As usually, chemistry and mechanical properties of the capote carriers have been evaluated.

[%]	Si	Fe	Cu	Mn	Mg	Zn	Ti	Be	Others
Min.	1,8			0,5	5,0				
Max.	2,6	0,2	0,05	0,8	6,0	0,07	0,20	0,004	0,2
Measured (LH 1)	2,3	0,2	0,05	0,7	5,2	0,05	0,08	N.A.	Ni<0,05 Ga<0,1
Measured (LH 2)	2,3	0,14	0,05	0,7	5,7	0,05	0,10	0,004	Ni<0,05
Measured (RH 1)	2,6	0,2	0,05	0,7	5,8	0,05	0,07	-	Ni<0,05
Measured (RH 2)	2,4	0,2	0,05	0,7	5,1	0,05	0,09	-	Ni<0,05

Tab. 3.15: the chemical composition of the pre-series carriers.

Two capote carriers per batch and both dies, LH and RH have been tested, as this final sampling has been considered representative of the series manufacturing castings. The chemical tolerances for Magsimal[®]-59 are respected. Tensile samples have been cut-off out and tested according the modalities of par. 3.2.

YTS	150 MPa
UTS	248MPa
e%	8,8 %

Tab. 3.16: results of the tensile test according UNI EN 10 002 on a third sampling RH capote carrier.

Mechanical properties have been evaluated as average of three tests, both on LH and RH capote carrier brackets. The results are reported in tab. 3.16 and tab. 3.17. The requirements have been fulfilled and the third sampling has been released for series manufacturing.

YTS	179 MPa
UTS	246MPa
e%	8,9 %

Tab. 3.17: results of the tensile test according UNI EN 10 002 on a third sampling LH capote carrier.

As from the results of the first samples the main stressed areas have been found on the connections of the roll bar, a pull-out test of the screw threads has been performed. For the third sampling this procedure has been applied to a larger extent and has involved nine different threads, marked with letters from A to I in fig. 3.58.

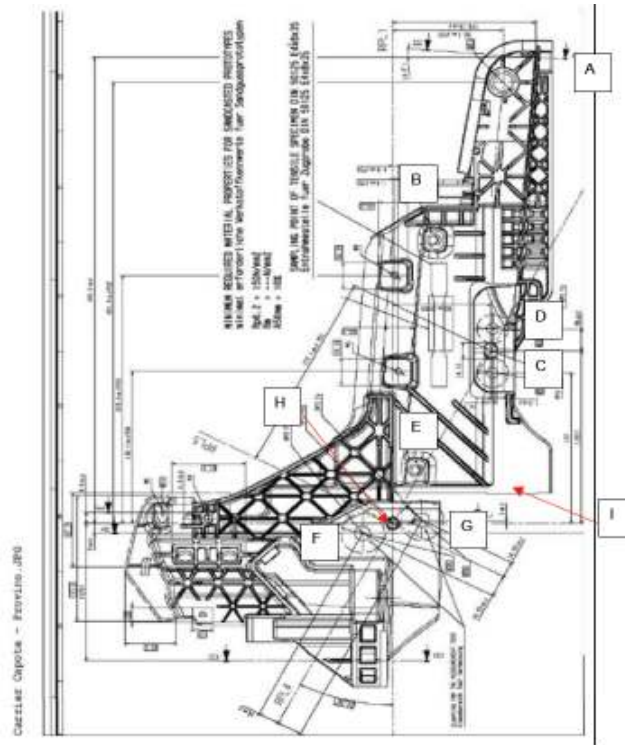


Fig. 3.58: threads tested to pull-out.

The tests have been performed on both RH and LH capote carriers and have been summarized in tab. 3.18. and 3.19 respectively.

Position	Load [N]
A	20 650
B	675
C	1 800
D	1 375
E	500
F	1 125
G	1 675
H	1 575
I	1 950

Tab. 3.18: pull-out results for threads A to I. Third sampling, RH capote carrier.

Position	Load [N]
A	17 600
B	1 875
C	1 600
D	2 325
E	1 300
F	3 100
G	3 400
H	2 100
I	1 400

Tab. 3.19: pull-out results for threads A to I. Third sampling, LH capote carrier.

The final customer has set requirements just on the thread corresponding to position A of fig. 3.58, with a minimum required value of 15 000 N. LH and RH carriers have therefore passed the test. As well as threads, eight nut and bushes with steel inserts have been designed into the bracket, in order to allow an easy assembly of the parts. They have been marked with letters A to H and a torsional moment has been applied on them, in order to determine at which moment the inserts decouple from the casting and turn. A USAG beam type torque wrench with an applicable torque of 10 to 50 Nm has been used. The instrument has a tolerance of $\pm 4\%$; the indicator bar remains straight while the main shaft bends proportionally to the force applied at the handle. The hexagonal head of the screw has been into contact with the raw casting in Magsimal[®]-59.

The results of the torque test with corresponding minimum required values have been reported in tab. 3.20.

Insert	Measured torque [Nm]	Min. required torque [Nm]
A	N.A.	40
B	> 50	40
C	30	40
D	35	40
E	35	20
F	35	20
G	25	10
H	15	10

Tab. 3.20: torques measured on the steel inserts of the carrier capote.

Finally, the castings have been observed under X-rays to evaluate the presence of casting defects. Micro-shrinkages have been detected in many areas of the capote carrier, but not considered critical to the performance extent.

The most significant shrinkages have been taken into account into details and corresponding countermeasures have been adopted. Shrinkages have been expected, looking to the filling simulation done with PROCAST, see par. 3.5.3.

3.4.1.5 Series manufacturing die

Although the third sampling has been approved for series manufacturing, proposal of improved design has been continuously provided, in order to prevent critical situations and to extend die-life.

The areas defined as “critical” in fig. 3.59 has shown sticking phenomena on the die and despite the increased lubrication, the sticking has not been completely eliminated, as the fins are located in a very unfavourable position.

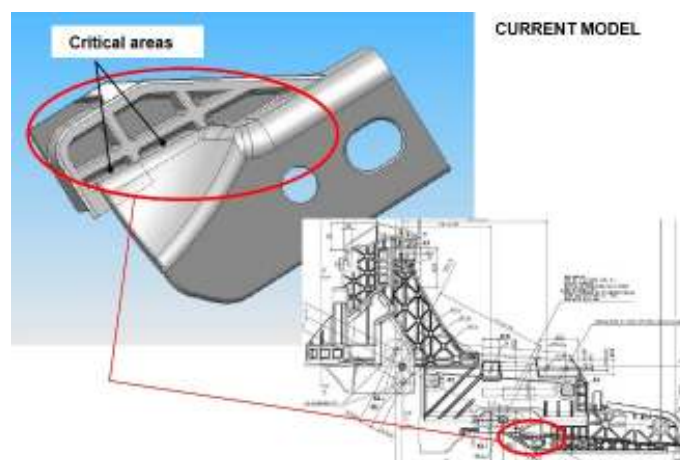


Fig. 3.59: critical area of the carrier capote.

The proposed solution is presented in fig. 3.60 and consists in moving the finning two millimetres under the current location. In this way, the metal has a more favourable filling and the connection to the main fixing plate is improved.

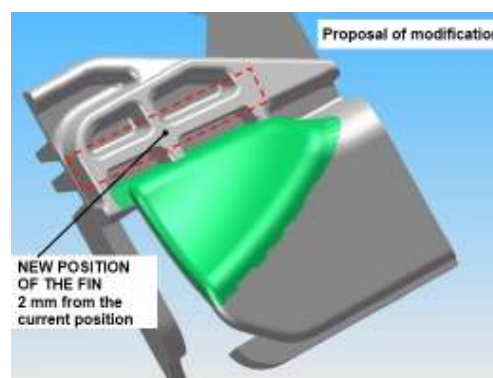


Fig. 3.60: proposed solution of the carrier capote.

Another suggested improvement is shown in fig. 3.61, on the fin circled in red. As it broke occasionally during ejection of the casting, a proposal of increasing the connecting radii to 1,5 to 2 millimetres has been made.

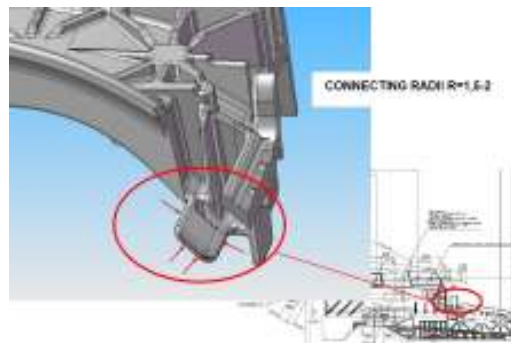


Fig. 3.61: proposed connecting radii.

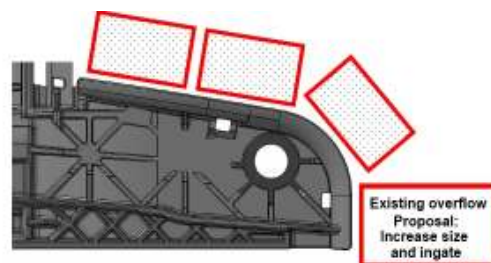


Fig. 3.62: overflows on the capote carrier.

The overflows of fig. 3.62 have been increased in their size and ingate, in order to improve as much as possible the quality of the casting in its “closed wing” and around the fixing point. Die air vent evacuation has been provided a well. The steel cores, introduced to close the two passing holes of fig. 3.63, have been levelled to the casting plane, as a slight unevenness has been observed. The height of the planes of the finning in fig. 3.64 has been brought at the same level as well.



Fig. 3.63: casting defect.



Fig. 3.64: casting defect.

3.4.1.6 Protection from cataphoretic painting and machining

In order to protect the threads from the cataphoretic painting process, covering plugs have been introduced in the areas marked in fig. 3.67.

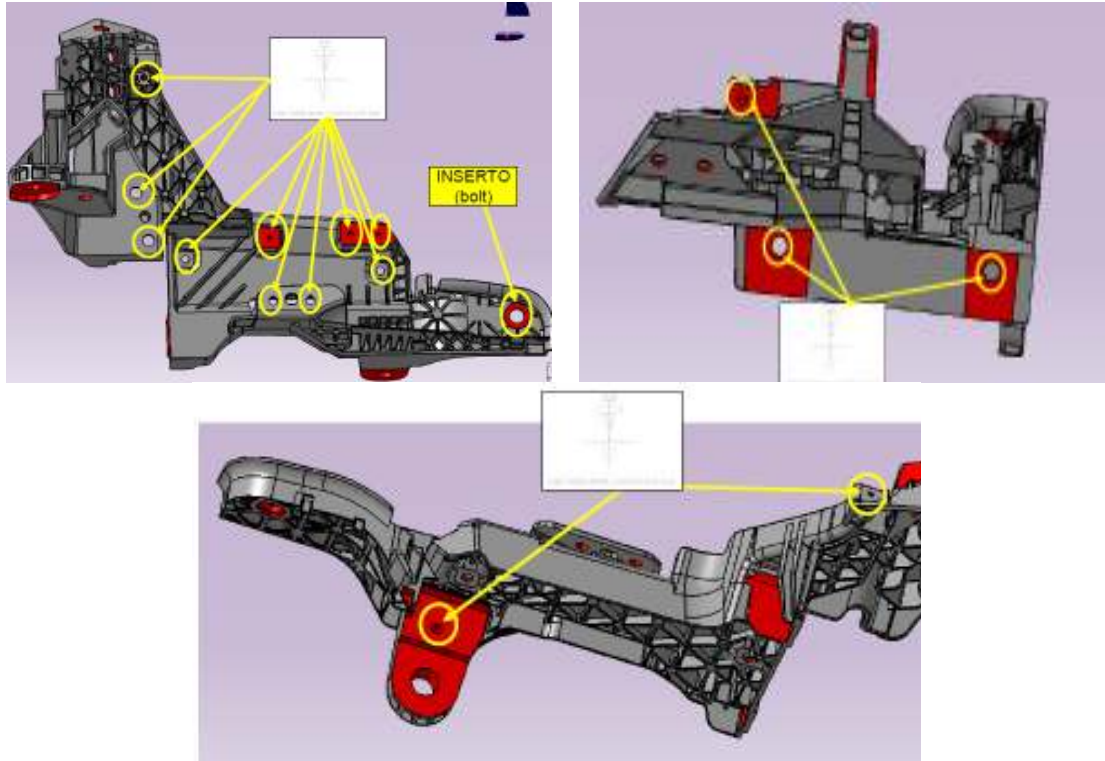


Fig. 3.67: protected threads. Plugs have been inserted before coating.

After coating, the side frames have been machined. A request for modification has been done, in order to obtain, with due machining allowance, a radius of $R=5$ mm in the marked zones of fig. 3.68. The proposal has been accepted.

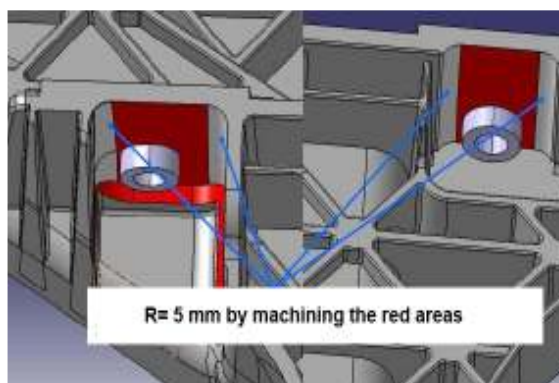


Fig. 3.68: request of machining modification.

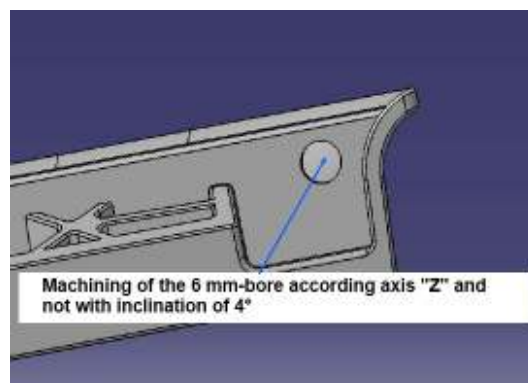


Fig. 3.69: request of machining modification.

The $\varnothing 6$ mm bore of fig. 3.69 should have been machined with an inclination of 4° , according to the casting designer. A modification of the machining direction to the parallel axis “z”, i.e. perpendicular to the casting has been asked and obtained. The designed tool has provided the possibility of machining two capote carrier brackets in a rotating double-faced carousel, see fig. 3.70.

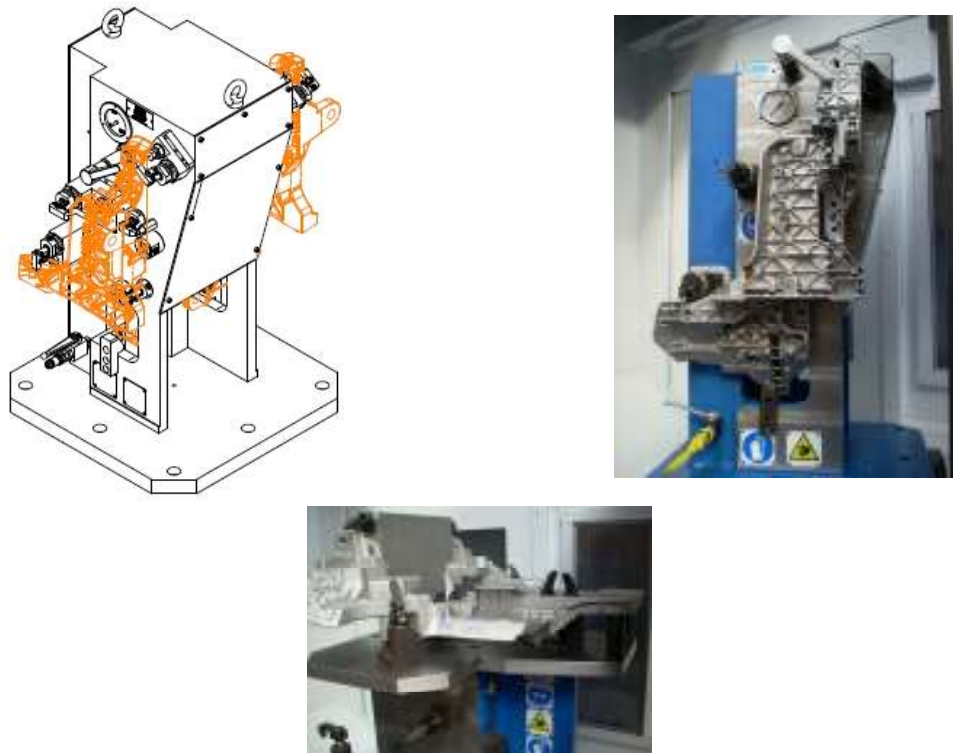


Fig. 3.70: machining tool of the capote carrier brackets.

3.4.2 Roof main bracket

The roof main brackets have not shown difficulties in their prototyping phase. The requirements of $YTS > 150$ MPa and $e\% > 1$ % have been reached easily on sand cast parts. However, shifting to high-pressure die-casting has implied several changes on the die configuration through three sampling campaigns, in order to improve the casting quality. This paragraph presents the sequence of interventions made on the die before approval of its final configuration.

3.4.2.1 First sampling

The visual control of the first sampled roof main brackets has shown a poor filling of the extractors both on the fix side and on the moving side of the die. Therefore, the five extractors of the fix side with $\varnothing 3$ mm have been removed and levelled to the die plane, see fig. 3.71, sight 1. The same operation has been carried out on the moving die for the extractor indicated in fig. 3.72, sight 2.

The gating system has been connected to the brackets with $R=4$ and in the area of the blank indicated in fig. 3.73 – position 1 of the moving die - the radii have been increased. The vertical walls next to the ingate have been polished and the die inclination increased in order to favour the flow of the melt into the cavity, see fig. 3.73, position 2 of the moving die. The overflows of fig. 3.74 – position 2 - have been enlarged to a total thickness of 10 mm; the ingates increased in their width to 22 mm and in their thickness to 1,5mm. The overflows of position 3 have been enlarged of 2 mm in their gate; a further 1,2 mm-thick overflow has been placed in position 4, see fig. 3.74 to better evacuate air in the upper part of the roof carrier. Every overflow has been provided with a “S”- shaped ventilation shaft, with a wall-thickness of 0,35 to 0,40 mm at its gating on the overflow and of 0,15-0,20 mm at its second neck.



Fig. 3.71: removed steel cores of the roof main bracket. Sight of the fix die.



Fig. 3.72: removed steel core of the roof main bracket. Sight of the moving die.

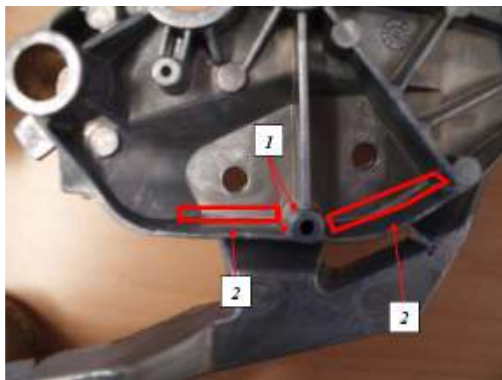


Fig. 3.73: ingate area.
Sight of the moving die.

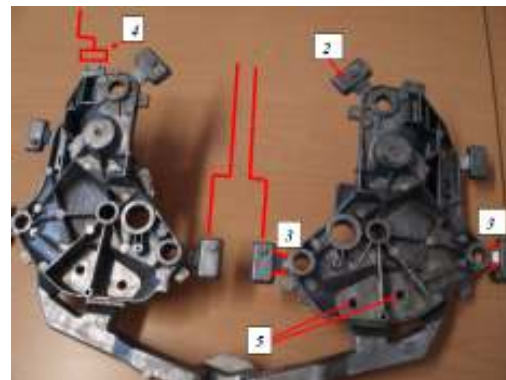


Fig. 3.74: overflow placement on the two cavities of the roof main brackets.
Sight of the moving die.



Fig. 3.75: shortened steel cores of the roof main bracket.
Sight of the fix die.

The passing openings marked with 5 have been reduced to blind holes, in order to create a connection flash, which does not disaggregate the metal flow during casting. The steel cores have therefore been substituted, while reducing their length of 0,3 mm and making their intersection with the fix die perpendicular without any connecting radii. The holes have been obtained with a subsequent machining operation. The above described operations have been repeated for both cavities of the die. Finally, the two steel cores marked by red arrows of fig. 3.75 have been shortened respectively of 0,06 mm and 0,04 mm for the left and right roof bracket, in order to respect the given tolerances. Date stamps have been regularly updated to trace back production batched. Article code RH 9221572 and LH 9221571 have been carved respectively onto the right and left roof bracket. The writing “Magsimal-59” has been carved onto the ingate in order to make the selection of scraps and returns easier into the shop floor.

3.4.2.2 Second sampling

After the second sampling, further modifications have been carried out on the die. One steel core has been re-introduced according the layout of the first sampling, but eliminating the internal diameter of 3,5 mm and therefore leaving a “full” core. This has been done on both die cavities, see fig. 3.76.



Fig. 3.76: the re-introduced steel core
Fix die.



Fig. 3.77: elimination of the hole.
Sight of the moving die.



Fig. 3.78: the polished area in the ingate and the points where flashes have been introduced. Sight on the moving die.

The moving side of the die has been levelled, thus eliminating the $\text{Ø } 7 \text{ mm}$ hole, obtained with a subsequent machine operation, see fig. 3.77. The aim of this modification is once again improving the die filling.

The moving die has been further polished in the sections marked by red arrows of fig. 3.78 in order to make the opening of the die and the ejection of the casting easier. The connection flashes of position 1, fig. 3.78 have been increased to 0,4 mm wall-thickness. Dimensional control of the castings have been carried out on the second sampling, with a positive result: all given quotas and tolerances have been maintained.

3.4.2.3 Third sampling

The third sampling has brought to the final configuration of the die for the roof main brackets. Due to the high speed of the metal after injection around the ingate, a further polishing of the moving side of the die has been done in the areas indicated by red arrows, see fig. 3.79. The main rib has been provided with a higher die inclination, reaching thus 2° and connecting radii increased to $R=5$.



Fig. 3.79: ingate area and rib.
Sight on the moving side of the die.



Fig. 3.80: enlarged overflows on the two cavities. Moving die.

The overflows of fig. 3.80 have been enlarged.

Tensile tests have been carried out on bracket roof after the carrying out of these modifications and according to the modalities described in par. 3.2. The results are summarized in tab. 3.21. Tests have been carried out at room temperature. Although the UTS has not reached the minimum required value, the final customer has accepted the results, exceptionally, as valid, as the YTS has been used as design property and the deviation from requirement not considered critical.

YTS	158 MPa
UTS	240 MPa
e%	10 %

Tab. 3.21: results of tensile test on a left roof main bracket.

3.4.2.4 Series manufacturing die

The die with two cavities has been approved for the series manufacturing. Ordinary maintenance has been carried out every 20 000 shots, see fig. 3.82. The two steel cores depicted in fig. 3.81 – position A – have been polished before every batch production, as they have shown a more pronounced wear.

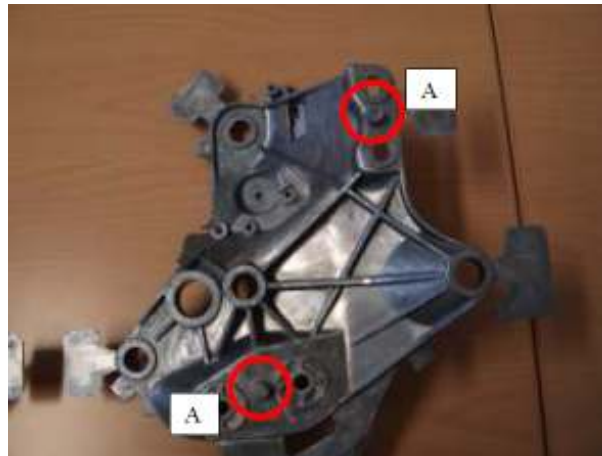


Fig. 3.81: steel cores.

After casting and sand blasting, the roof brackets have been machined. The designed tool has allowed the machining of two left plus two right roof brackets, as visible in fig. 3.84.

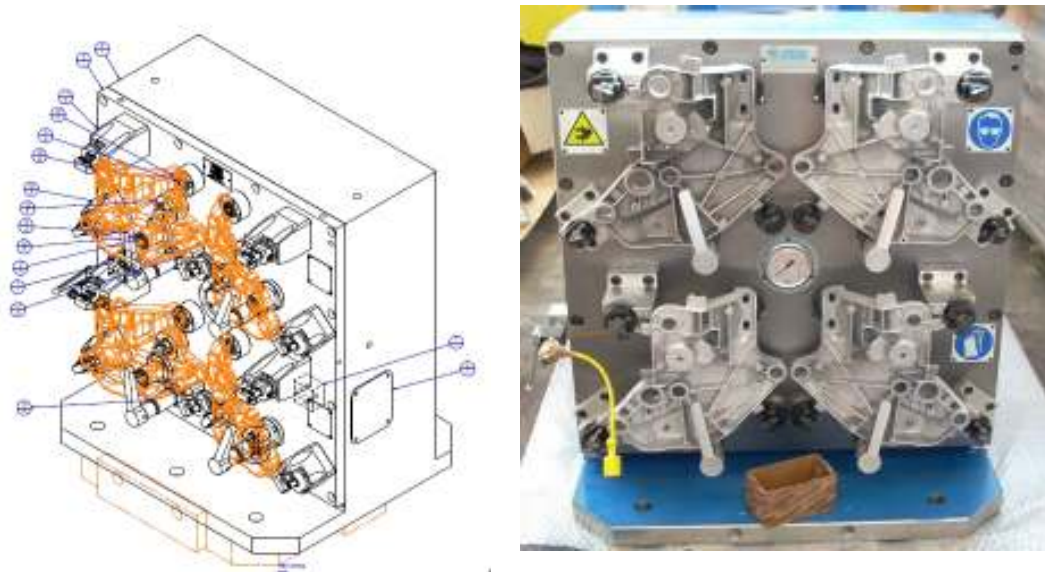


Fig. 3.84: machining tool of the roof main brackets.

3.4.3 Side frame

The side frames have not shown difficulties in their prototyping phase. Shifting to the high-pressure die-castings has implied several changes on the die configuration through two sampling campaigns. This paragraph presents the sequence of interventions made on the die before approval of its final configuration.

3.4.3.1 Preliminary modifications

Preliminary changes have been asked on the drawings of the side frame, on the basis of the simultaneous experience made on the roof main brackets.

The rib indicated by the red arrows in fig. 3.85 has been thickened of one millimetre from 2,9-3,3 mm to 3,9-4,3 mm, in order to give more stiffness to the casting where a bolt has been designed to a later stage of development.

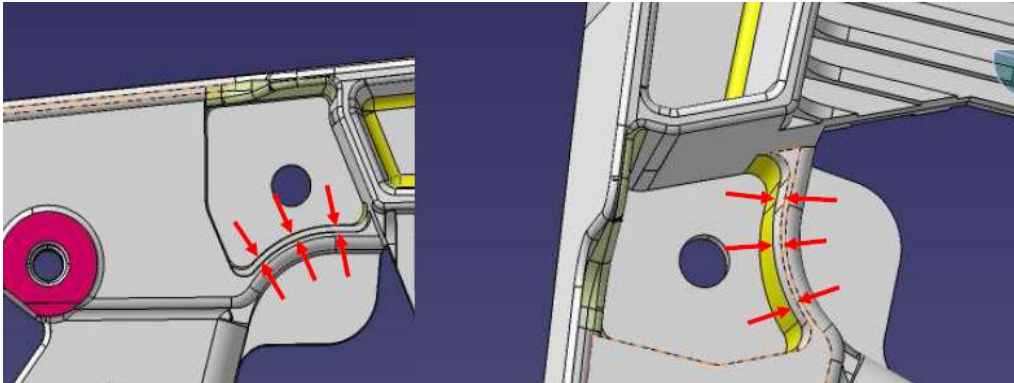


Fig. 3.85: the fin which has been increased of 1 mm. Side frame.

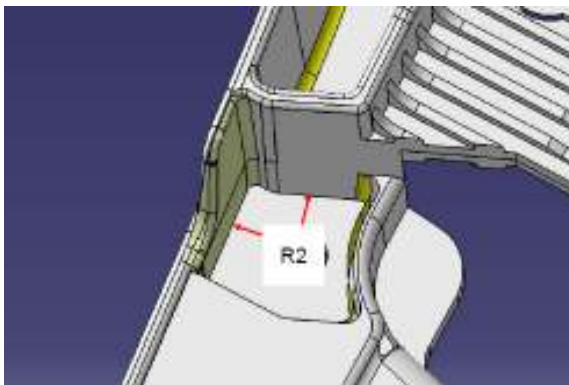


Fig. 3.86: the connecting radius $R=2$ in the bolt area. Side frame.

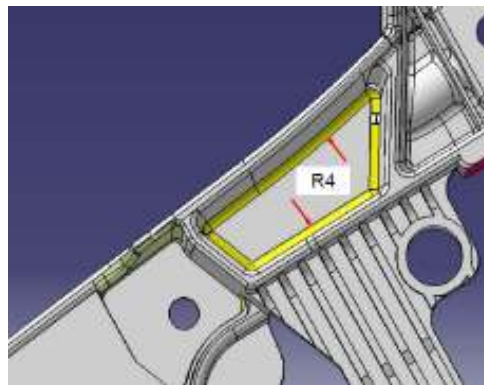


Fig. 3.87: the connecting radius $R=4$ next to the bolt area. Side frame.

On the entire profile around the bolt area a connecting radius of $R=2$ has been approved, see fig. 3.86. The yellow contour of fig. 3.87 has been changed to $R=4$ to make the ejection of the casting easier, as the die presents a wall height of more than 3 mm. The rib of fig. 3.88 has been also changed, maintaining its thickness in A, while increasing it on one millimetre in position B.

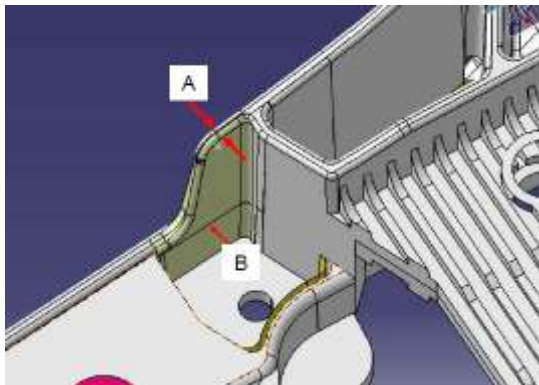


Fig. 3.88: machining tool of the roof main brackets.



Fig. 3.89: machining tool of the roof main brackets.

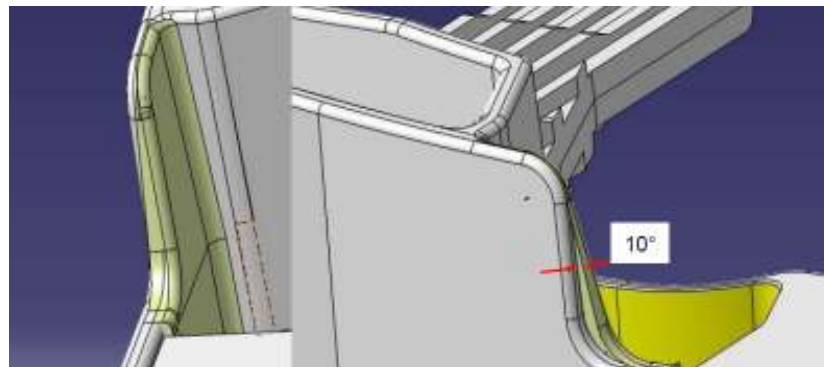


Fig. 3.90: profile of the changed rib with its 10°. Side frame.

A modification of the rib profile with a connecting radius of 10° has additionally been requested, as shown in fig. 3.90. The designer has however rejected this option, as the physical connection to the other parts of the rear trunk would have been compromised. The final configuration of this area is presented in fig. 3.89, which shows a picture of a series manufacturing casting.

3.4.3.2 First sampling

The pilot die has been tested for the first sampling, after which some further changes into the fix and moving sides have been carried-out. The steel cores with Ø 3 mm have been removed from the moving side of the die, see fig. 3.91 – sight 1. The steel cores with Ø 3,5 mm have been removed from the fix side of the die, see fig. 3.92 – sight 2. The ejectors have been therefore levelled to the corresponding planes. The operation has been done for the RH and LH die.



Fig. 3.91: elimination of steel cores.
Moving side frame die.



Fig. 3.92: elimination of steel cores.
Fix side frame die.

Some marking have been added on the moving side of the side frame dies. The writing “Magsimal-59” has been inserted in position 1; the identification codes LH and RH with corresponding part number have been inserted respectively on the left-

and right-hand side die in position 2 and 3; the revision code with \varnothing 6 mm has been put in position 4; the date stamp has been located in position 5. See fig. 3.93.



Fig. 3.93: markings of the side frame.



Fig. 3.94: steel core and slide position of the RH side frame.

The right side frame die has presented some problems during the opening/closing phase. In fact, while the slide has been operated in idling conditions without casting, a friction between die and slide with the breaking of two ejectors has been observed. Therefore, the movements of the slide have been double-checked, in order to confirm it is perpendicular to the axis of the die. The steel core of fig. 3.94 has been eliminated and the ejector levelled to the plan of the fix die.



Fig. 3.95: connection ingate/casting with modified radii.

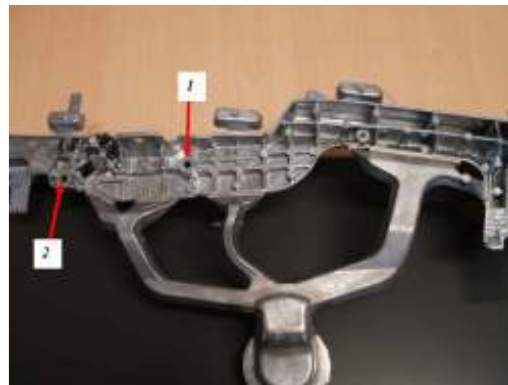


Fig. 3.96: downsized steel cores. Side frame.

The profile connecting the ingate to the casting has been changed to $R=3$ before and after the rib, see fig. 3.95. Measurements carried out on the M8 holes presented in fig. 3.96 have shown non-conformities. The steel core "1" has been downsized from \varnothing 6,85 mm to \varnothing 6,45 mm; the steel core "2" from \varnothing 6,8 mm to \varnothing 6,5 mm. All overflows have been modified in their geometry, providing a "S"-shaped ventilation shaft, with a wall-thickness of 0,15 to 0,20 mm at its connection to the casting and of 0,35-0,40 mm at its second neck. Additionally all passing holes have been reduced to blind holes of a height of 0,3 mm, in order to create a

connection flash, which does not disaggregate the metal flow during casting. Quotas and all given tolerances have been controlled on the side frames.

3.4.3.3 Second sampling

Following to the second sampling, further modifications have been carried out on the die. The diameter of the two steel cores has been increased to min. 15,10 to max 15,45 mm, see fig. 3.97.

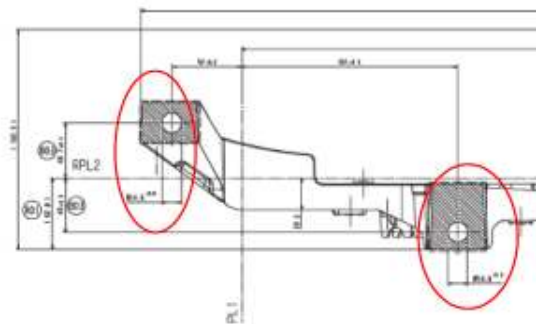


Fig. 3.97: increase of diameter of the steel cores. Side frame.

Moderate sticking phenomena have been observed in the area circled in red of fig. 3.98 on the fix side of the die. Polishing of this large and smooth surfaced has been carried-out.

The ejection system has been double-checked in the area marked in fig. 3.99, as a slight deformation of the plane has been observed.



Fig. 3.98: sticking area on the fix side of die.



Fig. 3.99: deformed ejectors.

Tensile tests have been carried out on a RH side frame after the carrying out of the above mentioned modifications, according to the modalities described in par. 3.2. DIN 50125 E3x8x35 tensile bars have been cut-off and tested to room temperature. The results are summarized in tab. 3.22 and meet the requirements for series production.

YTS	178 MPa
UTS	283 MPa
e%	8 %

Tab. 3.22: results of tensile test on a right side frame.

3.4.3.4 Series manufacturing die

Although if the changes introduced after the second sampling have delivered positive results in terms of tensile testing on side frames, further light modifications of die layout have been done before shifting to series production.

The integrity of all casting steel cores has been verified; the steel core marked as “a” in fig. 3.100 has been substituted on the right side frame, as broken. On the moving side of the die a fix steel core has been introduced to close the ejector area and therefore levelling the plane with the parting line, see fig. 3.101.

The connecting radii on the entire profile represented by the dotted yellow line of fig. 3.102 have been increased to $R=3$. The corresponding fix die surfaces have been polished.



Fig. 3.100: broken pin. RH Side frame.

Fig. 3.101: elimination of ejector.
Fix die.

As slight sticking to the die and tearing of the castings could be observed during the second sampling, the die inclination on the moving die side has been increased, see yellow profile of fig. 3.103. The possibility of moving the opening of the slide marked with “a” has been evaluated as efficient solution to improve the fault-free ejection of the castings.



Fig. 3.102: increasing the inclination of die. Side frame.



Fig. 3.103 increasing the inclination of die. Moving slide.

3.4.3.5 Shearing die

In order to optimize the final configuration of the HPDC process, some changes have been introduced on the shearing dies. This paragraph presents briefly the modifications suggested by the caster. In order to improve the local filling of the die, a flash of 0,3 mm has been introduced in the area ECR281 of fig. 3.104 and the shearing die accordingly modified. The diameter of the shearing core has been increased to 4,5 mm in ECR 284, see fig. 3.105.

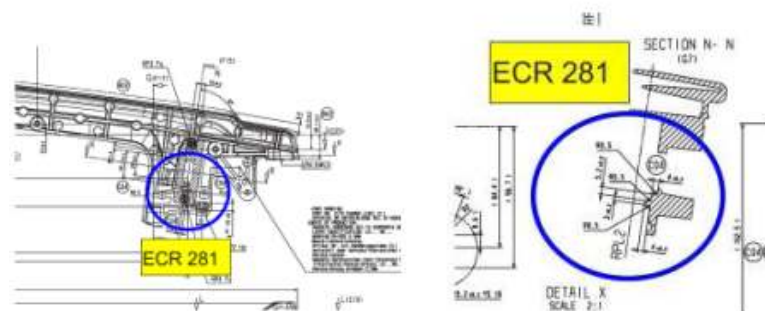


Fig. 3.104: introduction of connecting flashes.



Fig. 3.105: shearing steel core.

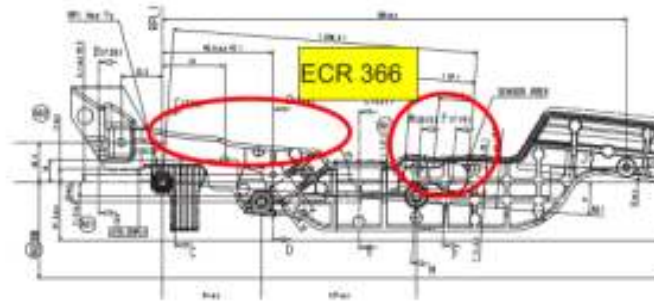



Fig. 3.106: new plugs of the shearing die.

According to the modification ECR 366, which has been requested by the final customer, two new plugs of the holding matrix have been manufactured. The adapter and the superior shearing die have been lightened. All shearing steel cores have been controlled and the coupling between high-pressure die-casting and shearing matrix has been optimized for both LH and RH side frames. The final configuration of the shearing press and die next to the HPDC machine is shown in fig. 3.107.



Fig. 3.107: the shearing die.

As for the roof main brackets, the final die has been approved for the series manufacturing and 100 000 shots have been granted. Ordinary maintenance has been carried out according to the maintenance plan of fig. 3.108.




Descrizione **Stampo di PRESSOFUSIONE** **Order** **8**
Articolo **SIDE FRAME SX** **Ord. Art.** **9121874** **Quantità** **100.000**

N°	Descrizione	Data In	TIPO	Stato	Richiesta da	Fornitore	Data Fine	Rel. Istruttore di Lavoro
1	Sistemazione stampo dopo prima campagna	21.12.07	M	C	Microtech	SOM		SI
2	Sistemazione stampo dopo seconda campagna	25.06.08	M	C	Microtech	SOM		SI
3	Riveduta stampo F.O. 261-264-366	23.10.08	S	C	WEBSPD	SOM		SI
4	Manutenzione Stampo	30.01.09	O	E	Microtech	SOM		SI

Mod. M Rev. 2 del 06/02/08
 Microtech Srl via Garibaldi, 34 - 25020 FLEPO (Italy) www.microtech-italia.it info@microtech-italia.it

Fig. 3.108: ordinary tool maintenance sheet for the side frames.

As for the roof main brackets, manufacturing batches have been recorded with their date, quantity, scraps and scrap rate, according to the corresponding paperwork, see fig. 3.109.



Descrizione **ATTREZZATURE** **Order** **8**
Articolo **SIDE FRAME SX** **Ord. Art.** **9121874** **Quantità** **100.000**

Comparto / Ordine	Quantità/Quantità	Data In	C. in Ord.	Scarti	Residuo	Data Fine
1000	100000	01.01.08	100	0	0	01.01.08
1001	100000	01.01.08	100	0	0	01.01.08
1002	100000	01.01.08	100	0	0	01.01.08
1003	100000	01.01.08	100	0	0	01.01.08
1004	100000	01.01.08	100	0	0	01.01.08
1005	100000	01.01.08	100	0	0	01.01.08
1006	100000	01.01.08	100	0	0	01.01.08
1007	100000	01.01.08	100	0	0	01.01.08
1008	100000	01.01.08	100	0	0	01.01.08
1009	100000	01.01.08	100	0	0	01.01.08
1010	100000	01.01.08	100	0	0	01.01.08
1011	100000	01.01.08	100	0	0	01.01.08
1012	100000	01.01.08	100	0	0	01.01.08
1013	100000	01.01.08	100	0	0	01.01.08
1014	100000	01.01.08	100	0	0	01.01.08
1015	100000	01.01.08	100	0	0	01.01.08
1016	100000	01.01.08	100	0	0	01.01.08
1017	100000	01.01.08	100	0	0	01.01.08
1018	100000	01.01.08	100	0	0	01.01.08
1019	100000	01.01.08	100	0	0	01.01.08
1020	100000	01.01.08	100	0	0	01.01.08
1021	100000	01.01.08	100	0	0	01.01.08
1022	100000	01.01.08	100	0	0	01.01.08
1023	100000	01.01.08	100	0	0	01.01.08
1024	100000	01.01.08	100	0	0	01.01.08
1025	100000	01.01.08	100	0	0	01.01.08
1026	100000	01.01.08	100	0	0	01.01.08
1027	100000	01.01.08	100	0	0	01.01.08
1028	100000	01.01.08	100	0	0	01.01.08
1029	100000	01.01.08	100	0	0	01.01.08
1030	100000	01.01.08	100	0	0	01.01.08
1031	100000	01.01.08	100	0	0	01.01.08
1032	100000	01.01.08	100	0	0	01.01.08
1033	100000	01.01.08	100	0	0	01.01.08
1034	100000	01.01.08	100	0	0	01.01.08
1035	100000	01.01.08	100	0	0	01.01.08
1036	100000	01.01.08	100	0	0	01.01.08
1037	100000	01.01.08	100	0	0	01.01.08
1038	100000	01.01.08	100	0	0	01.01.08
1039	100000	01.01.08	100	0	0	01.01.08
1040	100000	01.01.08	100	0	0	01.01.08
1041	100000	01.01.08	100	0	0	01.01.08
1042	100000	01.01.08	100	0	0	01.01.08
1043	100000	01.01.08	100	0	0	01.01.08
1044	100000	01.01.08	100	0	0	01.01.08
1045	100000	01.01.08	100	0	0	01.01.08
1046	100000	01.01.08	100	0	0	01.01.08
1047	100000	01.01.08	100	0	0	01.01.08
1048	100000	01.01.08	100	0	0	01.01.08
1049	100000	01.01.08	100	0	0	01.01.08
1050	100000	01.01.08	100	0	0	01.01.08
1051	100000	01.01.08	100	0	0	01.01.08
1052	100000	01.01.08	100	0	0	01.01.08
1053	100000	01.01.08	100	0	0	01.01.08
1054	100000	01.01.08	100	0	0	01.01.08
1055	100000	01.01.08	100	0	0	01.01.08
1056	100000	01.01.08	100	0	0	01.01.08
1057	100000	01.01.08	100	0	0	01.01.08
1058	100000	01.01.08	100	0	0	01.01.08
1059	100000	01.01.08	100	0	0	01.01.08
1060	100000	01.01.08	100	0	0	01.01.08
1061	100000	01.01.08	100	0	0	01.01.08
1062	100000	01.01.08	100	0	0	01.01.08
1063	100000	01.01.08	100	0	0	01.01.08
1064	100000	01.01.08	100	0	0	01.01.08
1065	100000	01.01.08	100	0	0	01.01.08
1066	100000	01.01.08	100	0	0	01.01.08
1067	100000	01.01.08	100	0	0	01.01.08
1068	100000	01.01.08	100	0	0	01.01.08
1069	100000	01.01.08	100	0	0	01.01.08
1070	100000	01.01.08	100	0	0	01.01.08
1071	100000	01.01.08	100	0	0	01.01.08
1072	100000	01.01.08	100	0	0	01.01.08
1073	100000	01.01.08	100	0	0	01.01.08
1074	100000	01.01.08	100	0	0	01.01.08
1075	100000	01.01.08	100	0	0	01.01.08
1076	100000	01.01.08	100	0	0	01.01.08
1077	100000	01.01.08	100	0	0	01.01.08
1078	100000	01.01.08	100	0	0	01.01.08
1079	100000	01.01.08	100	0	0	01.01.08
1080	100000	01.01.08	100	0	0	01.01.08
1081	100000	01.01.08	100	0	0	01.01.08
1082	100000	01.01.08	100	0	0	01.01.08
1083	100000	01.01.08	100	0	0	01.01.08
1084	100000	01.01.08	100	0	0	01.01.08
1085	100000	01.01.08	100	0	0	01.01.08
1086	100000	01.01.08	100	0	0	01.01.08
1087	100000	01.01.08	100	0	0	01.01.08
1088	100000	01.01.08	100	0	0	01.01.08
1089	100000	01.01.08	100	0	0	01.01.08
1090	100000	01.01.08	100	0	0	01.01.08
1091	100000	01.01.08	100	0	0	01.01.08
1092	100000	01.01.08	100	0	0	01.01.08
1093	100000	01.01.08	100	0	0	01.01.08
1094	100000	01.01.08	100	0	0	01.01.08
1095	100000	01.01.08	100	0	0	01.01.08
1096	100000	01.01.08	100	0	0	01.01.08
1097	100000	01.01.08	100	0	0	01.01.08
1098	100000	01.01.08	100	0	0	01.01.08
1099	100000	01.01.08	100	0	0	01.01.08
1100	100000	01.01.08	100	0	0	01.01.08

Mod. P Rev. 2 del 06/02/08
 Microtech Srl via Garibaldi, 34 - 25020 FLEPO (Italy) www.microtech-italia.it info@microtech-italia.it

Fig. 3.109: production batch sheet of the side frames.

3.4.3.6 Protection from cataphoretic painting and machining

In order to protect the threads from the cataphoretic painting process, covering plugs have been introduced in the areas marked with a red circle in fig. 3.110.

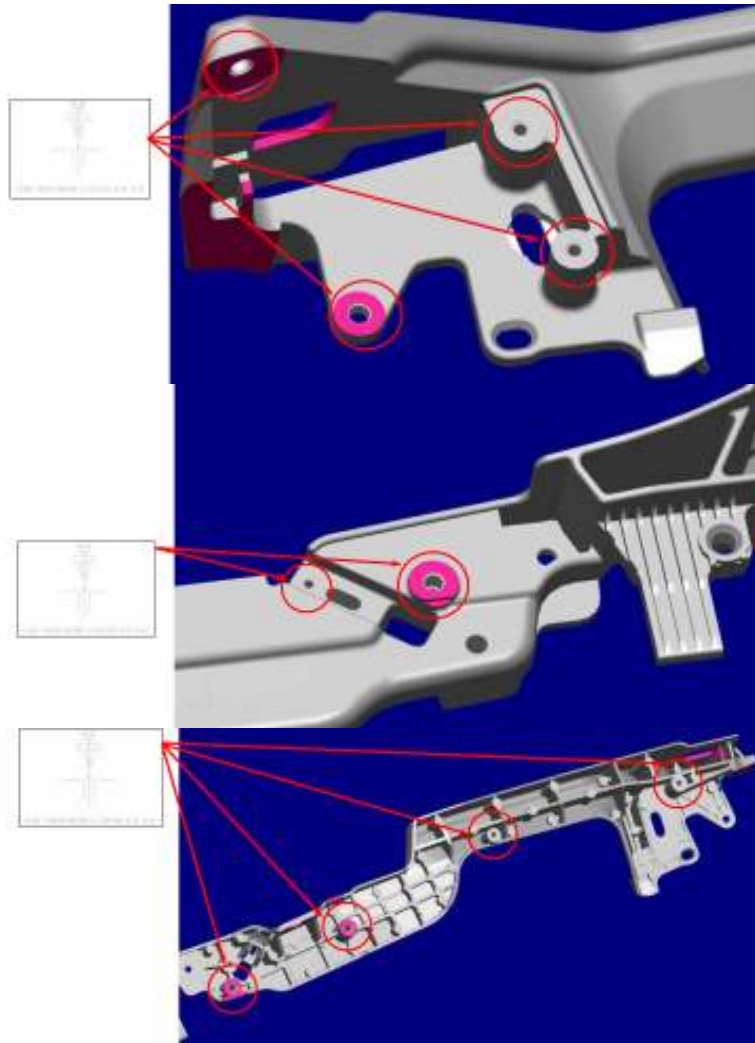


Fig. 3.110: protected threads. Plugs have been inserted before coating.

After coating, the side frames have been machined. The designed tool has provided the possibility of machining four side frames in a rotating carousel, see fig. 3.111.

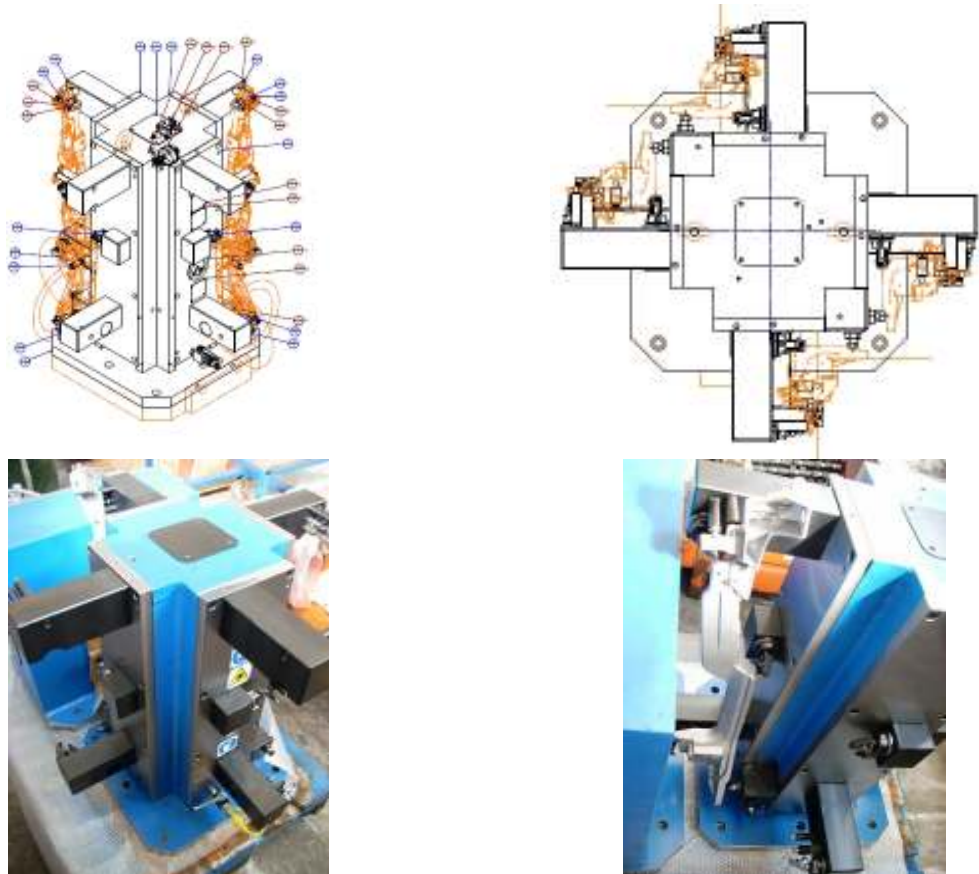


Fig. 3.111: machining tool of the roof main brackets.

3.4.4 Series production of the car set

Pre-series parts have been validated for final series-production. Series HPD-Castings in Magsimal[®]-59 for the car set of the F149 are reported in fig. 3.112.



Fig. 3.112: series part production.

3.5 Outcomes

The main difficulties arising from the use of Magsimal[®]-59 for the production of the car sets have been summarized in this paragraph, underlining the main differences in the everyday foundry practice compared to common AlSi-alloys. Some of these operative hurdles are strictly connected to the nature of Magsimal[®]-59; some ones are mainly to be referred to the intrinsic difficulty of the casting geometry; some other need to be linked to both contributes.

To this extent, it has to be pointed out, that the foundry layout and main hardware of the caster have been thought for secondary HPDC-alloys. Many observations have been reported as feedback by the foundry people, according to their experience. Evaluations have been made therefore oft on a qualitative basis.

However, it has been attempted to quantify the impact of processing Magsimal[®]-59 in terms of additional costs in the foundry. Real values have been rescaled for confidential reasons.

3.5.1 Shop floor and melting

On the shop floor, the main issue has been managing the shift from secondary alloys to Magsimal[®]-59 on the basis of the current production planning.

In particular, keeping the melt into its specifications by adequate furnace cleaning and granting a stable melt quality has proven being time consuming, as well as expensive in terms of additional work procedures.

Despite the use of covering salts, during the whole melting procedure, higher magnesium losses have been observed. Mg losses of around 0,1 % per melting procedure are normally to be expected [26]; measurements in the maintenance furnace showed an average Mg-loss or ca. 0,2 %. This major Mg-oxidation is not harming the final properties of the melt and no Mg-reintegration has been needed; however this is a symptom of non-optimal melting conditions. The main cause could be found in the construction of the maintenance oven.

Two roof gas burners maintain the set temperature with an accuracy of $\pm 10^{\circ}\text{C}$ by a simple three step control – off, low, high. The burning front is oriented vertically on the bath, i.e. with direct contact to the melt surface. These local hot spot favours the oxidation of magnesium.

Additionally, a higher tendency to the segregation of manganese could be observed, especially when holding the melt overnight. No melt stirring has been provided in the furnace and this could be the main reason for the precipitation of Mn crystals. Therefore, holding temperature has been set at 650°C overnight and the future adoption of a melting furnace with electromagnetic stirrer has been discussed.

HPDC-isles operated with Magsimal[®]-59 call for a dedicated operator.

3.5.2 Down-times and cycle-times

Downtimes with Magsimal[®]-59 have been caused mainly by deformation of the part during ejection. Slight sticking at the hot spots corresponding to the ingates could be observed, but have been solved improving the lubrication parameters and the die geometry.

Compared to benchmark, downtimes with Magsimal[®]-59 have been quantified in additional 5 %. Cycle time with Magsimal[®]-59 is 5 seconds longer to allow the complete solidification of the part.

3.5.3 Scrap rate, shrinkages and porosities

Side frames and roof carriers have not shown sensible shrinkages or concentrated localization of porosities, thanks to their lightweight geometry and average wall thickness of 3 mm.

The capote carrier bracket has shown some critical areas, marked with red circles in fig. 3.113. Position A corresponds to the fixing ring to chassis, as presented in fig. 3.24. The wall-thickness of the ring is of 10 mm in the front-part, 23 mm in its inner part, 28 and 12 mm on its two sides. Deepness of the ring and of the thread is 22 mm. Considering the features of Magsimal[®]-59, the geometry of the ring is unfavourable. Soon after the first sampling a lightening of the ring has been suggested, see 3.4.1.2. The simulation, run soon after the third sampling, shows the critical aspects of this area. The solidification of the ring and the next “plateau” takes place very late. Additionally, the filling speed around position “A” is very high, with resulting spraying of the metal, see fig. 3.114. Shrinkages on the first sampled carriers can be easily detected under x-rays, see fig. 3.119, left. The overflows have been heavily increased all around the ring; the improvements on the final product are remarkable, see fig. 3.119, right.



Fig. 3.113: fraction solid in position A, according to a CAD simulation.

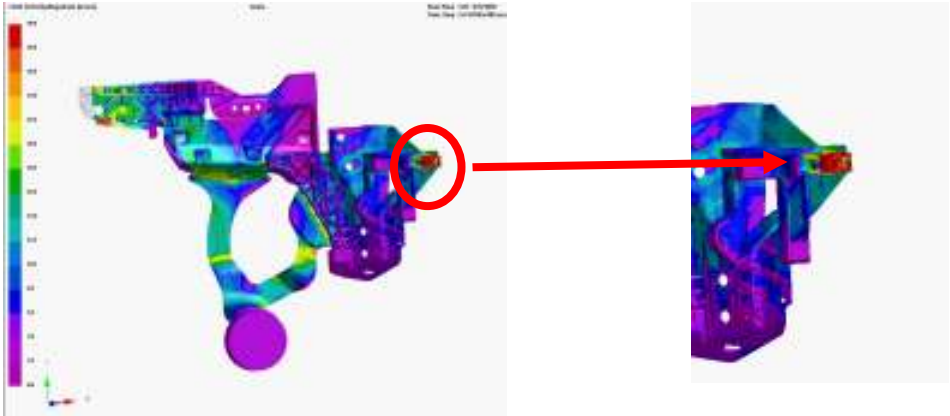


Fig. 3.114: filling speed over 30 m/s in position A, bearing ring.

Position B corresponds to the second fixing point on the roll bar. The wall-thickness of the ring is of 15 mm in the front-part, 20 mm in its inner part, 14 mm its two sides. Deepness of the ring and of the thread is 22 mm. As expected, shrinkages porosities are concentrated in the internal side of the ring, see fig. 3.120, left. The region solidifies very late and can be therefore considered a hot spot of the casting, see fig. 3.115. According to the caster’s experience, a thinning of this area has been suggested after the first sampling. The possibility of introducing a step of additional metal, in order to make the feeding of the region easier, has been accepted, see par. 3.4.1.2.



Fig. 3.115: fraction solid in position B according to the simulation.

Position C corresponds to the fixing point to the chassis. This area has proven to be difficult to be filled with a corresponding good quality level, as it represents a one-way peripheral region.

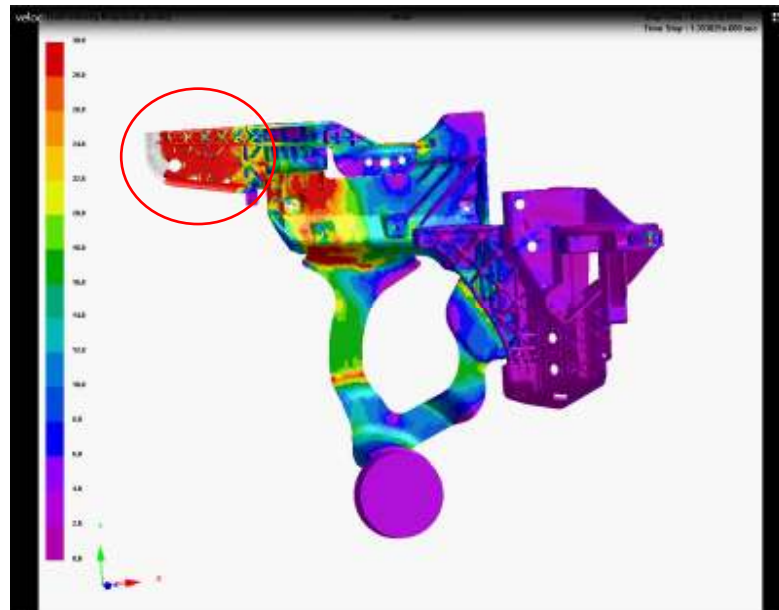


Fig. 3.116: filling speed in the position “C”.

The metal flows in fact at high speed in the wing of the carrier, see fig. 3.116. Additionally, the solidification proceeds with an open front back to the direction of the feeding ingate. In order to improve the die filling, the passing hole has been closed after the first sampling through a modification of the die. The melt flow has been kept closer and more compact. Significant improvements have been achieved by carrying-out the modifications suggested in par. 3.4.1.5, see fig. 3.62. The achieved quality can be compared to the results of the first sampling in fig. 3.121, left versus right.

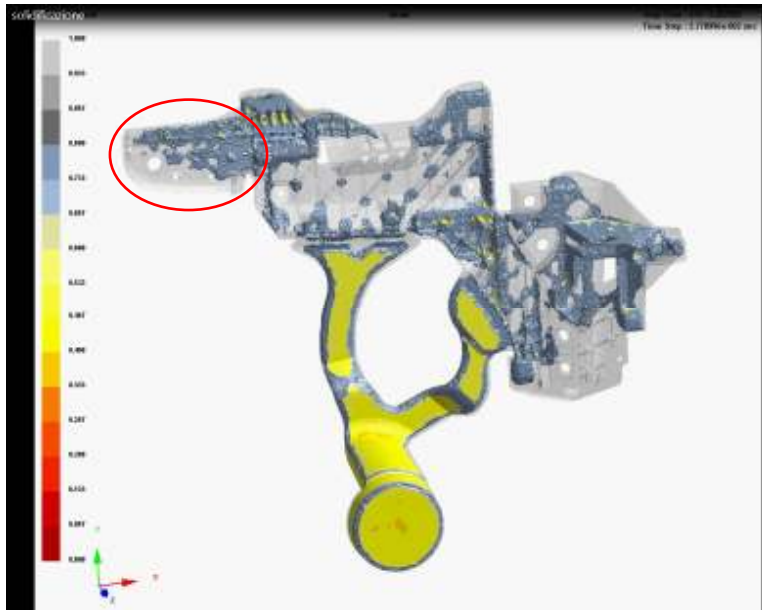


Fig. 3.117: solidification of the wing of the carrier.

The finning area still remains one critical area of the capote carrier brackets. Generally speaking, problems have been solved by a step-by-step approach, i.e. by subsequent die modifications: the overflows around the rings A and B, as well as around the bore hole C have been widened in size and ingate, taking into account the simulation results and the sampled parts. The quality improvements on real castings can be observed in fig. 3.119 to 3.121; on the left-side the areas A, B, C before modification of the die; on the right-side the areas A, B, C after modification of the die.

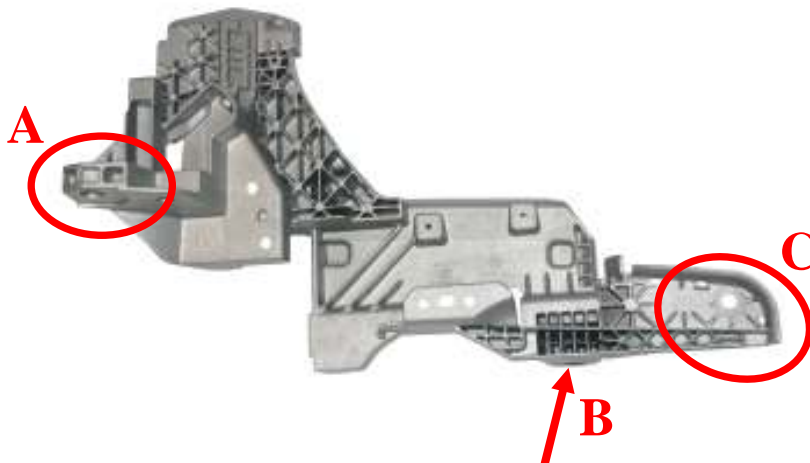


Fig. 3.118: critical porosity area of the capote carrier.

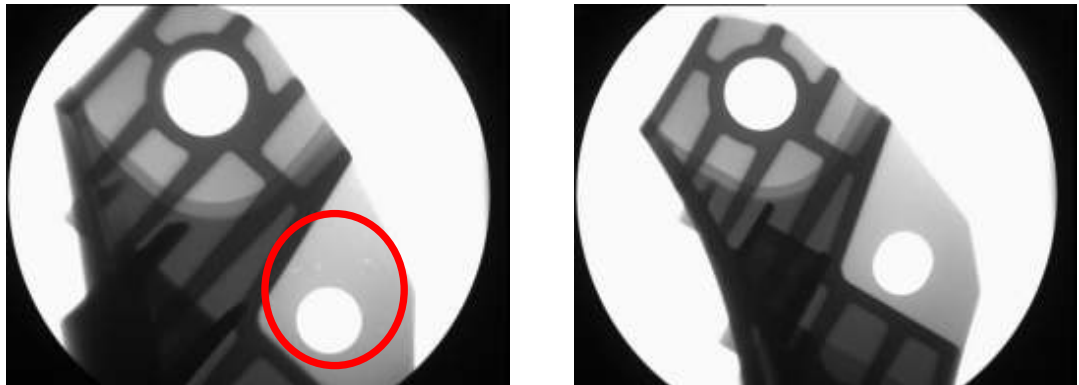


Fig. 3.119: position A before (left) and after (right) die modification.

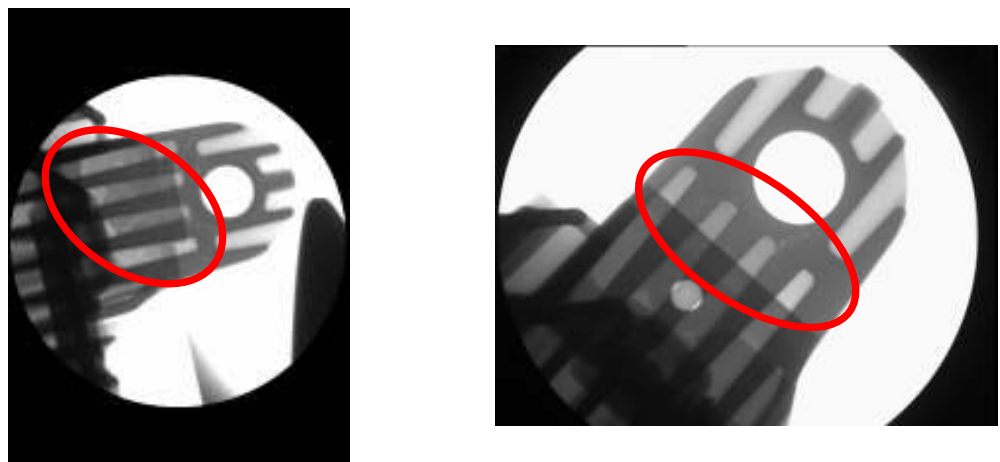


Fig. 3.120: position B before (left) and after (right) die modification.

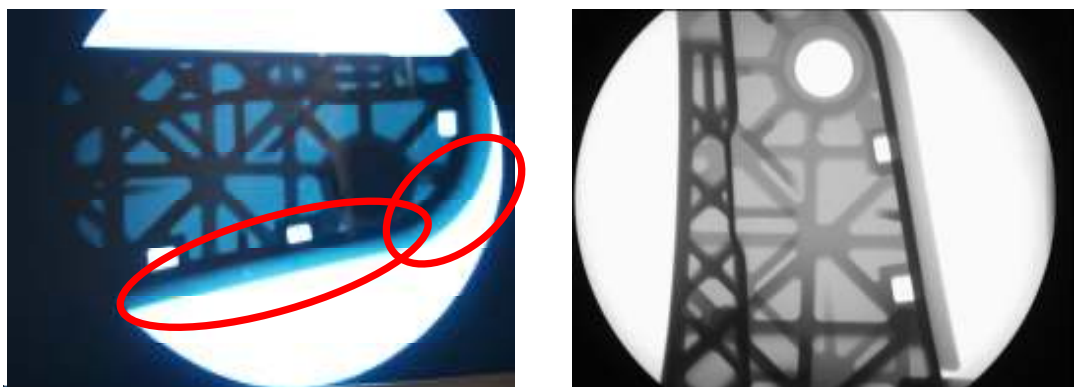


Fig. 3.121: position C before (left) and after (right) die modification.

3.5.4 Die-lubrication

Magsimal[®]-59 has been cast at 720-730°C, while a traditional AlSi9Cu3(Fe) is normally cast at 680-690°C. The cooling curves of the two alloys is reported in fig. 3.122 for comparative reasons.

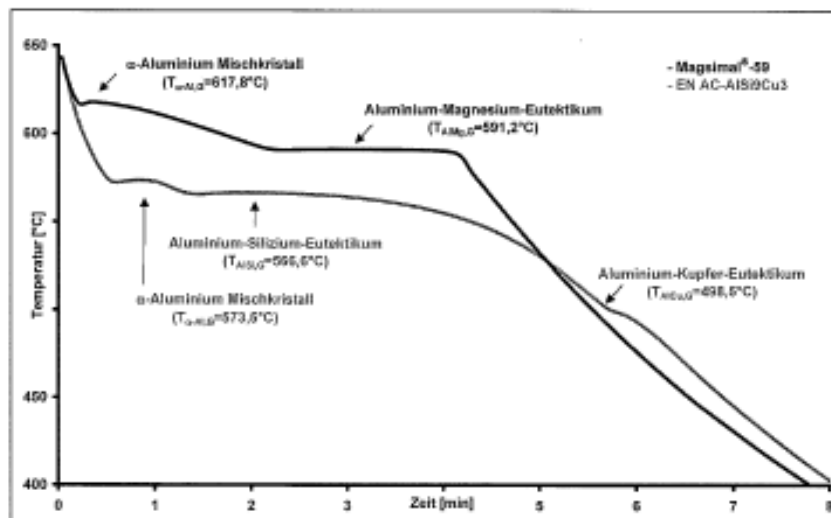


Fig. 3.122: cooling curve of Magsimal[®]-59 and of AlSi9Cu3(Fe).
The differences concerning solidus and liquidus temperatures are clear

Due to the higher thermal stress on the die and to the special chemistry of Magsimal[®]-59, a special modern die-lubricant, originally developed for AlMg-HPDC-alloys, has been used. Compared to traditional products, it allows the protection of the die at ca. 30°C higher, improving at the same time the flowing properties of the melt into the cavity. Concentrations up to 3,3 to 3,4 % have been necessary to get the desired quality of the castings in Magsimal[®]-59. If using the same lub, typical concentration values for a common AlSi9Cu3(Fe) are around 2,0 - 2,2 %, depending on the geometry of the part.

3.5.5 Die-wear

Recent studies [27] have shown that the main levers to act on in order to improve die-life when casting Magsimal[®]-59 are the following:

- die-lubrication;
- die-coating;
- die-steel;
- manufacturing parameters, i.e. die temperature, casting parameters and casting temperature.

Casting experiences with Magsimal[®]-59, showed that maintaining the die every 5 000 - 10 000 by a basic ionitriding treatment helps significantly the die-life. 30-50°C higher operating conditions of the die and lower injection pressures as well as casting temperatures are however the main leverages to improve die-life. At this extent just a compromise can be reached. Hot-resistant die-steel should be chosen whenever possible. The die and the inserts have been produced in H11 steel with no additional coating. Sensible wear of the tooling has been observed already at 5 000 shots, with appearance of thermal fatigue cracks. At 20 000 shots die attendance by welding resumption have been necessary.

Despite the use of improved lubricants, the wear of the die has been evaluated qualitatively critical compared to common secondary alloys for which 50 000 shots can be expected with no significant damages.

3.5.6 Shot-sleeve lubrication and wear

External and internal drop lubrication of the shot sleeve by mineral oil has been adopted. Nevertheless, the copper head of the shot sleeve showed increased wear: after 4 000 shots, the piston head has been substituted. Average 2 000 shots are reference values for EN AB 46100. Integral plungers and ring plungers have been adopted for secondary alloys and showed a prolonged life, respectively 8 000 and 35 000 shots before substitution, which makes their use interesting for Magsimal[®]-59.

3.5.7 Dimensional stability

Dimensional stability of the castings in Magsimal[®]-59 seems to be strongly influenced by stocking times. Measuring carried-out on castings made in AlSi9Cu3(Fe) - after 15 days from casting - showed constant tolerances of $\pm 0,1$ mm; measurements carried out on side frames soon after casting and after 15 days showed deviations of $\pm 0,3-0,5$ mm. These sensible deviations has not been observed on the capote carriers and o the roof brackets; therefore, the low dimensional stability of side frames can be traced back to the geometry of the casting itself, which is predominant in one direction (length).

3.6 Cost impact

The handling of Magsimal[®]-59 has implied several additional work procedures and tunings on the HPDC cell. Tab. 3.23 summarizes the main changes introduced, giving an estimation of its impact of the final operative costs. Price for consumables have been communicated by suppliers, as average prices in 2009. Operative costs of the HPDC-isle have been defined for two presses of different tonnage and are specified in tab. 3.24. Evaluations made on raw materials have been always referred to the nominal shot weight of the carrier capote (3,150 kg of the castings + 2,150 kg of ingate and overflows = 5,300 kg shot weight). The impact in terms of additional costs have been referred to the yearly planned volumes of the carrier capote (7 000 parts/year). Real prices and figures have been translated into percentages for confidential reasons.

	AlSi-secondary alloys	Magsimal [®] -59	Impact on costs
Operators	1 for 2 HPDC isles	1 for 1 HPDC isle	+ 15 %
Melting Procedure	Melting furnace Ladling Maintenance furnace	Melting and maintaining furnace next to the press	- 20 %
Metal loss during melting	5 %	10 %	+ 5 %
Metal cost	1,71 €/kg ¹ 1,89 €/kg ²	2,48 €/kg ³	+ 45 % + 31 %
Recycle of overflows	100 %	50 % - 50 % declassified to secondary alloys	+ 10 %
Skimming salts	No	Yes	+ 3 %
HPDC press	1 100 t - 150 €/hour - cycle time: 75 sec - p.rate: 640 parts/day - real: 600 parts/day	1 100 t - 150 €/hour - cycle time: 75 sec - p.rate: 640 parts/day - real: 260 parts/day 1 600 t - 170 €/hour - cycle time: 85 sec - p.rate: 560 parts/day - real: 520 parts/day	+ 13 % ⁴
Shot sleeve lub	No	Yes	+ 5 %
Die-lub dilution	1,8-2,2 %	3,3 %	+ 10 %
Downtimes	1	1,1	+ 10 %
Rejects	1	1,05	+ 5 %
Shot sleeve wear			
- copper head	4 000 shots	2 000 shots	+ 20 %
- integral	8 000 shots	N.A.	
- ring plunger	35 000 shots	N.A.	
Die wear	20 000 shots	5 000 shots	+ 20 % ⁵
Wear of wall of the furnaces	1x 6 months	1x 5 months	+ 10 %
Total			+ 150 %

Tab. 3.23: comparison table between Magsimal[®]-59 and AlSi-secondary HPDC-alloys.

¹ average of WVM's pricelists of 2009 for a 226 – AlSi9Cu3

² average of WVM's pricelists of 2009 for a 233 – AlSi10Mg(Cu)

³ average of Rheinfelden's official pricelists of 2009

⁴ see tab. 3.24 for details

⁵ considering a ionitring treatment of the die

One single operator taking care of the HPDC isle run with Magsimal[®]-59 is necessary. The melting procedure has been simplified by the introduction of the melting/maintaining furnace and sensible savings have been achieved by eliminating the separate melting and the transport phase.

Magsimal[®]-59 ingots are average 38 % more expensive than AlSi-secondary alloys. Metal losses are 5-8 % higher with Magsimal[®]-59, as AlMg-alloys tend to oxide

faster than common AlSi-alloys. The value of 5 % has been considered as average after the introduction of the salt covering and skimming treatment.

Returns of Magsimal[®]-59 can be recycled just once and a maximum ratio scraps/virgin ingots of 50 %-50 % results in an increased operative cost of 10 %. Costs for raw material are therefore contributing at the highest extent to the total increase of the manufacturing costs.

Additional costs for skimming salts are considered by the addition of 1 kg salt for 1 ton metal; the ones rising from the use of a modern die-lubricant are based on the correspondence 1 shot = ca. 6 litres water.

Operating a 1 600 t-HPDC has caused additional expenses quantified in a +13 %, compared to a 1 100 t machine. Break-down of cost units are listed in tab. 3.24, considering their percentage share on the total amount. A 10 s longer cycle time has been cost out.

Cost Unit	Press 1 100 t [%]	Press 1 600 t [%]
Paying-back press	20	17
Paying-back facility	4	3
Direct personnel	15	13
Indirect personnel	16	13
Consumables	6	11
Power – general	2	4
Methane	6	8
Power – HPDC isle	5	8
Maintenance	4	8
General costs	22	15
Total	100	100
Operative costs	Benchmark	+ 13 %

Tab. 3.24: percentage operating costs of a 1 100 versus a 1 600 t- HPDC press.

Downtimes and rejects are respectively 10 % and 5 % more frequent with Magsimal[®]-59, if comparing the manufacturing of the carrier capote to the production of a casting of the same weight in UNI EN AB 46 100. Shot-sleeve wear could be determined only on simple copper-headed pistons. Die wear has been evaluated considering real manufacturing conditions of the carrier capote in Magsimal[®]-59 compared to analogue castings in AlSi9Cu3(Fe) under similar casting conditions and a ionitriding treatment of the die after 5000 shots. Wear of walls has been intended as the building of oxide layers in the melting/maintaining furnace.

Magsimal[®]-59 proves being more aggressive towards refractories and additional maintaining procedures are necessary. A new lining of the brick lay must be planned with an average time frame of 5 months.

Summing up all contributes of tab. 3.23 results in an additional percentage cost of + 150 %. Manufacturing of HPD-castings in Magsimal[®]-59 is therefore considerably more expensive in comparison to standard materials. Severe profiles of requirements

and new technical solutions are the key parameters to evaluate the use of the alloy. In different circumstances, profitability is bare to expect.

However, the main economic efforts for the use of Magsimal[®]-59 are linked to the purchase of the raw material and to the melting and casting phases. No additional expenses have been traced back during after casting operations, see tab 3.26.

Phase	Magsimal [®] -59
Melting and casting	+ 25 %
Raw materials	+ 38 %
	Cost + loss
After casting operations	0 %
Shearing, sand blasting, machining,	

Tab. 3.25: additional costs arising from the use of Magsimal[®]-59.
Benchmark: UNI EN AB 46 1000.

Conclusions of tab. 3.23 are confirmed by the figures of tab. 3.26. Considering the cost units building up the price offer to the final customer, raw material costs are taking part to the 37 % of the total amount quoted for the carrier capote.

After casting operations, among which the cataphoretic painting plays a major role, are the second voice with 28 %. Casting, transport and after castings operations until machining follow respectively with 18 %, 10 % and 7 %.

Carrier capote	Cost [%]
Raw material (carrier capote + metal loss)	37 %
Casting	18 %
After casting operations: Shearing, sand blasting, machining	7 %
After casting operations: Machining and cataphoretic painting	28 %
Transport	10 %
Total	100 %

Tab. 3.26: percentage incidence of the manufacturing phases on the total cost of the carrier capote.

3.7 Conclusions

The use of Magsimal[®]-59 in HPDC often fascinates the final end-user, as highest performances are targeted in the as-cast state. The design engineer is required being well-experienced on casting alloys, as the requirements in terms of mechanical properties need to be translated in the correct design of the parts, in order to suit the features of Magsimal[®]-59. The HPD-Caster is in most cases the key ring of the whole supply chain, as the turning point from theory to practice and as manager of operative problems. In most cases, the final results on real castings are a reasonable

compromise between designed properties and the post-mortem analysis of the sampling or pre-series production parts.

The outcomes of 3.5 and the figures of 3.6 could strongly influence the evaluation of new projects where Magsimal[®]-59 is adopted. Many arisen difficulties have been solved “afterwards”, by means of a back-up solution. By way of examples, the need of maintaining the chemistry of Magsimal[®]-59 into strict intervals has called for the changes described in 3.3.3.1; the shrinkage phenomena on the carrier capote, see 3.5.3, required some intervention on the die and its geometry; the behaviour of the die to wear could have been improved to a great extent, if manufactured using better performing steels.

The driving factor “cost” calls for solutions which are in most cases contrasting with the technical requirements set on the parts. However, if insufficient resources are invested in the development of the casting, also taking into account the hardware needed for its manufacturing, significant if not even higher-than-budget costs are falling due.

According to the author, there is some potential for improving the general performance and productivity of the entire HPDC process. The most interesting areas to act on have been identified with:

1.) Designing, of castings and process.

The use of CAD/CAE tools reveals being more and more important for challenging parts. Simulations of die-filling, metal solidification, filling speed and temperature distribution have been run for the capote carrier brackets, as they are the most complex parts of the car set. However, the use of this tool has been implemented, say, in a “static” way, according to the diagram of fig. 3.123. The HPDC, shearing and machining dies have been manufactured at the very beginning of the project and modified through three samplings, according to the results achieved step-by-step. The simulations have been therefore merely used as a confirmation of the carried-out operations and have not played an active role in avoiding or shortening the optimisation phase. The approval for series manufacturing has been obtained through several modifications of the tooling until the achievement of the desired quality level.

The correct approach to the design of casting and process can be represented as per fig. 3.124 and could be named “CAE design chain concept”. It includes a complete virtual loop, able to analyse any steps of a casting component through its life, meaning manufacturing process, possible heat-treating, machining, assembling and life test.

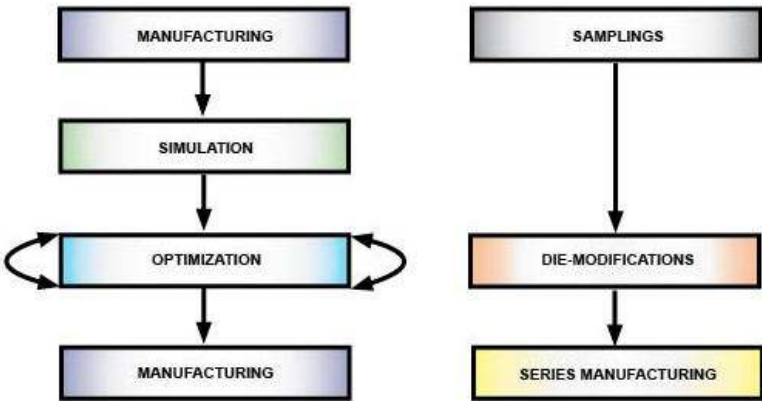
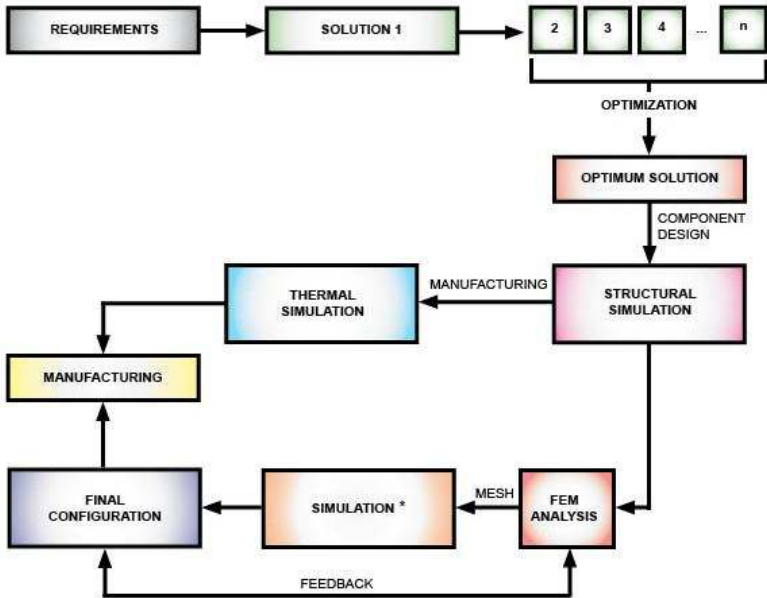


Fig. 3.123: CAE/CAD approach used for the F149 car set.

An accurate and reliable integrated methodology, based on virtual prototyping², allows the control of original investments, product costs, time to market and, in particular, can avoid start-up problems.



* if heat-treatment is performed, the simulation of residual stresses through Von Mises should be done

Fig. 3.124: the CAE design chain approach.

² IDP: Intelligent Digital Prototyping

The analysis of requirements leads to the definition of a first solution, which can be optimized automatically by software iterations, until the best one has been computed. By comparison of several possible solutions, the one which grants the highest safety coefficients and the best process conditions can be selected.

Hence, the thermal analysis can be run in order to define the fluid-dynamic aspects, relevant to the manufacturing process. On the other side, the structural analysis can be run in order to fine design and tune the component in its structure/geometry. Die filling simulation allows changing die geometries very quickly in the early phase of designing. After the first concept of the product, a FMEA identifies the weak points, allowing a cost-free re-engineering solution. Its integration with a process simulation analysis estimates the mechanical properties of the casting and therefore its behaviour during operation, often reducing unwelcome manufacturing defects and connected costs.

Through a FEM analysis and the meshing of the part, the final configuration of the casting can be defined, even before starting with the tool manufacturing.

If on one hand-side, a CAE design chain approach is much more complex and more work-intensive in its early stage than traditional solutions, modern softwares are able to link and blend different disciplines, in order to bring light on the following points:

- double-check and confirm the feasibility of the component in terms of smooth running and cost efficiency of the production process.
- compare several solutions or even different casting processes or different process layouts. i.e. to assess the convenience of running certain jobs before or after others.

The same tools can be used for having a closer look to the key variables of the process, such as the HPDC die and its heat balance, which is in turn strongly connected to die-wear. In the design phase, long before tooling manufacturing, the numerical approach allows to search for new solutions to improve die-life (thermoregulation, new materials, new release agents, deposit/coating) [28].

2.) Process stability

The set-up phase of the casting process has required longer than planned: the melting procedure has been changed and tuned; the optimal solution would imply the purchase of new hardware; the HPDC-machine has been changed after a start batch, increasing its closing force in order to get the required productivity. Full process stability has not really been achieved, if not after many efforts. Learning by doing is for sure an important rule; however, considerable savings can be pursued by designing the HPDC process to suit Magsimal[®]-59 with dedicated casting facilities.

The cast nodes in Magsimal[®]-59 for the F149 are a challenging application, at the state-of-the art on a 100 % aluminium chassis car. The parts can be considered the results of a continuous work-in-progress phase, which calls for increasingly high mechanical properties in terms of yield strength, elongation and fatigue strength. Deformability and ductility need to be granted, as the castings have to absorb the highest amount of energy in case of crash. High-pressure die-castings are nowadays required to be heat-treated, welded, ductile and stronger; they become larger, integrate several functions, but with lower wall thickness, in order to save weight.

This trend is rapidly bringing casting materials close to their physical limits.

The results of 3.4 and previous experiences with Magsimal[®]-59 have shown that the sensitivity of elongation to HPDC is enormous. The presence of shrinkages, gas pores or other casting defects locally influence elongation to a high extent, reducing its values even by 80 %.

Under the light of these considerations and of the strong dependence of the mechanical properties, inter alia elongation, of AlMg-alloys on SDAS, a research study has been conducted on Magsimal[®]-59 solidified at high cooling rates. The aim of the research is the understanding of how much the performance of Magsimal[®]-59 can be improved by changing the solidification rate and correlating the variation of mechanical properties to the achieved microstructure.

The results of the study are reported in chapter 4.

Chapter 4
Twin-roll casting

4.1 Introduction

The results of chapter 3 have shown one of the weak points of modern HPDC technology: delivering invariant quality and granting the same performance of the castings through all series production.

In fact, the carrier capote asked for a long optimization phase, before being able to satisfy the required mechanical properties and the challenging 8 % elongation. The tests on the fix bench have been successful only after significant changes in the melt shop of the foundry.

This “post-mortem” approach, which calls for improvements after the assessment of deviations from requirements, can somehow be related to the common logic of designing of the castings.

Traditionally, in fact, after the definition of the geometry according to the main functionalities and the boundary conditions, the casting is designed with the help of CAD tools. The profile of requirements comes as result of FEM simulations, where the stresses and critical areas can be evaluated in their details. According to the FEM output, suitable corresponding casting alloys are sorted out from a database or selected from the technical information by the suppliers of raw materials.

To the light of the most recent design criteria, this phase can be difficult. Generally speaking, in fact, modern automotive high-pressure die-castings are designed with less wall thickness to save weight and in turn lowering CO₂ emissions. High absorption of energy is of vital importance in case of crash; therefore, structural, crash relevant and ductile parts are designed with increased mechanical properties and fatigue strength. In most cases, additional requirements such as weldability, corrosion resistance or ability to be riveted are required; elimination of heat-treatment is an option. In such complex scenarios, the missing link is often the correct evaluation of the material properties and the knowledge of its metallurgy and direct impacts on the floor shop.

Additionally, for practical reasons and to get a statistical reliability, many suppliers cast their specimens apart, in laboratory conditions. The resulting nominal mechanical properties of a casting material are often superior compared to the ones delivered by real castings, as the influence of casting defects is not considered. Reductions to 70 % of YTS or UTS or even to just 10 % of the nominal declared elongation have been observed by the author on foundry cast products.

However, there is still currently no norm handling this theme.

UNI EN 1706:1998 gives just guidelines and defines mechanical properties for sand, gravity and investment casting cast-apart specimens. For high-pressure die-casting, appendix A has been inserted, which is clearly stated as “orientation” for the casting design engineer and roughly classifies the main common casting alloys in five groups. The scattering of indicated properties is referred to casting technology and kind of heat-treatments. This is the reason why in HPDC the profile of requirements, the position of tensile specimens and the details of assessment are traditionally stated by the final customer or handled face-to-face between the caster and his customer. UNI EN 1706:2010 has added some new alloys to the standardized materials, but has not brought light on the open point.

If the castings are structural parts, the design engineer appreciates having a higher safety factor and the stress is always put on the elongation and ductility of the material, as it “advises” before cracking. Available materials are thus brought very close to their physical limits.

Elongation and ductility are the most sensitive tensile properties and are influenced at highest extent by the presence of casting defects or even by the cutting-off modalities of the specimens. Among others, the so-called skin effect particularly influences elongation. As the standard deviation of $e\%$ is in most cases one order of magnitude higher than the one of YTS or UTS, it is important collecting data linking elongation to the main responsible levers of their increase and scattering.

Generally speaking, materials with high elongation show an improved ductility, which is in turn measured or evaluated with several testing methods, such as Charpy impact test, tear toughness test or Erichsen cupping test. In aluminium casting alloys, a metal which shows a fine dendritic microstructure as well as a eutectic phase with convenient size, morphology and spacing performs positively to this extent.

The key link to define an improved aluminium alloy of the next generation looks like: microstructure → elongation → ductility → toughness → strengthening. In other words, a strengthening of a material can be tuned to desirable results, if its microstructure can be somehow controlled.

Many control levers play a role at this extent, whereas the most relevant ones can be identified with the following four topics:

- 1.) Alloying, i.e. influencing the mechanical properties of a material by the chemical addition of elements which are expected to strengthen the material and to improve their elongation and ductility.
- 2.) Heat-treating, i.e. modifying the mechanical properties of a material by the realization of a well-directed thermal procedure, either with or without solutionizing.
- 3.) Manufacturing process, i.e. influencing the mechanisms of growth of specific phases or constituent parts of a casting alloy during its production and solidification in form of a semi-finished product. The induce alteration in the microstructure is expected to reflect improved mechanical properties.
- 4.) Casting process, i. e. influencing the final microstructure obtained on a casting by tuning the casting parameters in order to enhance one targeted aspects of solidification.

Concerning alloying, the turning point has been set in the 1990s by the introduction of low-iron primary HPDC alloys, which allowed a huge enhancement in terms of material performance, especially elongation [40]. Values of 5 to 10 % elongation have been reached in temper F; considering full-heat-treatments elongations of 20-25 % have been made possible. High-pressure die-castings could suddenly be heat-treated, welded, being at the same time ductile and stronger [41] [42].

According to the author, a similar turning point can not be expected again. AlSi-alloys have been chemically fully optimized and improvements can be achieved just in terms of heat-treatments [15][37]. AlMg-alloys would have still a potential in their chemistry.

In fact, foundry trials with HPDC-AlMg alloys with less than 0,3 % silicon have shown the possibility of reaching elongations over 20 %, while maintaining yield strengths above 170 MPa in the as-cast state. The drawback consists in the absence of silicon, which makes the castability of the metal very poor and not applicable in HPDC [38].

HPDC AlZnSiMg-alloys are not considered an alternative, as to the light of automotive requirements, waiting 10-30 days for the self-ageing of the castings and introducing a protective coating on the parts to prevent corrosion by zinc is not economical. Further improvements by means of simple alloying seem therefore not feasible any more. Promising aluminium materials are composite alloys, which have the intrinsic difficulty of creating a homogeneous matrix and reinforcement distribution. Ductility results always hindered. Additionally, MMCs did not find wide application in the automotive industry as the cost of raw materials is very high and the stability of the casting process can be hardly confirmed.

Aluminium nano-materials are the current research trend. However, there is still no evidence of successful alloys available for HPDC processing. Apart from the high manufacturing cost of nanoparticles, the main issues are connected to their poor wettability by aluminium and to their toxicity, especially for carbon containing nano-reinforcements [39].

Heat-treating can be very effective for the improvement of mechanical properties of casting alloys. Through the well-visible morphological modification of the eutectic phases or even through the simple recovery of a material, highest values in elongation and toughness can be reached. Amazing results have been obtained with heat-treated AlSi alloys modified with Te. Fluidized bed treatments or accelerated treatments, e.g. SST[®], have also shown positive results.

Nevertheless, the incidence of heat-treatments on the final cost of a casting and their disadvantages in the after-casting sessions call for their reduction and even their elimination. The average size of automotive castings is increasing, making the carrying-out of the heat-treatment challenging, as corresponding furnaces must be available. Therefore, compromises with the mechanical properties of temper F are strongly targeted and if a heat-treatment must be carried-out, the choice is in most cases made on a single-step heat-treatment without solutionizing.

Ideally, a casting material of the next generation exhibits superior properties, ductility and toughness in the as-cast state.

The influence of the manufacturing process and parameters have been the key topics of the 1990s, leading, for example, to the developing and patenting of Silafont[®]-36, AlSi9MgMn in 1994 and Magsimal[®]-59, AlMg5Si2Mn in 1995. The “manufacturing recipe” guaranteed superior performance of these metals compared to the standard ones available. Par. 2.4 and 2.5 show how the special production process of Magsimal[®]-59 influences its final mechanical properties. The manufacturing of the latter has been optimized in the last 25 years and, if further improvements will be carried-out, they are expected to be of a small scale.

Further experiences have been done with AlSiMg and AlMgSi casting alloys according to the so-called AMS¹ technology.

¹ Alloy Memory Structure

Melts have been solidified after the undergoing to a magnetic-electric field, with the aim of generating nuclei without adding grain refiners and homogenising the poured ingots, thus avoiding segregation and local differences in their microstructure. Encouraging results have been obtained on pilot castings and casting temperature of the metal could be lowered by 80°C. An improvement of the mechanical properties could be observed, thank to the more globular and homogeneous microstructure. Unfortunately, the obtained cast ingots do not always show the same “level of memory” of the previous manufacturing phases and switching to a stable manufacturing process seems not possible.

The lever of a modified casting process looks like the Trojan horse, hiding the biggest improvement potential. In fact, semi-solid processes, squeeze casting, liquid forging and similar are currently further investigated: the artificial modification of the microstructure, achieved during the final forming of a part, seems to be considered the most effective way of improving the basic properties of a material, see fig. 4.1. Highest attention is paid to the solidification phase, as the passage from the liquid to the solid state is the key step for achieving the desired final microstructure.

As reported in par. 1.4, the AlMgSi system has superior performances, but shows a more pronounced decay of its mechanical properties by increasing wall thicknesses in comparison to AlSiMg alloys. Besides, considering the more pronounced tendency to solidification shrinkage, the AlMgSi-system results technologically interesting for castings with wall-thicknesses up to maximum 6 mm.

This drawbacks could be minimized by the dimensional refinement of the metal structure, which could make its use even more interesting in the common thickness of 2-3 mm, typical of HPDC, or at least more competitive on thicknesses over 6 mm. AlSiMg and AlMgSi casting alloys form dendrites during solidification. As generally known, their strength and elongation are increasing with the decrease of the SDAS [30]. The SDAS is in turn strictly connected to the local solidification time, which can be finally controlled by the cooling rate.

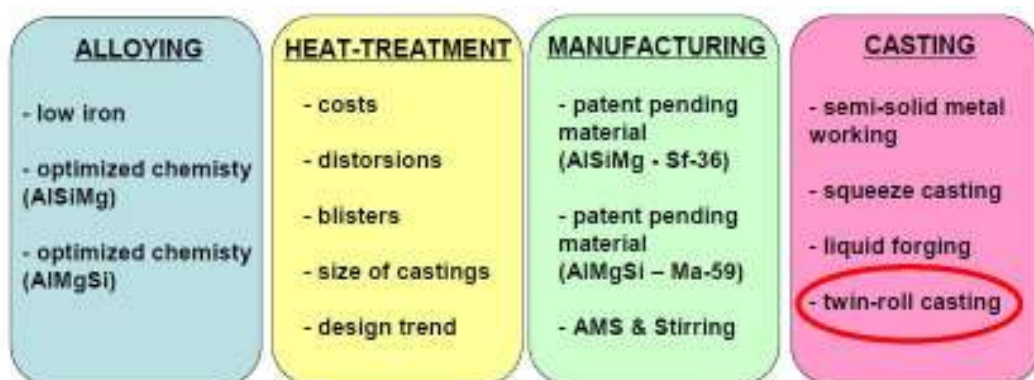


Fig.. 4.1: the four main levers of inducing morphological changes into the microstructure of an aluminium casting alloy.

From the literature, it is well-known that, in aluminium alloys, a ductile fracture causes the formation of dimples, which are resulting from the fracture of particles present in the microstructure or from its tearing-off from the matrix.

The finer, the particles, the higher the stress needed to their breaking or tearing-off. Additionally, according to some in-situ SEM observations on AlMgSi A6061 alloys and further analysis, it has been established that Mg₂Si particles of 1 to 1,51 μm diameter have a fracture strength of ca. 440 MPa [30].

Following this track and fitting the concept on Magsimal[®]-59, a microstructure refinement by a rapid cooling has been attempted, with the aim of assessing the potential improvement on the basic material performance. To this extent, a casting technology, called “twin-roll casting” has been introduced and presented in its details in par. 4.2. Its setting-up increases dramatically the cooling rate during casting (estimated between 1 000 to 4 000°C/s) and therefore solidifies the metal under improved conditions.

The particles present in the ternary eutectic of Magsimal[®]-59 are Mg₂Si, whose growth is induced globularly during manufacturing. Assuming that the solidification of Magsimal[®]-59 in the twin-roll caster would result into a eutectic Mg₂Si of micro dimensions and that the mechanism of fracture would initiate at the interface within α-aluminium dendrites and Mg₂Si particles, a sensible improvement of the material performance would be possible. In fact, taking into account the nominal mechanical properties indicated in [12] for a 2 mm wall-thickness plate, the improvement of UTS could be quantified as + 33,3 %. A morphological refining of the secondary phases and intermetallics can also be expected.

This chapter introduces the basics on traditional and high-speed twin-roll casting along with its relationship to toughness and Erichsen test. The adopted experimental procedure and its design of experiments are presented. Corresponding results on twin-rolled plates of Magsimal[®]-59 are discussed, setting as benchmarks HPDC plates of the same alloy with a wall-thickness of 2, 3, 4 and 6 mm, in temper F, T5, T4 and T7. Conclusions and outlooks close this chapter.

4.2 Twin-roll casting

The twin-roll casting is a manufacturing process widely used for steel and represents one of the various processes for its near-net-shape casting. Recently it has been applied to aluminium wrought alloys, as well as to magnesium alloys, with encouraging results [52].

Generally speaking, the core of a traditional twin-roll caster consists of two oppositely rotating water-cooled rolls, which are independently driven. The two rolls are rotating to a well-defined distance, creating thus a gap which corresponds to the thickness of the strip being cast. The molten aluminium is poured into the head-box of the casting machine, often connected to a planar pouring nozzle, which is in turn formed by thin-lipped slabs, usually of ceramic material. The melt forms a “puddle”, enters the roll bite and is instantly cooled down at its contact with the rolls. It solidifies under the load performed by the rotating cylinders and leaves the casting machine in the form of a sheet or a strip; the solidification of the metal is totally completed before the kissing point, i.e. the point where the two rolls are at the closest.

The main advantages related to this steel casting technology can be summarized as following:

- high productivity;
- increased mechanical properties, thanks to the rapid solidification;
- improved cast surface quality;
- low equipment costs;
- low running costs;
- energy saving;
- elimination of repeated rolling and annealing phases used in conventional sheet manufacturing methods;
- compactness and space saving;

On the other hand-side, the main issues connected to the twin roll process are:

- control of the casting operation and metal flow in order to minimise the start-up stabilisation phase;
- metal-mould heat transfer;
- metal delivery system;
- homogeneity of solid shell formation and corresponding characteristics of the strips;

4.2.1 Conventional Twin-Roll Caster for Aluminium alloys (CTRCA)

Conventional Twin-Roll Casters for Aluminium alloys (CTRCA) are typically horizontal casting systems, which have additional disadvantages as per par. 4.2, such as limitations of the processable materials: alloys with wide solidification intervals, in fact, can not be cast.

A CTRCA is commonly tooled with steel rolls, which need to be sprayed with a suitable parting lubricant in order to provide cooling and to avoid sticking phenomena. This affects in turn the casting speed, which is normally not higher than 10 m/min, normally 2m/min. If the rolling speed is set too high or cooling is not adequate, the contact time between the roll and the strip is too short and not sufficient to grant a good quality strip.

Additionally, the loads applied on the rolls of a CTRCA are of one or two orders of magnitude lower compared to the ones applied by more advanced devices. If the load applied on the rolls is too low, the transfer of heat between roll and metal is weak. This can lead to a partial solidification of the strip with consequent poor quality of the final product.

4.2.2 High-speed Twin-roll Caster for Aluminium Alloys (HSTRC)

An improved version of the CTRCA is the so-called High-Speed Twin-Roll Caster (HSTRC), which denotes remarkable functional differences. A schematic sketch of the high-speed twin roll-caster, used for the experiments of par. 4.6, is represented in fig. 4.2.

The HSTRC adopts water-cooled copper rolls with higher thermal conductivity than steel rolls. Furthermore, conventional rolls have 25 to 60 mm-thick shells, while high-speed casters have normally a 6 mm-thin shell, see fig. 4.3.

Copper rolls do not require any lubricant or release agent, which introduce a resistance to heat exchange between roll and strip. Therefore, higher heat transfer coefficient and higher thermal conductivity are guaranteed by a HSTRC in comparison to a CTRCA.

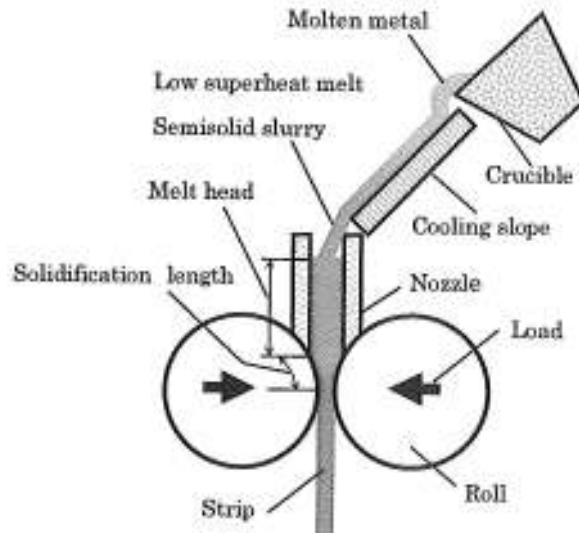


Fig. 4.2: sketch of a high-speed twin-roll caster.

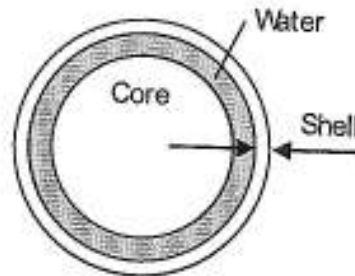


Fig. 4.3: section of a HSTRC roll.

The load applied by the high-speed rolls is 10 to 100 times higher than common ones and this increases the heat exchange coefficient as well. The casting of alloys with a wide solidification interval is therefore made possible.

The integrity of the cast strip is a function of its final temperature at the exit from the twin-roll caster. An increased thermal exchange allows the reduction of strip temperature and therefore an increase of the casting speed, which is up to 10 times higher than with a CTRCA. Higher rolling speeds means higher cooling rates, shorter solidification times and therefore finer microstructures.

At the same time, the reduction of the melt and casting temperature can be achieved. In fact, a cooling slope allows for the casting of a low superheated melt with the feeding of semi-solid metal. This would not be possible in a CTRCA as the metal could solidify in the nozzle.

The nozzle of a HSTRC is adjustable and formed by 4 walls (two moving nozzle plates and two dam plates) and is put in straight contact with one roll. The feeding of metal is thus direct and the hydrostatic pressure by the metal is higher. As consequence, the turbulence during casting is lowered and limited to the meniscus of the molten metal. The oscillation of the meniscus occurs at the corners of the nozzle and can be traced-back by the marks visible on the final cast strip product. The marks are symptoms of a non-perfect adherence between roll and melt and become more and more visible with increasing rolling speeds.

The strip does not solidify according to a straight trajectory, but according to the circular profile of the roll: the solidification length can be thus introduced, see fig. 4.2. The solidification length can be easily controlled by the position of the nozzle, which in turn determines the solidification time of the strip together with the rotating speed.

Previous experiences with a HSTRC have shown that casting of 3 mm-thick strips of 6016 aluminium alloy can be carried-out at 60 m/min, with satisfying mechanical properties and with the passing of the 180 degrees bending test after cold-rolling and a T4 heat-treatment [43]. Sensible refining of the microstructure has been observed and the as-cast strips have been rolled down to 1,0 mm without homogenization or intermediate annealing [44].

If the width of the twin-roll cast strips could be increased over 1500 mm, the application of the technology to the series manufacturing of skin door outer panels for cars could be applied, shooting down the cost difference between the steel and the aluminium solution. At this extent, casting trials have been done with 3084, 5182 and 6022 wrought alloys cast at 20 m/min with an unequal diameter HSTRC and a roll width of 400 mm. The process has shown feasibility through its easiness and positive mechanical properties of the strip after a T4 heat treatment. However, the presence of casting defects needs to be targeted [50].

Similar results have been obtained with an AlSi3Mg alloy, with even higher casting speeds, ranging from 60 to 90 m/min. The presence of silicon has shown a further improvement of the casting quality and no influence on its ductility. Additionally, a geometrical modification of the eutectic silicon has been observed as main effect of the high cooling rate: platelets have been turned into spherical particles of 5 μm [45]. Analogue silicon eutectic dimensions have been measured on A356 strips [48]. Elongations over 20 % have been obtained on T4 heat-treated strips of 6061 wrought alloy, even with iron contents up to 0,7 %. The refining effect of the twin-roll caster on Fe-intermetallics has been confirmed and the precipitation of needle-like phases can be avoided up to 2 % iron content. The technology could be therefore be applied for the efficient recycling of aluminium alloys [46] [49] or to innovative composite materials. In fact, the combination of two different alloys in one multilayer product has been attempted by the casting of a clad trip through a HSTRC provided with a scribe. Two melts have not been mixed and the two resulting single strips have been firmly joined, not debonding during a peeling bending test [51].

4.3 High speed twin-roll casting and toughness

Kumai et al. have established that AlSiMg heat-treatable alloys and AlMg non heat-treatable alloys with similar strength and ductility show improved toughness, respectively 1,8 and 3 times higher, if twin-roll cast compared to vacuum HPDC products [31]. The effect is even more remarkable with a secondary AlSi11Cu2 alloy, whose microstructural refinement has led to the increase of the toughness of a factor 6 compared to HPDC samples [32]. Toughness has been evaluated by means of the UE_p , the unit crack propagation energy, expressed in kNm^{-1} and defined as the ratio between the crack propagation energy and the net area of the specimen, see orange area of fig. 4.4. UE_p is considered representative of the tear toughness of a material [33]. UE_i is defined as the unit crack initiation energy, see sky-blue area of fig. 4.4. The sum of UE_p and UE_i is called UE_t , i.e. unit total crack energy.

The samples of fig. 4.5 have been tested according to the ASTM B871-96² whose typical load-displacement output curve is shown in fig. 4.4. The sharp-notched specimens are set under static load until a crack initiates at the notch and propagates across the width of the specimen itself.

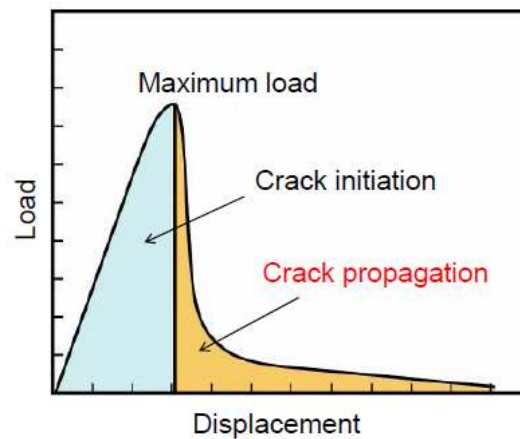


Fig. 4.4: key values of a load-displacement curve for tear toughness test.

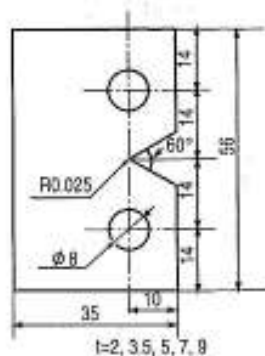


Fig. 4.5: tear toughness test samples.

²

Standard test method for tear testing of aluminium alloy products.

Tear toughness is strictly related to the SDAS: decreasing SDAS values correspond to higher toughness. In particular, the refinement of SDAS and of the grain size increases both UE_p and UE_i . In other words, the area under the load-displacement curve of fig. 4.4 as well as the maximum load increases with diminishing SDAS values. The HSTRC is therefore very effective to improve toughness and ductility of a metal. However, the impact on increasing cooling rates on UE_p and UE_i is different: the quantitative balance between the two values is favoured to UE_p by increasing solidification rates. The same effect has been observed with decreasing wall-thicknesses. For an A356 aluminium alloy, this has been referred to the different features of crack propagation path depending on the fineness of microstructure [33]. Tear toughness has been evaluated on samples or reduced size compared to the standardized ones. Additionally, the numerical results of the tear test are known to depend not only on the specimen size, but also on their thickness. In particular, maximum load, UE_i and UE_t increase with increasing wall-thicknesses, while UE_p shows the opposite trend [34].

Generally, UE_p is considered more representative of tear toughness, as the correlation between wall thickness and the unit crack propagation energy is almost linear and not dependent on the geometrical and surface finishing conditions of the material. For this reason, a new evaluation method of tear toughness has been developed by Kumai et al., fitting the second part of the load-displacement diagram with a cosine curve. The tear test results have been thus expressed by a logarithmic chart, useful to compare quickly different alloys.

4.4 Tear toughness of Magsimal-59

Tear toughness values have been collected for several alloys and different casting technology, in order to compare them and to build up a database. The results presented in tab. 4.1 have been extracted from [35] and completed with the values for high-speed twin rolled Magsimal[®]-59 obtained from [36].

Alloy	Chemistry	Technology	Temper	Tear toughness	Unit
ADC12	AlSi11Cu2(Fe)	HPDC	F	1,7	kNm ⁻¹
AC4C	AlSi7Mg(Fe)	Gravity	F	2,5	kNm ⁻¹
A356	AlSi7Mg	Gravity	T6	10,6	kNm ⁻¹
	AlSi11MgMn	HPDC	F	18,0	kNm ⁻¹
	AlMg3SiMn	HPDC	F	21,0	kNm ⁻¹
AC4CH	AlSi7Mg	Squeeze	F	25,0	kNm ⁻¹
	AlSi11MgMn	Twin-roll	F	26,0	kNm ⁻¹
	AlMg3SiMn	Twin-roll	F	26,3	kNm ⁻¹
AC4CH	AlSi7Mg	Squeeze	T6	30,0	kNm ⁻¹
	AlSi11MgMn	HPDC	T6	31,0	kNm ⁻¹
Ma-59	AlMg5Si2Mn	HPDC	F	34,6	kNm-1
A356	AlSi7Mg	Direct Chill	T6	52,6	kNm ⁻¹
Ma-59	AlMg5Si2Mn	Twin-roll	F	58,8	kNm⁻¹

Tab 4.1: tear toughness values of aluminium alloys cast with different technologies.

Conventional casting alloys, such as ADC12, show a very brittle behaviour. Primary metals cast under gravity do not achieve improved values, even if treated to temper T6, as the cooling rate is very low. HPDC favours significantly tear toughness: Magsimal[®]-59 in temper F has the same tear toughness as AlSiMg casting alloys treated to T6.

HSTRC strips of Magsimal[®]-59 have achieved the value of 58,8 kNm⁻¹, which is 1,7 times larger than the HPDC one. It has been observed that the microstructure of Magsimal[®]-59 has been significantly refined; eutectic Mg₂Si particles have shown typical dimensions around 1 µm and a globular morphology; SDAS has been reduced by 70 % compared to 3 mm-thick HPDC plates, resulting into 1,1 to 3,4 µm; the geometry of Mn-intermetallics has not been influenced, but their size have been reduced to 1 µm. The refining effect has the same effectiveness on the near-to-surface region of the plates as well as at their core [36]. As consequence, the fracture mechanism has been extremely ductile.

In order to assess if the increased tear toughness of the HSTRC technology has reflected on the static mechanical properties of Magsimal[®]-59, tensile tests of HPDC plates with varying thickness and of HSTRC in different tempers have been carried-out, see par. 4.7.2.

4.5 Tear toughness and Erichsen test

The procedure for tear testing can result time-consuming, as samples of given geometry need to be prepared. According to the author, an alternative criterion to evaluate tear toughness and/or the ductility of aluminium casting alloys could be the so-called Erichsen cupping test.

The adoption of this test would make the comparison between different casting alloys easier, faster and simpler. In fact, Erichsen test is a very popular in the field of metal sheets, pressed and deep drawn components as it gives a rapid response to the capability of deformation and ductility of a material stressed under biaxial load conditions. The reference norm is the UNI EN ISO 20482. Fig. 4.6 shows the equipment adopted for the test.

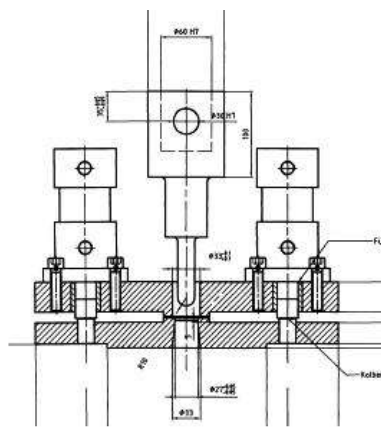


Fig. 4.6: Erichsen test standard equipment.

Once the test plate has been clamped between the two holders, a punch is put into contact with the sample. Indentation is started with a rate of 5 to 20 m/mm and the load-displacement curve is recorded. The key moment of the test is the appearance of a crack on the lower surface of the test plate, which can be observed by means of a lens or a mirror and determines the end of the test itself. The bulge depth represents the so-called Erichsen Number or Erichsen Index (IE), expressed in mm. Crack position and progress, as well as internal cup surface conditions reflect the behaviour of the metal; a smooth surface featured by a circular crack following the contour of the bulge denotes a fine and ductile microstructure; a radial crack with a rough sharp surface defines a poor ductility. The slope of the recorded curve is function of the chemistry and temper of the alloy: the lower, the more ductile the metal.

The integration of the load-displacement curve until crack results in the crack initiation energy. Within the meaning of the Erichsen test, the crack propagation energy does not have a relevant meaning, as at this point the material is fractured and therefore not considered in service conditions. To such an extent, the tear test value of UE_i gains in importance, as it reflects the ability of a metal to absorb energy, while deforming in a ductile way until fracture. The load-displacement curve of Erichsen test looks very similar to the tear toughness one. However, aluminium casting alloys behave with an almost linear response to the application of the load during the crack initiation phase. After the cracking of the metal, in most cases a pop-in can be observed.

Following this track, a design of experiments with HPDC and twin-rolled plates in Magsimal[®]-59 have been planned, in order to determine the following:

- IE values of HPDC and HSTRC products, with quantitative comparison of corresponding load-displacement curves
- correlation between results of tear toughness and Erichsen test, according to different wall thickness of the cast plates
- correlation between results of tear toughness and Erichsen test, according to the temper, i.e. heat-treated state of the cast plates

The aim is determining a new criterion for the assessment of toughness and ductility.

4.6 Experimental procedure

In order to compare the properties of Magsimal[®]-59 cast in HPDC and in HSTRC, specimens have been manufactured with both technologies. Tensile and Erichsen cupping tests have been carried out for each variant of tab. 4.2. Microstructural changes of HSTRC plates have been evaluated and correlated.

4.6.1 HPDC plates

HPDC plates in Magsimal[®]-59 have been cast on a 400 t Bühler B press with a forced venting system in the laboratory of Rheinfelden Alloys GmbH & Co. KG. The plates have typical dimensions of 220 x 60 mm. The wall thickness has been varied according the design of experiments of par. 4.6.3. Melt temperature has been recorded to 710-720°C and its density index has been determined lower than 1 % with the low pressure test. Degassing with Ar and N₂ has been performed for 6 minutes to 550 rpm. Die temperature has been set to 200°C and the gate speed to 30 to 40 m/s. Series manufacturing virgin ingots have been used, without recycling any returns or scraps.

4.6.2 Twin-rolled plates

The high-speed twin-rolled strips have been manufactured and kindly set to availability by the Tokyo Institute of Technology.

2,4 kg of Magsimal[®]-59 have been melted in a crucible. Casting temperature has been recorded to 633°C. The initial roll gap has been fixed to 1 mm and the separating force on the spring has been measured in 14,4 kN, being one roll fixed and one roll movable. The molten metal has been cast on a cooling slope, in order to achieve a ca. 10 % fraction solid metal before casting, falling into a small nozzle placed at the top of the two rolls. The copper rolls rotated while producing a strip at a linear speed of 50 m/min. The solidification length has been set to 100 mm. Resulting strips are presented in fig. 4.7. Their width is 100 mm, with a thickness of ca. 2,0-2,2 mm and a total length of 3 400 mm. Single plates with a length of 190 mm have been obtained from the main strip by simple cutting.

4.6.3 Design of experiments

In order to compare the mechanical properties of HPDC and HSTRC Magsimal[®]-59, the design of experiments represented in tab. 4.2 has been carried out. Totally 120 HPDC plates and 6 HSTRC strips have been tested: the figures on the columns represent the number of plates used for each variant.

	F	O	T4	T6	T7
HPDC - 2 mm	6	6	6	6	6
HPDC - 3 mm	6	6	6	6	6
HPDC - 4 mm	6	6	6	6	6
HPDC - 6 mm	6	6	6	6	6
HSTRC - 2 mm	3	3	-	-	-

Tab 4.2: design of experiments for HPDC and HSTRC plates in Magsimal[®]-59.

HPDC plates have been tested in the wall-thickness of 2, 3, 4 and 6 mm. Next to temper F, tempers O, T4, T6 and T7 have been introduced: although heat-treatments with solutionizing are known not having relevant effects on Magsimal[®]-59, test data have been collected in order to compare them with the ones of HSRTC. Each variant has been tested with 6 plates: 3 for tensile tests and 3 for Erichsen tests see par. 4.7.2 and 4.7.3. Tensile samples have been cut-off along the direction of casting according DIN 50125:2004-01, geometry E3x8x30.

HSTRC have been tested in the wall-thickness of ca. 2 - 2,5 mm. Tempers F and O have been chosen, as most effective on Magsimal[®]-59. Each variant has been tested with 3 plates: 2 for tensile tests and 1 for Erichsen tests. Temper T5 has not been tested, as the heat-treatment is not yet feasible with the high-speed twin-roll caster adopted for the plate manufacturing. The 6 twin-rolled plates have been marked as per tab. 4.3. Tensile tests have been performed both parallel (//) and perpendicularly (\perp) to the direction of rolling, in order to evaluate the sensitivity of mechanical properties at this extent, see fig. 4.7.

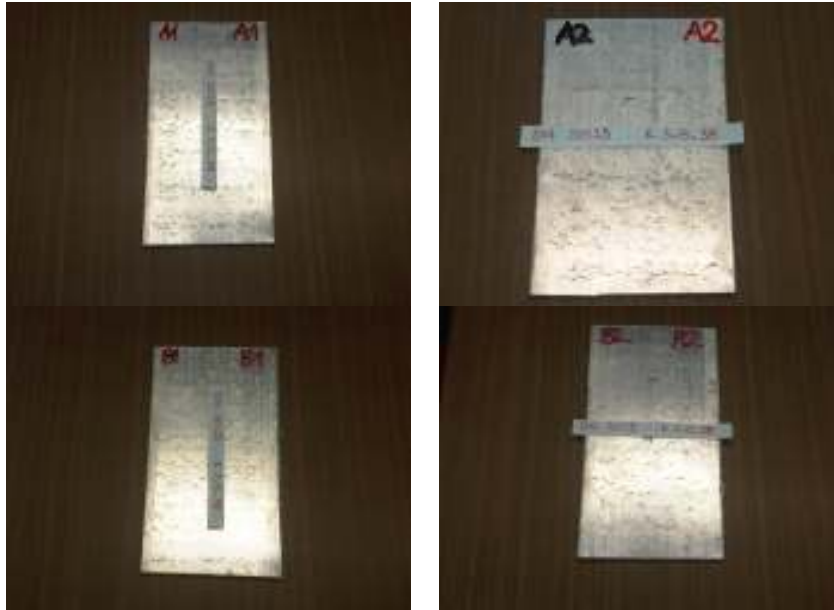


Fig. 4.7: cutting-off of tensile samples from the HSTRC plates.

Tensile samples have been cut-off along the direction of casting according DIN 50125:2004-01, geometry E3x8x30.

Tensile Test	F	O
Parallel (//)	A1	B1
Perpendicular (\perp)	A2	B2
Erichsen Test	C1	C2

Tab 4.3: marking of the HSTRC plates in Magsimal[®]-59.

The heat treatments have been performed according the following parameters:

- Temper F: as-cast state
- Temper O: 250°C for 60 minutes
- Temper T4: 490°C for 180 minutes + water quenching + 6 days to room temperature
- Temper T6: 490°C for 180 minutes + water quenching + 170°C for 120 minutes
- Temper T7: 490°C for 180 minutes + water quenching + 250°C for 120 minutes

The solutionizing and ageing times have been applied without heating-up time. Water quenching has been performed within 2 seconds from the extraction from the furnace. After ageing, the plates have been cooled down to room temperature by normal heat dissipation and with no forced cooling system.

4.7 Results and discussion

The results of the trials carried-out on the HPDC and HSTRC plates are presented in the par. 4.7.1 to 4.7.5.

4.7.1. Surface appearance and X-rays

The main difficulties arisen during the twin-roll manufacturing process have been connected to the surface aspect and to the wall thickness of the plates. The latter depends mainly on constancy of the pressure transferred by the spring to the copper roll. Its adjustment and fine tuning has proven to be difficult; this influences in turn the geometry of the strips, resulting in a slight concavity of the final cast shaped sheet along its width and in variable thickness along the rolling direction.

The profile measurements of the plates C1 and C2 are reported in fig. 4.8 and 4.9 and referred to the average of a double vertical (i.e. the direction of rolling) and horizontal (i.e. perpendicularly to the direction of rolling) assessment of their wall-thickness. The rolling wall thickness can be controlled with a tolerance of $\pm 0,5$ mm. The dimensional control of the strip can be done more accurately along its width, $\pm 0,2$ mm, with the exception of the two edges where non-stability of the melt meniscus has been observed. The concavity of thickness profile is caused by the different and non-uniform heat distribution of the roll surface. In the following paragraphs, the average wall-thickness of HSTRC strips will be referred as 2,5 mm. The plate surface has been observed with stereo magnifying glasses and an x-ray device.

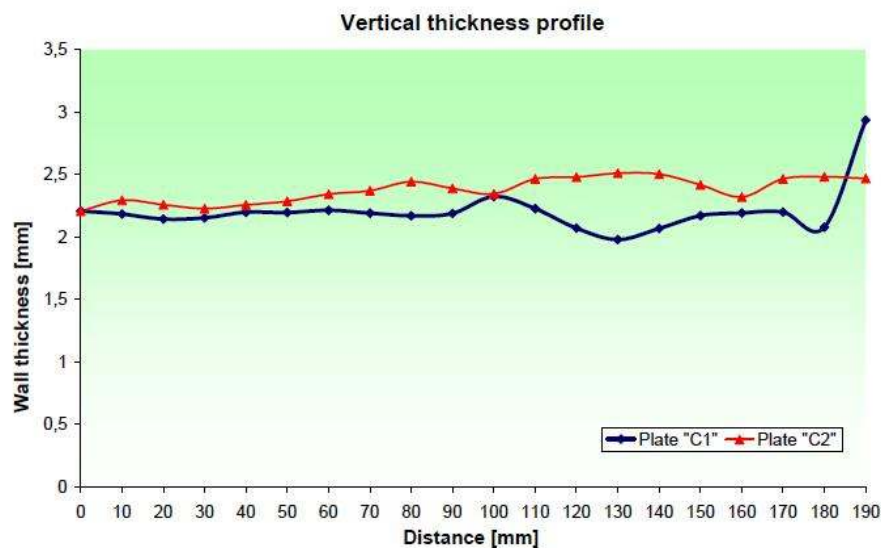


Fig. 4.8: vertical thickness profile of the plates C1 and C2.

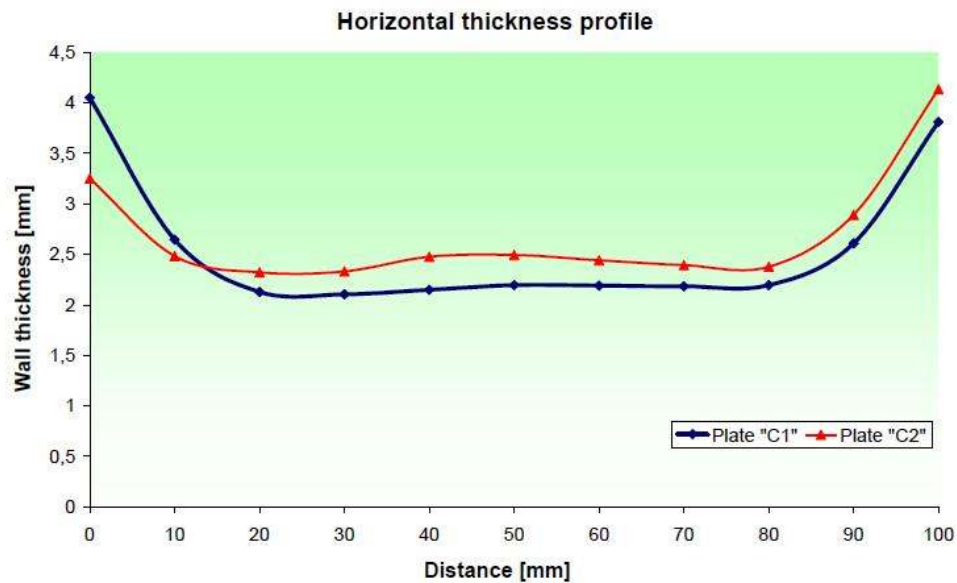


Fig. 4.9: vertical thickness profile of the plates C1 and C2.

Twin-rolled plates of Magsimal[®]-59 have a very bright metallic colour, with a grey surface lustre. However, the surface of the strips shows some casting defects. Ripple marks, of a cloudy white colour, can be observed on the plates A1, B1, C1 and C2, see sides "B" respectively of fig. 4.10, 4.11, 4.14 and 4.15. The phenomenon is not so pronounced on the plates A2 and B2. These patterns have been traced by the tip of the nozzle, which rubs on the roll, and are more pronounced during the start-up and end phase. Additionally, some superficial cracks have been observed on the side "A" of the plates and are located mainly at the grain boundaries. Zooming on this cracks shows that some of them are shrinkages – to be expected due to the low silicon content of the alloy. Cold-rolling has proven helpful to improve superficial shrinkages [44]. Furthermore, the adoption of parallel or cross grooved rolls can significantly help to reduce or eliminate the surface crack of the plates, as the contact surface can be increased and the wettability between melt and roll favoured [47]. The plates have been screened with X-rays, in order to trace the presence of internal casting defects. Plates A1, B1, A2 and B2 have been found fault-free. Small-sized shrinkages have been found on the plates C1 and C2. Fault-free plates have been chosen for tensile testing; the others have been used for Erichsen test.

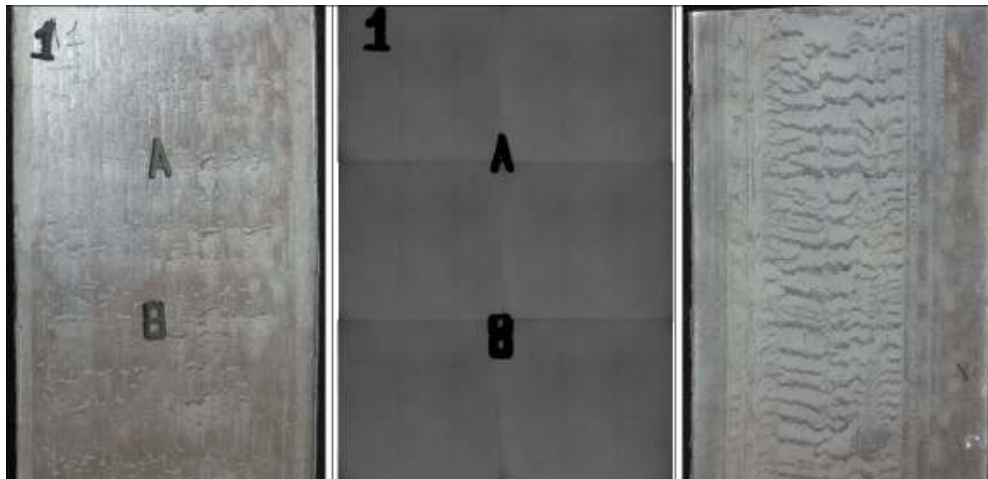


Fig. 4.10: plate A1. Side A (left), x-ray image (centre) and Side B (right).

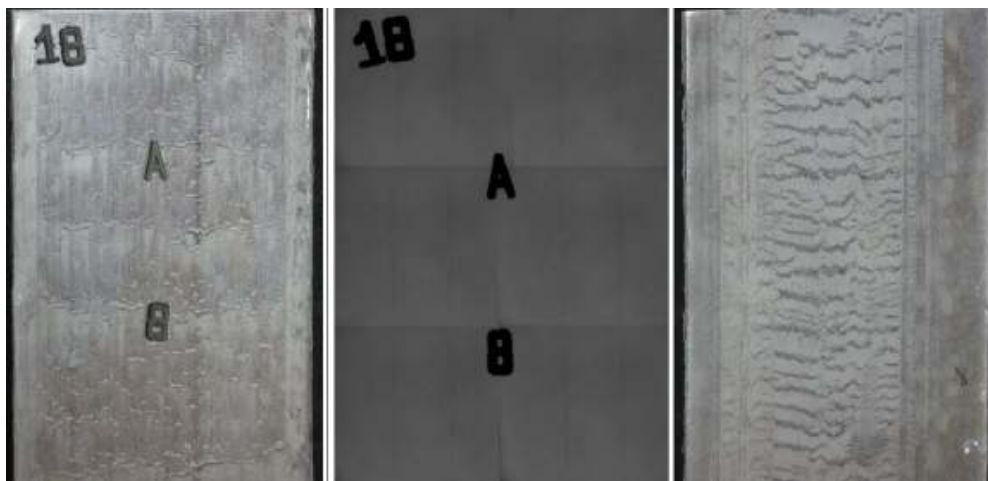


Fig. 4.11: plate B1. Side A (left), x-ray image (centre) and Side B (right).

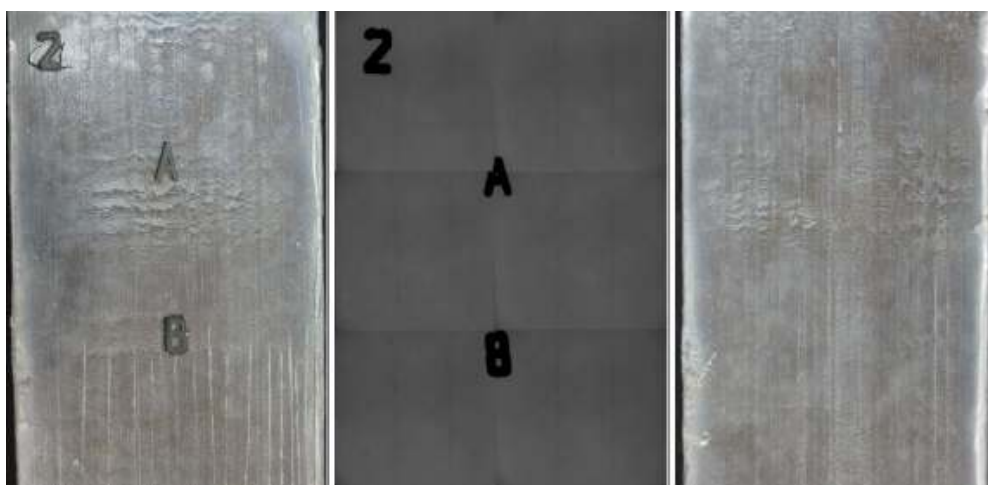


Fig. 4.12: plate A2. Side A (left), x-ray image (centre) and Side B (right).

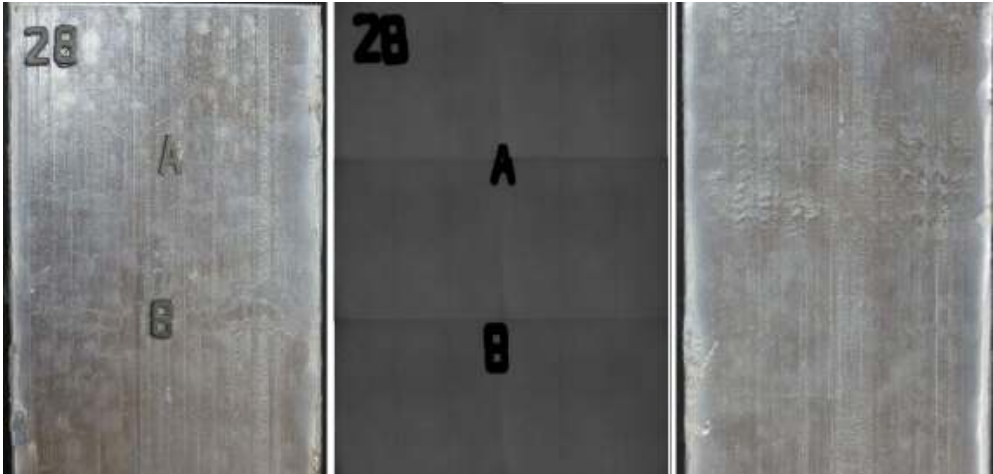


Fig. 4.13: plate B2. Side A (left), x-ray image (centre) and Side B (right).

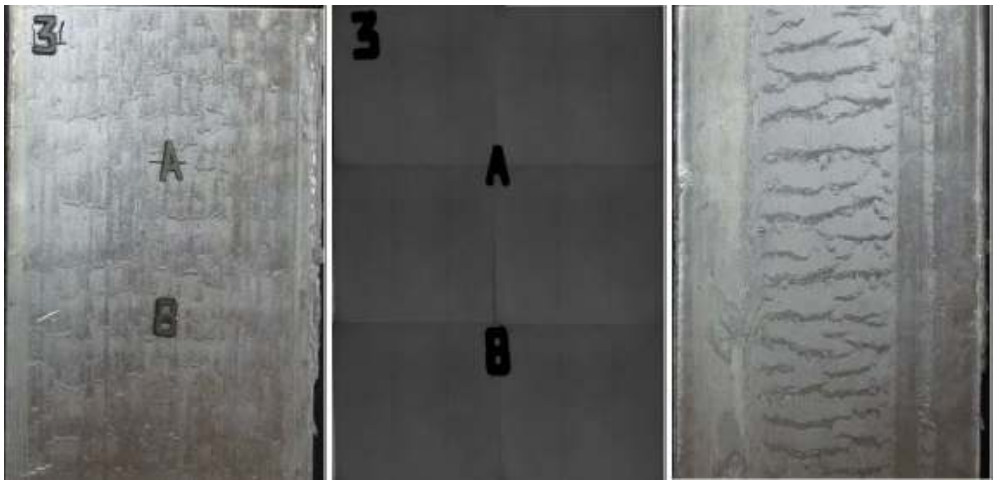


Fig. 4.14: plate C1. Side A (left), x-ray image (centre) and Side B (right).

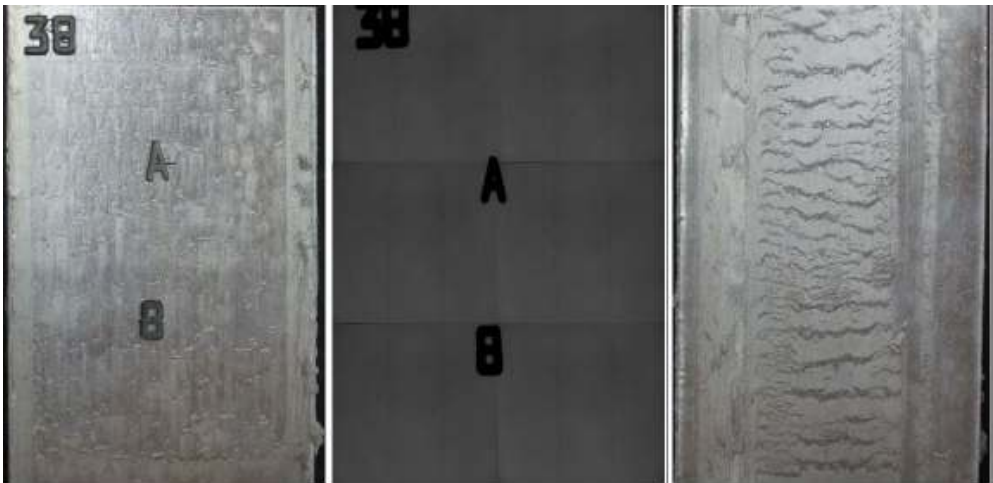


Fig. 4.15: plate C2. Side A (left), x-ray image (centre) and Side B (right).

4.7.2 Tensile tests

The results of tensile tests are reported in tab. 4.4, summarizing the average values, according varying wall-thicknesses and tempers. The mechanical properties of HPDC and HSTRC plates have been evaluated for each variant as average of respectively 6 and 10 specimens. Non-valid tests have been discarded. The tests have been carried-out according EN 10002, setting a traction speed of 10 MPa/s until YTS and of 10 mm/min from YTS until fracture. Pre-load has been reached at 1 mm/min.

Casting process	Wall-thickness [mm]	Temper	YTS [MPa]	UTS [MPa]	e [%]
HPDC	2	F	230	354	10,3
HPDC	3	F	186	320	10,5
HPDC	4	F	173	313	9,7
HPDC	6	F	149	281	7,1
HPDC	2	O	257	358	9,7
HPDC	3	O	203	311	7,4
HPDC	4	O	190	309	8,9
HPDC	6	O	160	280	6,0
HPDC	2	T4	111	241	15,3
HPDC	3	T4	111	243	15,3
HPDC	4	T4	103	239	16,7
HPDC	6	T4	97	235	13,0
HPDC	2	T6	113	240	16,9
HPDC	3	T6	109	247	15,5
HPDC	4	T6	103	239	16,3
HPDC	6	T6	97	230	11,5
HPDC	2	T7	118	240	16,4
HPDC	3	T7	115	235	15,0
HPDC	4	T7	111	240	14,5
HPDC	6	T7	96	220	13,1
HSTRC	2,5	F - (A1)	122	221	4,1
HSTRC	2,5	F - (A2)	132	241	5,1
HSTRC	2,5	O - (B1)	138	232	4,6
HSTRC	2,5	O - (B2)	142	246	4,9

Tab. 4.4: average results of tensile testing on HPDC and HSTRC plates.

To the sake of completeness, the single tensile tests for HSTRC strips have been reported from tab. 4.5 to tab. 4.8, listing macroscopic casting defects observed on the fracture surface of specimens, such as cold shuts and oxides. The presence and typology of defects have been investigated in the details in par. 4.7.4.

Brinell hardness has been calculated as average of two measurements, resulting slightly lower than the common minimum value of 80 HB_{5/250-30} for HPDC Magsimal[®]-59 in 2 to 4 mm wall-thickness.

Test	YTS [MPa]	UTS [MPa]	e [%]	Brinell Hardness [HB _{5/250-30}]	Notes
1	129	205	2,6		Cold shut
2	112	242	6,7		
3	118	237	5,5		
4	114	235	5,2		
5	114	230	4,9		Cold shut
6	146	196	1,0		
7	123	238	5,3		Cold shut
8	109	171	1,2		Head fracture
9	N.A	N.A	N.A		Head fracture
10	131	232	4,7	76,3	
Average	122	221	4,1	76,3	

Tab. 4.5: average results of tensile testing on the plate “A1”.

Test	YTS [MPa]	UTS [MPa]	e [%]	Brinell Hardness [HB _{5/250-30}]	Notes
1	130	242	5,0		
2	N.A	N.A	N.A		
3	135	233	3,6		Cold shut
4	132	248	5,0	70,0	
5	125	227	6,7		
6	139	245	4,7		
7	138	229	3,7		
8	127	253	6,4		
9	132	244	5,3		
10	131	247	5,8		
Average	132	241	5,1	70,0	

Tab. 4.6: average results of tensile testing on the plate “A2”.

Test	YTS [MPa]	UTS [MPa]	e [%]	Brinell Hardness [HB _{5/250-30}]	Notes
1	137	245	4,8		
2	133	230	4,4		
3	108	184	1,4		
4	178	263	7,5		
5	130	247	7,1	74,3	
6	134	243	4,5		
7	129	238	5,3		
8	155	179	1,1		
9	134	258	5,6		
10	N.A	N.A	N.A		Head fracture
Average	138	232	4,6	74,3	

Tab. 4.7: average results of tensile testing on the plate “B1”.

Test	YTS [MPa]	UTS [MPa]	e [%]	Brinell Hardness [HB _{5/250-30}]	Notes
1	143	263	8,2		
2	134	245	4,0		Cold shut
3	138	240	3,6		
4	155	258	5,0		Oxides
5	124	232	4,2		
6	138	255	6,3	72,0	
7	153	235	3,2		
8	143	251	5,1		
9	135	238	4,1		
10	161	247	5,1		
Average	142	246	4,9	72,0	

Tab. 4.8: average results of tensile testing on the plate “B2”.

The results of twin-roll plates are sensibly lower than the ones of high-pressure die-cast plates. This depends on the nature of twin-roll casting. In fact, the solidification of metal starts contemporarily on both sides and the plates solidify at last in their longitudinal central fibres. Due to the high casting speed, feeding the centre of plates results more difficult and casting defects are generated. Of course, the stress-strain response of the strip is controlled by the location of the defects.

Benchmarking HSTRC strips to 3 mm wall-thick HPDC plates results in tab. 4.9.

In temper F, YTS and UTS are decreased of 24,7 % to 34,4 %; elongation is even more influenced, with a reduction of 51,4 to 61,0 %., depending on the direction of rolling. After annealing at 250°C for 60 minutes, the decrease gap results slightly narrower. In fact, YTS and UTS decrease of 20,9 % to 32,0 %; the value of elongation decreases of 33,8 % to 37,8 %, being function of the rolling direction. As known, performing a single-step heat-treatment reduces therefore the incidence of casting defects on the cross section of specimens.

Casting process	Wall-thickness [mm]	Temper	YTS [MPa]	UTS [MPa]	e [%]
HPDC	3	F	186	320	10,5
HSTRC	2,5	F - (A1)	122	221	4,1
HSTRC	2,5	F - (A2)	132	241	5,1
Benchmark A1			- 34,4 %	- 30,9 %	- 61,0 %
Benchmark A2			- 29,0 %	- 24,7 %	- 51,4 %
HPDC	3	O	203	311	7,4
HSTRC	2,5	O - (B1)	138	232	4,6
HSTRC	2,5	O - (B2)	142	246	4,9
Benchmark B1			- 32,0 %	- 25,4 %	- 37,8 %
Benchmark B2			- 30,0 %	- 20,9 %	- 33,8 %

Tab. 4.9: benchmark and HSTRC strips.

Tensile test performed perpendicularly to the twin-rolling direction have resulted in better mechanical properties. In temper F, YTS and UTS improve respectively of 8,2 % and 9,0 %. A more pronounced impact can be observed on the elongation value, which is 24,4 % higher if measured perpendicularly to the metal flow direction. Heat-treating the strips to temper O has once again a “milding” effect on the mechanical properties, providing their more uniform distribution. Average YTS and UTS result respectively 2,9 % and 6,0 % higher on plate B2, in comparison with B1. Elongation has been measured as 6,5 % higher on B2 than on B1.

Casting process	Wall-thickness [mm]	Temper	YTS [MPa]	UTS [MPa]	e [%]
HSTRC	2,5	F - (A1)	122	221	4,1
HSTRC	2,5	F - (A2)	132	241	5,1
Comparison A2 versus A1			+ 8,2 %	+ 9,0 %	+ 24,4 %
HSTRC	2,5	O - (B1)	138	232	4,6
HSTRC	2,5	O - (B2)	142	246	4,9
Comparison B2 versus B1			+ 2,9 %	+ 6,0 %	+ 6,5 %

Tab. 4.10: comparison between tensile tests carried out in the parallel and perpendicular direction of twin-rolling.

This could depend on the fact that the probability that casting defects result located in the gauge length - L_0 - of the specimen is lower. In fact, the nature of twin-roll guarantees constant casting conditions in the direction of the roll axis, as at a certain moment the metal flows into a fix roll gap. Variation of the roll distance and in turn of the wall-thicknesses of the strip can cause oscillations of the meniscus and a major incidence of casting defects. Twin-roll strips present however higher YTS, and in most cases higher UTS, compared to full-solutionized HPDC plates.

4.7.3 Erichsen test

The results of Erichsen tests are reported in tab. 4.11, summarizing the average values, according varying wall-thicknesses and tempers. The Erichsen Index (IE_{40}) of HPDC and HSTRC plates has been evaluated for each variant as average of respectively 9 and 8 specimens. Non-valid tests have been discarded. The figure “40”, in subscript position, defines the adoption of holders with a 40 mm diameter, necessary for testing pieces with a wall thickness beyond 2 mm. The punching ram has a diameter of 20 mm. Every plate has been marked with positioning and progressive test number. The tests have been carried-out according EN ISO 20482, setting a testing speed of 5 mm/min and a pre-load of 100N. The holding dies of the 200 kN measuring cell testing equipment has been closed with a holding force of 10 kN. The 2,5 mm-thick plates have been punched on their side A, see fig. 4.14 and 4.15, after being greased with a lubricant called Zwick NLGI 00. The criterion for the ending of the test has been established in 5 % decay of the maximum applied force F_{max} . If a drop of load has not recorded instantaneously, the test has been stopped manually as soon as the crack has been visible to the naked eye.

Casting process	Wall-thickness [mm]	Temper	F_{max} [N]	IE_{40} [mm]
HPDC	2	F	7 962	3,7
HPDC	3	F	10 924	2,8
HPDC	4	F	18 587	2,9
HPDC	6	F	38 826	4,0
HPDC	2	O	7 351	3,4
HPDC	3	O	10 922	3,1
HPDC	4	O	18 648	3,0
HPDC	6	O	38 229	3,8
HPDC	2	T4	14 498	7,3
HPDC	3	T4	15 682	5,7
HPDC	4	T4	18 806	4,5
HPDC	6	T4	35 746	4,8
HPDC	2	T6	13 976	7,0
HPDC	3	T6	15 434	5,3
HPDC	4	T6	18 480	4,4
HPDC	6	T6	35 663	5,2
HPDC	2	T7	13 416	6,9

HPDC	3	T7	15 055	5,7
HPDC	4	T7	18 545	5,0
HPDC	6	T7	34 210	4,5
HSTRC	2,5	F	9 745	5,1
HSTRC	2,5	O	8 905	5,2

Tab. 4.11: average results of Erichsen tests on HPDC and HSTRC plates.

No AC potential drop method could be applied, because of the lack of apposite hardware. In most cases, however, a sudden pop-in along with a simultaneous cracking metallic sound has been recognized. Erichsen tests have been conducted also on wall-thicknesses beyond 3 mm and tempers T4, T6 and T7, in order to collect comparative values. To the sake of completeness, single Erichsen tests for HSTRC strips have been reported in tab. 4.12.

Test	Temper	F_{max} [N]	IE_{40} [mm]
1	F	11 092	5,4
2	F	9 575	5,0
3	F	8 437	4,6
4	F	12 013	5,6
5	F	11 357	5,4
6	F	8 811	4,8
7	F	7 787	5,0
8	F	8 884	4,7
Average	F	9 745	5,1
1	O	10 722	5,4
2	O	7 810	4,6
3	O	8 851	4,9
4	O	9 135	5,4
5	O	9 057	5,8
6	O	8 249	5,1
7	O	7 972	5,1
8	O	9 442	5,3
Average	O	8 905	5,2

Tab. 4.12: results of Erichsen tests on HSTRC plates.
Strip C1 and C2 have been tested respectively in temper F and O.

Concerning Erichsen test the main benchmark has been set with 2 and 3 mm HPDC wall-thick plates. Twin-rolled plates shown an increase of the bearing load of 22,4 % if compared to 2 mm-HPDC plates, while a decrease of load of 10,8 % has been observed in comparison to 3 mm-thick HPDC plates.

In the hypothesis that a 2,5 mm HPDC plate of Magsimal[®]-59 would bear the average value of load³, no remarkable effect on maximum carried load would have been recorded for HSTRC products.

The same trend has been confirmed by the results on the plate C2, in temper O. The bearing load has been increased of 21,1 % in comparison to the one recorded for 2 mm-thick HPDC plates, but a decrease of 18,5 % in comparison to 3 mm thick plates has been observed.

However, the effectiveness of the twin-rolling can be traced on the Erichsen Index, IE₄₀. 2,5 mm twin-rolled strips have shown superior displacements compared to HPDC plates. An increase of 37,8 % and even of 82,1 % has been recorded in comparison to respectively 2 and 3 mm high-pressure products of the same alloy. Analogue considerations are valid for temper O, where the increase of the IE₄₀ for twin-rolled strips is 52,9 % and 67,7 % in comparison respectively to 2 and 3 mm HPDC plates, see tab. 4.13.

Casting process	Wall-thickness [mm]	Temper	F _{max} [N]	IE ₄₀ [mm]
HPDC	2	F	7 962	3,7
HPDC	3	F	10 924	2,8
HSTRC	2,5	F	9 745	5,1
Benchmark C1 versus 2 mm			+ 22,4 %	+ 37,8 %
Benchmark C1 versus 3 mm			- 10,8 %	+ 82,1 %
HPDC	2	O	7 351	3,4
HPDC	3	O	10 922	3,1
HSTRC	2,5	O	8 905	5,2
Benchmark C2 versus 2 mm			+ 21,1 %	+ 52,9 %
Benchmark C2 versus 3 mm			- 18,5 %	+ 67,7 %

Tab. 4.13: benchmark and HSTRC strips.
Plate C1 (temper F) and C2 (temper O).

A limited influence of a single-step heat-treatment to temper O can be observed, if comparing the results of Erichsen test on plates C1 and C2, see tab. 4.14. The HSTRC strip in temper O has shown a decrease of the bearing load of 8,6 % and an increase of the IE₄₀ of 2,0 %. Therefore, the results for temper F and O can be considered almost equivalent.

Maximum loads borne by HSTRC strips are always lower than the ones carried by full heat-treated plates of Magsimal[®]-59, as expected. However, the displacements achieved by HSTRC are comparable to 3 mm HPDC plates in temper T4, T6 and T7. Additionally, the IE₄₀ are always superior to the ones achieved by 4 and 6 mm HPDC plates full heat-treated to temper T4, T6 and T7. This evident improvement can be

³ 9 443 N

made possible through the microstructural change induced by the ultra-high rapid cooling, see par. 4.7.4.

Casting process	Wall-thickness [mm]	Temper	F_{max} [N]	IE_{40} [mm]
HSTRC	2,5	F	9 745	5,1
HSTRC	2,5	O	8 905	5,2
Benchmark C2 versus C1			- 8,6 %	+ 2,0 %

Tab. 4.14: comparison between Erichsen tests carried out on strip C1 and C2, respectively in temper F and O.

4.7.3.1 Real-time Erichsen test

Real-time data have been collected during the Erichsen test. An average curve, representing the ideal progress of each variant has been extrapolated. Fig. 4.16 shows a comparative diagram of Erichsen curves in temper F, according varying wall-thicknesses. Confirming the trend observed in [34] for real-time tear toughness tests, the Erichsen cupping test shows increasing bearing loads for increasing wall thicknesses and a clear correlation between absorbed initiation crack energy and wall-thickness of the specimen.

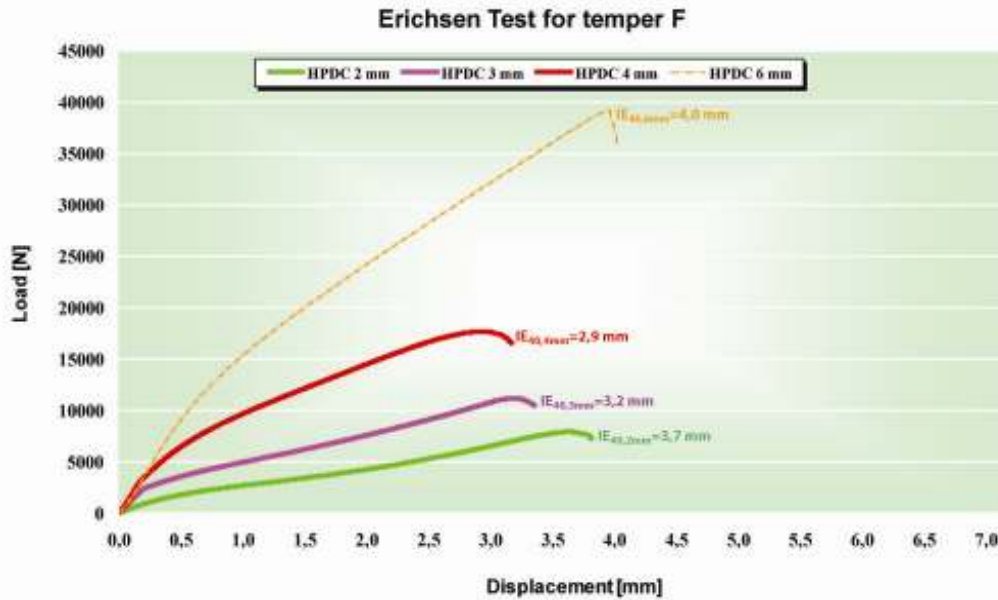


Fig. 4.16: comparison between Erichsen tests carried out in temper F, according varying wall-thicknesses.

However, IE_{40} values do not vary proportionally to the thickness of specimen: a progressive decrease of the value is recorded; shifting from 2 to 3 to 4 mm, in fact, the Erichsen Index is respectively 3,7, 3,2 and 2,9 mm; afterwards the trend is

inverted and the IE_{40} increases: a value of 4,0 mm has been recorded for 6 mm HPDC plates.

Similar considerations can be done on HPDC plates heat-treated to temper O.

Fig. 4.17 compares the average Erichsen curves: F_{max} increases with increasing wall-thicknesses. IE_{40} values have been recorded as 3,4, 3,1 and 3,0 mm, respectively for 2, 3 and 4 mm HPDC wall-thick plates. Afterwards the trend is inverted and the IE_{40} increases: a value of 3,8 mm has been recorded for 6 mm HPDC plates.

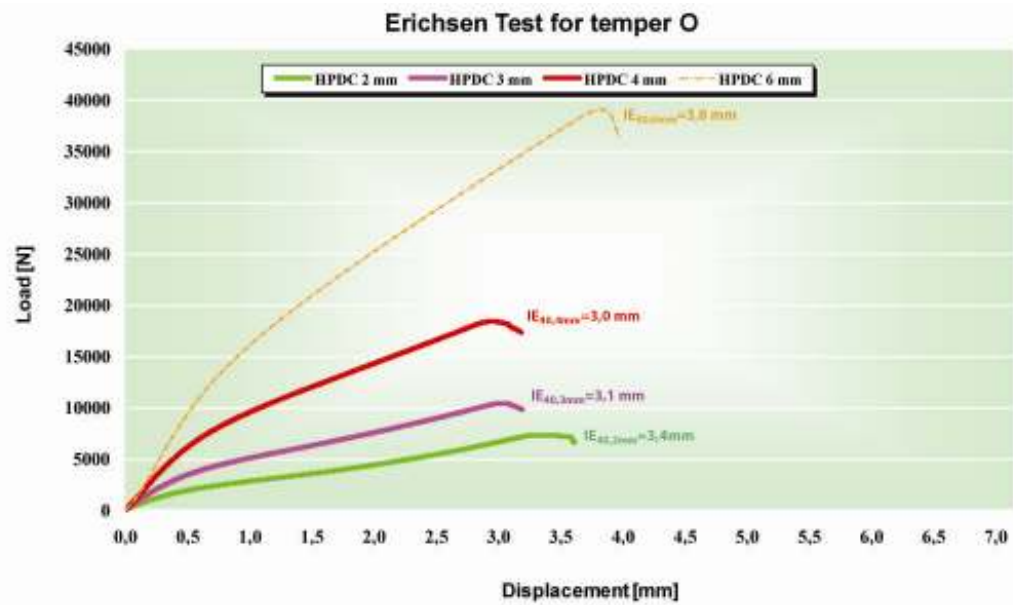


Fig. 4.17: comparison between Erichsen tests carried out in temper O, according varying wall-thicknesses.

This trend can be explained as the balancing effect of two factors: mechanical properties and bearing section. Decreasing wall-thicknesses result in higher solidification rates, finer microstructures and therefore improved mechanical properties. On one hand-side, plates of 2 mm respond better than 3 and 4 wall-thick plates to Erichsen test, as the mechanical performance of the alloy prevails on the resisting section. On the other hand-side, 6 mm plates have a better behaviour than other plates, as the increased bearing section can counterbalance the negative effects of coarser structures. Considering real-data of HSTRC plates and setting HPDC plates of similar wall-thickness (i.e. 2 and 3 mm) as benchmark, further considerations can be done.

Fig. 4.18 represents the superimposing of cupping tests respectively for temper F. Despite the slight influence on the maximum bearing force F_{max} , the strong improvement of the value IE_{40} determines a change in the morphology of the load-displacement curve recorded on HSTRC plates. The different slope of the load-displacement curve is evident and the IE_{40} increases from 3,2-3,7 mm for HPDC plates to 5,4 mm for 2,5 mm thick HSTRC strips.

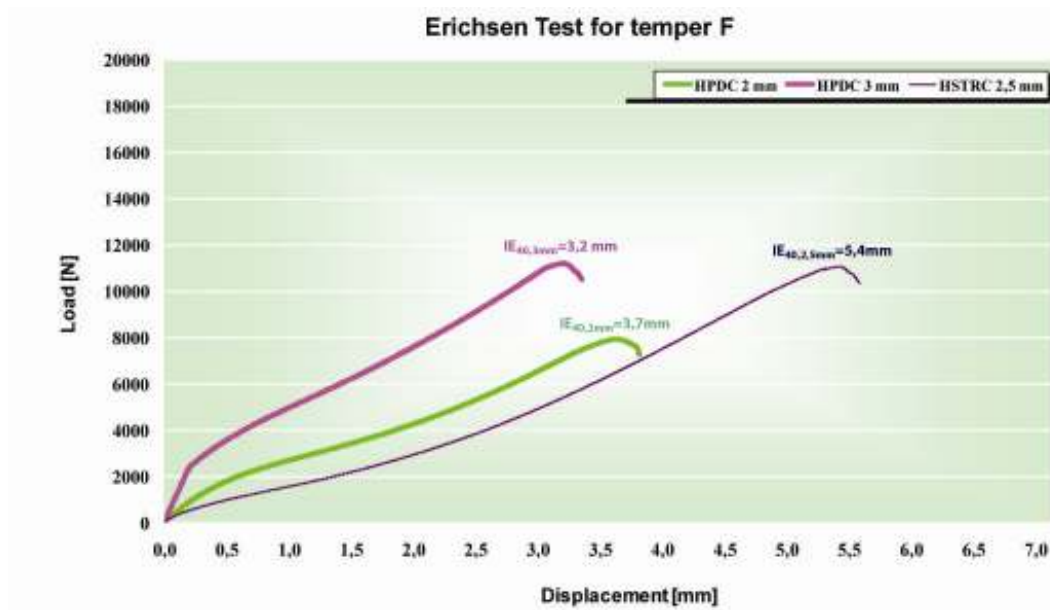


Fig. 4.18: comparison between Erichsen tests carried-out on HPDC and HSTRC plates. Temper F.

The same trend has been observed in temper O. In fact, IE₄₀ value increases from 3,1-3,4 mm for HPDC plates to 5,1 mm for 2,5 mm thick HSTRC strips, see fig. 4.19.

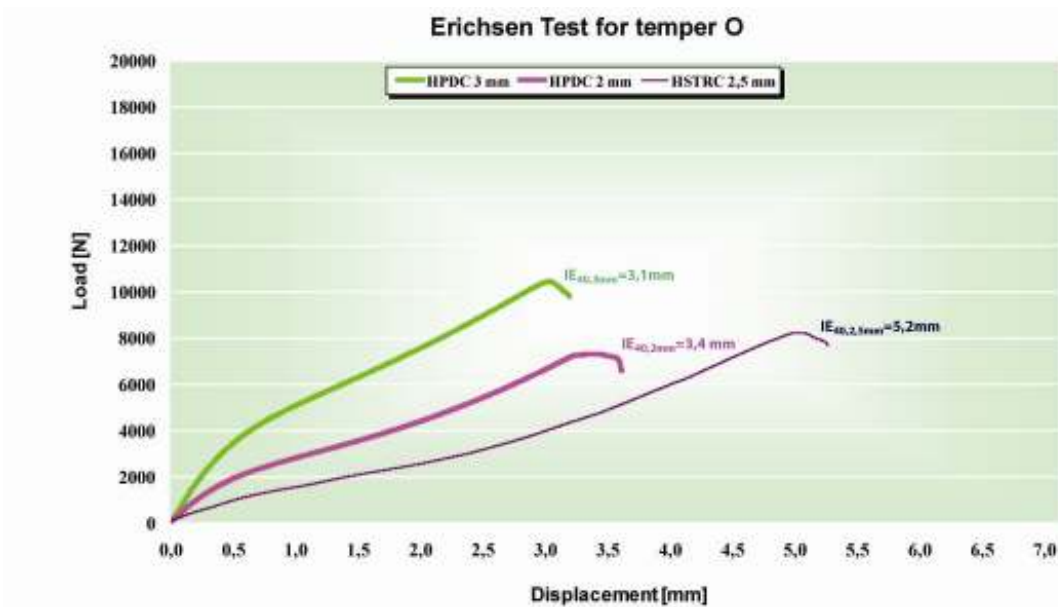


Fig. 4.19: comparison between Erichsen tests carried-out on HPDC and HSTRC plates. Temper O.

4.7.3.2 Absorbed energy and unit initiation crack energy

Generally speaking, the higher the value of IE_{40} , the more ductile the alloy, the more the energy absorption. In order to quantify the improvement in terms of energy absorption through twin-rolling, the area subtended by Erichsen curves of different variants has been integrated as function of the displacement.

The algorithm used is the Trapezium Method, an easy technique of approximation for integrals of mathematic functions. The area subtended by the load-displacement curve has been decomposed in n different trapeziums with height h , bases f_i and f_{i+1} , and therefore area $0,5 \cdot h \cdot (f_i + f_{i+1})$. Of course, the higher the number of intervals, the more accurate the approximation, see fig. 4.20.

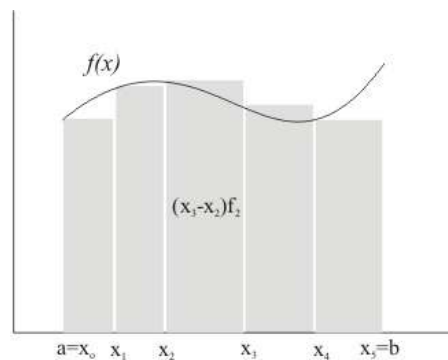


Fig. 4.20: the approximation of a function with the Trapeziums method.

The sum of all trapeziums area approximates the real integral, according to the following equation:

$$I = \int_a^b f(x) dx = \frac{h}{2} \sum_{i=0}^n (f_i + f_{i+1})$$

Fig. 4.21 shows this concept applied to the Erichsen curves for temper F according different wall-thicknesses. “a” corresponds to the zero of the Erichsen test, “b” to the index IE_{40} . “n” represent the number of intervals considered and depends on the sampling rate of the real-time software⁴. The area subtended by the curve represents the total energy absorbed by the plate before cracking; in other words, the energy of crack initiation, E_i .

⁴ Labmaster v. 1.7.12.4

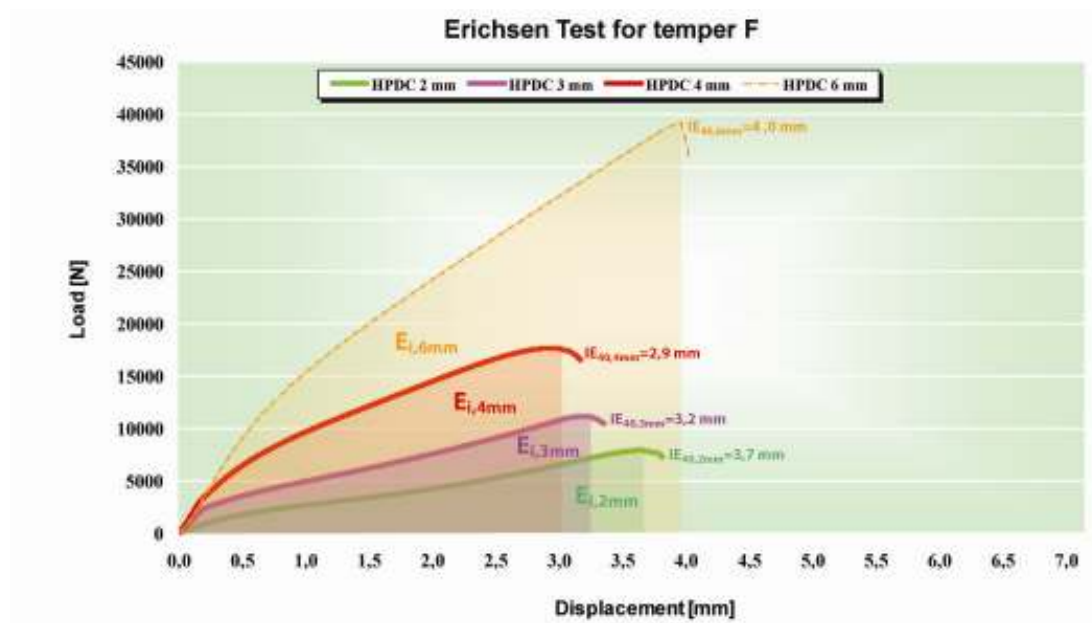


Fig. 4.21: absorbed energy. HPDC plates in temper F:

$$E_{i,2\text{mm}} = 15,9 \text{ J}$$

$$E_{i,3\text{mm}} = 21,0 \text{ J}$$

$$E_{i,4\text{mm}} = 33,5 \text{ J}$$

$$E_{i,6\text{mm}} = 90,8 \text{ J}$$

Assuming that the contact area between the punching system and the testing plate can be approximated to the maximum ram section⁵, the unit crack initiation energy UE_i can be calculated as ratio between E_i and loaded surface.

Absorbed energy E_i and unit crack initiation energy UE_i have been computed for all tested variants and summarized in tab. 4.15. E_i has been expressed in Joule; UE_i in Nmm^{-1} .

Casting process	Wall-thickness [mm]	Temper	E_i [J]	UE_i [Nmm^{-1}]
HPDC	2	F	15,9	50,6
HPDC	3	F	21,0	66,9
HPDC	4	F	33,5	106,6
HPDC	6	F	90,8	289,0
HPDC	2	O	15,3	48,6
HPDC	3	O	19,1	60,7
HPDC	4	O	33,6	107,0
HPDC	6	O	88,5	281,5
HPDC	2	T4	46,0	146,5
HPDC	3	T4	39,5	125,7

⁵ $100\pi \text{ mm}^2$

HPDC	4	T4	49,0	155,9
HPDC	6	T4	96,9	308,4
HPDC	2	T6	44,4	141,3
HPDC	3	T6	56,1	178,5
HPDC	4	T6	45,1	143,7
HPDC	6	T6	105,9	336,9
HPDC	2	T7	43,1	137,2
HPDC	3	T7	48,7	155,0
HPDC	4	T7	47,9	152,4
HPDC	6	T7	90,8	289,1
HSTRC	2,5	F	26,6	84,7
HSTRC	2,5	O	20,1	63,9

Tab. 4.15: absorbed initiation energy E_i and unit crack initiation energy UE_i for HPDC and HSTRC plates.

The integrated curves and corresponding subtended area have been represented for the benchmark – again 2 and 3 mm HPDC plates - and the twin-rolled plate C1, see fig. 4.22.

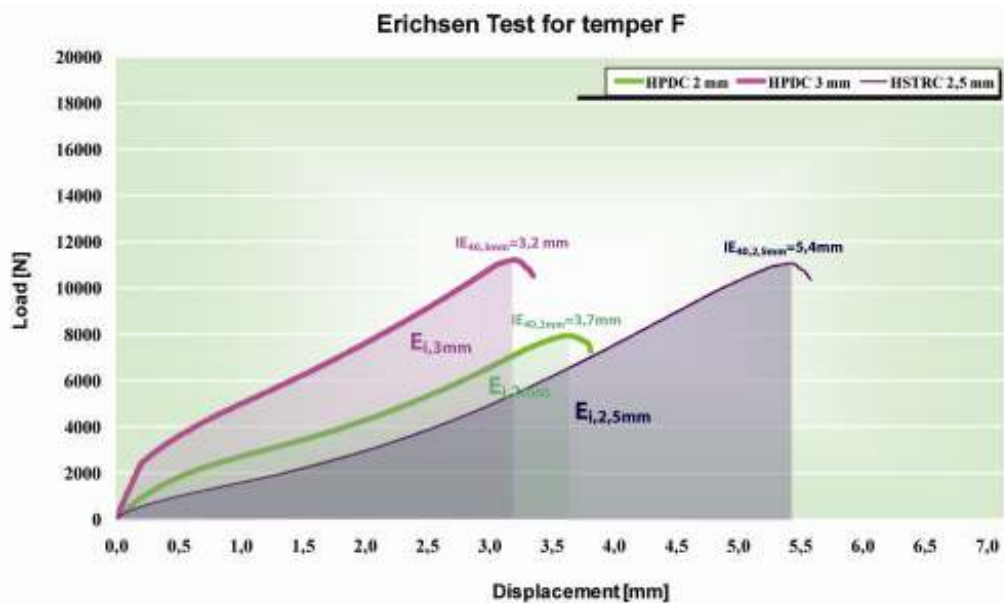


Fig. 4.22: absorbed energy. Benchmark versus HSTRC in temper F:

$$E_{i, 2mm, F, HPDC} = 15,9 \text{ J}$$

$$E_{i, 3mm, F, HPDC} = 21,0 \text{ J}$$

$$E_{i, 2,5mm, F, HSTRC} = 26,6 \text{ J}$$

Twin-rolled plates absorb 26,6 J in temper F. Compared to 21,0 J of 3 mm HPDC plates and to 15,9 J of 2 mm HPDC plates, this corresponds to percentage increases respectively of 26,6 % and 67,4 %, see tab. 4.16.

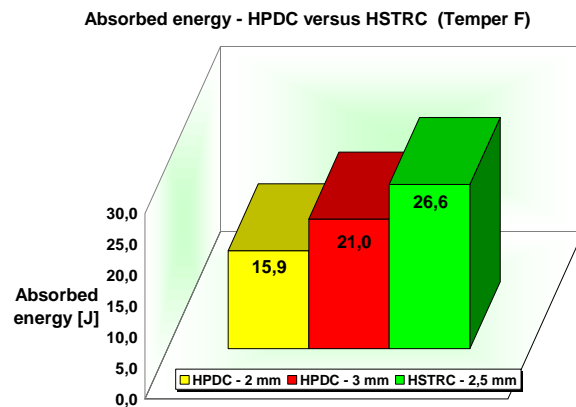


Fig. 4.23: E_i of HSTRC in temper F. Benchmark: 2 and 3 mm HPDC plates.

Unit crack initiation energy for twin-rolled plates of Magsimal[®]-59 is $84,7 \text{ Nmm}^{-1}$, followed by $66,9$ and $50,6 \text{ Nmm}^{-1}$ of 3 and 2 mm HPDC plates. These values are very consistent with the ones found by Kumai et al. in [34] for casting alloys and with the reference values for unit crack propagation energy of Magsimal[®]-59 as per [36].

Casting process	Wall-thickness [mm]	Temper	E_i [J]	UE_i [Nmm^{-1}]
HPDC	2,0	F	15,9	50,6
HPDC	3,0	F	21,0	66,9
HSTRC	2,5	F	26,6	84,7
C1 versus 2 mm			+ 67,4 %	
C1 versus 3 mm			+ 26,6 %	

Tab. 4.16: benchmark and HSTRC strips.
Plate C1 (temper F).

The improvements obtained on the basic material in temper F have been somehow hindered or mitigated in temper O. The integrated Erichsen curves and corresponding subtended area have been represented for the benchmark and the twin-rolled plate C2 in temper O as well, see fig. 4.24.

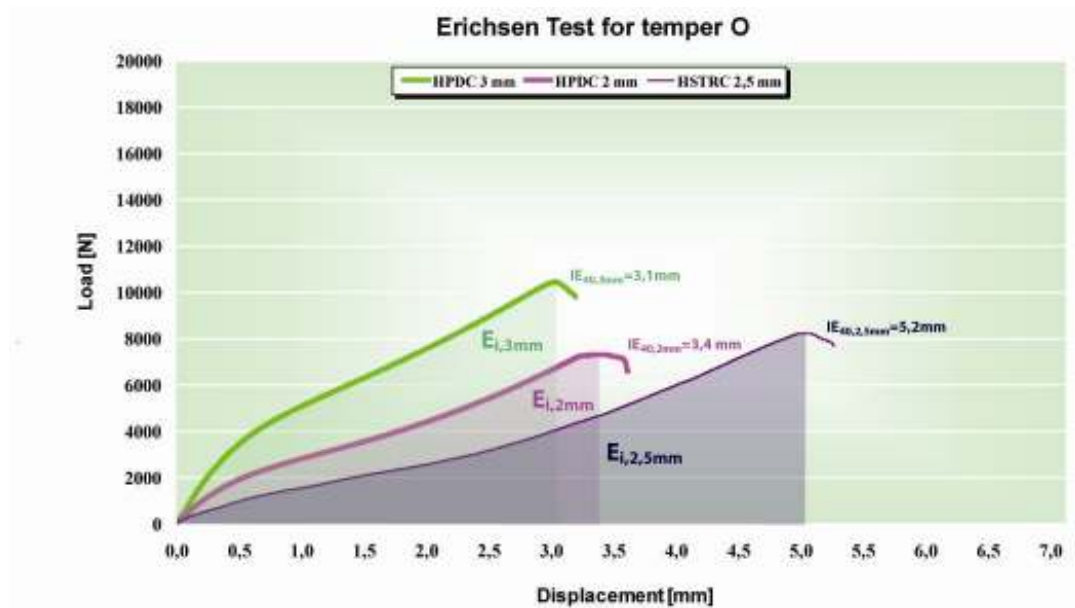


Fig. 4.24: absorbed energy. Benchmark versus HSTRC in temper O:

$$E_{i, 2\text{mm}, O, \text{HPDC}} = 15,3 \text{ J}$$

$$E_{i, 3\text{mm}, O, \text{HPDC}} = 19,1 \text{ J}$$

$$E_{i, 2,5\text{mm}, O, \text{HSTRC}} = 20,1 \text{ J}$$

Twin-rolled plates absorb 20,1 J in temper O. Compared to 19,1 J of 3 mm HPDC plates and to 15,3 J of 2 mm HPDC plates, this corresponds to percentage increases respectively of 5,2 % and 31,5 %, see tab. 4.17.

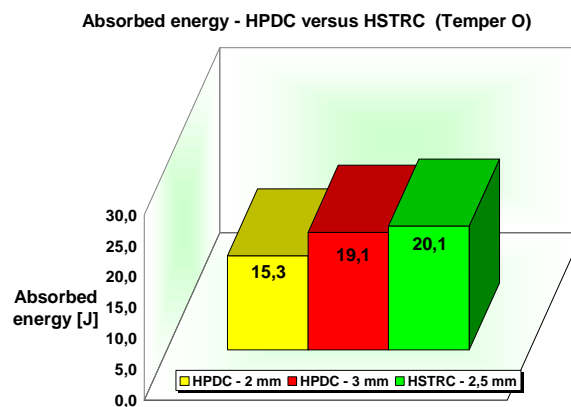


Fig. 4.25: E_i of HSTRC in temper O. Benchmark: 2 and 3 mm HPDC plates.

Unit crack initiation energy for twin-rolled plates of Magsimal[®]-59 is $63,9 \text{ Nmm}^{-1}$, followed by $60,7$ and $48,6 \text{ Nmm}^{-1}$ of 3 and 2 mm HPDC plates.

Casting process	Wall-thickness [mm]	Temper	E_i [J]	UE_i [Nmm ⁻¹]
HPDC	2,0	O	15,3	48,6
HPDC	3,0	O	19,1	60,7
HSTRC	2,5	O	20,1	63,9
C1 versus 2 mm			+ 31,5 %	
C1 versus 3 mm			+ 5,2 %	

Tab. 4.17: benchmark and HSTRC strips.
Plate C1 (temper O).

It is worth underlining that the heat-treatment to temper O seems to have an influence on the course of the Erichsen test, diminishing its slope and therefore the final subtended area, in comparison to temper F. This phenomenon has not been observed on HPDC plates, see fig. 4.26.

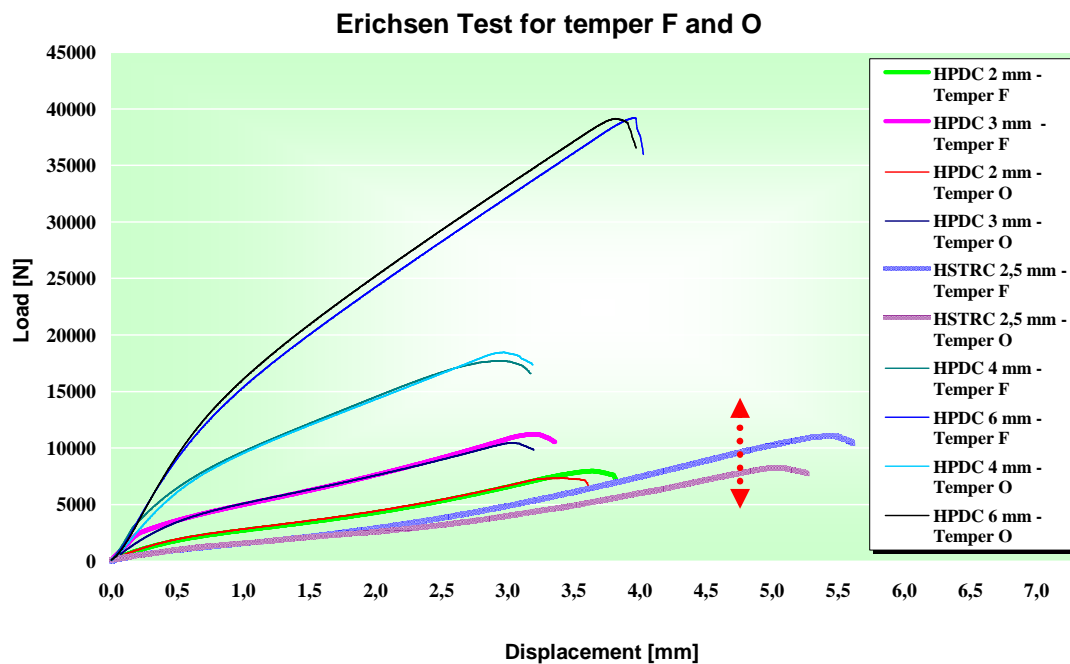


Fig. 4.26: overlapping of HPDC and HSTRC Erichsen tests.
Temper F and O.

This fact could depend on the very fine induced microstructure and Mg_2Si particles in the HSTRC strip.

4.7.4 Microstructural evaluation

Tensile specimens with interesting mechanical results have been observed on their fracture surface, see par. 4.7.4.1. Metallographic samples have been prepared for the evaluation of microstructure to the light microscope, see par. 4.7.4.2 and 4.7.4.3.

4.7.4.1 Fracture surfaces

Fracture surface of samples A1-5, A1-6, A2-6, A2-8, B1-2 and B2-9 are reported in fig. 4.27 to 4.32 with the corresponding mechanical properties. Sample A1-5 has shown a satisfactory elongation to fracture. The fracture surface shows an evident internal segregation of a blue colour, concentrated in the middle fibres of the metal. This reflects a change in the microstructure, induced by the ultra-high cooling rate. The phenomenon is not so pronounced on sample A1-6, which has shown higher YTS, but has fractured to 1,0 % elongation.

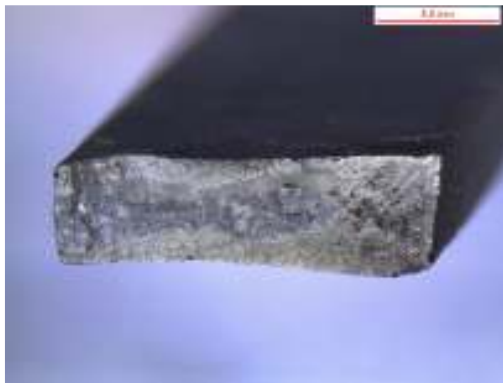


Fig. 4.27: sample A1-5.16X.

YTS: 114 MPa;
UTS: 230 MPa;
e%: 4,9 %.



Fig. 4.28: sample A1-6. 16X.

YTS: 146 MPa
UTS: 196 MPa
e%: 1,0 %

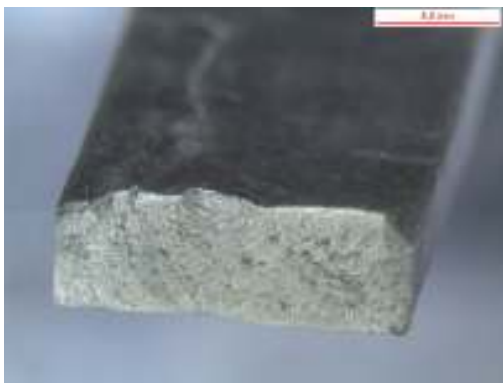


Fig. 4.29: sample A2-6. 16X.

YTS: 139 MPa
UTS: 245 MPa
e%: 4,7 %



Fig. 4.30: sample A2-8. 16X.

YTS: 127 MPa
UTS: 253 MPa
e%: 6,4 %

Samples A2-6 and A2-8 show a cleaner and more regular fracture surface, with a ductile behaviour.



Fig. 4.31: sample B1-2. 16X.

YTS: 133 MPa
UTS: 230 MPa
e%: 4,4 %



Fig. 4.32: sample B1-9. 16X.

YTS: 134 MPa
UTS: 258 MPa
e%: 5,6 %

Samples B1-2 and B1-9 have shown a change of microstructure in the middle of fracture surface. The blue-shaded layers appear of constant thickness through the section, in contrast with samples A1-2 and A1-6, where the layer appears irregular.

4.7.4.2 Light microscopy on tensile specimens

Cross sections of the tensile specimens have been polished, 2 to 3 mm under the location of fracture. Pictures taken at the light microscope have been pasted together in order to obtain overviews of the entire cross section of the samples.



Fig. 4.33: cross section of sample A1-5. 100X.

Sample A1-5 show an irregular distribution of the microstructure: a skin of irregular thickness is progressively substituted by a central layer with a coarser structure, see fig. 4.33. The cross section of fig. 4.33 is reported in fig. 4.35 together with the different microstructures, which can be observed contemporary on the same specimen. The near-to-surface region presents a non-dendritic structure, due to the extreme high cooling rates applied. However, the spot presence of globular dendrites shows that at the moment of casting, a semisolid melt has entered the roll bite.

In literature, these dendrites are called ESC, Externally Solidified Crystals, see fig. 4.35 top-left. The same microstructure can be observed in the lower part of the sample, see fig. 4.35, bottom-left. However, the layer of the bottom skin is lower than the upper one, confirming the irregular heat exchange during solidification.

The central part of the sample A1-5 shows a very fine microstructure, see fig. 4.35 bottom-middle. The eutectic is very fine and spongy. Mg_2Si solidifies in form of spheroids with a diameter of ca. 0,5 to 1 μm . Dendrites have not the time to grow in their typical dendritic shape, due to the fast solidification time and to the pressure applied by the rolls, fig.4.35 bottom-right.

In the right part of the cross section a pre-solidified area of metal has been observed, see fig. 4.35, top-middle. The eutectic dimensions are significant higher and the Mg_2Si crystals are present in the form of platelets, which confirms that the metal has entered the rolls already at the solid state, fig. 4.35 top-right.



Fig. 4.34: cross section of sample A1-6. 100X.

The same considerations can be done on the sample A1-6 of fig. 4.34. The skin layers are more regular on their thickness. The microstructural fineness of the upper layer is higher than the one of lower, see fig. 4.36 top-left vs. bottom-left. The central region of the sample shows an increased presence of α -aluminium and a very low rate of eutectic, see fig. 4.36 top-middle. As in A1-5, dendrites have a globular shape. The eutectic is very fine. The area in the right part of the sample looks enriched in eutectic; the dendrites have been broken during solidification by the roll pressure, but show a more dendritic ratio and lower dimensions compared to the area at the immediate left-side. In this region the crack during tensile test has been initiated.

Observing the specimens in the perpendicular direction of rolling confirms once again the irregular distribution of temperature along the axis of twin-rolls. Specimen A2-6 has a thinner skin region compared to A1-5 and A1-6. However, sample A2-8 has a very thick skin and a thin core region. This is the symptom that the heat is extracted irregularly and the applied cooling rates variable in time and position.

The heat-treated variant B1 do not show any differences in the microstructure. 250°C for 60 minutes have not influenced the dimension of dendrites and Mg_2Si . However, as also the effects of a T5 heat-treatment are not visible to the light microscopy, micro-hardness profiles have been traced on plate B1, see par. 4.7.5, in order to have a confirmation of different behaviour to Erichsen test. Considerations made for samples A1-5 and A1-6 can be repeated. Sample B1-2 shows an ever more random structure, with a skin which covers almost the entire cross section in the left part of the specimen, being completely absent in the right part of the same specimen.

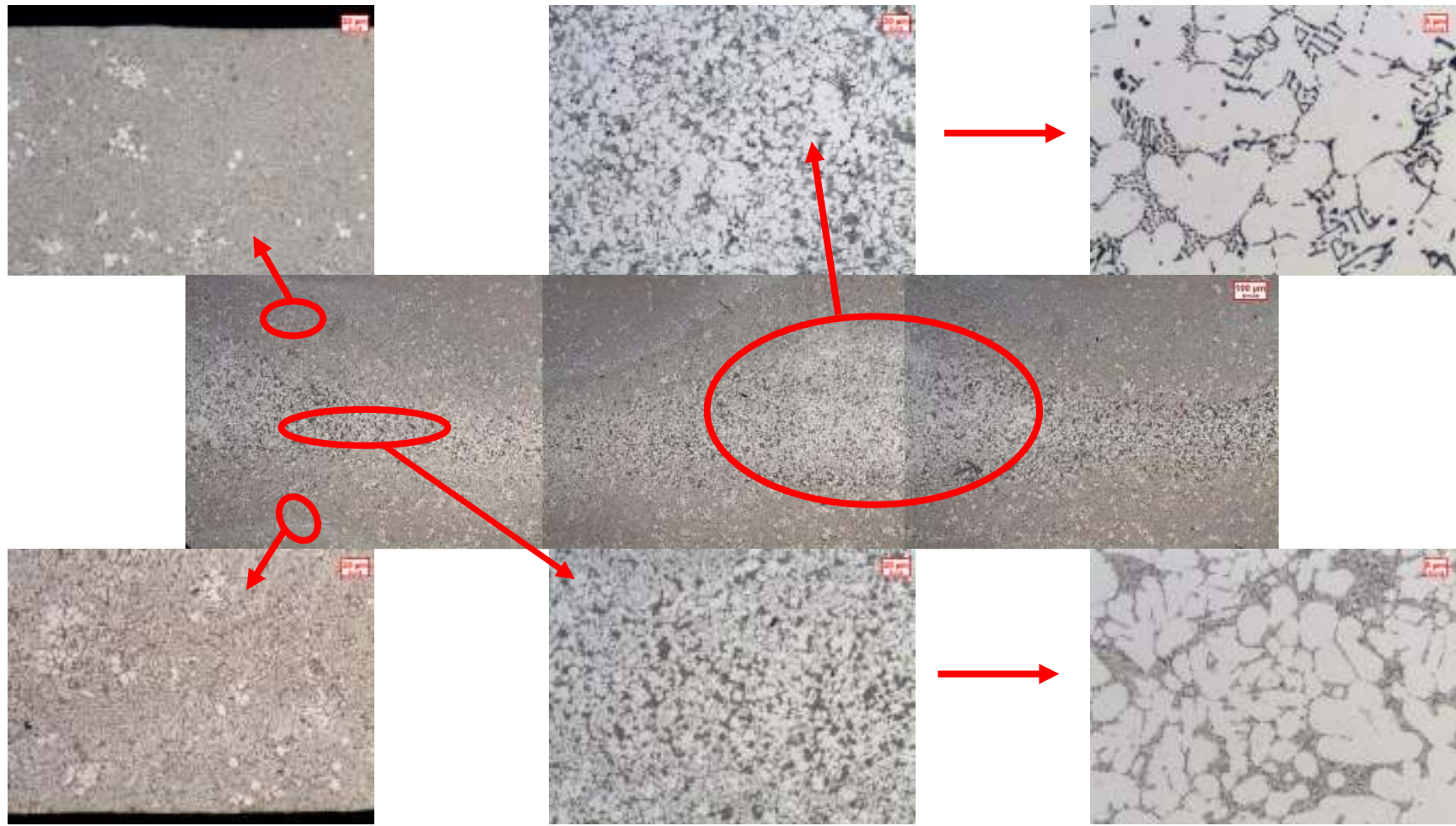


Fig. 4.35: cross section of sample A1-5 and its different coexistent microstructures.

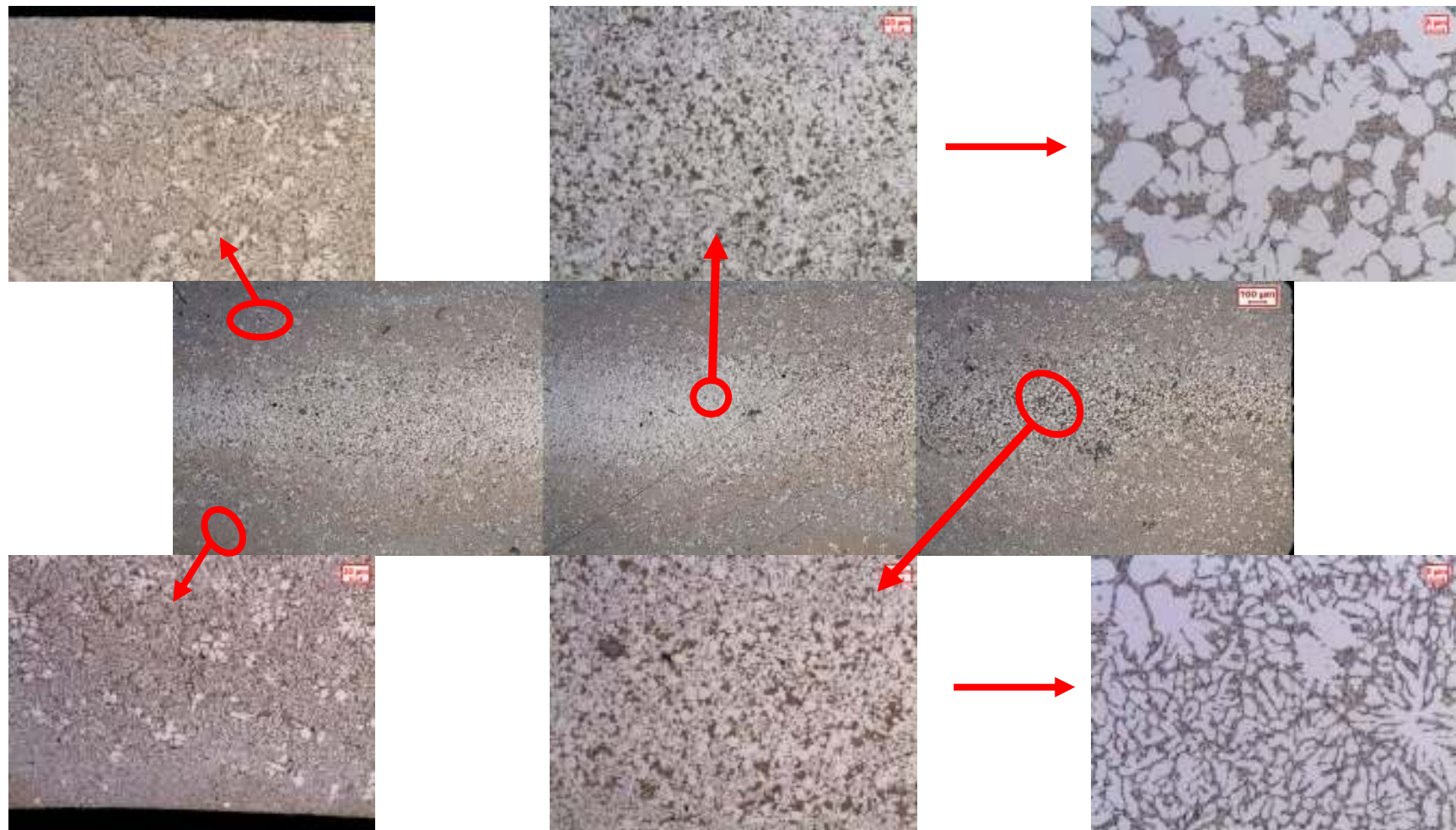


Fig. 4.36: cross section of sample A1-6 and its different coexistent microstructures.



Fig. 4.37: cross section of sample A2-6. 100X.



Fig. 4.38: cross section of sample A2-8. 100X.



Fig. 4.39: cross section of sample B1-2. 100X.



Fig. 4.40: cross section of sample B1-9. 100X.

The secondary dendrite arm spacing (SDAS) of the samples B1-2 and B1-9 has been measured at the edge and at the core of sample, at 1000X, see fig. 4.41 and 4.42. The average results have been reported in tab. 4.18.

Sample	Edge [μm]	Core [μm]
B1-2	2,3	7,0
B1-9	2,1	12,5

Tab. 4.18: SDAS of samples B1-2 and B1-9.

The results are aligned with the measurements carried-out in [34]. No influence of heat-treatment O can be observed on the SDAS.

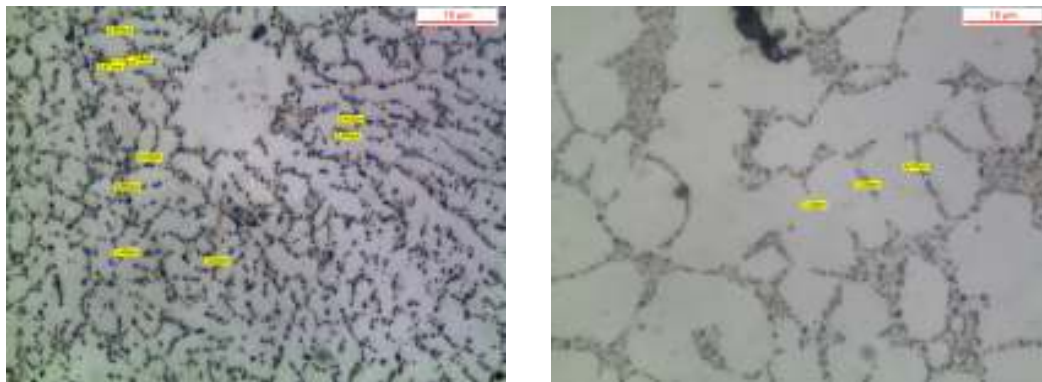


Fig. 4.41: SDAS at the edge (left) and at the core (right) of sample B1-2. 1000X.

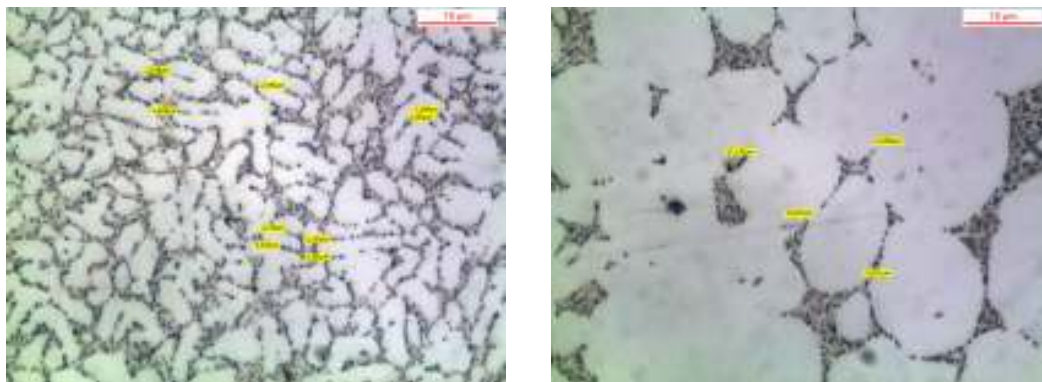


Fig. 4.42: SDAS at the edge (left) and at the core (right) of sample B1-9. 1000X.

4.7.4.3 Light microscopy on Erichsen plate

Metallographic samples have been taken also from plate C1, twin-rolled in temper F and used for Erichsen test. Cross sections of the plate are presented in fig. 4.43 to 4.46. Macro-segregations can be observed once again: the eutectic is concentrated in the central fibres of the material, which solidify at latest.



Fig. 4.43: segregation of eutectic.
25X.



Fig. 4.44: segregation of eutectic.
25X.

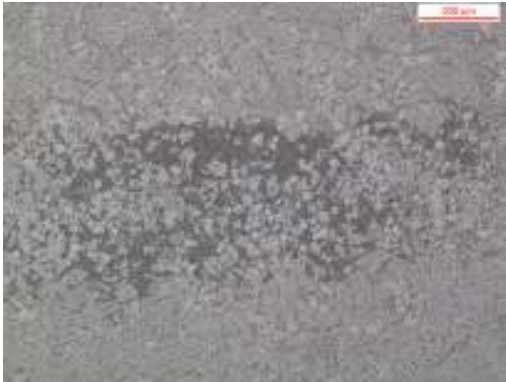


Fig. 4.45: segregation of eutectic.
50X.



Fig. 4.46: segregation of eutectic.
100X.

Crack patterns - observed on the surface of the HSTRC strips have been found running into the plate, as per fig. 4.47. The crack of fig. 4.48 is ca. 150 μm long and eutectic islands can be observed at its end.

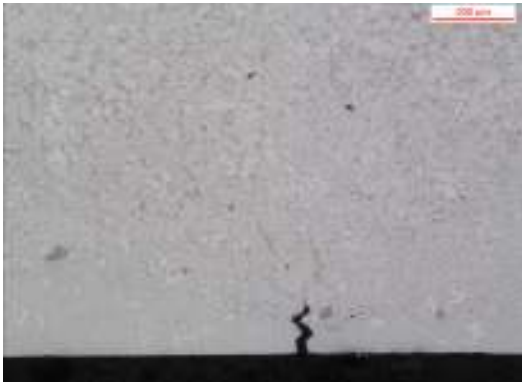


Fig. 4.47: crack initiation at the border
of plate C1.
50X.



Fig. 4.48: crack initiation at the border
of plate C1.
Zoom of fig. 4.47. 200X.



Fig. 4.49: externally solidified dendrite. Plate C1. 500X.

The phenomenon of pre-solidified zones is confirmed by fig. 4.49, where a dendrite has been included in the strip at the solid state, during its growing phase. Manganese intermetallics have grown to 30-50 μm before casting. Metal shrinkages have been traced to a very low extent. A sensible refining of the microstructure has been observed from the edge to the core of the plate. No dendritic structure has been noticed for layers of 100-150 μm from the plate border. Globular primary aluminium dendrites and Mg_2Si have been remarked around 200 μm under the casting skin.

A comparison between twin-roll microstructures at the edge and at the core of the plate have been reported in fig. 4.50 to 4.53, from 100 to 500 magnifications.



Fig. 4.50X: HSTRC microstructure.
Edge. 100X.



Fig. 4.51: HSTRC microstructure.
Core. 100X.

SDAS of 1,6 to 3,4 μm have been determined in the near-surface region, while the core area has typical SDAS dimensions of 6,7 to 10,2 μm . It is worth underlining that the morphology of Mg_2Si particles remains globular even at the core of the twin-roll plate, confirming the effectiveness of the rapid cooling by the HSTRC technology.

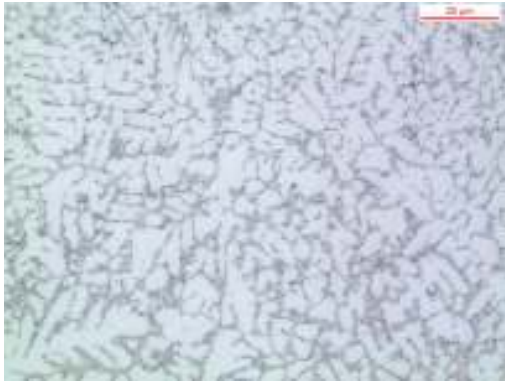


Fig. 4.52: HSTRC microstructure. Edge. 500X.

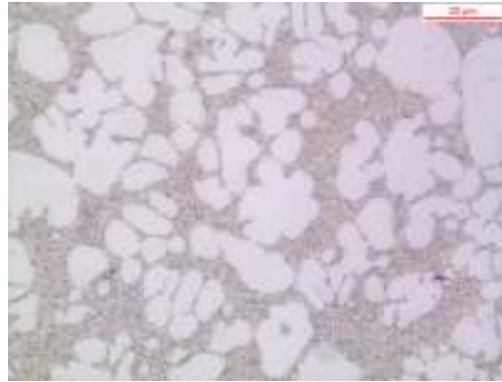


Fig. 4.53: HSTRC microstructure. Core. 500X.

4.7.5 Microhardness

Microhardness profiles have been generated on the samples A2-6 and B2-1, in order to evaluate possible effects of the heat-treatment O. Two measurements have been carried-out for each sample; the average is represented in fig. 4.54. Sample A2-6 in temper F show a slightly higher hardness compared to B2-6, around 5 to 10 HV₃₀ from the border to the middle of the sample; afterward the trend is inverted.

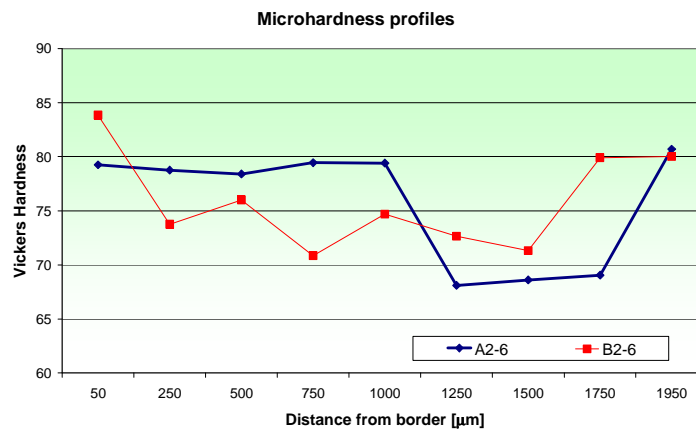


Fig. 4.54: microhardness profiles for sample A2-6 and B2-6.

Hardness can be therefore considered equivalent on both samples.

4.8 Conclusions

The comparison between the results obtained on HPDC plates and HSTRC strips of Magsimal[®]-59 have shown the potential of improvement by ultra-high cooling-rate technologies. Some final considerations can be done at the light of the experimental part carried-out in this work, evaluating plus and cons of twin-roll casting applied to a premium primary casting alloy.

Tear toughness can be significantly increased by higher quenching rates. In accordance with [30], higher cooling rates have proven to be significantly more effective than strengthening or heat-treating.

The expected improvements of HSTRC technology on the tensile properties of Magsimal[®]-59 have not been observed, due to the lack of an adequate and invariant casting quality of twin-rolled strips. In particular, the presence of casting defects and the non-homogeneity to a microstructural level have been considered the main factors for the impairing of mechanical properties of twin-rolled plates. The further optimization of casting parameters has therefore to be implemented. Nevertheless, interesting conclusions can be drawn. Mechanical properties of HSTRC Magsimal[®]-59 result in average better in the perpendicular than in the parallel direction of rolling. Carrying-out a one-step heat treatment mitigates significantly the impact of casting defects on the material performance, despite its non traceability in the microstructure and in the microhardness.

As well as the tear-toughness test, the Erichsen test has shown its reduced sensitivity to the presence of internal casting defects and provides therefore a good alternative for the evaluation of the effective ductility or resilience of a material. The test, originally drawn from the sheet manufacturing sector, can be thus usefully applied to casting materials as well. Experimental results on twin-rolled cast strips in Magsimal[®]-59 tested to Erichsen have shown interesting correlations:

- the change induced on the growing kinetic of Mg₂Si particles through HSTRC does not reflect in increased maximum bearing loads F_{max} of Erichsen. Nevertheless, the Erichsen Index IE_{40} improves dramatically. Twin-rolled strips show values of IE_{40} comparable to the ones of solutionized 3 mm-thick samples of the same alloy and are considerably higher than IE_{40} of 4 and 6 mm wall-thickness
- the absorbed energy until cracking E_i and the unit crack initiation energy UE_i is ca. 1,7 times higher in comparison to HPDC plates of similar wall-thickness. These results are in full accordance with the correlations of [34] concerning absorbed energy after cracking E_p and unit crack propagation energy UE_p
- heat-treating a HSTRC strip to temper O has a “mildening” effect on the values of IE_{40} , E_i and UE_i and should therefore be avoided. The behaviour of the alloy after a T5 heat-treatment has not been investigated, but should be examined, if the providing of an immediate quench in water after rolling becomes feasible.
- the Erichsen test is operatively easier than tear toughness tests, as the specimen consist in non-machined plates. Additionally, E_i and UE_i seems not being a function of the specimen geometry; surface treatment conditions has not been evaluated

Finally, casting defects as intra-granular cracks, eutectic segregations, ESCs, shrinkages and locally coarsened regions have been observed. Generally, the achieved microstructure is non uniform, due to the locally and timely different solidification conditions. Several kinds of microstructures coexist within few millimetres of distance. These factors affect the performance of the metal to tensile testing to a high extent.

However, the local microstructural fineness achieved by HSTRC is impressive, though not uniform throughout the whole plate section. SDAS values have been measured within a range of 1,6 to 3,4 μm and of 6,7 to 10,2 μm respectively at the edge and at the core of a 2,5 mm strip. 3 mm-thick HPDC plates have typical dimensions 3 times larger [36]. Mg_2Si particles have been observed in globular spheroids. The cooling rate of the HSTRC has been estimated around 4 000°C/s and 1 000°C/s, respectively at the surface and at the core of the casting [45].

4.9 Applications and outlooks

The results of chapter 3 have shown one of the weak points of modern HPDC technology: delivering invariant quality and granting the same performance of the castings through all series production.

Chapter 4 underlines how a significant improvement of the basic material is still theoretically possible via an accelerated solidification. Tuning the HSTRC until the achievement of constant good quality of the strips could allow either the casting of the same product with improved mechanical properties or the realisation of thinner walls with equivalent performance.

From a practical point of view, many applications could take advantage of this new technology for casting alloys. For example, sheet doors outer panels for cars could be cast with this technology, substituting steel panels or at least approaching their manufacturing costs. Hemming has proven to be successful on full heat-treated twin-rolled strips of 3084, 5182, 6022, 6061 and 6063 wrought alloys, as well as on A356 foundry alloy in T4. Additionally, door connection nodes, windscreens, backdoors and similar could be produced by HSTRC instead of traditional HPDC, due to their flat geometry.

Chapter 5
Weldability of primary aluminium HPDC alloys

5.1 Introduction

Aluminium casting alloys can be welded with a wide combination of materials, filler metals and welding techniques. The transportation industry has been one of the first sectors taking advantage of this possibility. In fact, welded castings or joining between mixed aluminium materials, such as cast and wrought alloys are state of the art, used for the lightweight design in vehicle bodies. Cooling and EGR systems, compressor units, chassis and connecting parts are just few further examples. Lighter assembled units mean in turn energy savings, in terms of lower masses, which need to be accelerated and braked [53]. Large constructions in energy plants are designed through welded aluminium solutions. In many cases, welding between steel and aluminium or even copper and aluminium has been taken into account, as able to deliver long-term mechanical resistance of the seams [54].

Traditional high-pressure die-casting alloys are generally quite difficult to weld with common arc welding technologies, as the generated thermal cycles cause in most cases the precipitation of brittle phases in the Heat-Affected Zone (HAZ). The chemistry of casting and filler alloys need to be controlled in the iron and copper content, if joined ductile castings and corrosion resistant welding seams are required. Air entrapments, melt gas content and use of lubricant have to be minimised, in order to obtain weldable parts [55]. The considerations of par. 1.7.1 on the control of casting process are furthermore very important.

The most common joining techniques are arc welding processes, usually working in protective atmospheres, such as TIG or MIG. The latter is often preferred for series manufacturing, thanks to its higher welding speed and the possibility of easy integration with robotics and monitoring systems. However, in many circumstances the given geometry of castings can be incompatible with the adopted welding technique, e. g. clear spacing or interstices which can not be reached easily with traditional welding torches. Hence, the need for alternative joining processes such as Laser Beam Welding (LBW), Electron Beam Welding (EBW) and Friction Stir Welding (FSW). LBW and EBW are classified as high-energy processes, due to the concentration of high power in welding profiles of limited size¹. FSW is a welding technique, which allows the joining of the metallic chamfers by a mechanical action and without reaching their melting points.

This chapter presents a study on these modern welding processes, carried-out on HPDC plates in Silafont[®]-36, AlSi9MgMn and Castasil[®]-37, AlSi9Mn. The experiments have been done with these alloys because the AlSi-system shows notoriously a very good weldability. Additionally, both materials are widely used in automotive, where the requirements and the demands in term of ductile high-pressure die castings are constantly increasing. Aim of the study is the understanding of compatibility of modern welding processes with premium casting alloys and the definition of the correct welding parameters in order to obtain sound weld seams. LBW and EBW have the advantage of reducing significantly the size of the HAZ and

¹ LBW~ 1MW/cm²; EBW~ 10MW/cm²; traditional arc welding techniques ~ 0,01 MW/cm²

therefore of limiting the drawbacks of traditional arc welding methods. FSW does not generate a HAZ at all, but a nugget of mixed material.

The main issues of standard arc welding techniques are briefly exposed on par. 5.2. Material tested to welding, design of experiments and corresponding results are presented in par. 5.3 and 5.4. Conclusions have been summarized in par. 5.5. For a detailed explanation of traditional and modern welding techniques, the reader should make reference to dedicated literature.

5.2 Traditional welding techniques and aluminium alloys

Despite the low melting range, the welding of aluminium alloys requires roughly the same amount of energy required for steel, because of the higher thermal conductivity and specific heat. Due to its physical and mechanical properties, aluminium responds differently to welding procedures than ferrous materials and needs some specific precautions. The design of the weld joint is crucial for aluminium. In fact, welding edges have to be accurately shaped, prepared and cleaned. The stable oxide layer on the surface has to be removed or torn off. An accurate welding procedure under protective atmosphere has to be implemented.

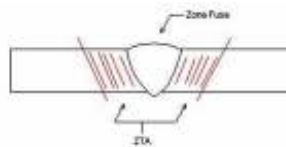


Fig. 5.1: ZTA and welding seam.

Arc welding processes cause the partial melting of the metals to be joined with the genesis of a welding seam, see fig. 5.1. In correspondence of the HAZ, the induced microstructural changes affect the strength of the final joint, depending on several factors, such as:

- base material
- heat-treatment state
- filler metal
- welding technique
- product geometry

The base materials show a decay of their mechanical properties in the HAZ. UTS and YTS are influenced to a lighter extent than elongation. Fig. 5.2 represents the mechanical properties of basic materials - a wrought alloy AlMgSi0,5 and a casting alloy AlSi9MgMn – and of the welded seam. In the worst case, strengths may fall to levels of as-cast tempers of gravity die castings. A self-ageing alloy ages again after welding. Materials which have already been aged show higher decays after welding. Strength values can only be recovered at a level corresponding to a T5 state. If heat-treatment has been or will be performed on welded seams, appropriate welding and design measures should be taken to avoid straightening of welded areas. An annealing to temper O eliminates the stresses induced by the welding procedure.

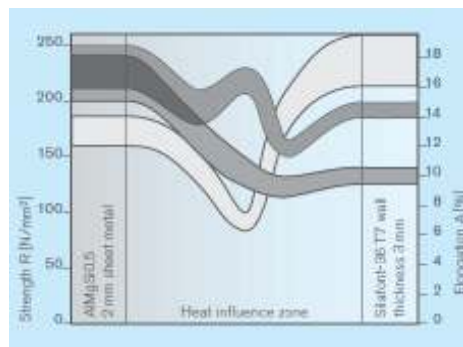


Fig. 5.2: influence on the mechanical properties in the HAZ.
MIG welding with filler metal AlSi12.

The choice of filler metal depends on the composition of the base materials and the properties required of the weld seam. An overview of filler metals used for casting and wrought alloys are listed in tab. 5.1. Usually, filler metal of a similar alloy is chosen; exceptions are possible if required due to particular requirement on the welding.

Casting alloy	AlSi5Mg AlSi7Mg	AlSi9Mg AlSi11Mg AlSi13	AlZn10Si8Mg	AlMg3 AlMg5 AlMg5Si2Mn AlZn5Mg AlZn3Mg3	AlCu4MgTi AlCu4Mg
AlSi5Mg AlSi7Mg	AlSi5				
AlSi9Mg AlSi11Mg AlSi13	AlSi5	AlSi5 AlSi10			
AlZn10Si8Mg			AlMg4,5Mn AlSi10		
AlMg3 AlMg5 AlMg5Si2Mn AlZn5Mg AlZn3Mg3	AlMg3 AlMg5	AlSi5 AlMg3 AlMg5		AlMg3 AlMg5	
AlCu4MgTi AlCu4Mg		AlSi5 AlMg5		AlSi5 AlMg5	AlMg5
Wrought alloys					
AlMgSi1	AlSi5	AlSi5	AlSi5 AlMg5	AlSi5 AlMg5	AlSi5
AlZn4,5Mg1	AlSi5 AlMg5	AlSi5 AlMg5	AlMg4,5Mn	AlMg5 AlMg4,5Mn	AlSi5 AlMg4,5Mn
AlMg2,7Mn	AlSi5 AlMg5 AlMg4,5Mn	AlSi5 AlMg5 AlMg4,5Mn	AlMg4,5Mn	AlMg5 AlMg4,5Mn	AlSi5 AlMg5 AlMg4,5Mn

Tab. 5.1: recommended filler metals for casting and wrought alloys.

The most common defects observed during arc welding procedures are blowholes, gas porosities, segregations and inclusions of oxides. Welding cracks and distortions on the welding seams are generated by internal stresses due to shrinkage during solidification of the HAZ.

5.3 Materials and samples

High-pressure die-cast plates of Silafont[®]-36, AlSi9MgMn and Castasil[®]-37, AlSi9Mn have been used for this study. The plates have been manufactured according to the same parameters of par. 4.6.1 and tested in a wall-thickness of 2 and 4 mm. The nominal chemical composition of the specimens is reported in tab. 5.2 and 5.3.

%	Si	Fe	Cu	Mn	Mg	Zn	Ti	Sr	Others
Min.	9,5			0,5	0,1		0,04	0,010	
Max.	11,5	0,15	0,03	0,8	0,5	0,07	0,15	0,020	0,10

Tab. 5.2: chemical composition of plates in Silafont[®]-36, AlSi9MgMn.

Magnesium is alloyed in Silafont[®]-36 as active strengthening element and tunes the final mechanical properties of the alloy. The same function is played by Mo and Zr for Castasil[®]-37, while magnesium is absent, in order to prevent undesired age-hardening phenomena. Both alloys have been modified with strontium, in order to modify the eutectic silicon.

%	Si	Fe	Cu	Mn	Mg	Zn	Mo	Zr	Ti	Sr	Others
Min.	8,5			0,35						0,0060	
Max.	10,5	0,15	0,03	0,60	0,06	0,07	0,3	0,3	0,15	0,0250	0,10

Tab. 5.3: chemical composition of plates in Castasil[®]-37, AlSi9Mn.

5.4 Design of experiments

High-pressure die-casting plates have been tested in with 3 different welding technologies:

- Laser Beam Welding (LBW)
- Electron Beam Welding (EBW)
- Friction Stir Welding (FSW)

Welding seams have been performed according to the approach “beads-on-plate”, i.e. directly on base material. Despite its non-applicability in real operating conditions, this technique can quickly reflect the feasibility of a welding process. Chamfers welded with EBW have been either brushed or etched with a NaOH solution before testing, in order to remove the surface layer of alumina. Edged joined with FSW and LBW have been simply degreased.

Testing conditions and parameters set for each welding technique have been described in par. 5.4.1, 5.4.2 and 5.4.3. After welding, cross sections of the seams have been polished. Light microscopy has been used to evaluate the presence of defects; micro-hardness profiles collected to quantify the softening of welded seams compared to base materials.

5.4.1 Laser Beam Welding

The functional design of a laser and its use as LBW is presented in fig. 5.3. A CO₂ laser with a power of 6 kW and a typical wave-length of 10,6 μm has been used. The welding cell has a working field of 1200 · 700 mm². The head of the laser can move vertically and change the focus length with a travel of 340 mm. The welding parameters which can be adjusted before operating the laser are the following:

- power profile in the welding start-up phase
- laser power during welding
- power profile in the welding end-up phase
- flow rate of the protective gas
- flow rate of the anti-plasma gas
- welding speed
- inclination of the welding head

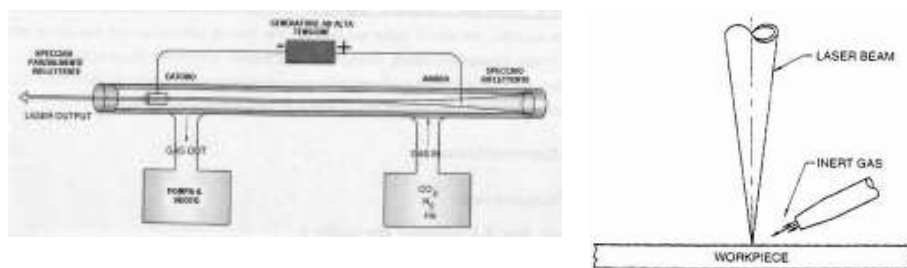


Fig. 5.3: LBW process.

The possibility of tuning the power input during the start-up and end-up phases allows the optimization of the most critical stages of the process. The protective gas is blown in the parallel direction of laser through a jet nozzle, while the anti-plasma gas is blown through a copper jet nozzle in the tangent direction of welding. Welding runs have been carried-out for each alloy and wall thickness, varying the following parameters:

- flow rate of protective gas
- protective gas (He or N₂)
- laser power during welding
- welding speed

Tab. 5.4 and 5.5 summarize the welding trials respectively for Silafont[®]-36 and Castasil[®]-37. Selected tests, whose results are presented in par. 5.4.1.3, are marked with a green-shadowed colour.

Weldability of primary aluminium HPDC alloys

Test	Wall thickness [mm]	Welding speed [mm/s]	Power [kW]	Protective gas	Flow rate [l/h]
1	2	41,7	3,1	He	6
2	2	41,7	3,1	He	6
3	2	45,0	3,1	He	6
4	2	50,0	3,1	He	6
5	2	53,3	3,1	He	6
6	2	53,3	3,1	He	6
7	2	56,7	3,1	He	6
8	2	66,7	3,5	He	6
9	2	83,3	3,5	He	6
10	2	41,7	3,3	He	6
11	2	45,0	3,3	He	6
12	2	45,0	3,1	He	6
13	2	50,0	3,1	He	6
14	2	58,3	3,1	He	6
15	2	58,3	3,1	N ₂	9
16	2	58,3	4,0	N ₂	9
17	2	58,3	4,2	N ₂	9
18	2	58,3	4,4	N ₂	9
19	2	61,7	4,2	N ₂	9
20	2	65,0	4,2	N ₂	9
21	2	68,3	4,2	N ₂	9
22	2	68,3	4,2	N ₂	9
1	4	41,7	4,5	He	6
2	4	41,7	4,3	He	6
3	4	41,7	4,1	He	6
4	4	41,7	3,9	He	6
5	4	41,7	4,0	He	6
6	4	41,7	4,1	He	4
7	4	41,7	4,1	He	2
8	4	41,7	4,1	He	8
9	4	41,7	4,1	He	10
10	4	41,7	4,1	He	12
11	4	53,3	5,5	N ₂	9
12	4	50,0	5,5	N ₂	9
13	4	53,3	5,5	N ₂	9
14	4	46,7	5,0	N ₂	9
15	4	43,3	5,0	N ₂	9

Tab. 5.4: design of LBW experiments for Silafont®-36, AlSi9MgMn.

Test	Wall thickness [mm]	Welding speed [mm/s]	Power [kW]	Protective gas	Flow rate [l/h]
1	2	58,3	3,1	N ₂	9
2	2	58,3	4,0	N ₂	9
3	2	58,3	4,2	N ₂	9
4	2	58,3	4,4	N ₂	9
5	2	61,7	4,2	N ₂	9
6	2	65,0	4,2	N ₂	9
7	2	68,3	4,2	N ₂	9
8	2	68,3	4,2	N ₂	9
1	4	58,3	5	N ₂	9
2	4	58,3	5,3	N ₂	9
3	4	58,3	5,5	N ₂	9
4	4	53,3	5,5	N ₂	9
5	4	50,0	5,5	N ₂	9
6	4	53,3	5,5	N ₂	9
7	4	46,7	5	N ₂	9
8	4	43,3	5	N ₂	9
9	4	46,7	5,5	N ₂	9
10	4	53,3	5,5	N ₂	9
11	4	50,0	5,5	N ₂	9
12	4	43,3	5,5	N ₂	9
13	4	43,3	5,5	N ₂	9
14	4	43,3	5,5	N ₂	9
15	4	43,3	5,5	N ₂	9
16	4	53,3	5,5	N ₂	9

Tab. 5.5: design of LBW experiments Castasil[®]-37, AlSi9Mn.

5.4.1.1 Results of LBW test procedure

Porosities and microporosities have been observed in most welding seams, with a major incidence on 2 mm wall-thick plates. The LBW seam of test 6 carried-out on a 4 mm thick plate in Silafont[®]-36 is shown in fig. 5.4. The presence of blowholes is significant and the quality of the seam not satisfactory. The tuning of welding speed has not led to remarkable improvements. Changing shielding gas has proven to be ineffective.

In order to improve the soundness of LBW seam, a second run has been performed. However, a decrease of the gas content has not been observed. This could depend on external sources of H₂, which could be introduced by the adopted welding system in form of humidity.

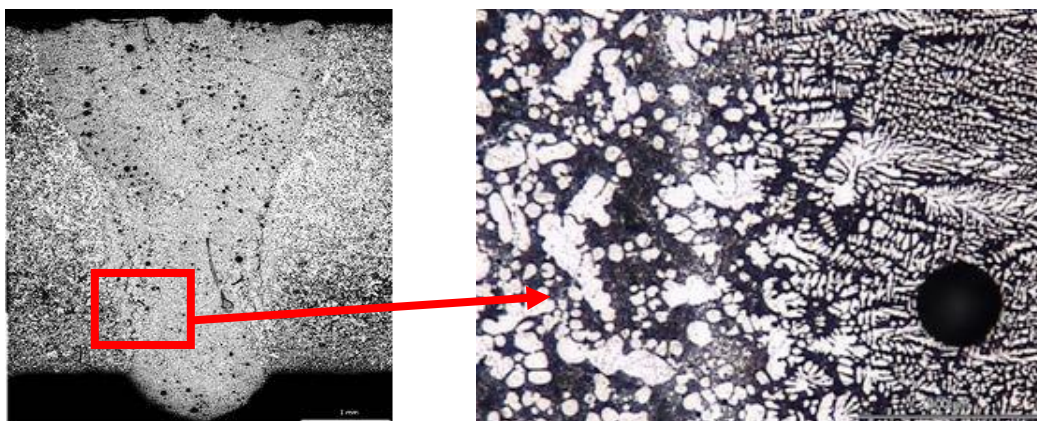


Fig. 5.4: LBW welding seam on a 4 mm wall-thick plate in Silafont[®]-36.

LBW seams in Castasil[®]-37 are of the similar quality level. Increasing the power of the CO₂ laser has shown some improvements on the gas content of seams: fig. 5.5 shows the seam obtained in test 2 with a power of 4 kW; fig. 5.6 the seam of test 4 welded at 4,4 kW.



Fig. 5.5: LBW seam. Test 2. Castasil[®]-37.



Fig. 5.6: LBW seam. Test 4. Castasil[®]-37.

However, a strong deformation of the welded area makes the seam unacceptable.

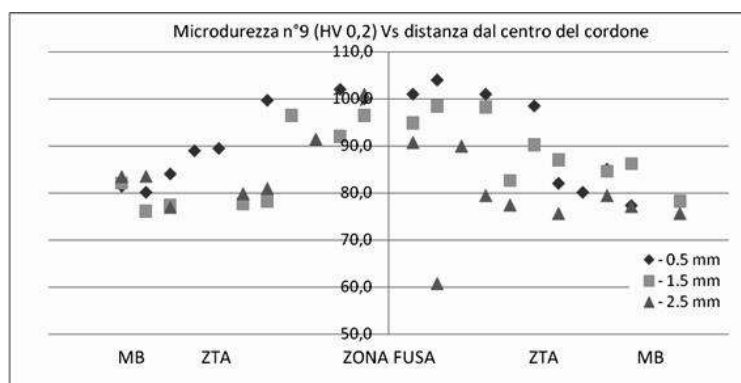


Fig. 5.7: microhardness profiles on a 4 mm LBW plate in Silafont[®]-36.

Microhardness profiles have been generated for seams 9 and 11, respectively for Silafont[®]-36 and Castasil[®]-37 in 4 mm plates. Three measurements at 0,5, 1,5 and 2,5 mm under the cast skin have been carried out, see fig. 5.7 and 5.8. The increase of Vickers hardness in the melted zone has been measured within 30 HV_{0,2} for both alloys compared to base material and HAZ.

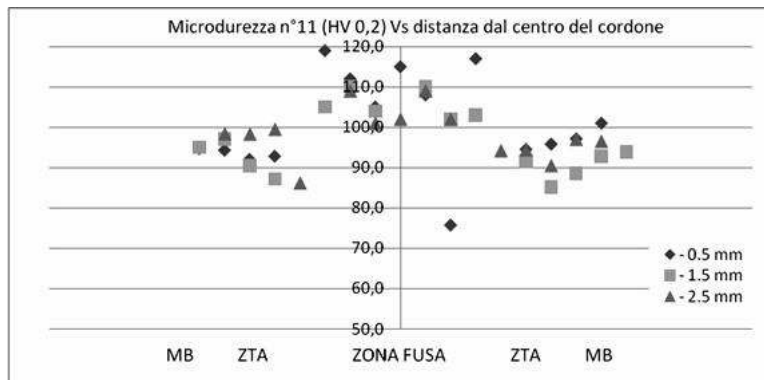


Fig. 5.8: microhardness profiles on a 4 mm LBW plate in Castasil[®]-37.

5.4.2 Electron Beam Welding

In the EBW the electrons emitted by a cathode are accelerated by an electrostatic field and focussed of the chamfers by electromagnetic fields, see fig. 5.9.

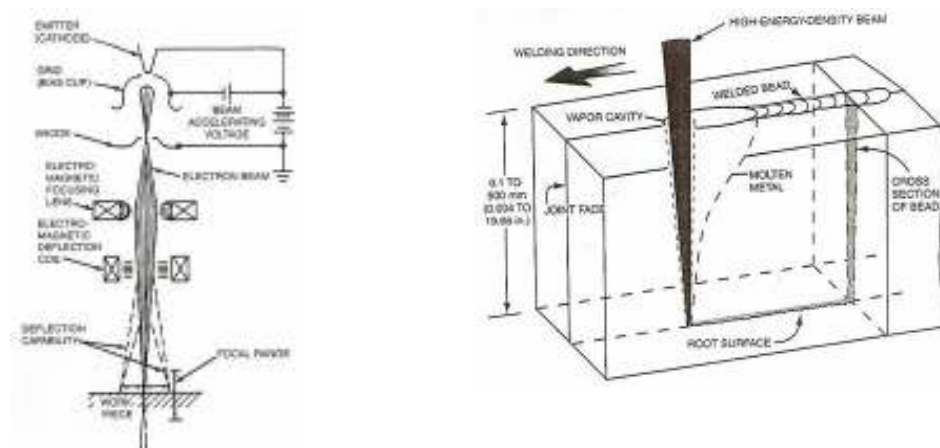


Fig. 5.9: EBW process.

The welding parameters which can be adjusted before operating the laser are the following:

- filament current
- voltage, i.e. potential between anode and cathode
- welding speed
- focus position

Tab. 5.6 and 5.7 summarize the welding trials respectively for Silafont[®]-36 and Castasil[®]-37. Selected tests, whose results are presented in par. 5.4.2.1, are marked with a green-shadowed colour.

Test	Wall thickness [mm]	Welding speed [mm/s]	Filament current [A]	Voltage [kV]	Notes
1	2	5	4	80	
2	2	5	5	80	
3	2	20	12	80	
4	2	50	20	80	
5	2	70	25	80	
6	2	90	28	80	
7	2	90	28	80	Double run
8	2	90	28	80	Cosmetic run
9	2	50	20	80	Cosmetic run
1	4	5	10	80	
2	4	5	11	80	
3	4	20	25	80	
4	4	20	23	80	
5	4	20	20	80	
6	4	20	18	80	Cosmetic run
7	4	40	25	80	
8	4	40	22	80	
9	4	40	22	80	Cosmetic run
10	4	60	25	80	
11	4	60	22	80	
12	4	50	20	80	

Tab. 5.6: design of EBW experiments for Silafont[®]-36, AlSi9MgMn.

Voltage has been kept constant to 80 kV, while welding speed and filament current have been varied within wide intervals. A double run has been adopted in some cases, in order to improve the internal soundness of EBW seams. A triple run has been done on a 2 mm-thick plate in Castasil[®]-37 with the same scope. A so-called “cosmetic run”, which is a welding run focussed on the surface of the chamfers, has been used to improve the visual appearance of EBW seams.

Test	Wall thickness [mm]	Welding speed [mm/s]	Filament current [A]	Voltage [kV]	Notes
1	2	20	12	80	
2	2	40	16	80	
3	2	60	20	80	
4	2	40	16	80	Double run
5	2	40	16	80	
6	2	40	16	80	Cosmetic run
7	2	20	12	80	Cosmetic run
8	2	60	20	80	Double run
9	2	60	20	80	Triple run
1	4	20	23	80	
2	4	20	20	80	
3	4	20	18	80	
4	4	40	25	80	
5	4	40	25	80	Double run
6	4	60	22	80	
7	4	60	22	80	Double run
8	4	20	23	80	Cosmetic run
9	4	20	18	80	Double run

Tab. 5.7: design of EBW experiments for Castasil[®]-37, AlSi9Mn.

5.4.2.1 Results of EBW test procedure

The presence of porosities and microporosities has been found comparable in EBW and LBW seams see fig. 5.9, if the welding procedure is carried-out with a single run. Although welding is performed in a vacuum chamber and sources of humidity are therefore absent, the hydrogen solutionized in the plates aggregated in form of gas bubbles.

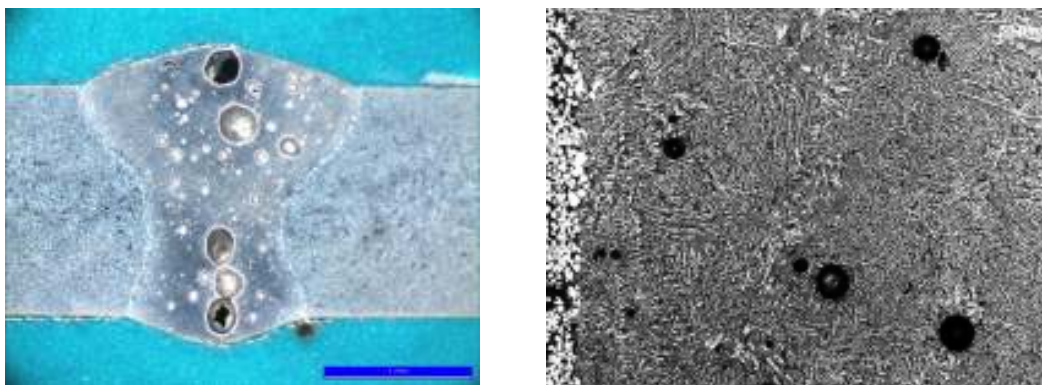


Fig. 5.9: macro- (left) and micro- (right) porosities in a 4 mm plate in Silafont[®]-36.

However, differently from LBW, the double run has shown remarkable positive effects, eliminating almost completely internal blowholes. In fact, the metal has time to re-melt and H₂ to be evacuated. This consideration is valid for both alloys and wall-thicknesses, see fig. 5.10 and 5.11.

The triple run has not shown further remarkable improvements. If EBW is used with a double run, the welding speed can be increased up to 90 mm/s without observing drawbacks in the quality of seams.

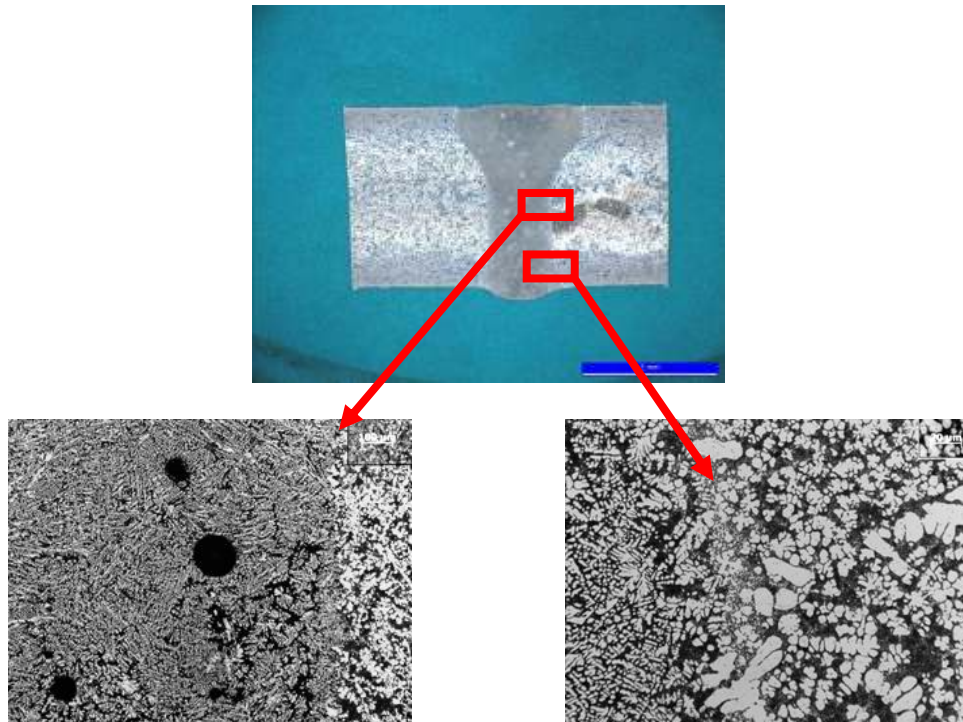


Fig. 5.10: EBW welding seam on a 4 mm wall-thick plate in Silafont[®]-36.

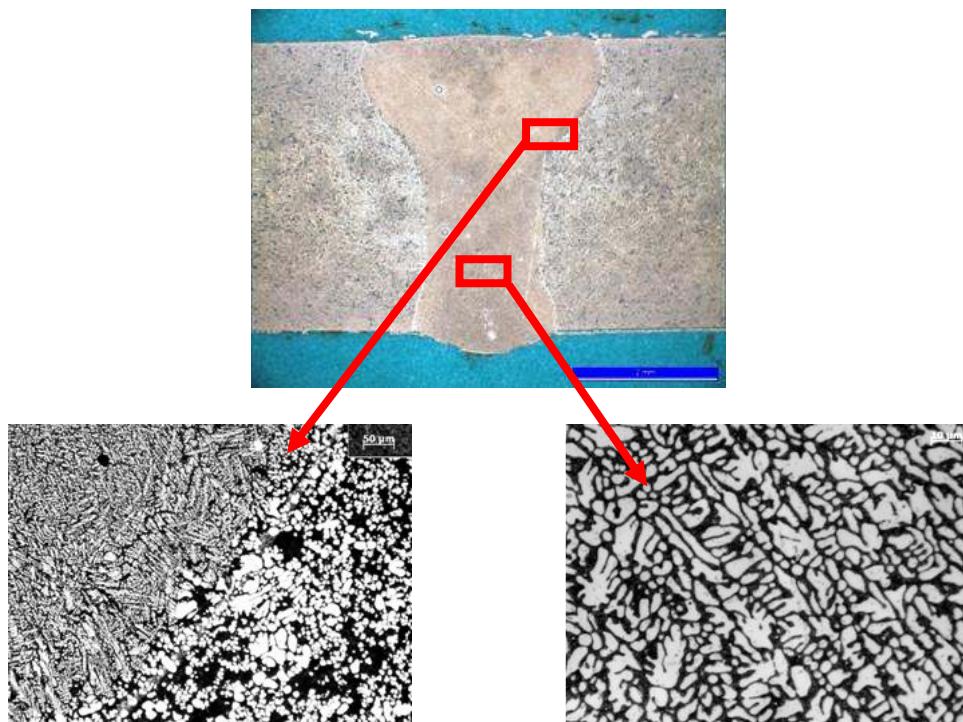


Fig. 5.11: EBW welding seam on a 4 mm wall-thick plate in Castasil[®]-37.

The width of the HAZ slightly increases, if the second run is made immediately after the first one; see comparison between fig. 5.12 and 5.13. However, if an intermediate cooling is carried out between the two runs, the dimension of the weld seam remains unvaried; see comparison between fig. 5.14 and 5.15. The aspect of the seam is significantly improved with the cosmetic run, which makes the joined area flat, clean and almost perfectly smooth.

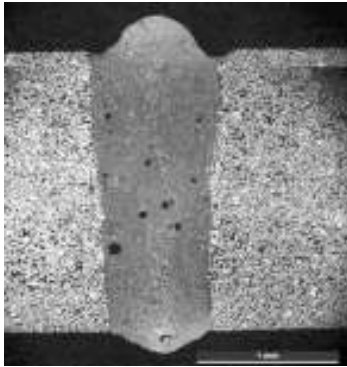


Fig. 5.12: EBW seam. Silafont®-36.

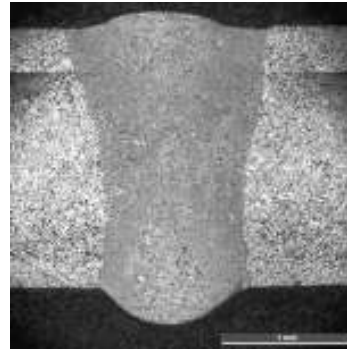


Fig. 5.13: EBW seam. Silafont®-36.



Fig. 5.14: EBW seam. Test 3, single run. Castasil®-37.

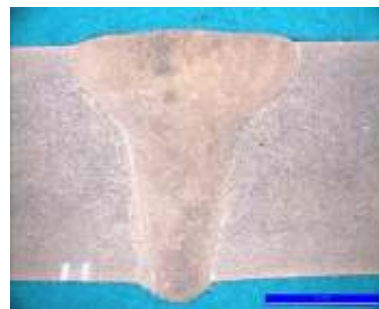


Fig. 5.15: LBW seam. Test 9, double run Castasil®-37.

The quality of EBW seams is therefore very satisfactory, if a double run process is set as default.

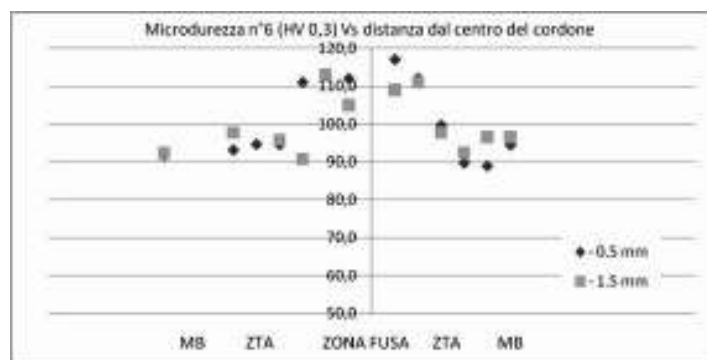


Fig. 5.16: microhardness profiles on a 2 mm EBW plate in Silafont®-36.

Microhardness profiles have been generated for seams 6 and 7, respectively for Silafont[®]-36 and Castasil[®]-37 in 2 mm plates. Two measurements at 0,5 and 2,5 mm under the cast skin have been carried out. The increase of Vickers hardness in the melted zone has been measured within 25 HV_{0,3} for both alloys compared to base material and HAZ.

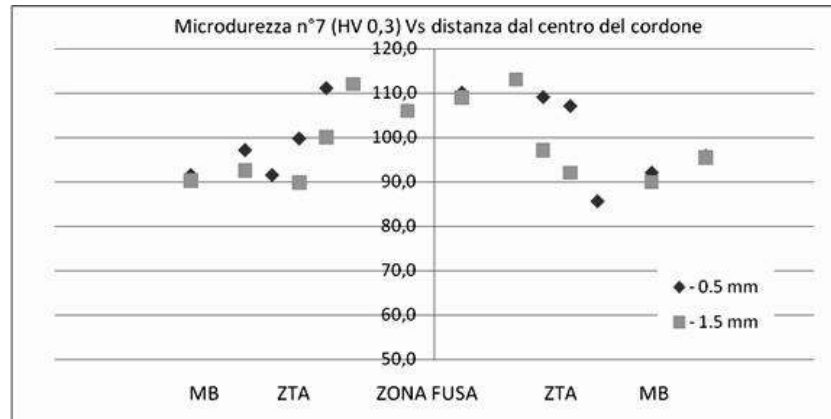


Fig. 5.17: microhardness profiles on a 2 mm EBW plate in Castasil[®]-37.

5.4.3 Friction Stir Welding

FSW process is a modern welding technique developed for aluminium and low-melting point metals. The heat, which is generated by the friction between a pin and the surface of the welding piece, softens the chamfers without causing their metal. The rotating movement of the pin mechanically “mixes” the metal, welding the two edges together, see fig. 5.18.



Fig. 5.18: FSW process.

A FSW seam has the typical aspect shown in fig. 5.19. Next to the basic material (A) and a HAZ (B), a so-called Thermo-Mechanical Affected Zone, TMAZ (C) can be defined. The core of the welding seam is called nugget (D). The width of area “C” corresponds to the pin shoulder.



Fig. 5.19: FSW seam.

The FSW equipment used in this study has a maximum force of 60 kN on its vertical axis and of 20 kN on its horizontal axis. Maximum welding speed is 160 mm/s. The pin length can be varied and the rotation speed can reach 6 000 rpm. The equipment can be operated either controlling its position or the applied force in real-time. In this study the control of position has been adopted; therefore, the following parameters have been set-up before welding:

- initial rotating speed (during penetration)
- rotating speed (during welding)
- pin length
- “touch-point” quote²
- welding speed
- pin head inclination

Initial rotating speed has been always set at 2 000 rpm, i.e. higher than welding speed. This favours a stable first contact between pin and metal. Pin length and inclination, as well as touch point have been kept constant.

Test	Wall thickness [mm]	Rotating speed [rpm]	Welding speed [mm/s]
1	2	800	4
2	2	800	6
3	2	800	8
4	2	800	10
5	2	1 000	8
6	2	1 000	10
7	2	1 000	12
8	2	1 500	16
9	2	1 500	18
10	2	800	8
11	2	1 000	10
12	2	1 500	18
13	2	1 500	20
14	2	1 500	23
15	2	1 500	25
16	2	1 500	28
17	2	1 500	34
18	2	1 800	38
19	2	1 800	40
1	4	1 500	7
2	4	2 000	8
3	4	1 500	6

² i.e. the position in which the pin head comes into contact with the chamfers

Weldability of primary aluminium HPDC alloys

4	4	1 500	5
5	4	2 000	7
6	4	2 000	6
7	4	800	2
8	4	800	3
9	4	800	4
10	4	800	5
11	4	1 000	5
12	4	1 000	6
13	4	800	10
14	4	800	12
15	4	800	16

Tab. 5.8: design of FSW experiments.
Silafont[®]-36, AlSi9MgMn.

Test	Wall thickness [mm]	Rotating speed [rpm]	Welding speed [mm/s]
1	2	800	8
2	2	800	10
3	2	1 000	12
4	2	1 000	16
5	2	1 000	20
6	2	1 500	22
7	2	1 500	26
8	2	1 500	30
9	2	1 500	34
10	2	1 800	38
11	2	1 800	40
12	2	1 800	16
1	4	1 500	7
2	4	1 500	7
3	4	1 000	5
4	4	1 500	7
5	4	1 500	7
6	4	2 000	8
7	4	2 000	10
8	4	1 500	7
9	4	800	4
10	4	1 500	12
11	4	1 500	16
12	4	1 500	10
13	4	800	5
14	4	800	10

Tab. 5.9: design of FSW experiments.
Castasil[®]-37, AlSi9Mn.

Rotating speed has been varied between 800 and 200 rpm and welding speed could have been set to a maximum of 40 mm/s on 2 mm-thick plates. Tab. 5.8 and 5.9 summarize the FSW trials respectively for Silafont[®]-36 and Castasil[®]-37.

5.4.3.1 Results of FSW test procedure

Generally, the quality of FSW seams has been considered very satisfactory and the parameters of welding, in particular the rotating speed of the pin, have been varied within wide intervals without affecting the joining ability of basic metal.

Porosities and microporosities due to gas inclusions have not been observed in the TMAZ of FSW seams. In few cases, the presence of tunnel and microtunnel has been detected, see fig. 5.20. However, these defects have been solved simply by changing the welding parameters.

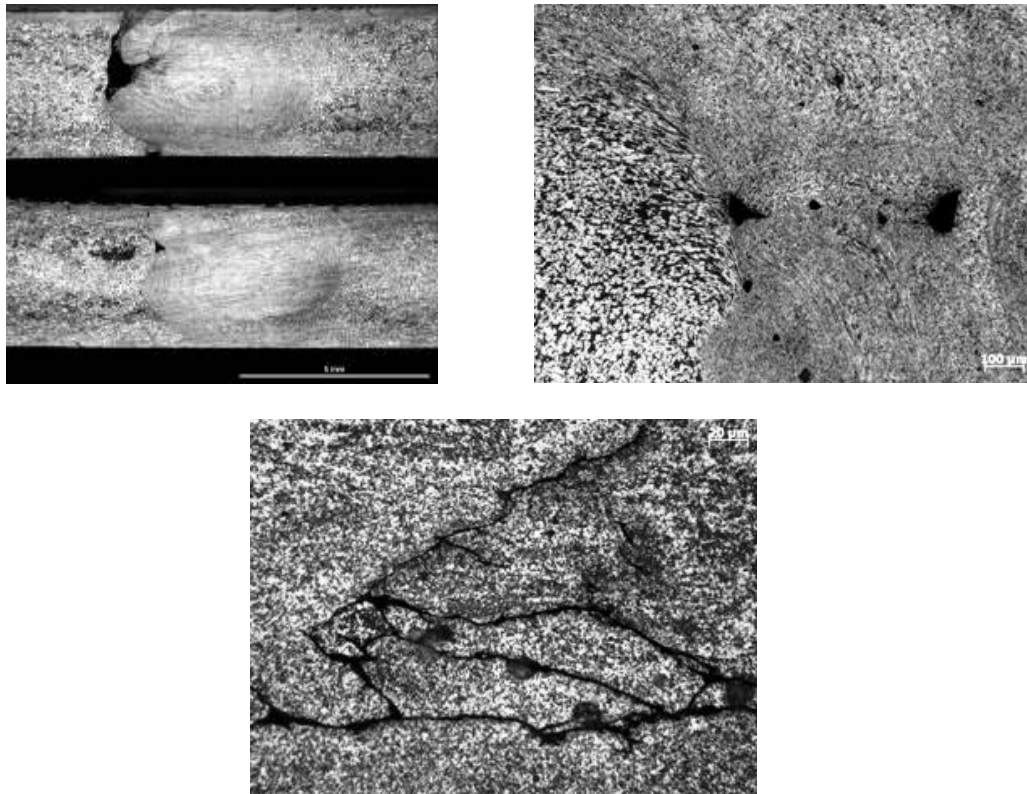


Fig. 5.20: FSW typical defects. Tunnels (top-left), microtunnel (top-right) and cracks (bottom). 4 mm wall-thick plate in Silafont[®]-36.

A FSW nugget has an asymmetrical aspect, see fig. 5.21, where the right-side is called advancing side, as the welding direction and the rotating direction coincide. The difference in the microstructure between basic material and nugget is evident macroscopically to the naked eye and microscopically, see fig. 5.21 and 5.23. The FSW has a refining effect on the eutectic phase of the metal: the “stretching” of the microstructure is a typical phenomenon caused by the plastic deformation induced by this method. This seam structure has been observed on both alloys in both wall-thicknesses.

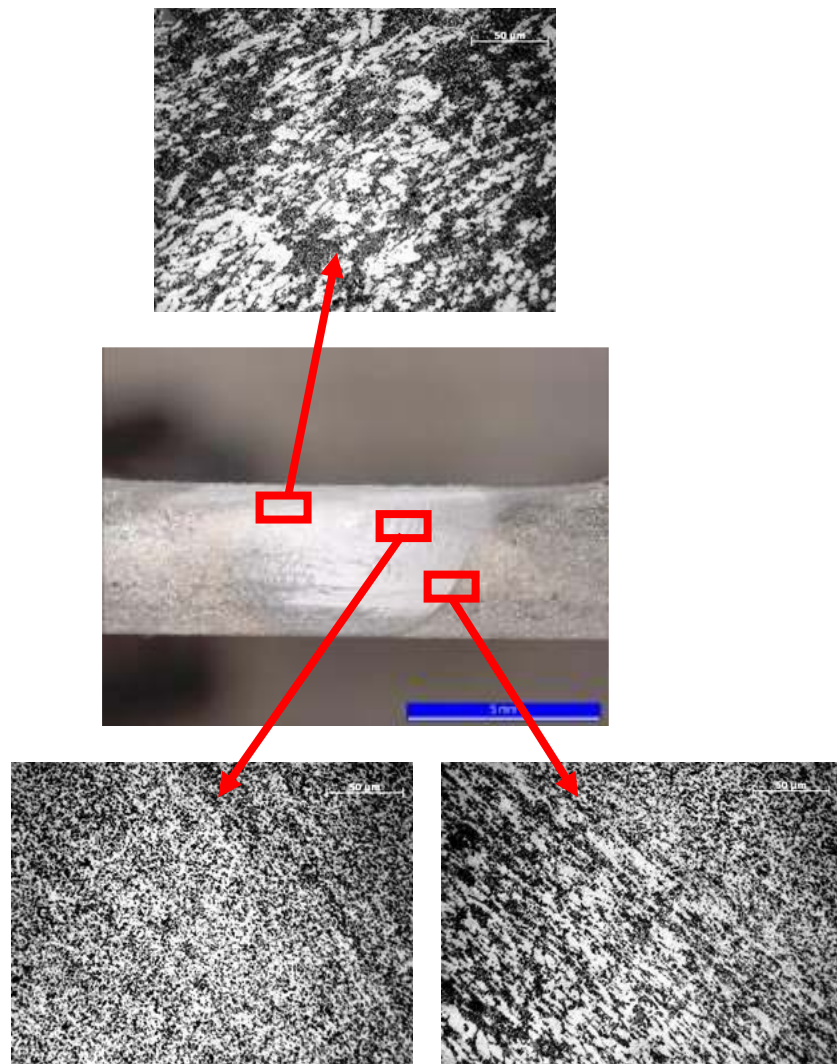


Fig. 5.21: FSW welding seam on a 4 mm wall-thick plate in Silafont[®]-36.

Microhardness profiles have been generated for seams 7 and 6, respectively for Silafont[®]-36 and Castasil[®]-37 in 4 mm plates. Three measurements at 0,5, 1,5 and 2,5 mm under the cast skin have been carried out, according fig. 5.22.



Fig. 5.22: micro-hardness profiles on a 4 mm thick plate.

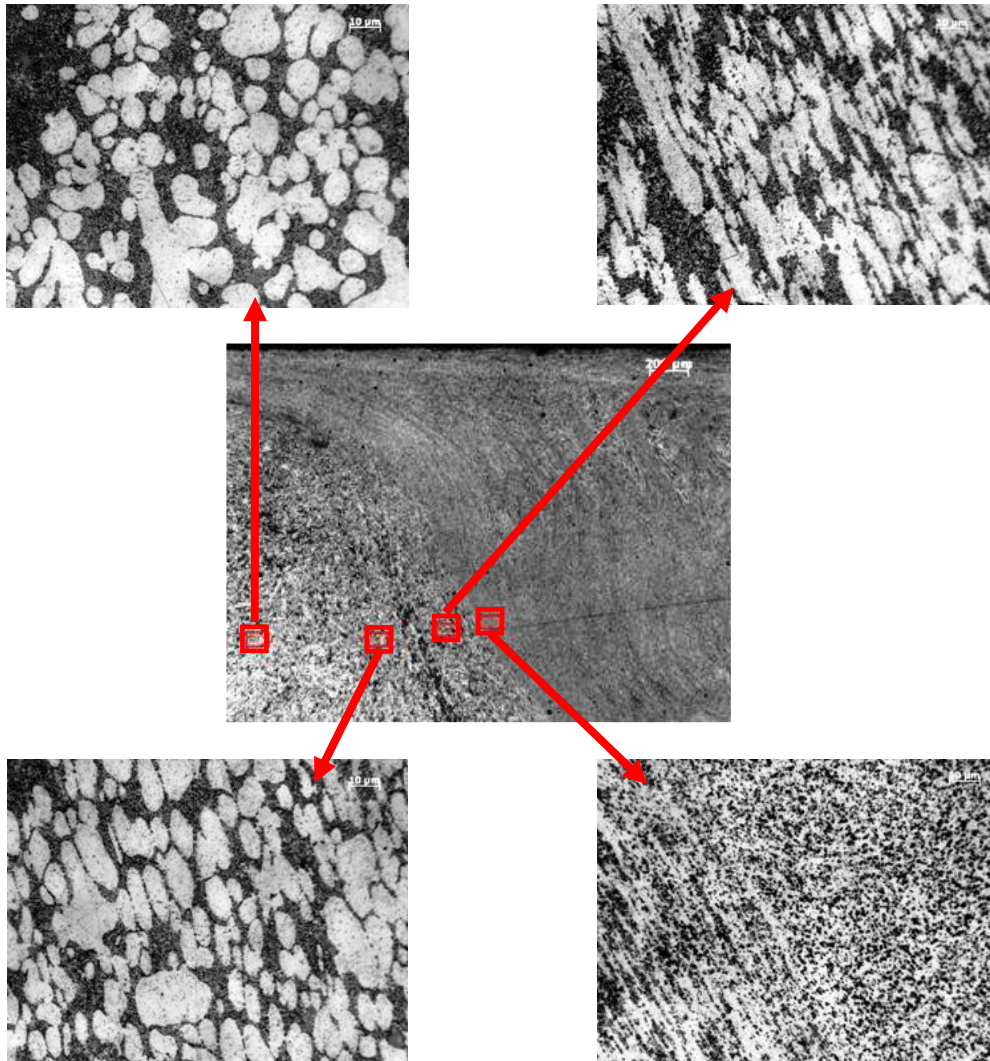


Fig. 5.23: FSW welding seam on a 4 mm wall-thick plate in Castasil[®]-37.

In contrast to LBW and EBW, FSW causes a softening of the seam. A decrease of Vickers hardness in the nugget has been measured within 25 HV_{0,3} for both alloys compared to base material and TMAZ, see fig. 5.24 and fig. 5.25.

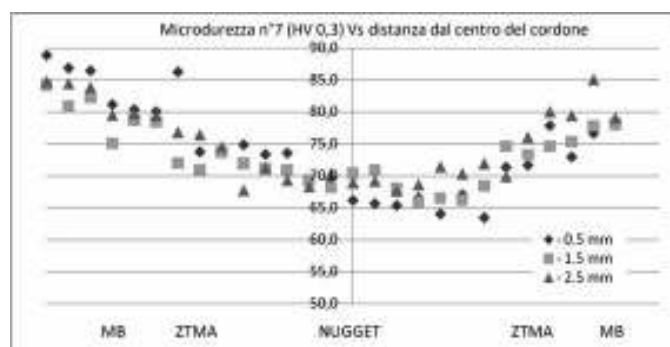


Fig. 5.24: microhardness profiles on a 4 mm FBW plate in Silafont[®]-36.

Heterogeneity of the microstructure can be observed in FSW seams comparing the near-to-surface region to the core area of the nugget. The micro-hardness profiles confirm it.

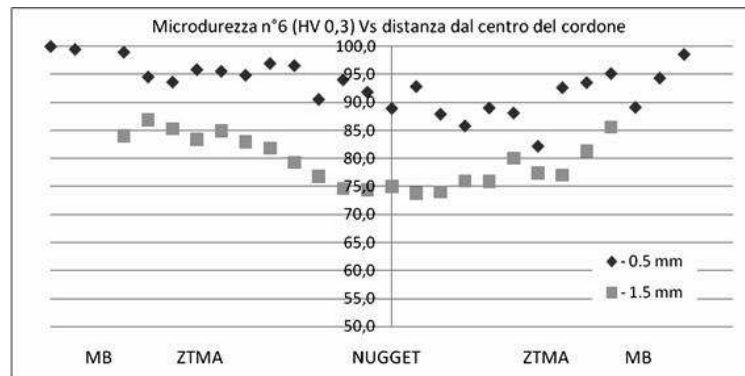


Fig. 5.25: microhardness profiles on a 2 mm EBW plate in Castasil[®]-37.

5.5 Conclusions

This study has been useful to determine the feasibility of modern welding processes applied to primary AlSi casting alloys.

Welding processes, which cause the melting of the chamfers, result in seams with gaseous porosities. High-energy processes have shown different results. The experimentation with LBW has proven to be unsuccessful, as fault-free welding seams could not be produced. The technology EBW has shown acceptable results with the adoption of a double run. Welding speeds of 90 mm/s could be reached with satisfactory seam quality. The vacuum chamber has to be managed properly to grant the repeatability of results. Generally, HAZs of LBW and EBW are very limited in their size, compared to traditional arc welding techniques. The increase on the microhardness of the melt zone is around 25-30 HV.

FSW technology has shown a higher degree of liberty in the tuning of welding parameters. Welding seams of satisfactory quality have been produced. A decrease of microhardness of around 25 HV has been observed in the nugget.

The results can be considered equivalent for both alloys.

Acknowledgements

This doctoral thesis is the result of three years of work and study, which have been precious, intense and continuously provided me enrichments on a professional and personal point of view.

I am particularly grateful to Professor Franco Bonollo, who was the supervisor of this script, for its thoughtful comments and more generally for his kindest support on all aspects of the work.

I am personally and professionally very grateful to Dr. A. J. Franke and R. Franke, who gave me the possibility of carrying out this PhD next to my working activities and showed full availability to my requests. I could not have found a better framework than Rheinfelden.

A huge help has been provided by Emanuele Ferrari and Claudio Gatti. The idea and the core activities of this work were born in Microtech. My deepest thanks for the time they spent for me, the precious material provided and the conversations that clarified my thinking on this matter. Their friendship and professional collaboration meant a great deal to me.

Thank you to Stefano Peli of Fonderie Cervati for the additional material he kindly provided on chapter 3.

I owe my gratefulness to Professor Shinji Kumai, from the Department of Materials Science and Engineering of the Tokyo Institute of Technology in Yokohama for kindly setting to my availability the twin-rolled plates and the technical information on HSTRC of chapter 4. A special thank to my friend Shui, always ready to offer his help and share with me his experience.

The study of chapter 5 has been made possible by Gianbruno Luvará, Luis Mario Volpone and Professor Paolo Piccardo. My thanks for their professional assistance.

Finally, I must acknowledge a number of colleagues, who actively helped me to conciliate work and study. In this regard, I am indebted to Anita, the one who really understood how important the PhD was to me, offering the best example of professional friendship. Special thanks to Herbert for his metallographic work in Rheinfelden and to Nicola Gramegna for his kind hosting in EngineSoft.

Some people made this time of my life unique and turned my worries into smiles. There are no words, but a huge hug to Michela as immense thank for bearing me three years long and for her spiritual support at critical and opportune times. I am extremely grateful also for the exquisite care she put in the review and new layout of the original manuscript, with helpful comments and creative tips.

Monica and Sonia stand by me as firm columns.

Last but first; this work is dedicated to Rosetta, who decided to sublimate her love to me through Eleonora. I wish I could hear her calling you “Nonna!”.

References

- [1] Aluminium Rheinfelden GmbH, Publication Code 630, *Producing low-iron ductile aluminium die castings*, 18th International Die Casting Congress and Exposition by NADCA, Indianapolis, 1995.
- [2] H. Koch, U. Sternau, H. Sternau, A. J. Franke, *Magsimal-59, an AlMgMnSi-Type Squeeze-Casting Alloy designed for temper F*, TMS Annual Meeting, Anaheim, LA, February 1996.
- [3] Aluminium Rheinfelden GmbH, Publication Code 633, *Experience of three years producing low iron ductile pressure die castings*, 19th International Die Casting Congress and Exposition by NADCA, Minneapolis, 1997.
- [4] Aluminium Rheinfelden GmbH, Publication Code 637, *Optimizing the manganese and magnesium content for structural part application, Silafont-36, AlSi9MgMn*, 22nd International Die Casting Congress and Exposition by NADCA, Indianapolis, 2003.
- [5] Aluminium Rheinfelden GmbH, *Primary aluminium alloys for pressure die casting*, 1. Edition, June 2007.
- [6] Aluminium Rheinfelden GmbH, *Neuentwickelte Druckgusslegierung mit ausgezeichneten mechanischen Eigenschaften im Gußzustand, Magsimal-59, AlMg5Si2Mn*, Sonderdruck aus GIESSEREI Ausgabe 3/98.
- [7] Aluminium Rheinfelden GmbH, Publication Code 632, *Erfahrung aus der Serienproduktion von druckgegossenen Lenkradskeletten in der Legierung Magsimal-59, AlMg5Si2Mn*, TMS Annual Meeting & Exhibition, San Diego, March 1999.
- [8] Aluminium Rheinfelden GmbH, Publication Code 636, *Potentials of aluminium pressure die casting. Application of this technology close to the limits, Magsimal-59, AlMg5Si2Mn*, Casting Plant and technology International, No. 2/2003.
- [9] http://en.wikipedia.org/wiki/Portevin%E2%80%93Le_Chatelier_effect
- [10] Aluminium Rheinfelden GmbH, Publication Code 545, *Magsimal-59, AlMg5Si2Mn, Anwendungsmerkblatt*, February 2004.
- [12] Rheinfelden Alloys GmbH & Co. KG, *Hüttenaluminium-Gusslegierungen, Leporello*, Ausgabe 06/2010.
- [11] Rheinfelden Alloys GmbH & Co. KG, *Hüttenaluminium-Gusslegierungen, Produktkatalogue*, Ausgabe 7, 01/2010.
- [13] O. Ozdemir, J. E. Gruzleski, R. A. L. Drew, *Effect of low-levels of strontium on the oxidation behaviour of selected molten aluminium-magnesium alloys*, Springer Science+Business Media, LLC 2009.

References

- [14] Rheinfelden Alloys GmbH & Co. KG, *Primary aluminium casting alloys*, Version 7, January 2010.
- [15] Dr. K. Greven, Dr. D. Dragulin, *Ductile high pressure die casting – heat treated or temper F?*, Proceedings of the 2nd International Light Metals Technology Conference 2005, 2005.
- [16] Aluminium Rheinfelden GmbH, *Aluminium Druckguss Legierungen*, 1 Edition, May 2003.
- [17] Aluminium Rheinfelden GmbH, *Primary Aluminium Casting Alloys*, February 2006.
- [18] Aluminium Rheinfelden GmbH, Publication Code 635, *Möglichkeiten des Aluminiumdruckgiessens. Anwendung dieser Technologie im Grenzenbereich. Berichte aus der Praxis. Magsimal-59, AlMg5Si2Mn*,. Sonderdruck aus Giesserei 90, Nr. 7, 2003.
- [19] Aluminium Rheinfelden GmbH, *Primary aluminium alloys for pressure die casting*, 1. Edition, June 2007.
- [20] Rheinfelden Alloys GmbH & Co. KG, *Hüttenaluminium-Gusslegierungen*, Ausgabe 7, 01/2010.
- [21] G. Luvará, *Studio di saldabilità (LBW-FSW-EBW) di leghe da pressocolata a base di alluminio*, Università degli Studi di Genova, Facoltà di Scienze M.F.N., A.A. 2008-2009, Genova, 2009.
- [22] Aluminium Rheinfelden GmbH, Publication Code 806, *Non aging ductile pressure die casting alloys for car construction, Castasil[®]-37, AlSi9Mn*, Edition 08/2004.
- [23] Aluminium Rheinfelden GmbH, Publication Code 638, *Economic production of ductile and weldable aluminium castings, Castasil[®]-37, AlSi9Mn*, Reprint from Casting Plant and Technology International, pages 22-27, February 2006
- [24] Aluminium Rheinfelden GmbH, Publication Code 623, *Qualitätsorientierte Schmelzprüfung in der Aluminiumgiesserei*, , Sonderdruck aus Giesserei Heft 23/1987, pages 695-700, 1987.
- [25] Aluminium Rheinfelden GmbH, Publication Code 518, *Silafont-36, AlSi9MgMn, Anwendungsmerkblatt*, Version 06, 2003.
- [26] Rheinfelden Alloys GmbH & Co. KG, *Leghe primarie da fonderia*, Edizione 7, Gennaio 2010.

-
- [27] R. Kasper, *Widerstandsfähigkeit von Formwerkstoffen gegenüber hochmagnesiumhaltigen Al-Legierungen*, Technische Universität Bergakademie Freiberg, Freiberg, April 2008.
- [28] N. Gramegna, *Analysis of the factors contributing to the heat balance of an high-pressure die-casting mould*“, Paper dal 31° Convegno AIM, Milano, Novembre 2006.
- [29] K. Greven, D. Dragulin, *Ductile high pressure die casting – Heat treated or temper F?*, Proceedings of the 2nd International Light Metals Technology Conference 2005, 2005.
- [30] T. Kobayashi, *Materials Science & Engineering*, 280, 8-16, 2000.
- [31] S. Kumai, K. Kobayashi, H. Zhu, K. Suzuki, T. Haga, *Microstructure and tear toughness of the vacuum die-cast and high-speed twin-roll cast aluminium alloys*, J. Jp Inst. Light Metals, 55, 500-506, 2005.
- [32] S. Kumai, Y. Nagata, A. Mukaiyama, *Improvement of tear toughness of ADC12 aluminium alloy by refined solidification structure*, J. JFS, 79, 717-7, 2007.
- [33] H. Zhu, S. Kumai, T. Tanaka, A. Sato, *Tear toughness of permanent mould cast and DC cast A356 aluminium alloys*, *Mat. Trans.*, 4, 1706-1713, March 2004.
- [34] H. Zhu, S. Kumai, T. Tanaka, A. Sato, *Tear toughness of permanent mould cast and DC cast A356 aluminium alloys using a small-size specimen*, *Mat. Trans.*, 4, 1714-1721, March 2004.
- [35] S. Kumai, A. Mukaiyama, *New expression method for tear toughness of cast and die-cast aluminium alloys*, J. JFS, 79, 671-675, 2007.
- [36] D. Shimosaka, M. Kim, Y. Harada, S. Kumai, F. Casarotto, S. Watanabe, *Microstructure refinement and toughness improvement of rapidly-solidified aluminium alloys including inherent brittle dispersed particles*, PFAM XVIII, Sendai, December 2009.
- [37] F. Casarotto, *Effects of eutectic silicon morphology on mechanical properties and ductile behaviour of Castasil-37*, DTG, Università di Padova, Facoltà di Ingegneria, A.A. 2003-2004.
- [38] E. Caruso, *Chemical optimization of Castasil-37 for the economic production of ductile high-pressure diecastings*, DTG, Università di Padova, Facoltà di Ingegneria, A.A. 2007-2008.
-

- [39] G. Raffaelli, *Strengthening while maintaining ductility in HPDC-Alloys for automotive application*, DTG, Università di Padova, Facoltà di Ingegneria, A.A. 2008-2009.
- [40] Aluminium Rheinfelden GmbH, Publication Code 803, *Duktile Druckgusslegierung mit geringem Eisengehalt, Silafont-36[®], AlSi9MgMnSr, Berichte aus dem Gusswerkstofftechnik*, Sonderdruck aus Giesserei 82, Nr. 15, 1995.
- [41] H. Koch, U. Hielscher, H. Sternau, A. J. Franke, *Silafont-36, the new low-iron high-pressure die-casting alloy*, TMS Annual Meeting, Las Vegas, February 1995.
- [42] A. J. Franke, J. C. Miske, *Low-iron diecasting alloy*, Foundry Management and Technology, March 1995.
- [43] H. Sakaguchi, T. Haga, H. Watari, S. Kumai, *High speed twin roll casting of 6016 aluminium alloy strip*, Journal of Achievements in Materials and Manufacturing Engineering, 20/1-2 (2007), 495-498.
- [44] T. Haga, M. Ikawa, H. Watari, S. Kumai, *High speed twin roll casting of 6016 strip*, Journal of Achievements in Materials and Manufacturing Engineering, 18/1-2 (2006), 371-374.
- [45] T. Haga, M. Ikawa, H. Watari, S. Kumai, *High speed twin roll casting of Al-3Si-0,6Mg strip*, Journal of Achievements in Materials and Manufacturing Engineering, 17/1-2 (2006), 337-340.
- [46] T. Haga, H. Sakaguchi, H. Watari, S. Kumai, *High speed twin roll casting of 6061 alloy strips*, Archives of Materials Science and Engineering, 31/1 (2008), 49-52.
- [47] T. Haga, K. Hirooka, H. Watari, S. Kumai, *Grooved roll for a high speed twin roll caster*, Archives of Materials Science and Engineering, 30/2 (2008), 117-120.
- [48] T. Haga, M. Ikawa, *High Speed Roll Casting of Aluminium Alloy*, 12th International Scientific Conference, Achievements in Materials and Manufacturing Engineering, Conference Proceedings.
- [49] T. Haga, H. Inui, H. Sakaguchi, H. Watari, S. Kumai, *High speed twin roll caster for aluminium alloy thin strip*, Journal of Achievements in Materials and Manufacturing Engineering, 24/1 (2007), 365-371.
- [50] T. Haga, H. Inui, H. Watari, S. Kumai, *Casting of aluminium alloy strip using an unequal diameter twin roll caster*, Archives of Materials Science and Engineering, 29/2 (2008), 113-116.

- [51] T. Haga, R. Nakamura, S. Kumai, H. Watari, *Clad strip casting by a twin roll caster*, Archives of Materials Science and Engineering, 37/2 (2009), 117-124.
- [52] H. Watari, T. Haga, Y. Shibue, K. Davey, N. Koga, *Twin roll casting of magnesium alloys with high aluminium contents*, Journal of Achievements in Materials and Manufacturing Engineering, 18/1-2 (2006), 419-422.
- [53] Aluminium Rheinfelden GmbH, Publication Code 620, *Aluminiumguß als Werkstoff für Schweißkonstruktionen*, Berichte aus der Praxis, March 1992.
- [54] U. Hielscher, Aluminium Rheinfelden GmbH, Publication Code 607, *Aluminium-Guß für Schweißkonstruktionen mit Aluminium-Knetwerkstoffen und für Drehgestell- Konstruktionen im Schienenfahrzeugbau*, Berichte aus der Praxis, Sonderdruck aus VDI Berichte Nr. 698, 101-115, 1988.
- [55] N. Grov, P. Lutze, H. Koch, *Schweißbaren Aluminium-Druckguss eignet sich für Sicherheitsbauteile*, Maschinenmarkt, 34/2001, 48-50, 2001.

